THE CATHOLIC UNIVERSITY OF AMERICA

Infrared Observations of Oxidized Carbon in Comet C/2002 T7 (LINEAR)

A DISSERTATION

Submitted to the Faculty of the

Department of Physics

School of Arts & Sciences

Of The Catholic University of America

In Partial Fulfillment of the Requirements

For the Degree

Doctor of Philosophy

By

William Michael Anderson Jr.

Washington, D.C.

2010

Infrared Observations of Oxidized Carbon in Comet C/2002 T7 (LINEAR)

William Michael Anderson Jr., Ph.D.

Director: Dr. Michael A. DiSanti, Ph.D.

Cometary nuclei are generally recognized as the most primitive remnants of the early Solar System. Their physical and chemical attributes allow a glimpse into the conditions under which icy bodies formed. Parent volatiles in comets are now routinely studied, and a significant diversity in composition among the comets sampled to date has been demonstrated. This forms the foundation of an emerging cometary taxonomy based on chemical composition.

In spring 2004, comet C/2002 T7 (LINEAR) was observed using the facility echelle spectrometer (CSHELL) at the NASA Infrared Telescope Facility on Mauna Kea, Hawaii. CSHELL offers seeing-limited spatial resolution and sufficiently high spectral resolving power ($R = \lambda/\Delta\lambda \sim 2.5 \times 10^4$) to permit line-by-line intensities to be measured along its 30 arc-second slit. Its small pixels favor measurement of molecules released from ices housed in cometary nuclei ("native" ices) over those released from spatially extended sources in the coma. Emission lines from multiple molecular species were targeted in the 3 to 5 μm wavelength region. The observations revealed an extremely rich volatile chemistry in C/2002 T7.

I present the chemical composition of oxidized carbon in C/2002 T7 (LINEAR). Carbon monoxide (CO), formaldehyde (H_2CO), and methyl alcohol (CH_3OH) were detected simultaneously or nearly simultaneously with H_2O on multiple UT dates spanning 2004 May 3-9 (heliocentric distance $R_h = 0.66 – 0.71$ AU) and May 30 - June 2 ($R_h = 0.99 – 1.03$ AU). I will discuss native production rates, rotational temperatures, and mixing ratios (abundances relative to H_2O) for oxidized carbon. My results illustrate that

C/2002 T7 (LINEAR) is enriched in CH_3OH, while CO is borderline depleted compared to other Oort cloud comets that have been measured.

I tested for chemical heterogeneity in C/2002 T7 (LINEAR), both diurnal, presumably associated with rotation of the nucleus, and serial (i.e., over a range in R_h). However, no evidence was seen for either short term or long term changes in the mixing ratios of CO, H_2CO, or CH_3OH, suggesting a homogeneous composition that did not vary with location on or depth in the nucleus. The gas production rates of C/2002 T7 (LINEAR) did however reveal short term variability having a rotational period of 2.32 days. This periodicity is consistent with an elongated nucleus having uniform activity per unit surface area, or alternatively with a more nearly spherical nucleus having distinct active regions, or some combination of these. This represents the first measure of a rotational light curve in a comet based on multiple parent volatiles.

This dissertation by William Michael Anderson Jr. fulfills the dissertation requirement for the doctoral degree in Physics approved by Dr. Michael A. DiSanti, Ph.D. in Physics, as Director, and Dr. Frederick C. Bruhweiler, Ph.D. in Astronomy, Dr. Steven B. Kraemer, Ph.D. in Astronomy, and Dr. Michael J. Mumma, Ph.D. in Physics, as Readers.

_____

Dr. Michael A. DiSanti, Ph.D., Director

_____

Dr. Frederick C. Bruhweiler, Ph.D., Reader

_____

Dr. Steven B. Kraemer, Ph.D., Reader

_____

Dr. Michael J. Mumma, Ph.D., Reader

Table of Contents

List of Figures

List of Tables

Acknowledgements

I would like to thank those who have provided me the help and support in the long journey in completion of this thesis and my doctoral degree. First of all, I would like to thank and give credit to my advisor, Dr. Michael DiSanti, for taking me on research assistant and granting me the amazing opportunity to study comets. I also want to express my gratitude to Dr. Frederick Bruhweiler for being an mentor throughout my entire graduate experience at Catholic University of America. I would also like to acknowledge my other committee members, Dr. Michael Mumma and Dr. Steven Kraemer, for their generous time, knowledge, and advice. It was an honor to meet and work with the other members of the Dr. Michael Mumma's Goddard Infrared Spectroscopy group: Dr. Boncho Bonev, Dr. Geronimo Villanueva, Dr. Neil Dello Russo, Dr. Karen Magee-Sauer, Dr. Erika Gibb, and Yana Radeva.

I would also like to thank all the Physics Department faculty of Catholic University of America at who have taught and assisted me throughout my graduate education, including Dr. Charles Montrose. I would also like to acknowledge my previous mentors and professors for their previous help and advice, including Dr. Stanley Dermont and Dr. Francisco Reyes from the University of Florida, and Dr. John Stane and Dr. Martin Posner at the University of Massachusetts at Boston.

Finally, I would like to thank my wife, Dianna, my two sons, Liam and Colin, my parents, and my brother for their constant support and encouragement. This work is dedicated to them.

CHAPTER I

INTRODUCTION

1.1. THE MYSTERY OF COMETS

Among the various celestial objects in the night sky, comets have attracted the interest of mankind throughout history. Bright streaks of light, comets moved of their own accord compared to the relatively predictable movement of the stars and planets. Strange, mysterious, and unknown, comets were seen by many cultures as herald of fortune or doom. Comets as the object of scientific study first occurred with Tycho Brahe, who intensely observed the comet of 1577 A.D. from various positions in Europe. The lack of parallax in these observations allowed Brahe to determine that comets were truly celestial objects as opposed to artifacts of the Earth's atmosphere. Edmund Halley would follow in Brahe's footsteps by using Newtonian mechanics to study the motion of the comet that would later bear his name. He correctly identified comets as solar system objects with calculable periods.

Centuries would pass as the brightness and orbital parameters of various comets were observed and studied. Such astrometry is useful for finding the positions of comets, but it sheds little light on the mystery of a comet's identity. What are comets? Where do they come from? Are comets all the same or are there different types?

1.2. THE SCIENTIFIC IMPORTANCE OF COMETS

The importance of comets in the scope of this thesis can be summarized in a few points:

1) Comets are essentially “fossils” of the early solar system. Cometary nuclei are theorized to have formed out of the early solar nebula far enough from the Sun that ices could be retained. It is also believed that comets were formed early in the solar system and subsequently ejected to its outer edge, and thus are though to be largely unaltered since their formation (Mumma, Weissman, & Stern, 1993). The molecular composition of cometary ices is very sensitive to the environment of their formation. With this knowledge, an examination of cometary chemistry can be used to study the physical and thermal conditions of the early Solar System.

2) The study of comets has direct implications to astrobiology. The comets that impacted on the Earth in its early history may have brought water and organic molecules that were necessary precursor materials for the emergence of life.

3) Comets are virtual chemical laboratories in space. Cometary activity occurs due to solar heating of the nucleus, resulting in sublimation of its surface or near-surface ices. The released gases expand adiabatically, and the associated pressure also drags dust grains, thereby forming a tenuous atmosphere (the coma). This present a unique opportunity to test molecular line fluorescence models at low temperatures.

1.3. COMET CLASSIFICATION BY ORBITAL PROPERTIES

Throughout much of history, the study of comets was largely focused on the determination of their orbits. Starting with Edmund Halley, the orbits of comets were calculated using Newtonian mechanics. Over time, the number of comets recorded increased to the point where it was feasible to form specific classes based on orbital parameters. The long period comets (or nonperiodic comets) were defined as comets with periods greater than 200 years and have no preferred inclination. Short-period comets were defined as with those of 200 years or less. These comets had the characteristic of lower inclinations to the ecliptic and often showed strong orbital resonances with the gas giant planets (especially Jupiter).

Computational models showed that comets could transfer between Jupiter-family and Halley-type orbits several times within their dynamical lifetimes. As a result, a more recent dynamical taxonomy (Carusi et al., 1987; Levison and Duncan, 1994) was developed based on the Tisserand parameter (T_J) relative to Jupiter and the Sun,

$$T_J = \frac{a_J}{a} + 2\left[\left(1-e^2\right)\frac{a}{a_J}\right]^{1/2}\cos(i) \tag{1.1}$$

where a_j is the semimajor axis of Jupiter, and a, e, i are respectively the semimajor axis, eccentricity, and inclination of the object. The Tisserand parameter is a dynamical value derived from the Jacobi integral of the restricted three-body problem (Tisserand, 1896),

and is relatively constant through a solar system object's dynamical lifetime. The Tisserand parameter was first devised as a matematical tool to verify the identity of two celestial objects, in particular for comparing a newly discovered comet with that of the a lost comet. Later, it was shown that the Tisserand parameter could be used to group solar system objects in to different classes, and indeed modern dynamical classifications incorporate the Tisserand parameter as the defining feature. Asteroids were found to have T_J of 3 or larger. Comets with $T_J < 2$ are associated with comets in Halley type orbits as well as long period and non-returning (from the Oort cloud) comets. Comets belonging to the Jupiter dynamical family (Jupiter Family comets) have T_J between 2 and 3.

1.4. COMET RESERVOIRS

Once comets were recognized as celestial objects, their origin became of scientific interest. Comets formed either from the same solar nebula as the planets or they formed somewhere external to the solar system. Short period comets, with their low inclinations, hinted toward a solar system origin. Long period comets, on the other hand, appeared to come from random directions. This debate would last centuries from Kepler to the mid-century 20th century.

In 1950, Jan Oort proposed a solution for the source of the long period comets. He saw that their orbits would cause them to be either ejected out of the solar system or altered into less eccentric orbits. These bright comets would have to be "new", meaning

they were most likely entering the inner solar system for the first time. To account for these comets, Oort proposed a reservoir that consisted of a spherical cloud ranging from 30,000 to 50,000 AU From the sun (Oort 1950). Today, this structure is called the *Oort cloud,* estimated to range from 10^3 to 10^5 AU and becoming spherical after 30,000 AU. The Oort cloud is thought to include 10^{11} to 10^{12} cometary nuclei and have a total mass of 1 to 50 earth masses (Stern, 2003). The return mechanism from the Oort cloud is gravitational interaction with nearby passing stars, molecular clouds, and galactic tides.

The Oort Cloud provided a likely explanation for the dynamically new and long period comets whose orbits had random inclinations relative to the ecliptic. Jupiter-family comets posed a problem as they have orbits that lie close to the ecliptic. Dynamically, it was very difficult to explain how comets originating in the Oort Cloud could preferentially end up in Jupiter-family orbits. A second reservoir for was proposed as the source of Jupiter-family comets. The Edgeworth-Kuiper Belt, a disc extending from the current orbit of Neptune (30 AU) to beyond 100 AU (Edgeworth, 1949; Kuiper, 1951). Numerical simulations of the evolution of comet orbits through the gravitational perturbation of the gas giants supported the existence of the Edgeworth-Kuiper Belt (Duncan et al., 1988). Direct observational evidence of the Edgeworth-Kuiper Belt followed in the early 1990's (Luu, J. et al., 1994).

The "Nice model" (named after the originating academia) was recently proposed as a dynamical model for the current formation of the Solar System (Gomes et al., 2005; Tsiganis, et al., 2005; Morbidelli et al. 2008), The "Nice model" theorized the migration

of the Jovian planets to their current orbits. The movements of the Jovian planets would disrupt much of the early solar system proto-disc. Comets formed in the giant planets' region was subsequently ejected, forming the Oort cloud, while Neptune's outward migration scattered planetesimals into high-eccentricity orbits, forming the scattered disc region of the Kuiper Belt. Within the "Nice" model, the scattered disc objects are thought to be the primary source of Jupiter Family comets, as their orbits continue to be subject to perturbations from Neptune's gravity.

1.5. PHYSICAL CLASSIFICATION OF COMETS

Another common criteria for classifying comets are to group them according to their physical features. Prominent features include their nuclei and ion and dust tails. Unfortunately, as of yet, no direct correlation between the physical appearance of a comet and its origin has been found. Both Oort Cloud comets and Kuiper Belt Comets have a range of dust poor to dust rich tails. The few direct observations of comet nuclei by spacecraft (only 4 in total as of 2010) show great differences in size, shape and surface structure (Huebner, 2008).

1.6. TAXONOMY ISSUES

Recent computational models of the early solar system have introduced additional dynamical considerations in connecting cometary orbits to their origin. It was once thought that Oort Cloud comets formed in the gas giants region (5-30 AU) of the

protoplanetary disk, while most Jupiter Family comets formed further out in the Kuiper Belt region (R_h > 30 AU). The computational model showed that Uranus and Neptune could not have formed at their current orbits as the densities of proto-planetary disc would be too low to account for their masses. A new Solar System paradigm was formed, the "Nice model" (Gomes et al., 2005; Tsiganis, et al., 2005; Morbidelli et al. 2008). As previously stated, the "Nice model" proposes that the migration of the giant planets from their original positions of formation to their current orbits occurred early in Solar System's history. Within the model, Jupiter is thought to have migrated inward through gravitational interactions with the proto-planetary disc, and scattered planetismal material outward. These planetismals interact with the other three gas giants, causing them to slowly drift to larger orbits. Eventually, Saturn migrates through the 2.:1 orbital resonance with Jupiter, which increases their orbital eccentricities and Saturn is moved to its current orbit. Saturn movement destabilizes the outer Solar System, moving Uranus and Neptune further out and scatters much more planetismals inward and outward. The "Nice model" is thought to explain the occurrence of the Late Heavy Bombard era (as evidenced from crater records on the Moon and terrestrial planets), as well as the formation of the Oort cloud and scattered disc of the Kupier belt. As a result, comet nuclei were scattered from their original locations to both cometary reservoirs, mixing the two populations. Based on this, dynamical characteristics alone cannot determine a comet's formation history, and indeed this is supported among comets observed to date. A different method must be used to trace cometary origins, namely the composition of ices in their nuclei.

1.7. CHEMISTRY AS A NEW BASELINE FOR COMET TAXONOMY

Chemistry (i.e., molecular composition) provides a means to understanding the origins of comets. The original composition of ices contained within a comet (i.e., the "native ices") should reflect the local environment (temperature, chemistry, and amount of radiation processing) in which the comet formed. As comets spend nearly their entire existence in the outer solar system (far more than any other bodies in the solar system), they are most likely to retain their primitive compositions. As a comet heads toward perihelion and crosses into the inner Solar System, the comet's nucleus will warm enough such that its native ices (i.e., those contained in its nucleus) will sublimate and release parent volatiles into the coma. These parent volatiles can be measured spectroscopically to assess the chemical composition of the native ices. In particular, a number of parent volatiles have strong fundamental vibrational bands at near infrared wavelengths ($\lambda \sim 2$-5 microns). Several of these molecules also have pure rotational transitions at sub-millimeter and millimeter wavelengths.

1.8. TECHNOLOGICAL REQUIREMENTS FOR INRFARED SPECTROSCOPY OF COMETS

The primary requirement to perform infrared spectroscopy of cometary parent volatiles is the ability to isolate individual emission lines from potential nearby (in wavenumber) lines and also from the underlying dust continuum. To accomplish this, a near-infrared (NIR) echelle spectrometer must have high spectral resolving power ($\lambda/\Delta\lambda$),

of order 10^4 (corresponding to 30 km s^{-1}) or higher. Gas outflow speeds in the coma are only ~ 1 km/s, therefore the cometary lines are not resolved by NIR spectrometers and the contrast between the lines and the background continuum increases with increasing resolving power. Sub-arc-second pixel size is also a necessary requirement, allowing the spatial distribution of line emission in the coma to measured at a high spatial resolution. High spatial resolution is very important, as it is necessary to measure the gas abundance accurately as function of distance from the nucleus. With low spatial resolution (as is the case in of single-dish radio receivers), it is much more difficult to separate parent volatile production from potential sources of release in the coma (referred to as extended or distributed sources).

1.9. WATER AS THE DOMINANT VOLATILE IN COMETS

Water is the most abundant ice in comets. Its sublimation effectively drives the overall volatile chemistry from a cometary nucleus within heliocentric distances of 3-4 AU (Mumma et al., 1986, 1996; Dello Russo et al., 2000). Historically, water has been theorized as a component of comets since the 1940's, starting with the detection of OH 3090 Å UV emission (see the historical review in Festou, Keller, & Weaver, 2004). Whipple (1950) later presented his "dirty snowball" hypothesis, stating that a comet was a solid nucleus a few kilometers in size and composed of water ice mixed with solid particles. Over the next couple of decades, there was only circumstantial evidence of water in comets. Whipple's model was verified with the arrival of Halley's comet in 1986. The Kuiper Airborne Observatory directly detected infrared fluorescent emission

of the 000-010 water band (Weaver et al. 1986). Later ground-based detection of water in comets was possible, targeting the weaker non-resonance fluorescence band (also termed "hot" bands). For these bands, rotational levels within the lower vibrational state are not significantly populated in the Earth's atmosphere, and so lines arising from these transitions are not subject to telluric extinction except in cases of accidental overlap with other absorptions (see section 3.6; Mumma et al., 1996; Dello Russo et al., 2000).

1.10. THE IMPORTANCE OF OXIDIZED CARBON (CO, H_2CO, AND CH_3OH) IN COMETS

Aside from water, a number of other cometary parent volatiles are measured in the near-Infrared (NIR). Three oxidized carbon molecules that are addressed in the research of this dissertation are introduced below in relation to cometary science. The addition of atomic hydrogen to organic molecules residing on the surface of icy-mantled grains prior to their incorporation into a cometary nucleus is thought to be a common process, based on high C_2H_6 to CH_4 abundances first observed in Comet Hyakutake (Mumma et al., 1996), and in subsequent comets (Mumma et al., 2003; DiSanti and Mumma, 2008).

Carbon monoxide should also experience hydrogenation on grain surfaces. Using ice compositions that match their interstellar analogs, laboratory irradiation experiments show that the abundances of H_2CO and CH_3OH resulting from this process are highly dependent on hydrogen density and temperature (from 10 to 25 K; Hiraoka et al., 2002, Watanabe et al., 2004). The relative abundances of CO, H_2CO, and CH_3OH can be used

to examine the hydrogenation efficiency, as was first done with 153P/Ikeya-Zhang (DiSanti et al., 2002). The process first creates the highly reactive formyl radical (HCO). The addition of a second hydrogen atom to HCO produces monomeric formaldehyde (H_2CO). Further hydrogen addition leads to methyl alcohol (CH_3OH) or formic acid (HCOOH) (Hudson and Moore, 1999).

Carbon monoxide (CO) is an organic molecule commonly observed in giant molecular clouds where star formation is active (Rank et al., 1971; Turner, 1989). A ubiquitous hyper-volatile species, CO is an excellent probe of cold (shielded) environments such as natal clouds around young planetary systems (Chiar et al., 1995, Whittet et al., 1996). CO ice is found to be dominant in the quiescent region between hot cores, where temperatures are low enough (~ 25 K) for carbon monoxide to condense directly as an apolar (i.e., water-poor) ice (e.g., Elias 16). Within a young planetary system, carbon monoxide can also be captured by polar (methanol-rich, water-rich) ices that form at small (< 5.0 AU) heliocentric distances (Whittet et al., 1996, Chair et al., 1998). Comets likely formed in the outer regions of the pre-solar nebula where carbon monoxide was abundant, though it is possible that some comets incorporate apolar ice from the natal cloud core while others incorporate polar ices of various compositions (DiSanti et al. 2001). This connection presents a good initial rationale for studying CO within comets. Correspondingly, CO was the first cometary molecule observed, in comet West (Feldman and Brune, 1976).

Formaldehyde (H_2CO) is commonly observed in interstellar clouds (Turner, 1994). If comets contain interstellar material, it is reasonable to expect that formaldehyde should be found within their nuclei. Formaldehyde was first securely detected in comets (Mumma and Reuter, 1989) by applying a new model for fluorescent emission in its ν_1 and ν_5 bands near 3.6 μm to the low-resolution infrared spectrum of comet 1P/Halley acquired with IKS on Vega 1 (Combes et al., 1988). Follow-up searches from ground-based telescopes returned upper limits only (Hoban et al., 1993), and it was first securely detected in the IR with CSHELL in Comet 153P/Ikeya-Zhang (DiSanti et al., 2002). The abundance of H_2CO in comets is of interest for two primary reasons. The first concerns astrobiology, as it is theorized that comets should have transported large amounts of pre-biotic molecules to the early Earth. The second reason is that H_2CO, along with methanol and CO, can be used as probe of the local conditions in which native cometary ices formed (Mumma et al., 1993; Bockelée-Morvan et al., 2005).

Methyl alcohol (methanol, CH_3OH) is a third organic molecule expected in comets based on abundances found in interstellar clouds. The first detection of cometary methanol was achieved in infrared observations of C/1990 V (Austin) (Hoban et al., 1991) through ν_3 band emission. Almost concurrently, millimeter radio observations also detected methanol in Comet Austin with abundances that matched the infrared results (Bockelée-Morvan et al., 1991). Methanol has since been detected in many comets, with abundances relative to water ranging from much less than 1% (0.15 % in LINEAR S4, Mumma et al., 2001 and 0.2% in 73P/S-W3, Dello Russo et al., 2006) to 5% (Bockelée-Morvan, et al., 2005).

1.11. SUMMARY

If the goal of a cometary taxonomy based on chemistry is to be accomplished, a larger sample size of measured comets is required to establish the existence of distinct categories as opposed to a more continuous distribution of native ice abundances. This work adds an integrating step through the presentation of infrared measurements and analysis of chemistry of the Oort cloud comet C/2002 T7 (LINEAR). Abundances of water and of chemically-related oxygen-bearing organic molecules (specifically CO, H_2CO, and CH_3OH) are presented on multiple UT dates (7 days in early May 2004 and 4 days in late May and early June 2004) during two separate observing runs that together spanned a range of heliocentric distances (0.66 – 1.03 AU). Abundances of these native ices are examined both day-to-day (for which a rotational period is fitted), and longer term through comparison of results from the two runs.

CHAPTER II

OBSERVATIONS OF C/2002 T7 (LINEAR)

2.1. OVERVIEW

In this chapter, I describe the observational techniques and present the spectral data for comet C/2002 T7 (LINEAR), the main object of this dissertation. The chapter starts with a background introduction of C/2002 T7, followed by a description of its orbital parameters and other important characteristics. I also briefly describe the Infrared Telescope Facility (IRTF) and introduce the CSHELL spectrograph, and discuss why it was chosen to observe C/2002 T7. I next describe the observing procedure and the analysis steps from raw data to calibrated spectra. Finally, I provide an observing log along with spectral extracts for all data included in this thesis.

2.2. BACKGROUND OF C/2002 T7 (LINEAR)

Comet C/2002 T7 (LINEAR) is an Oort cloud comet that was discovered on October 14, 2002 by the Lincoln Laboratory Near-Earth Asteroid Research (LINEAR) project, during a patrol observation of near-Earth asteroids. At the time of discovery its apparent magnitude was 17.5 and its heliocentric distance was 6.9 AU. Its orbital parameters were calculated to be: $1/a = 0.000051$ AU^{-1}, eccentricity $e = 1.005$, and inclination $i = 160.6$ deg. (Marsden, 2003; Nakano, 2003, 2006).With these values, this comet is dynamically new, coming into the inner Solar System for the first time (Rosenbush, 2006). As of March 1, 2010, C/2002 T7 still has an eccentricity of just less

than 1.005 and thus its hyperbolic orbit will take this comet out of the solar system (JPL HORIZONS, 2010).

The comet reached perihelion on April 23, 2004 UT. Its closest approach to Earth was on UT May 19, at a distance of 0.27 AU. However its solar elongation at this time was too small to permit observations. Dates of observation were selected in both early and late May with the objective of obtaining spectra during times of unusually large geocentric radial velocities and hence large Doppler shifts in the cometary emission lines. In particular this served to displace CO lines from their corresponding (opaque) terrestrial atmospheric absorptions. This provided very high transmittance for detailed study of the individual cometary CO lines targeted in this thesis.

C/2002 T7 (LINEAR) had an apparent visual magnitude of 4 at the beginning of May 2004 and peaked between 2.5 and 3.0 from May 20 to 25. Optical observations showed that Comet T7 had irregularities in brightness during mid-May (Seiichi Yoshida, 2008), in the sense that its light curve contained several unexplained minima and maxima. There are at least two possible causes for these observed variations in brightness. One could be regional heterogeneity on the surface ice of the nucleus, in which certain regions are more active (i.e. have higher concentrations of surface or near-surface ice) compared with the rest of the comet. As the comet approached perihelion, these more sensitive region became more or less exposed to the Sun. This would cause differences in the overall gas and dust outflow, and thereby bring about changes in the

comet's brightness. Rotation of the nucleus could also influence the exposure of these active regions to incident sunlight. Alternatively, the nucleus could initially have a uniform surface composition, but also have composition differences within the comet interior, as might be expected if the nucleus formed from material exposed to differing environments. As the comet approached perihelion, the exposure to the Sun would sublimate and remove the initial ice layers and reveal ice layers with a different composition with different volatility. In this case a seasonal (orbital) evolution in native ice abundances would be expected, and IR spectroscopy provides a critical test. Optical observations also revealed a visible dust tail ranging from between 1 and 2 arc-seconds to as long as 25 arc-seconds (Seiichi Yoshida, 2008).

2.3. THE NASA INFRARED TELESCOPE FACILITY

The NASA Infrared Telescope Facility (IRTF) is a 3.0-meter, f/35 telescope located atop Mauna Kea in Hawaii at an elevation of 4200 m above sea level. At this elevation, the column of water vapor in the atmosphere is greatly reduced, typically to about 10 percent of the column at sea level. This is very important for infrared observing, as water absorbs very strongly in the near- (and mid-) infrared. The location of the NASA IRTF also provides an addition benefit. Being atop a high mid-ocean island, a laminar flow of stable air runs across the observatory. The lack of turbulence typically provides sub-arc-second seeing. The NASA IRTF is optimized for infrared observing and is

managed and operated for NASA by the University of Hawaii Institute for Astronomy. Half of the observing time at the IRTF is allocated strictly for solar system research. The IRTF is unique among IR facilities in that it permits daytime observing, which offers great benefit for cometary observations as comets often have limited solar elongation during periods of highest activity. This was the case for C/2002 T7 (LINEAR) during May 2004 -- daytime observing was a necessary requirement for this study. The IRTF has a variety of instruments available including a CCD guide camera (1024 x1024 pixels – 1 arc-minute field of view) and two infrared spectrometers.

2.4. CRYOGENIC ECHELLE SPECTROGRAPH (CSHELL)

The Cryogenic Echelle Spectrograph (CSHELL; Greene et al., 1993, Tokunaga et al., 1990) is a long-slit spectrograph that uses a 31.6 lines/mm, 63.5-degree blaze angle echelle grating. CSHELL has narrow band circular variable filters that select the individual echelle order (ranging from 11 to 56) closest to blaze (see Appendix A.3). CSHELL incorporates a 256 x 256 InSb array detector (having sensitivity from 1 to 5.5 microns) with 0.2" pixels and achieves a spectral resolving power ($RP \equiv \nu/\Delta\nu$) of up to 42000 (or 7 km/s). This is the primary reason it was selected for comet infrared observations; for the observations presented here RP ~ 25,000, sufficient for studying individual molecular lines. The CSHELL also has a direct imaging mode. Because most observations of C/2002 T7 (LINEAR) were conducted during daytime (especially in

early May), the CCD guider could not be used, so direct infrared imaging was essential for placing (and maintaining) the comet in the slit.

2.5. OBSERVATIONAL METHOD

For the observations of C/2002 T7 (LINEAR), a 1.0 arc-second wide slit (oriented lengthwise East-West) was used. For a source that uniformly fills this slit, CSHELL delivers RP ~ 2 x10^4. For uniform expansion at constant speed, as assumed in our formalism (section 3.1), densities decrease as r^{-2} in the coma (r being distance from the nucleus), which translates to emission profiles falling as $1/\rho$, where ρ is projected distance (i.e., perpendicular to the line-of-sight) from the nucleus. The distribution of intensity in the slit is therefore not uniform, and this results in slightly higher RP in our comet spectra, at times approaching 3 x 10^4 (depending on seeing and accuracy in tracking the comet over the course of each exposure).

To maximize the total on-comet exposure time, the telescope was nodded along the slit in an ABBA sequence with the A and B beams placed equidistant from the slit center and separated by 15 arc-seconds (one-half of the slit length). The net comet spectrum was isolated by arithmetically combining the beams as A - B - B + A. Flat field spectra and dark frames were obtained after a series of ABBA sets were collected for each given echelle setting. A given echelle setting encompasses only about 0.23 percent

of the central wave number (ranging from ~ 5 cm^{-1} at 4.7 μm to ~ 8 cm^{-1} at 2.9 μm, so multiple settings are generally required to sample a sufficiently broad range in rotational energies (essential for determining rotational temperature; see Chapter 3). For example, a single setting only encompasses two CO lines, and these are close in rotational energy. Therefore, a minimum of two CO settings are required.

The following sequence of steps describes the processing of the two-dimensional (spatial-spectral) CSHELL frames. To illustrate this I use a setting from UT 2004 May 9.79 that simultaneously measures CO and H_2O (the CO_D setting, central wavelength about 4.7 microns). The upper left of Figure 2.1A is the difference image (A – B) showing C/2002 T7 (LINEAR) through the open aperture, with A-beam (white) and B-beam (black) positions indicated. A superposed schematic of the 1" wide CSHELL slit is shown in red. Each spectral frame is divided by a normalized (flat-dark) frame, cleaned through removal of "hot" pixels (caused by high dark current pixels and cosmic ray hits on the detector), straightened to achieve consistent spatial-spectral registration, and then differenced, which also achieves first-order subtraction of the thermal background and sky-line emissions (Fig. 2.1 (A), Upper Right). The processing is streamlined through set of IDL algorithms (DiSanti et al., 2001), resulting in a spatial-spectral frame in which the spatial dimension falls along columns and the spectral dimension runs along rows. Residual background thermal continuum and sky-line emissions are then next removed by combining the beams into a cropped frame, containing 256 spectral channels (columns) by 75 spatial channels (rows) (Figure 2.1 (A), Bottom). A wavelength scale is

established through comparison of each processed spectral frame with a synthetic spectrum of atmospheric transmittance and radiance, generated through GENLN2 - General Purpose Line by Line Atmospheric Transmittance and Radiance Model (Edwards, 1992) – using the HITRAN-2004 Molecular Data Base (Rothman et al., 2005). In addition to wavelength calibration, the GENLN2 transmittance model is also used to determine column burdens for each absorbing species in the terrestrial atmosphere. The fully resolved (RP ~ 10^6) atmospheric model is binned to the instrumental sampling, convolved to the spectral resolution of the comet observations, and normalized to the cometary continuum (Fig. 2.2 (B), Upper trace). The difference comet–scaled model yields the cometary emission spectrum (the "residuals") still multiplied by the atmospheric transmittance function (Fig. 2.2 (B), Lower trace).

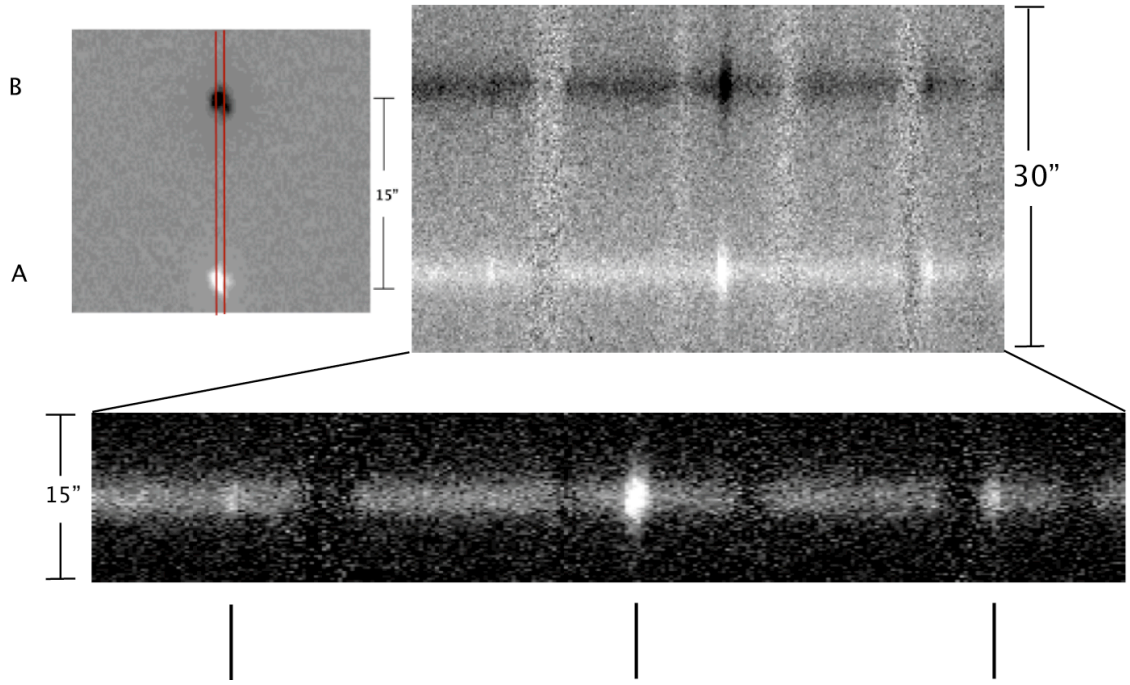

Figure 2.1 (A) (Upper Left): Difference image of comet C/2002 T7 (LINEAR) on May 9 2004, using a 30” by 30” aperture. The white and black represent the A-beam and B-beam positions respectively. They are separated by 15”. The red lines represent the 1” wide slit of CSHELL. (Upper Right): When switching from imaging mode to spectral mode, the spectral signal is shifted by 5” (25 rows in CSHELL) on the array to prevent contamination of the signal by residual afterglow from the bright comet image. The difference of spectral frames in CO_D setting, after both beams are individually spatially registered. (Bottom): The A and B beams are spatially combined and the spectral image is cropped to 15”. The CO P1 and P2 lines as well as a bright water line (center) is visible in the spectral signal.

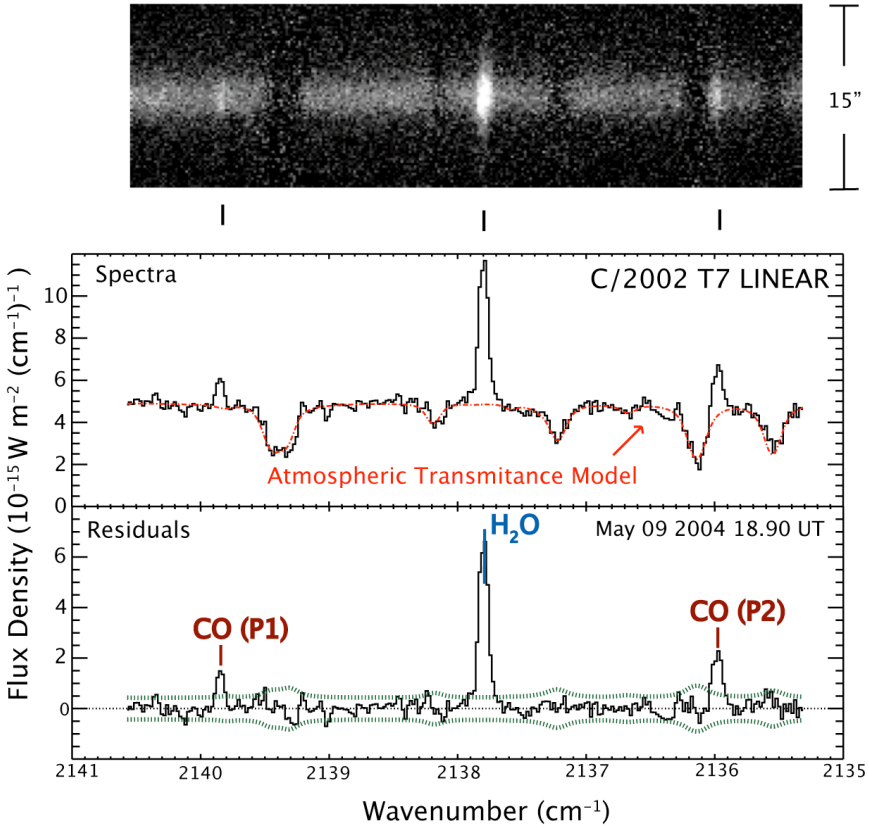

Figure 2.1 (B) – (Upper trace) – Comet spectra (solid) extracted from the comet signal contained in a 1” by 3” aperture centered on the row with the peak continuum intensity. An atmospheric transmittance model (dotted line) is applied, matching the terrestrial absorption features to H_2O and CO_2. (Lower trace): The observed comet residuals, from subtracting the comet spectra from the transmission model, shows the emission intensity above the continuum. Also displayed (dotted lines) is the +/- 1 stochastic noise (this also applies to the figures within the spectral gallery). For this figure, and for Figs. 2.2-2.5, observed frequency is plotted on the x-axis. Converting to emission line rest frequencies require correcting for geocentric Doppler shift.

Table 2.1. Log of C/2002 T7 (LINEAR) Observations

UT	Setting	R_h [a]	Δ [b]	V_Δ [c]	Lines	t_{int} [d]	Mid-UT [e]
3-May-2004	CH_3OH_A	0.657	0.709	-66.6	ν_3 Q-branch	480	18.22
	H_2O_3A	0.658	0.705	-66.3	γ	240	20.75
	CO_E	0.659	0.703	-66.2	R0, R1, α	480	21.85
	CO_H	0.659	0.703	-66.2	R7, R8	240	21.92
4-May-2004	H_2O_3A	0.665	0.671	-66.4	γ	240	16.03
	CO_F	0.665	0.674	-66.6	R2, R3	240	16.17
5-May-2004	CH_3OH_A	0.673	0.636	-66.1	ν_3 Q-branch	480	16.07
	CO_E	0.673	0.634	-66.0	R0, R1, α	240	16.87
	CO_G	0.674	0.634	-66.0	R5, R6	240	17.27
	CO_I	0.674	0.633	-65.9	R9, R10	480	17.95
	H_2O_3A	0.674	0.629	-65.6	γ	240	20.42
6-May-2004	CO_E	0.682	0.598	-65.5	R0, R1, α	240	15.75
	H_2O_3A	0.683	0.594	-65.1	γ	240	18.58
7-May-2004	CH_3OH_A	0.692	0.561	-64.6	ν_3 Q-branch	240	15.70
	CO_G	0.692	0.560	-64.5	R5, R6	240	16.05
	H_2O_3A	0.692	0.559	-64.4	γ	240	16.95
8-May-2004	CO_G	0.702	0.524	-63.3	R5, R6	240	16.20
	H_2O_3A	0.702	0.524	-63.3	γ	240	16.08
	CH_3OH_A	0.702	0.521	-63.1	ν_3 Q-branch	240	18.03
9-May-2004	CH_3OH_A	0.712	0.488	-61.7	ν_3 Q-branch	240	16.18
	H_2O_3A	0.713	0.485	-61.4	γ	420	18.07
	CO_D	0.713	0.484	-61.3	P2, P1, β	240	18.90
	CO_G	0.713	0.484	-61.3	R5, R6	240	19.02
	CO_C	0.713	0.483	-61.3	P3, P4	240	19.17
	CO_H	0.714	0.483	-61.2	R7, R8	240	19.32
30-May-2004	CH_3OH_A	0.989	0.521	60.8	ν_3 Q-branch	1920	4.70
	CO_D	0.989	0.523	60.9	P2, P1, β	1680	5.53
31-May-2004	CO_D	1.004	0.559	62.0	P2, P1, β	720	6.16
1-Jun-2004	CO_D	1.019	0.594	62.7	P2, P1, β	960	5.43
	H_2CO_B	1.020	0.596	62.9	ν_3 Q-branch	2400	6.80
2-Jun-2004	CO_D	1.034	0.629	63.2	P2, P1, β	480	5.00
	H_2CO_B	1.034	0.630	63.3	ν_3 Q-branch	960	5.40
	H_2O_3A	1.034	0.631	63.4	γ	480	5.88

[a] Heliocentric distance in Astronomical Units.
[b] Geocentric distance in Astronomical Units.
[c] Geocentric Doppler shift (km s^{-1})
[d] Total integration time on source (s)
[e] Mid-exposure UT (decimal date)

TABLE 2.2

Table 2.2. 2.9 and 4.7 μm H_2O Line Reference

Reference	H_2O Band	H_2O Line	ν_{rest}	$E_u - E_u(0_{00})$	g_{80K}	g_{100K}
α	100-010	2_{11}-1_{10}	2148.19	134.90	1.33E-07	1.42E-07
	001-010	1_{11}-1_{10}	2151.19	37.14	5.22E-07	4.54E-07
β	001-010	3_{22} -3_{21}	2137.33	206.30	4.90E-08	6.84E-08
		0_{00}-1_{01}	2137.37	0.0	6.28E-07	4.87E-07
γ	111-110	5_{15}-6_{16}	3448.72	326.6	5.59E-09	9.40E-09
	101-100	6_{06}-7_{07}	3448.74	446.7	2.01E-08	4.79E-08
	101-100	5_{24}-6_{25}	3449.38	416.2	2.15E-08	4.74E-08
	200-001	1_{10}-1_{11}	3450.29	42.4	1.26E-07	1.02E-07
	101-100	2_{02}-3_{21}	3453.15	70.1	8.05E-08	6.93E-08
	200-100	1_{10}-2_{21}	3453.30	42.4	8.50E-08	7.27E-08
	101-001	2_{11}-2_{20}	3454.69	95.2	5.07E-08	4.60E-08

Table 2.2 shows the various H_2O lines found within the corresponding CSHELL settings listed in Table 2.1. The α reference corresponds to the CO_E setting. The β reference corresponds to the CO_D setting. The γ reference corresponds to the H_2O_3A setting (see Dello Russo et al., 2004).

2.6. SPECTRAL GALLERY OF C/2002 T7 (LINEAR)

This section shows an overview of CO, H_2O, CH_3OH, and H_2CO emissions from May 3-9 and May 30-June 2, 2004 UT, all obtained with the 1-arc-second slit. All spectral extracts represent sums over 15 rows (3 arc-seconds) along the slit and centered on the row containing the peak continuum emission. As in Fig. 2.1 (B), for each extract the upper panel shows the comet spectrum in black and the convolved atmospheric transmittance model in red, while the lower panel shows the residuals along with the ±1σ

stochastic noise level (dotted). Prominent molecular emissions, both individual lines and blends are identified in each residual spectrum. For all spectra in Fig. 2.2, spatially integrated flux density is plotted against observed frequency (i.e., not corrected for geocentric Doppler shift). For these nucleus-centered extracts, differences in line intensities can be due to changes in cometary activity and/or differences in seeing/telescope tracking among CSHELL settings. We correct for seeing and placement of the comet in the slit in determining molecular production rates (see Chapter 3).

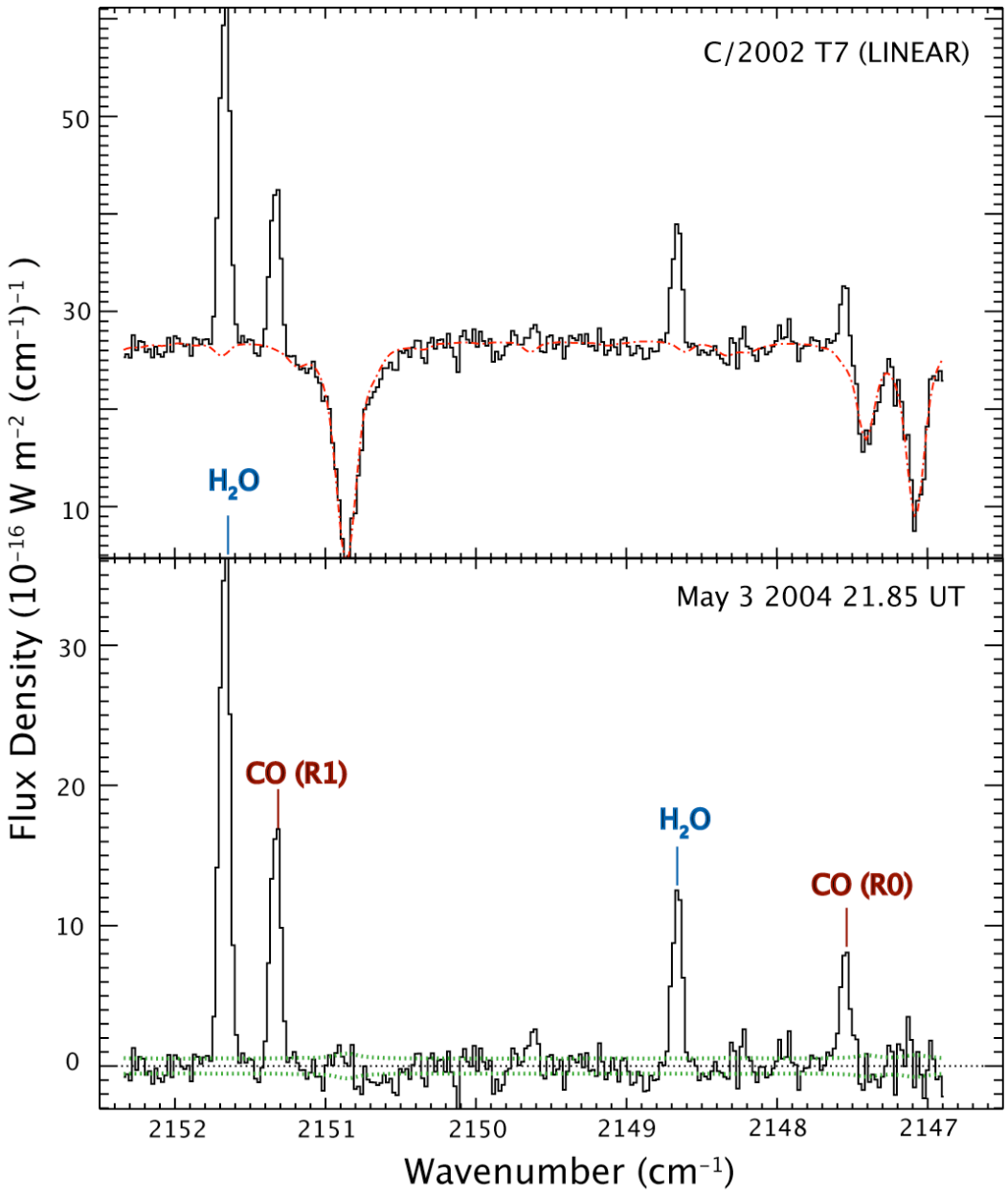

Figure 2.2 (A): Overview of May 3, 2004, CO and H_2O (CO_E setting) gas emission in C/2002 T7 (LINEAR) obtained with CSHELL through the 1 arc-second slit. The spectral revolving power is $\nu/\Delta\nu$ ~25,000. All extracts are centered on the row containing the peak emission. (Top): Comet spectra (solid) and atmospheric model (dotted line). (Bottom): Residuals with line identification and noise level (dotted line).

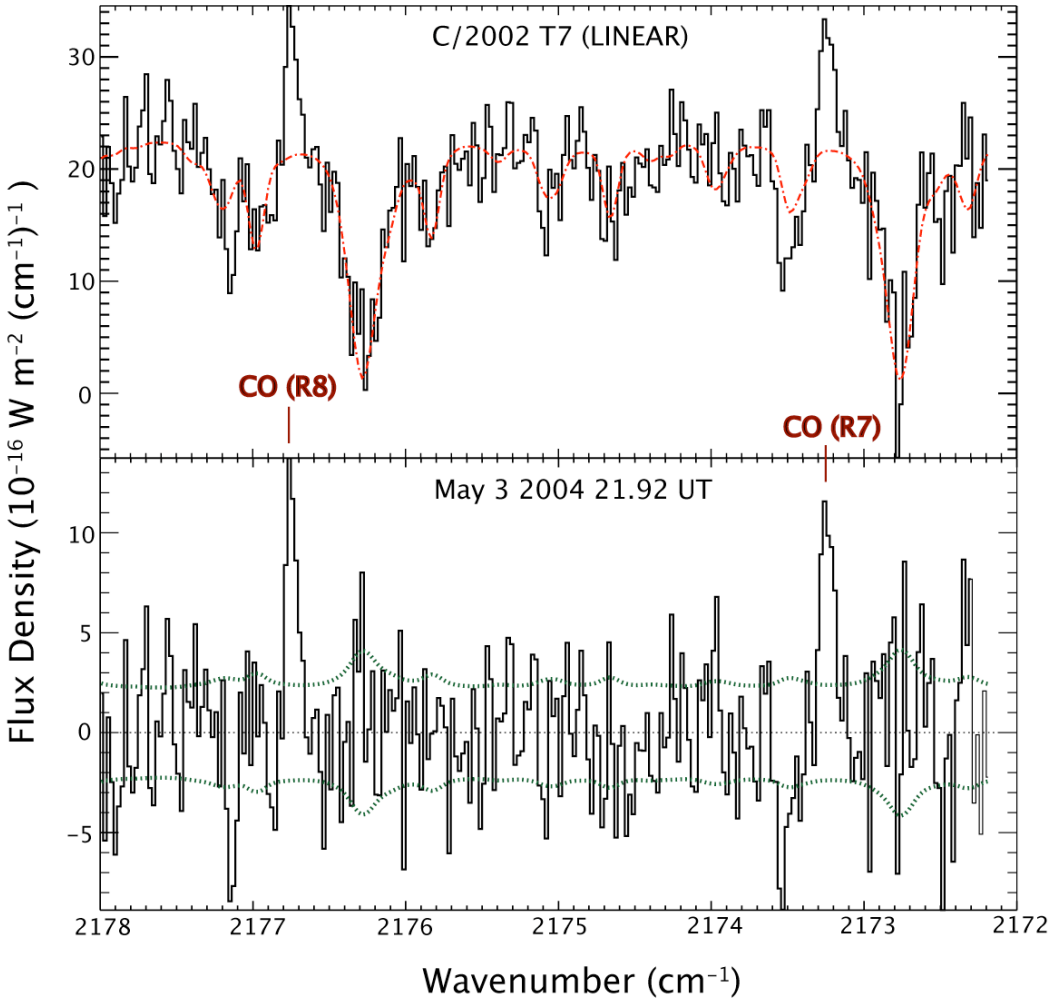

Figure 2.2 (B): Overview of May 3, 2004, CO (CO_H setting) gas emission in C/2002 T7 (LINEAR) obtained with CSHELL through the 1 arc-second slit. The spectral revolving power is $v/\Delta v$ ~25,000. All extracts are centered on the row containing the peak emission. (Top): Comet spectra (solid) and atmospheric model (dotted line). (Bottom): Residuals with line identification and noise level (dotted line).

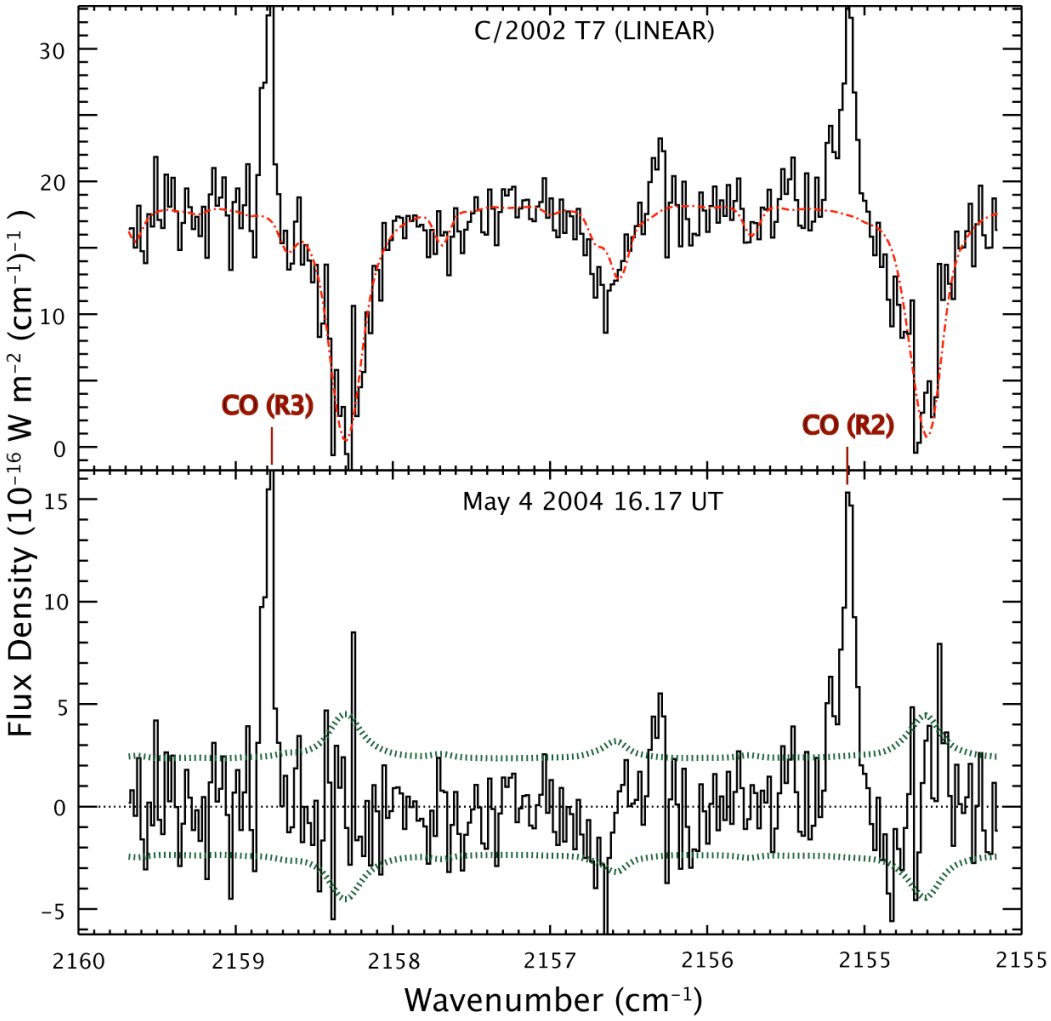

Figure 2.2 (C): Overview of May 4, 2004, CO (CO_F setting) gas emission in C/2002 T7 (LINEAR) obtained with CSHELL through the 1 arc-second slit. The spectral revolving power is $v/\Delta v$ ~25,000. All extracts are centered on the row containing the peak emission. (Top): Comet spectra (solid) and atmospheric model (dotted line). (Bottom): Residuals with line identification and noise level (dotted line).

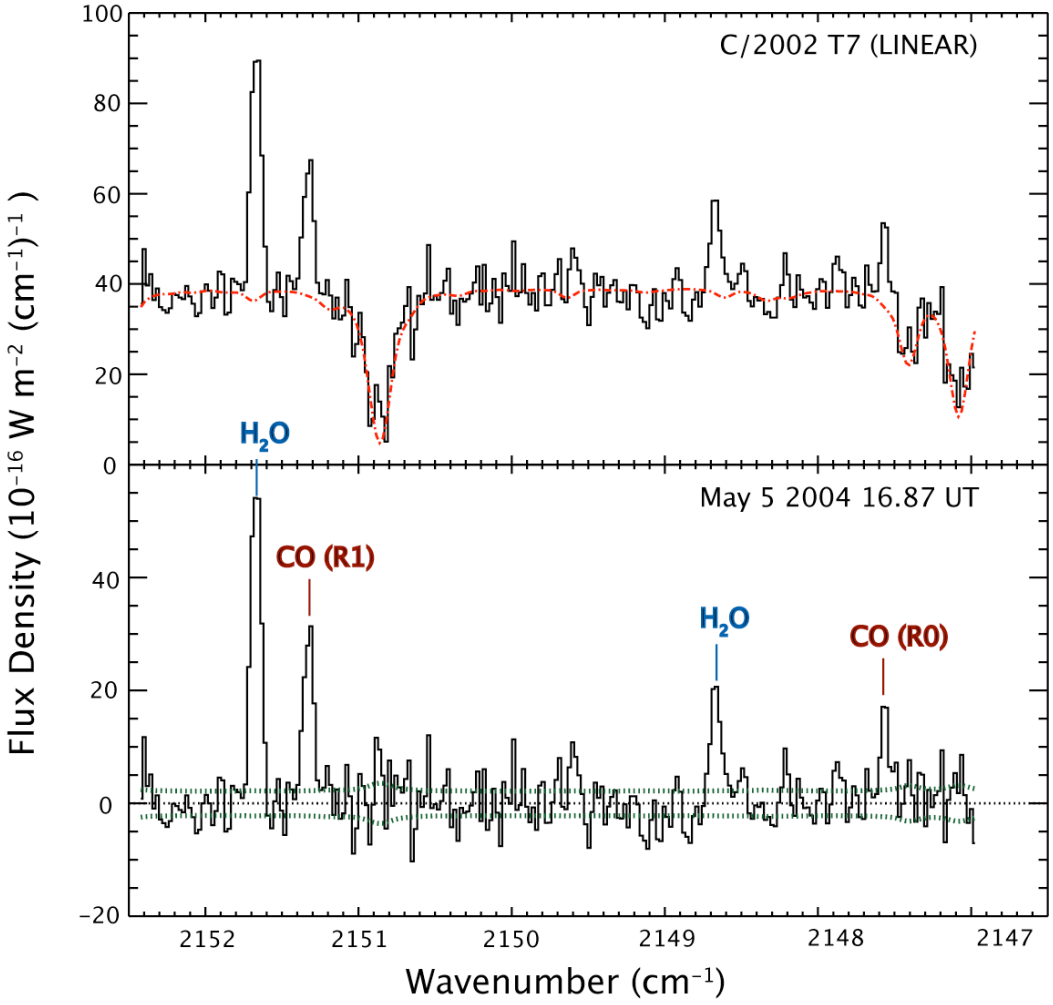

Figure 2.2 (D): Overview of May 5, 2004, CO and H_2O (CO_E setting) gas emission in C/2002 T7 (LINEAR) obtained with CSHELL through the 1 arc-second slit. The spectral revolving power is $\nu/\Delta\nu$ ~25,000. All extracts are centered on the row containing the peak emission. (Top): Comet spectra (solid) and atmospheric model (dotted line). (Bottom): Residuals with line identification and noise level (dotted line).

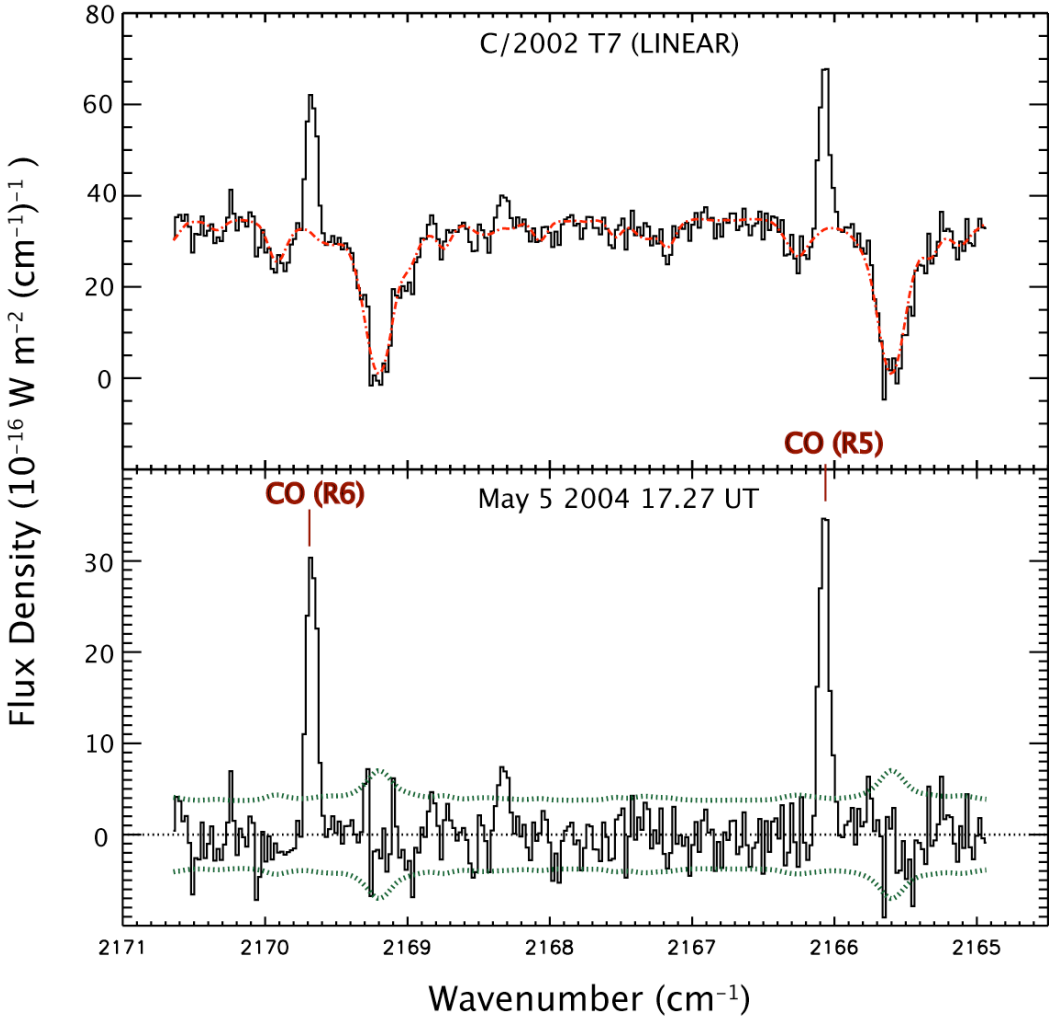

Figure 2.2 (E): Overview of May 5, 2004, CO (CO_G setting) gas emission in C/2002 T7 (LINEAR) obtained with CSHELL through the 1 arc-second slit. The spectral revolving power is $\nu/\Delta\nu$ ~25,000. All extracts are centered on the row containing the peak emission. (Top): Comet spectra (solid) and atmospheric model (dotted line). (Bottom): Residuals with line identification and noise level (dotted line).

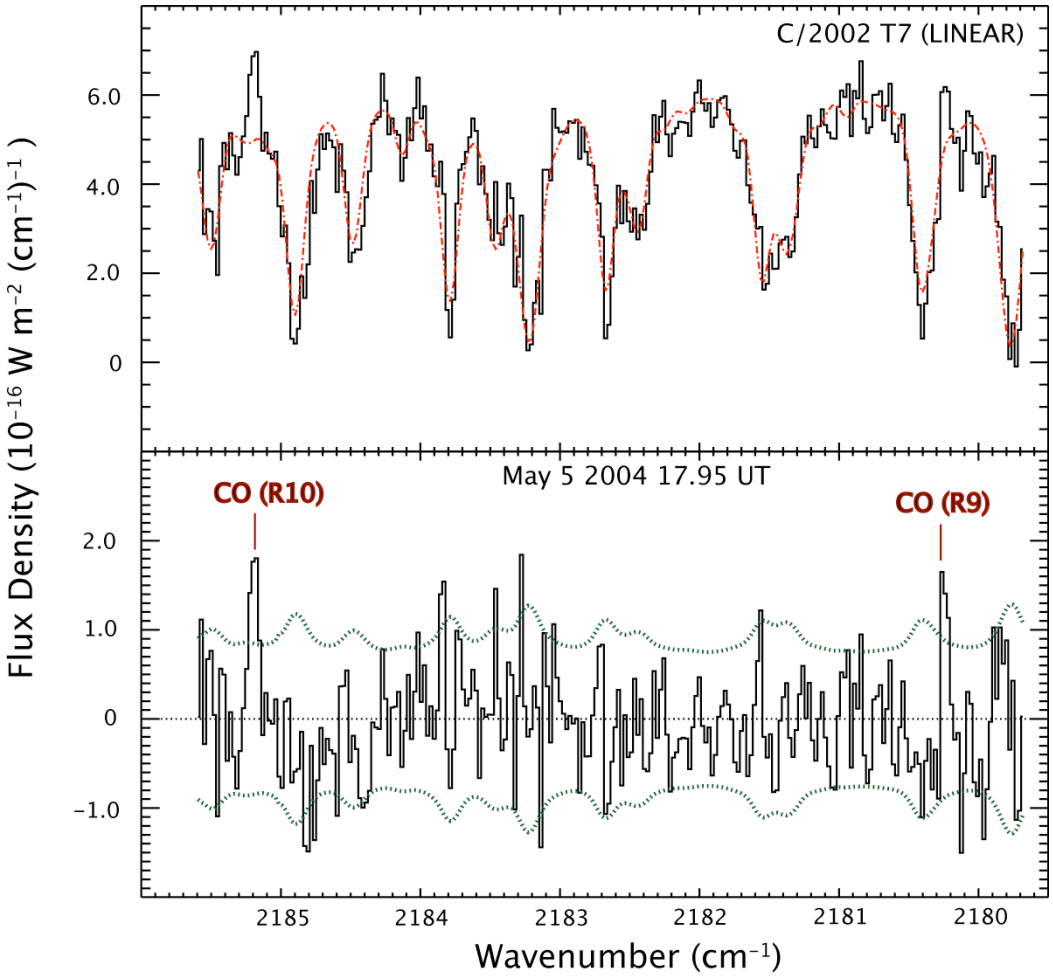

Figure 2.2 (F): Overview of May 5, 2004, CO (CO_I setting) gas emission in C/2002 T7 (LINEAR) obtained with CSHELL through the 1 arc-second slit. The spectral revolving power is $v/\Delta v$ ~25,000. All extracts are centered on the row containing the peak emission. (Top): Comet spectra (solid) and atmospheric model (dotted line). (Bottom): Residuals with line identification and noise level (dotted line).

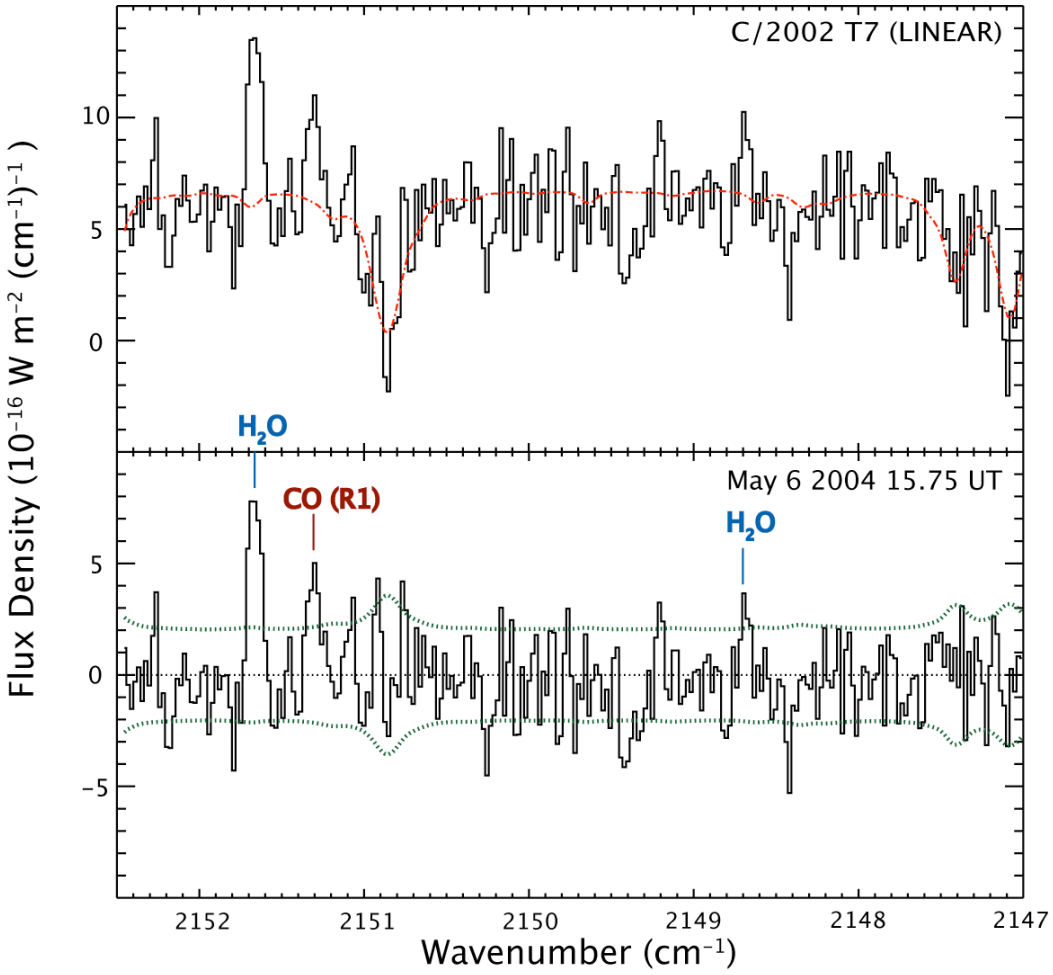

Figure 2.2 (G): Overview of May 6, 2004, CO and H_2O (CO_E setting) gas emission in C/2002 T7 (LINEAR) obtained with CSHELL through the 1 arc-second slit. The spectral revolving power is $v/\Delta v$ ~25,000. All extracts are centered on the row containing the peak emission. (Top): Comet spectra (solid) and atmospheric model (dotted line). (Bottom): Residuals with line identification and noise level (dotted line).

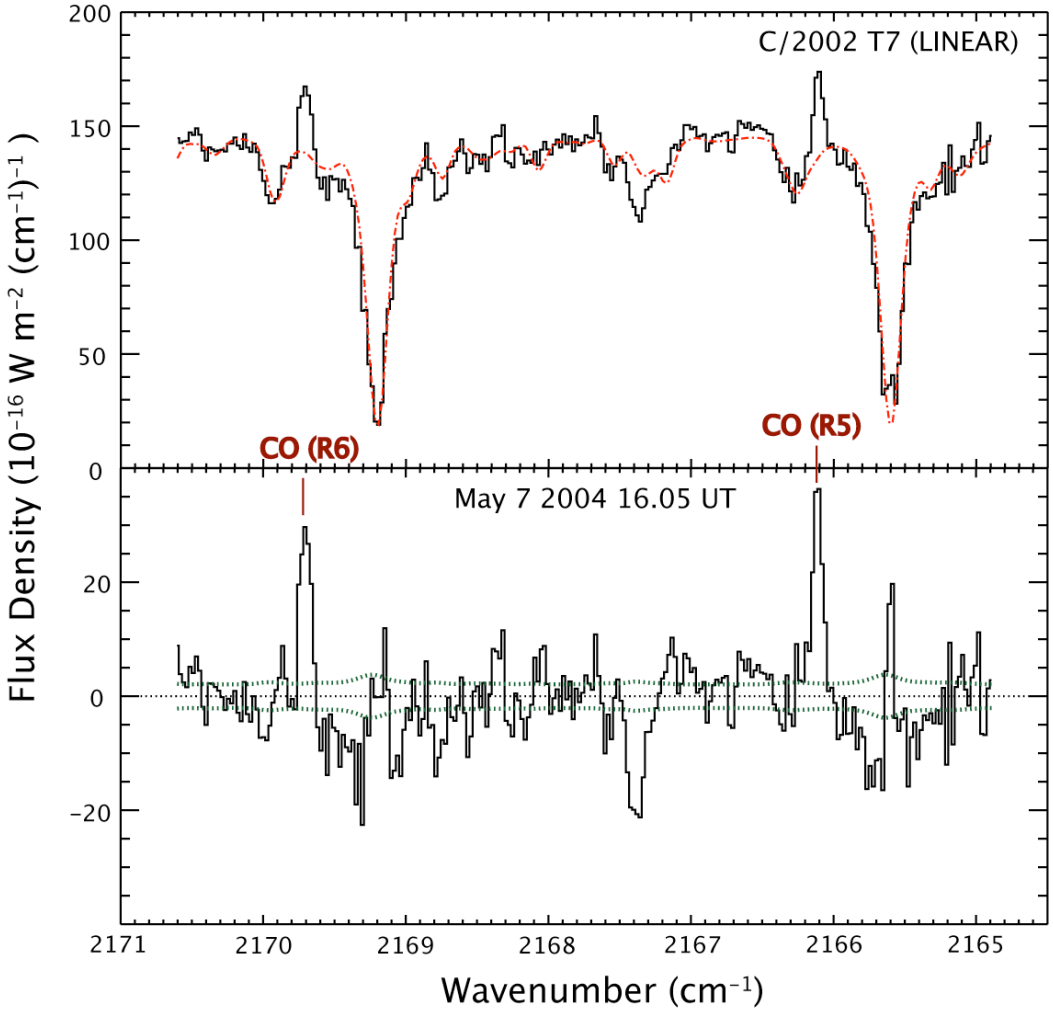

Figure 2.2 (H): Overview of May 7, 2004, CO (CO_G setting) gas emission in C/2002 T7 (LINEAR) obtained with CSHELL through the 1 arc-second slit. The spectral revolving power is $v/\Delta v$ ~25,000. All extracts are centered on the row containing the peak emission. (Top): Comet spectra (solid) and atmospheric model (dotted line). (Bottom): Residuals with line identification and noise level (dotted line).

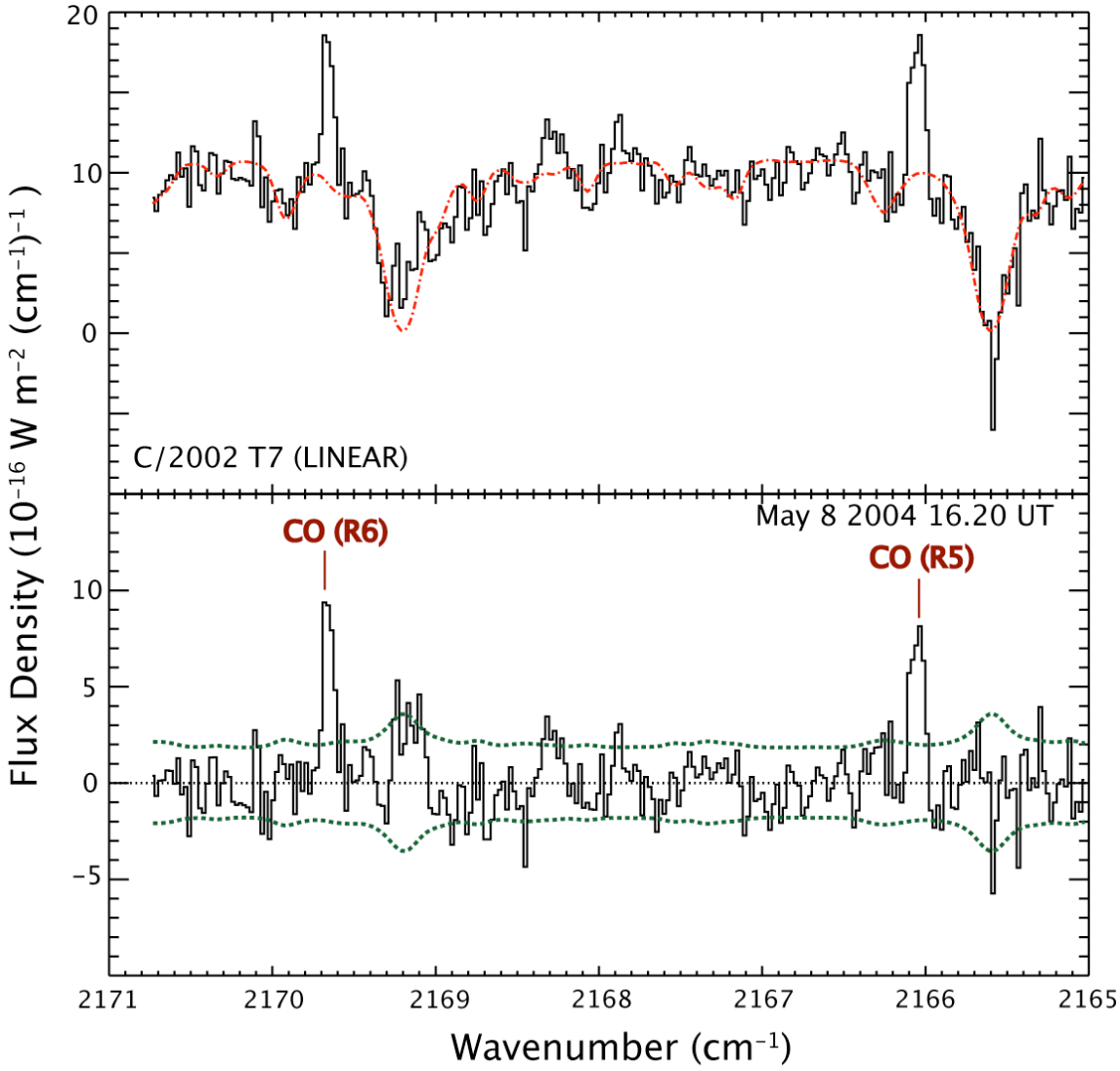

Figure 2.2 (I): Overview of May 8, 2004, CO (CO_G setting) gas emission in C/2002 T7 (LINEAR) obtained with CSHELL through the 1 arc-second slit. The spectral revolving power is $\nu/\Delta\nu$ ~25,000. All extracts are centered on the row containing the peak emission. (Top): Comet spectra (solid) and atmospheric model (dotted line). (Bottom): Residuals with line identification and noise level (dotted line).

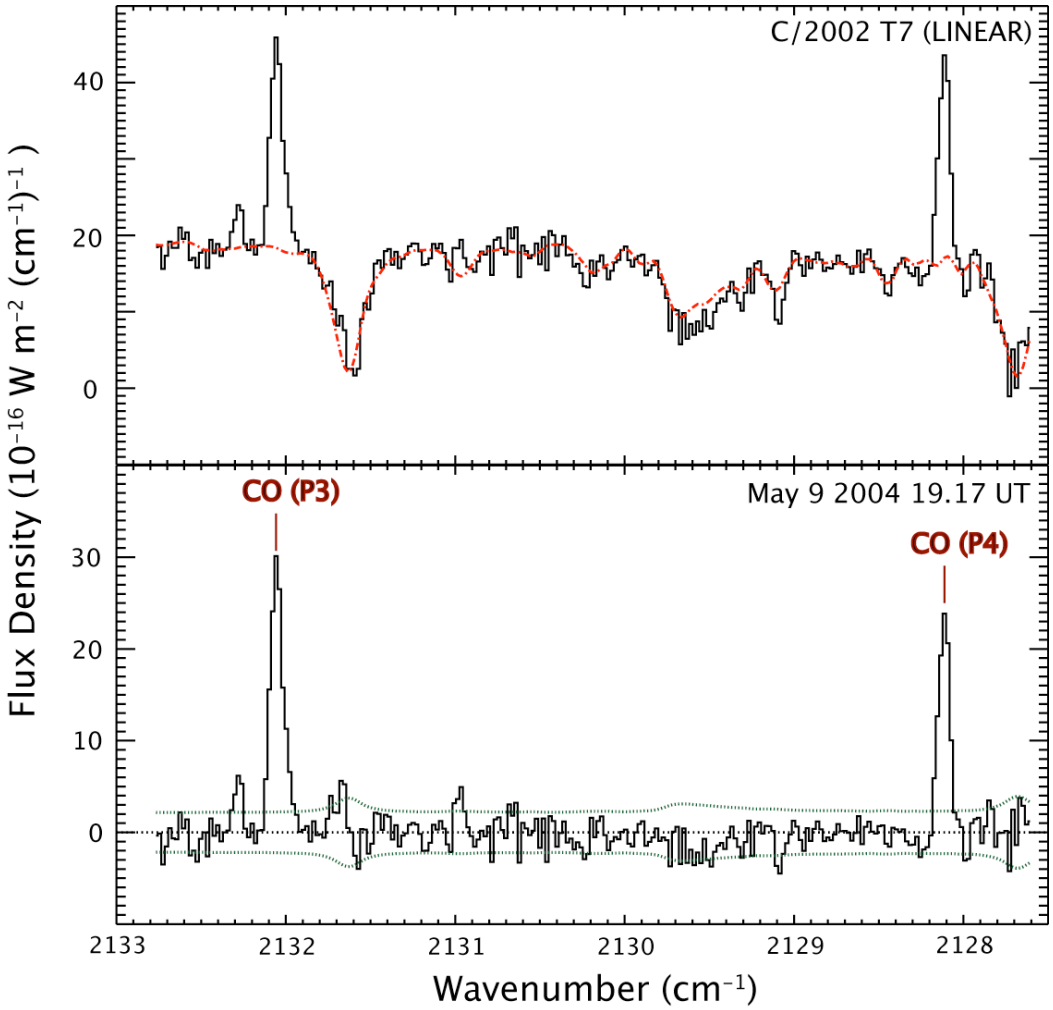

Figure 2.2 (J): Overview of May 9, 2004, CO and H_2O (CO_C setting) gas emission in C/2002 T7 (LINEAR) obtained with CSHELL through the 1 arc-second slit. The spectral revolving power is $\nu/\Delta\nu$ ~25,000. All extracts are centered on the row containing the peak emission. (Top): Comet spectra (solid) and atmospheric model (dotted line). (Bottom): Residuals with line identification and noise level (dotted line). The CO P3 line is blended with a weak H_2O line.

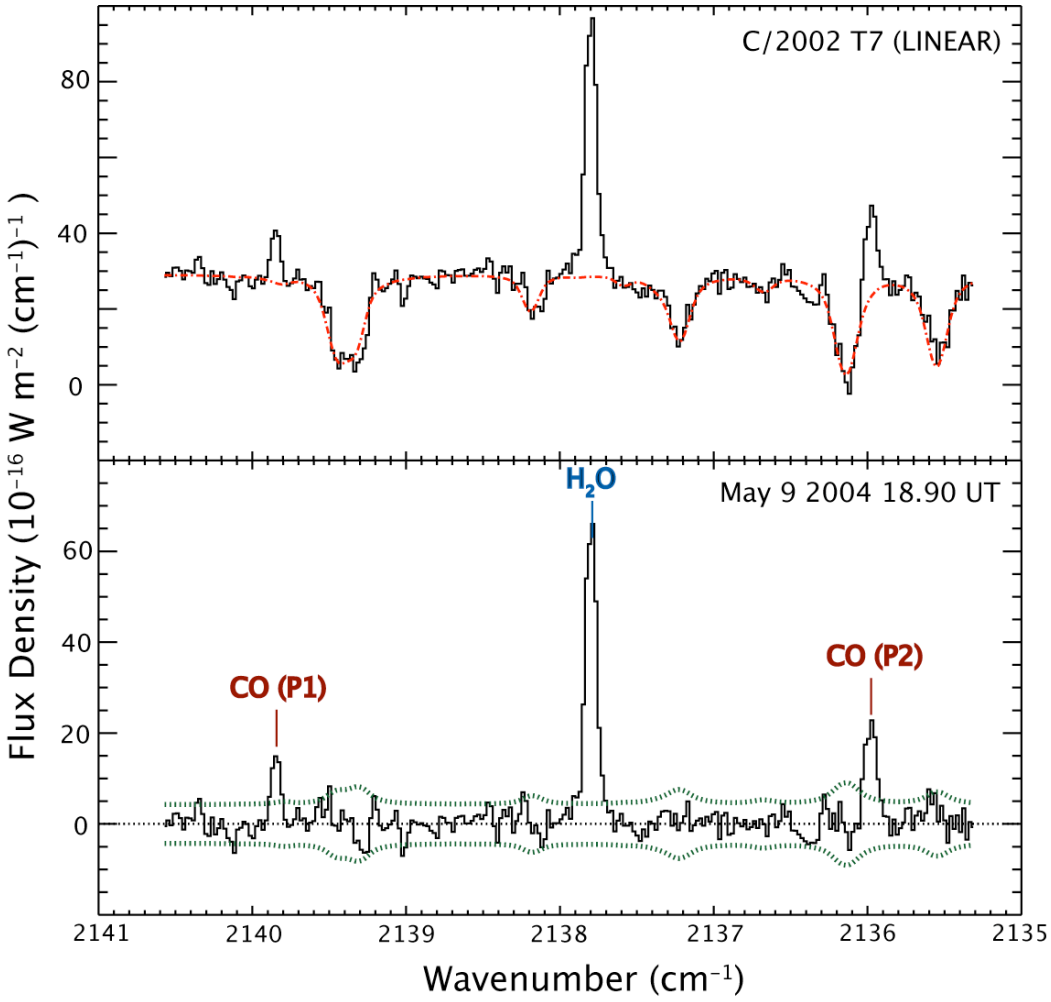

Figure 2.2 (K): Overview of May 9, 2004, CO and H_2O (CO_D setting) gas emission in C/2002 T7 (LINEAR) obtained with CSHELL through the 1 arc-second slit. The spectral revolving power is $v/\Delta v$ ~25,000. All extracts are centered on the row containing the peak emission. (Top): Comet spectra (solid) and atmospheric model (dotted line). (Bottom): Residuals with line identification and noise level (dotted line). The CO P2 line is blended with a weak H_2O line.

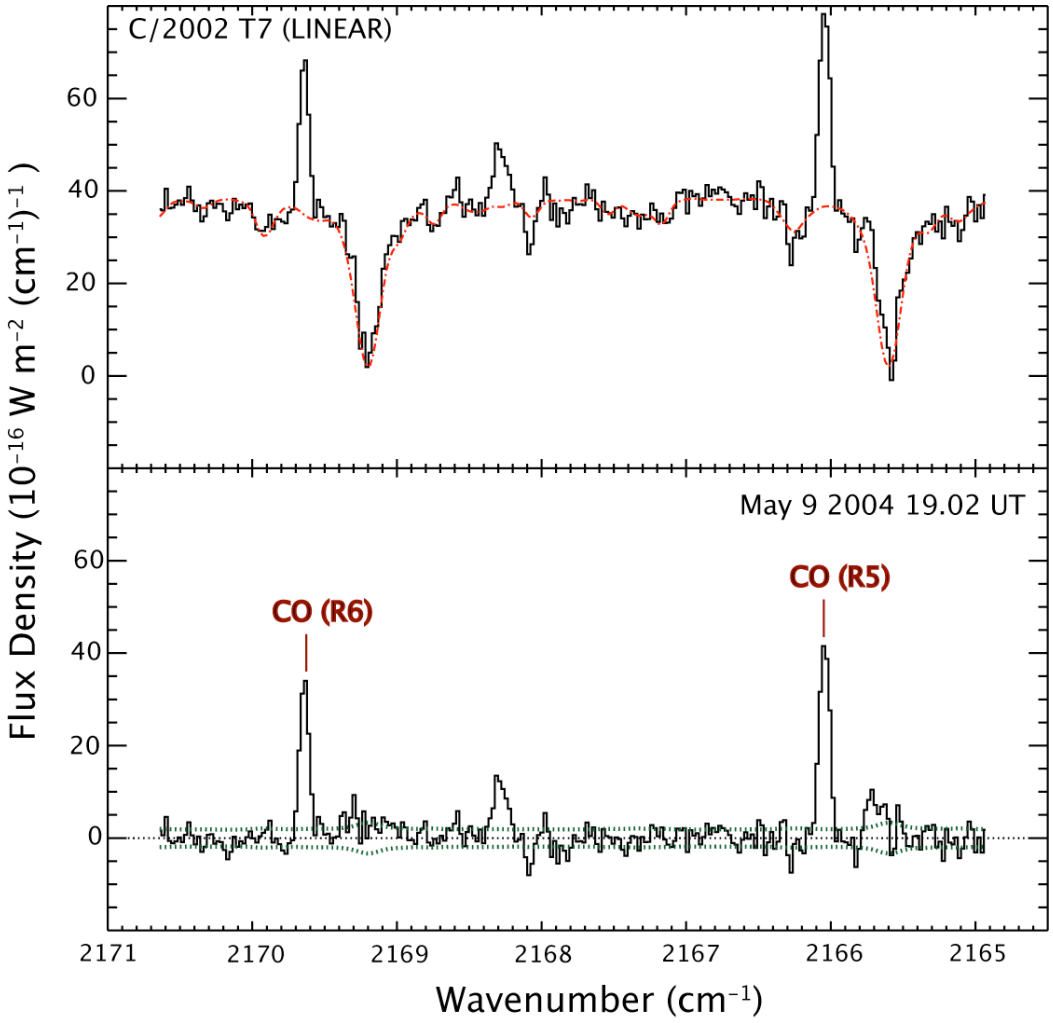

Figure 2.2 (L): Overview of May 9, 2004, CO (CO_G setting) gas emission in C/2002 T7 (LINEAR) obtained with CSHELL through the 1 arc-second slit. The spectral revolving power is $\nu/\Delta\nu$ ~25,000. All extracts are centered on the row containing the peak emission. (Top): Comet spectra (solid) and atmospheric model (dotted line). (Bottom): Residuals with line identification and noise level (dotted line).

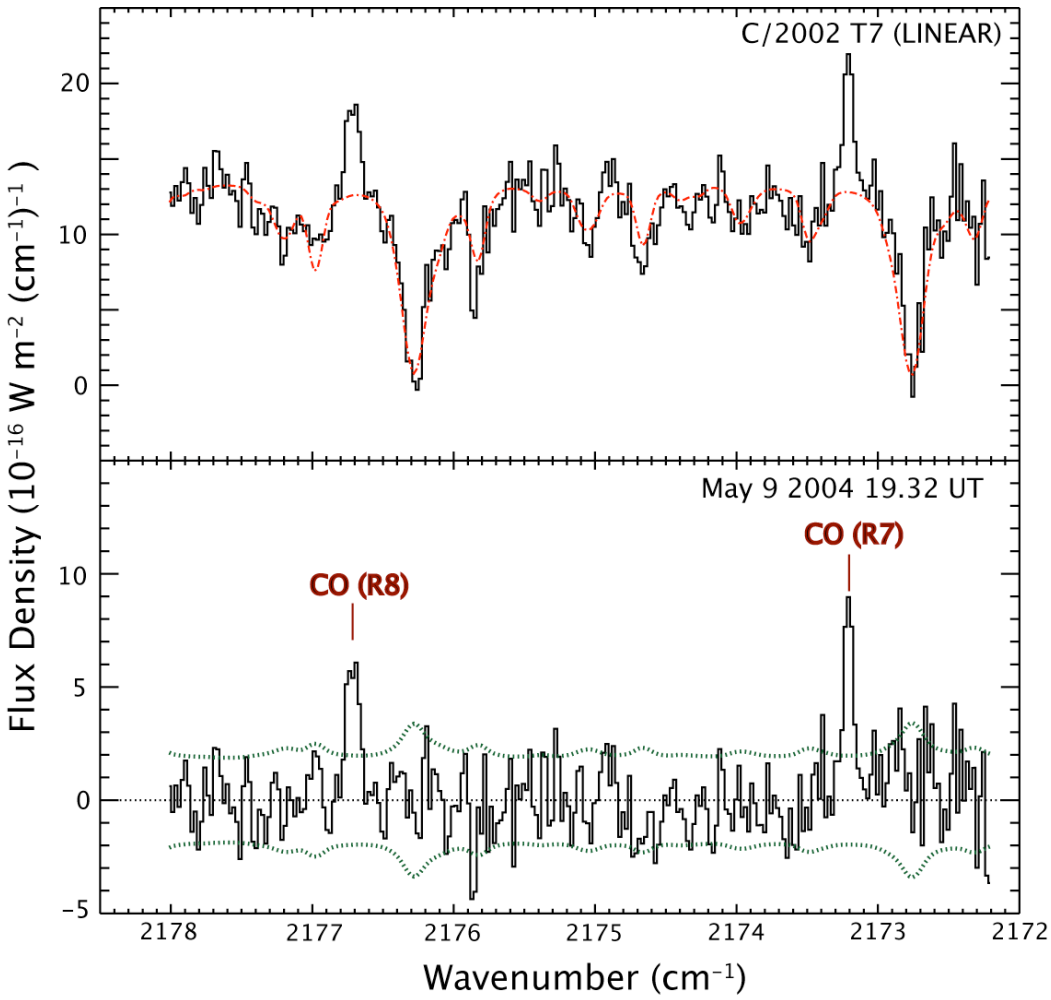

Figure 2.2 (M): Overview of May 9, 2004, CO (CO_H setting) gas emission in C/2002 T7 (LINEAR) obtained with CSHELL through the 1 arc-second slit. The spectral revolving power is $\nu/\Delta\nu$ ~25,000. All extracts are centered on the row containing the peak emission. (Top): Comet spectra (solid) and atmospheric model (dotted line). (Bottom): Residuals with line identification and noise level (dotted line).

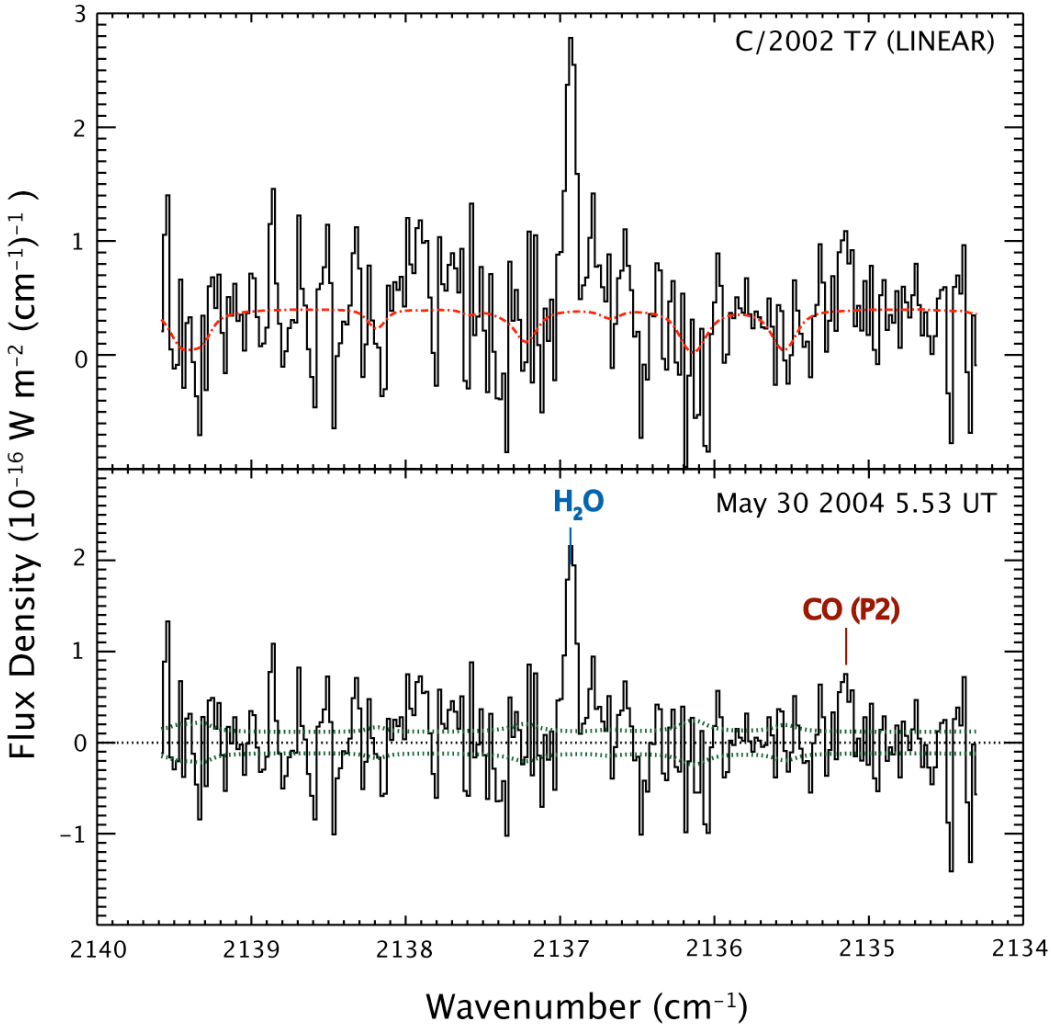

Figure 2.2 (N): Overview of May 30, 2004, CO and H_2O (CO_D setting) gas emission in C/2002 T7 (LINEAR) obtained with CSHELL through the 1 arc-second slit. The spectral revolving power is $\nu/\Delta\nu$ ~25,000. All extracts are centered on the row containing the peak emission. (Top): Comet spectra (solid) and atmospheric model (dotted line). (Bottom): Residuals with line identification and noise level (dotted line). The CO P2 line is blended with a weak H_2O line.

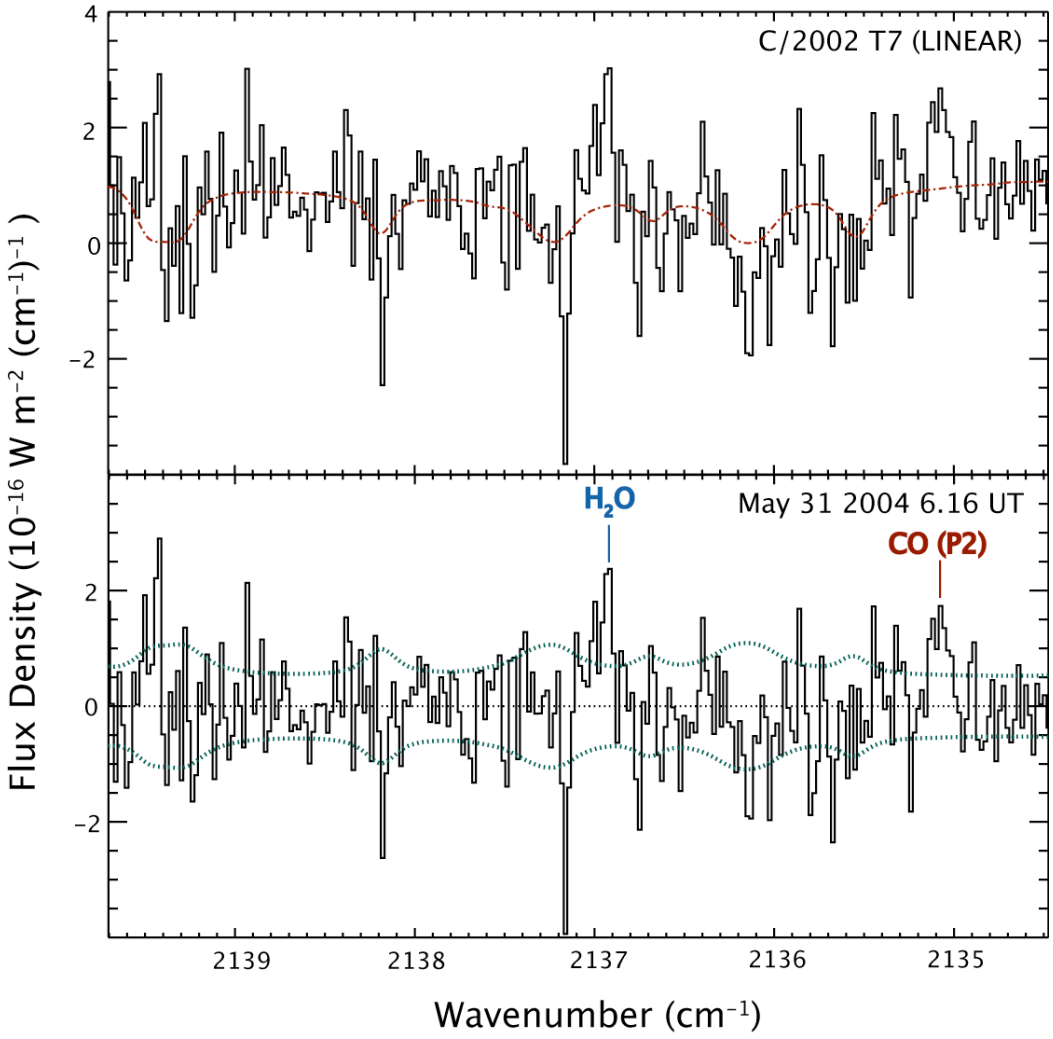

Figure 2.2 (O): Overview of May 31, 2004, CO and H_2O (CO_D setting) gas emission in C/2002 T7 (LINEAR) obtained with CSHELL through the 1 arc-second slit. The spectral revolving power is $\nu/\Delta\nu$ ~25,000. All extracts are centered on the row containing the peak emission. (Top): Comet spectra (solid) and atmospheric model (dotted line). (Bottom): Residuals with line identification and noise level (dotted line). The CO P2 line is blended with a weak H_2O line.

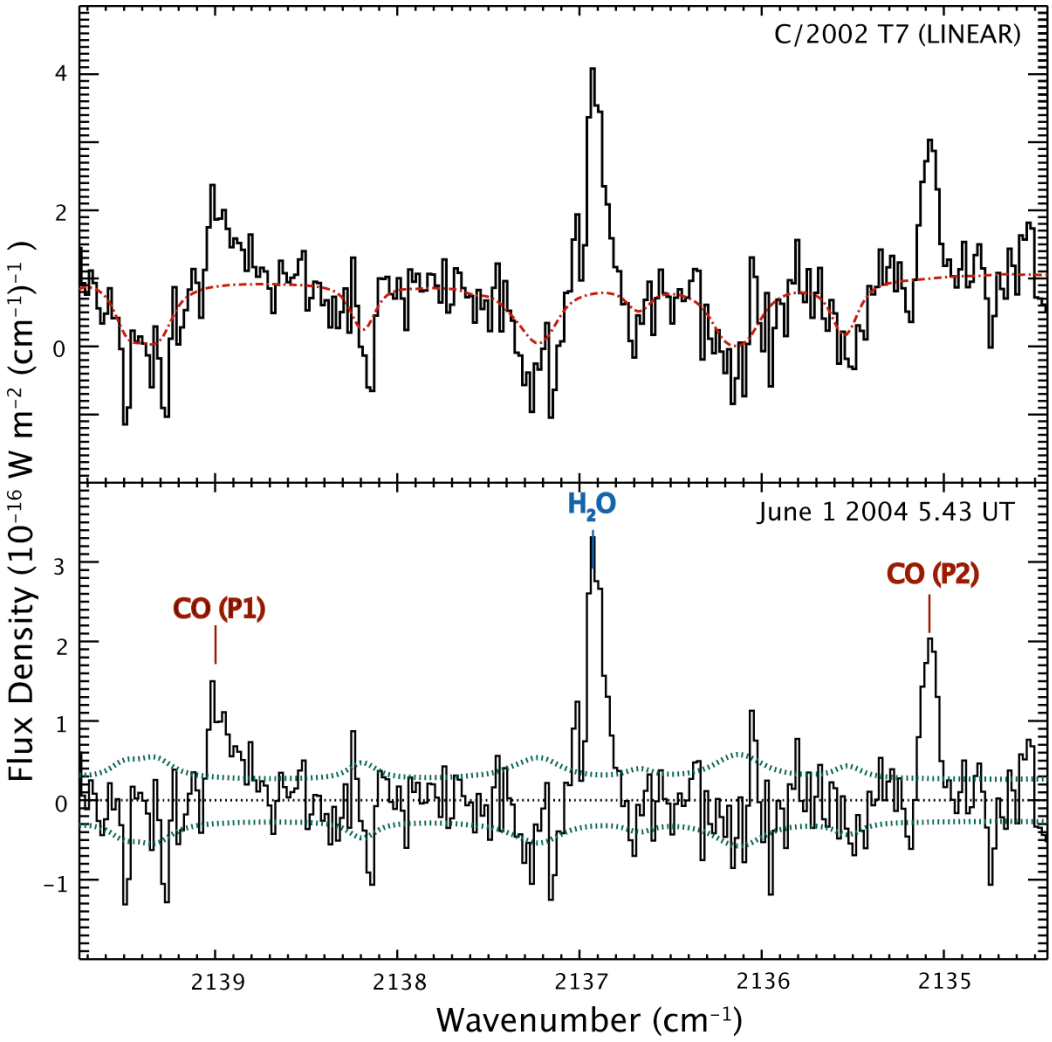

Figure 2.2 (P): Overview of June 1, 2004, CO and H_2O (CO_D setting) gas emission in C/2002 T7 (LINEAR) obtained with CSHELL through the 1 arc-second slit. The spectral revolving power is $\nu/\Delta\nu$ ~25,000. All extracts are centered on the row containing the peak emission. (Top): Comet spectra (solid) and atmospheric model (dotted line). (Bottom): Residuals with line identification and noise level (dotted line). The CO P2 line is blended with a weak H_2O line.

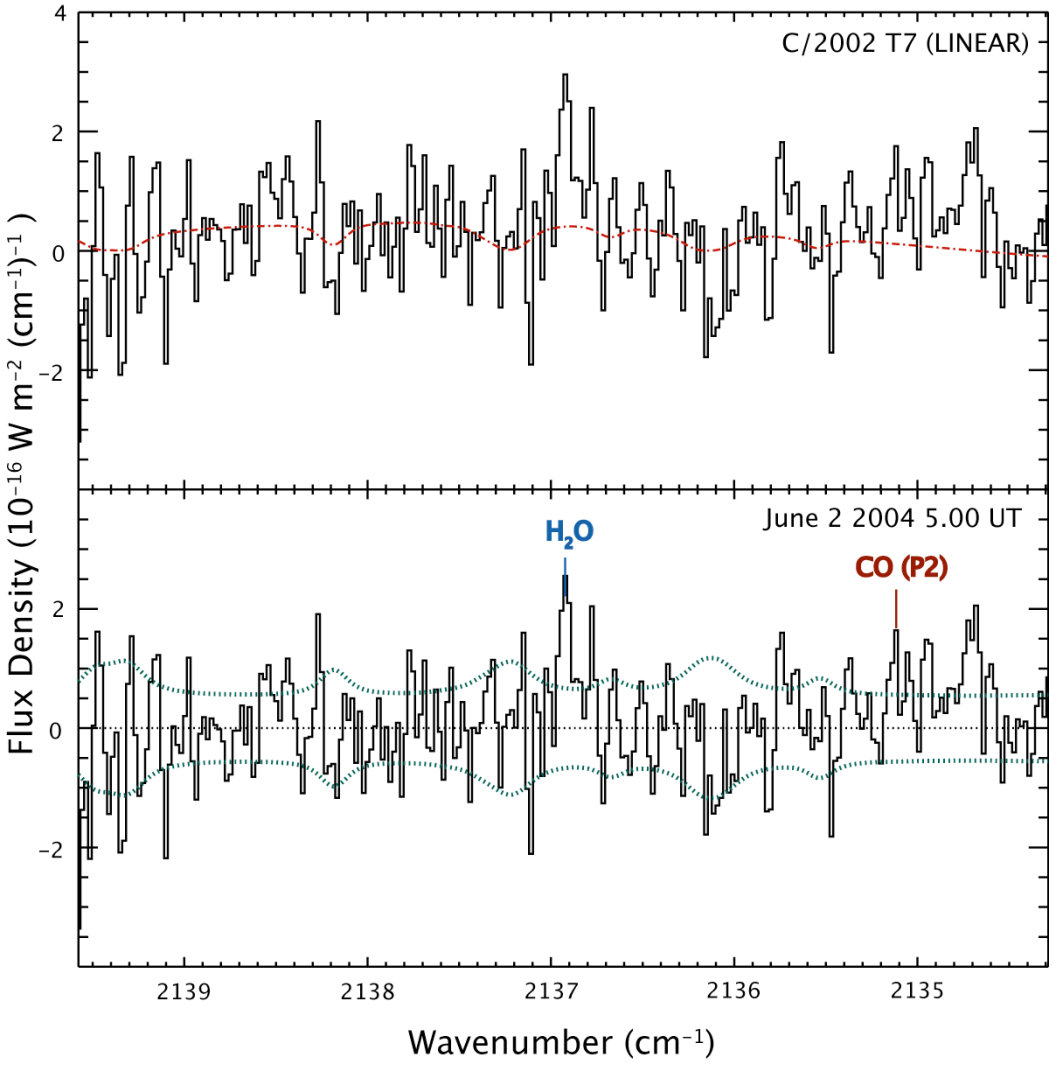

Figure 2.2 (Q): Overview of June 2, 2004, CO and H_2O (CO_D setting) gas emission in C/2002 T7 (LINEAR) obtained with CSHELL through the 1 arc-second slit. The spectral revolving power is $\nu/\Delta\nu$ ~25,000. All extracts are centered on the row containing the peak emission. (Top): Comet spectra (solid) and atmospheric model (dotted line). (Bottom): Residuals with line identification and noise level (dotted line). The CO P2 line is blended with a weak H_2O line.

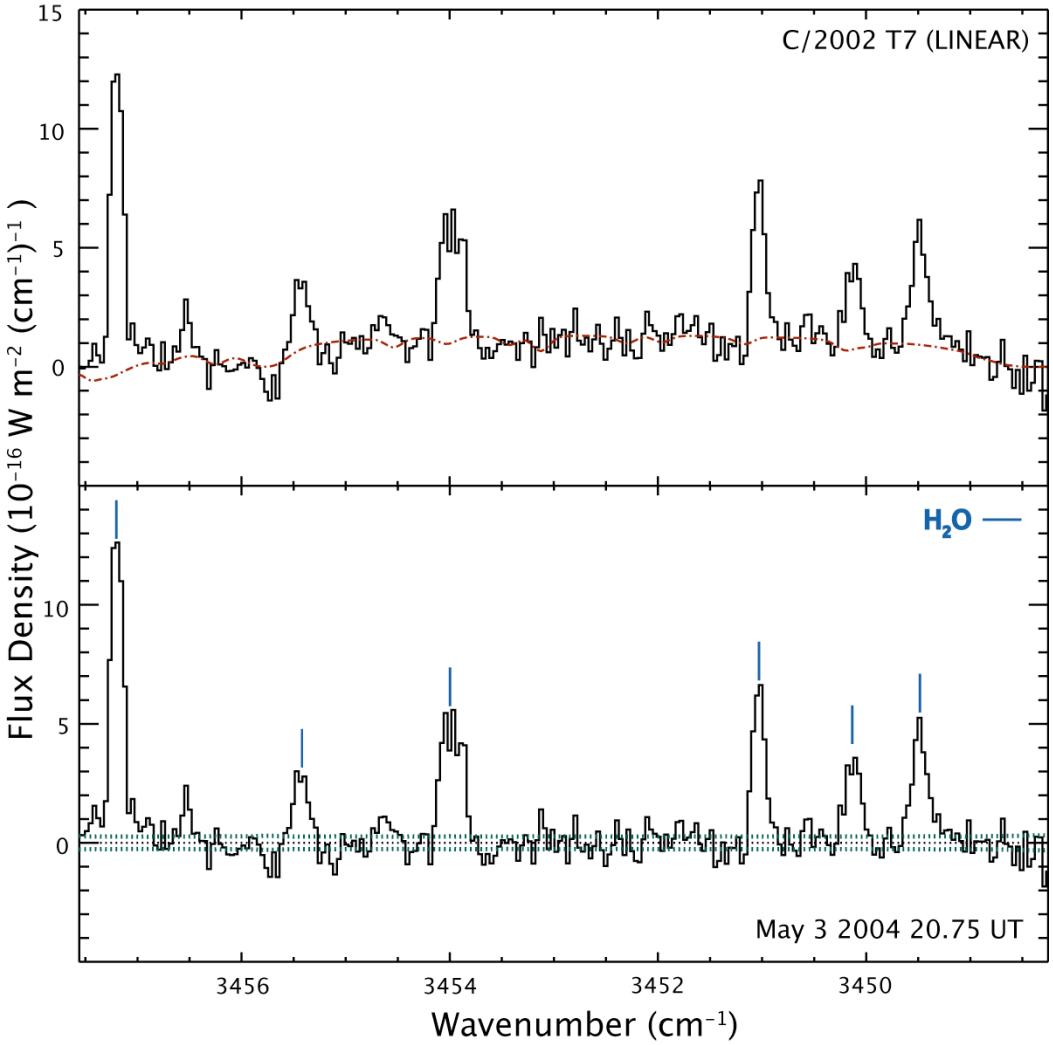

Figure 2.3 (A): Overview of May 3, 2004, 2.9 μm H_2O emission of C/2002 T7 (LINEAR) obtained with CSHELL through the 1 arc-second slit. The spectral revolving power is v/Δv ~25,000. All extracts are centered on the row containing the peak emission. (Top): Comet spectra (solid) and atmospheric model (dotted line). (Bottom): Residuals with line identification and noise level (dotted line).

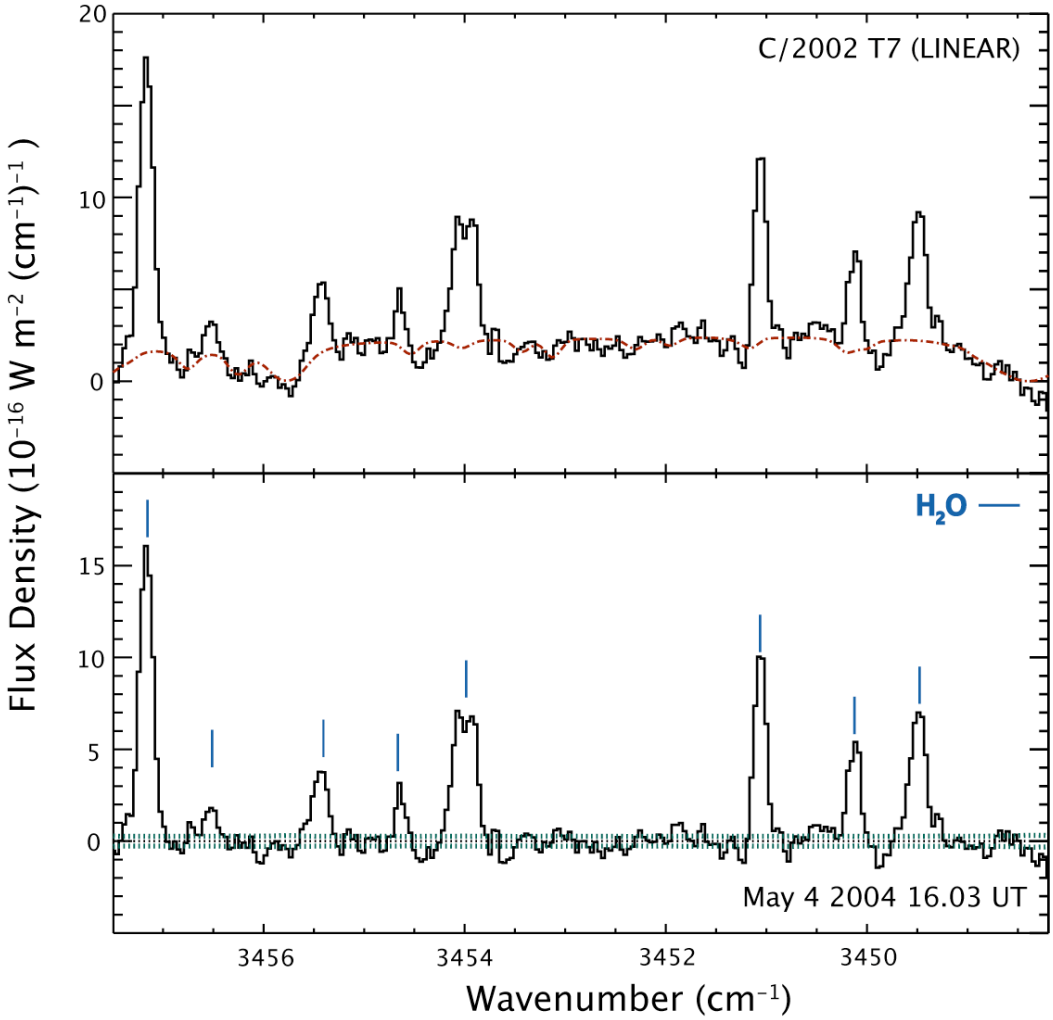

Figure 2.3 (B): Overview of May 4, 2004, 2.9 μm H_2O emission of C/2002 T7 (LINEAR) obtained with CSHELL through the 1 arc-second slit. The spectral revolving power is v/Δv ~25,000. All extracts are centered on the row containing the peak emission.
(Top): Comet spectra (solid) and atmospheric model (dotted line).
(Bottom): Residuals with line identification and noise level (dotted line).

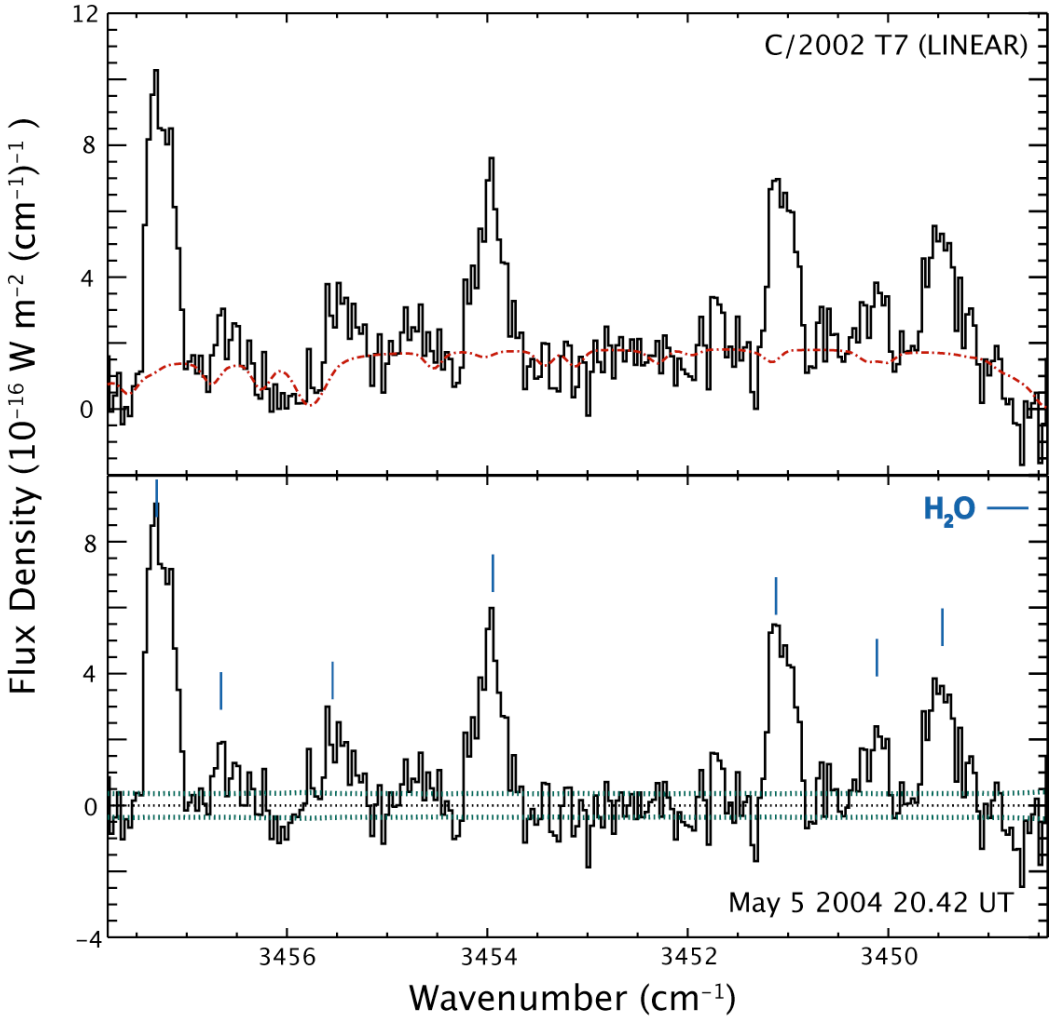

Figure 2.3 (C): Overview of May 5, 2004, 2.9 μm H_2O emission of C/2002 T7 (LINEAR) obtained with CSHELL through the 1 arc-second slit. The spectral revolving power is v/Δv ~25,000. All extracts are centered on the row containing the peak emission.
(Top): Comet spectra (solid) and atmospheric model (dotted line).
(Bottom): Residuals with line identification and noise level (dotted line).

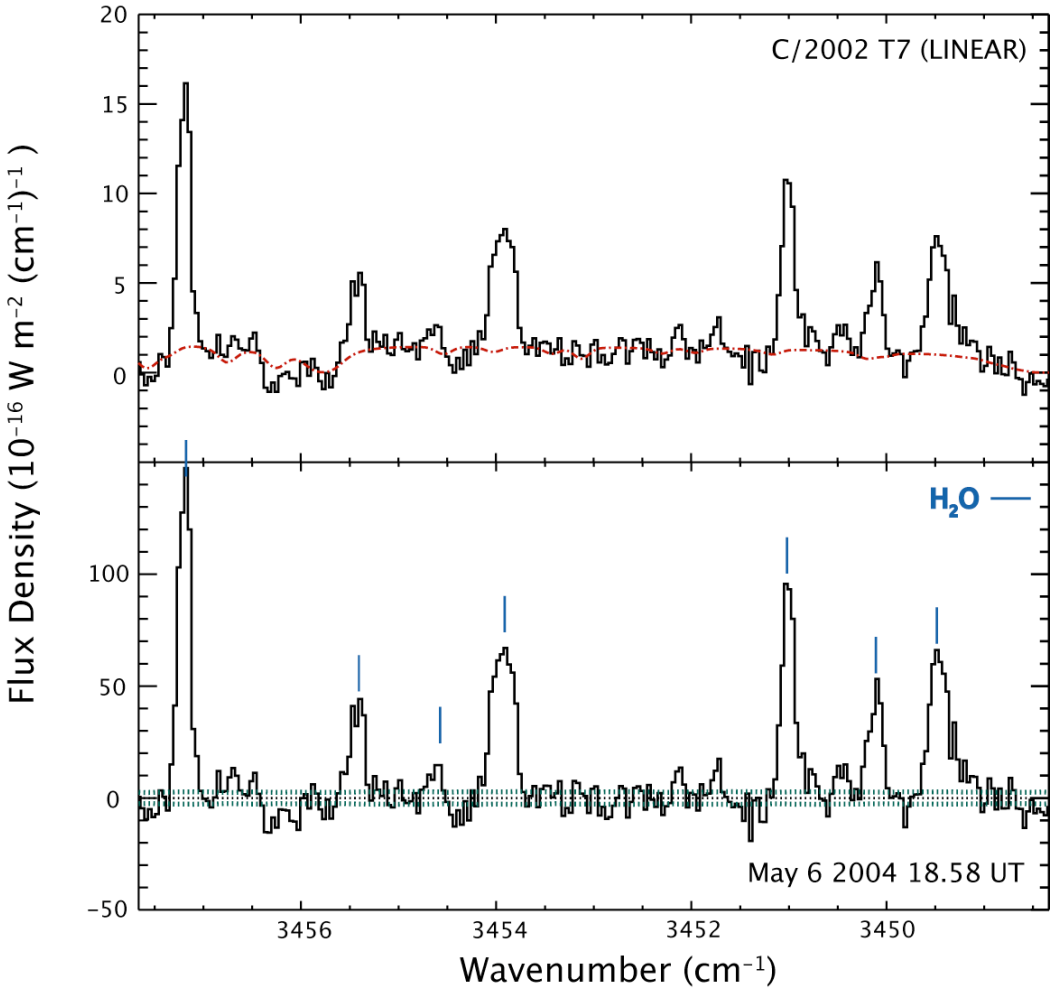

Figure 2.3 (D): Overview of May 6, 2004, 2.9 μm H_2O emission of C/2002 T7 (LINEAR) obtained with CSHELL through the 1 arc-second slit. The spectral revolving power is v/Δv ~25,000. All extracts are centered on the row containing the peak emission. (Top): Comet spectra (solid) and atmospheric model (dotted line). (Bottom): Residuals with line identification and noise level (dotted line).

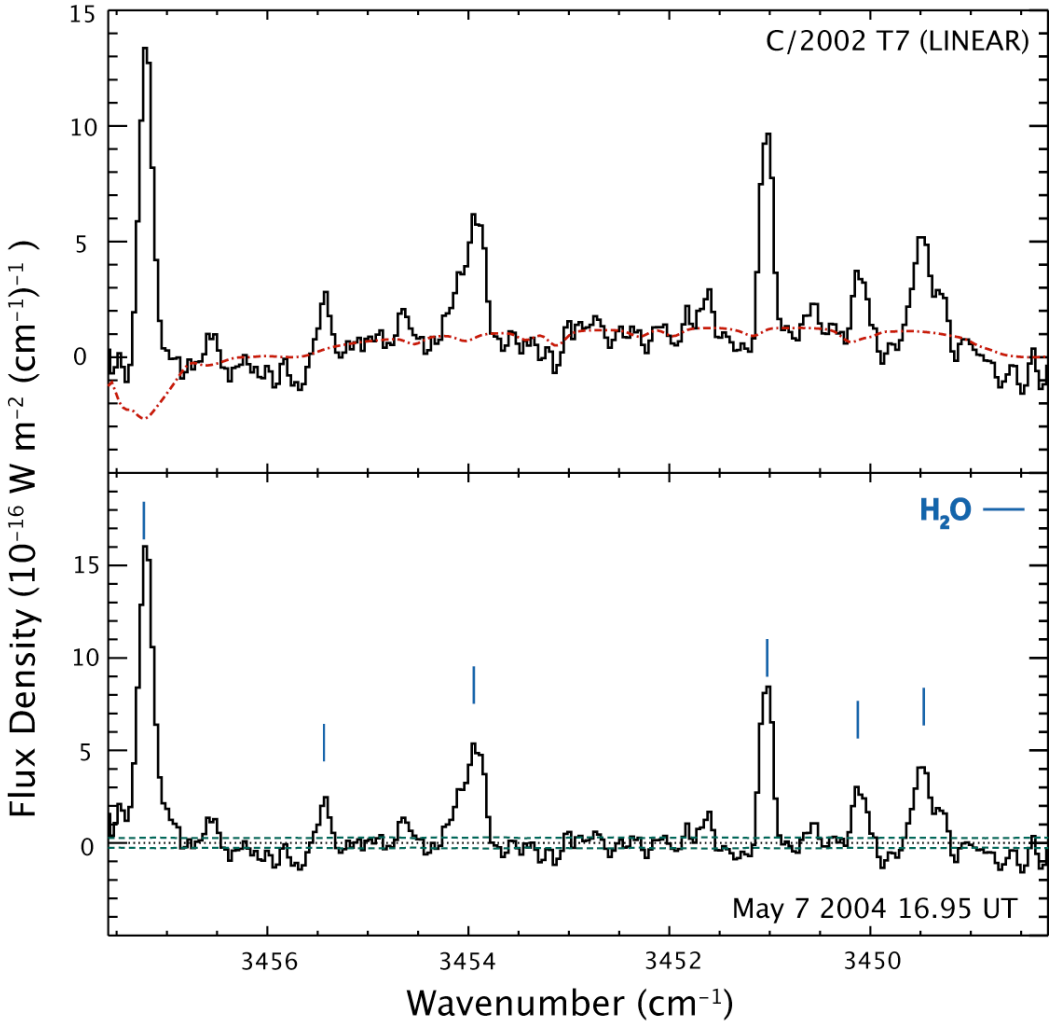

Figure 2.3 (E): Overview of May 7, 2004, 2.9 μm H_2O emission of C/2002 T7 (LINEAR) obtained with CSHELL through the 1 arc-second slit. The spectral revolving power is v/Δv ~25,000. All extracts are centered on the row containing the peak emission.
(Top): Comet spectra (solid) and atmospheric model (dotted line).
(Bottom): Residuals with line identification and noise level (dotted line).

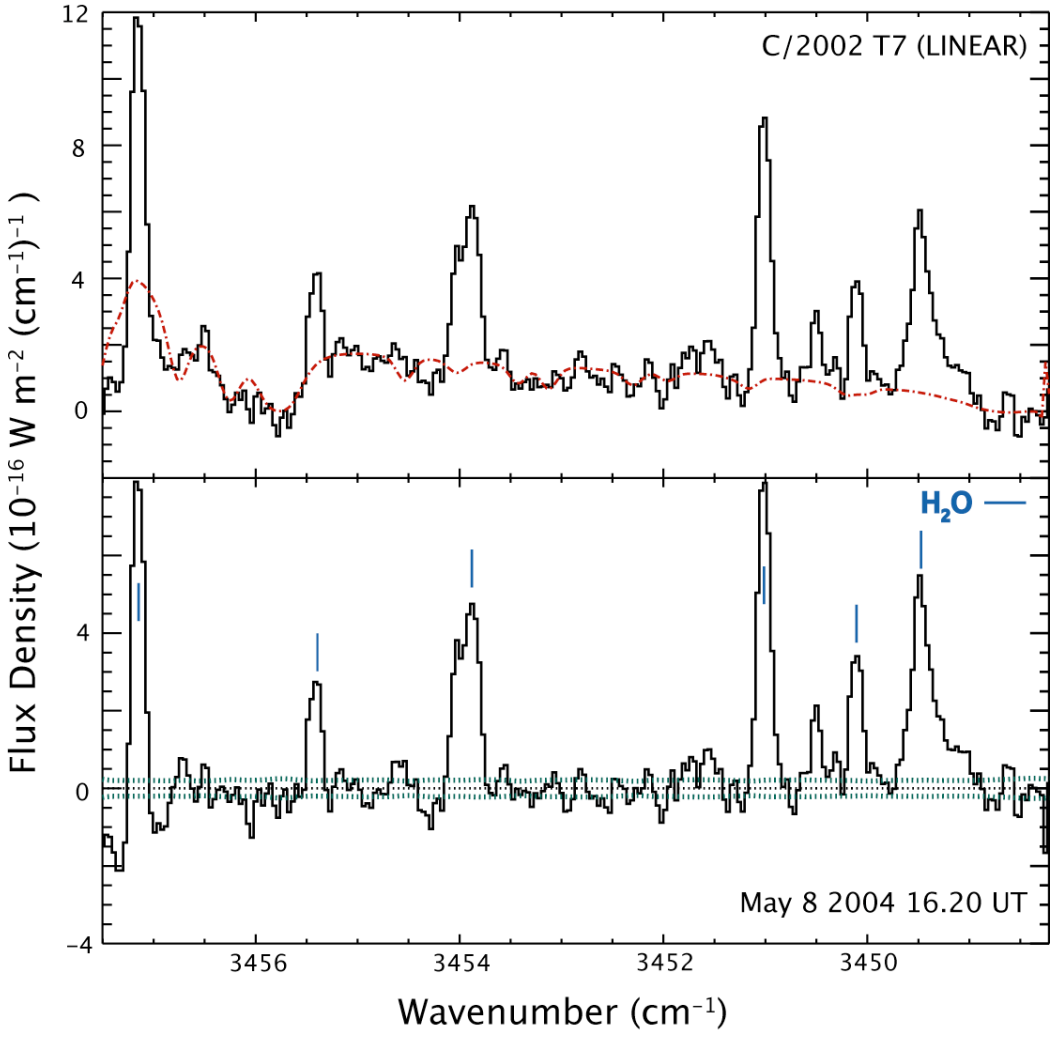

Figure 2.3 (F): Overview of May 8, 2004, 2.9 μm H_2O emission of C/2002 T7 (LINEAR) obtained with CSHELL through the 1 arc-second slit. The spectral revolving power is v/Δv ~25,000. All extracts are centered on the row containing the peak emission.
(Top): Comet spectra (solid) and atmospheric model (dotted line).
(Bottom): Residuals with line identification and noise level (dotted line).

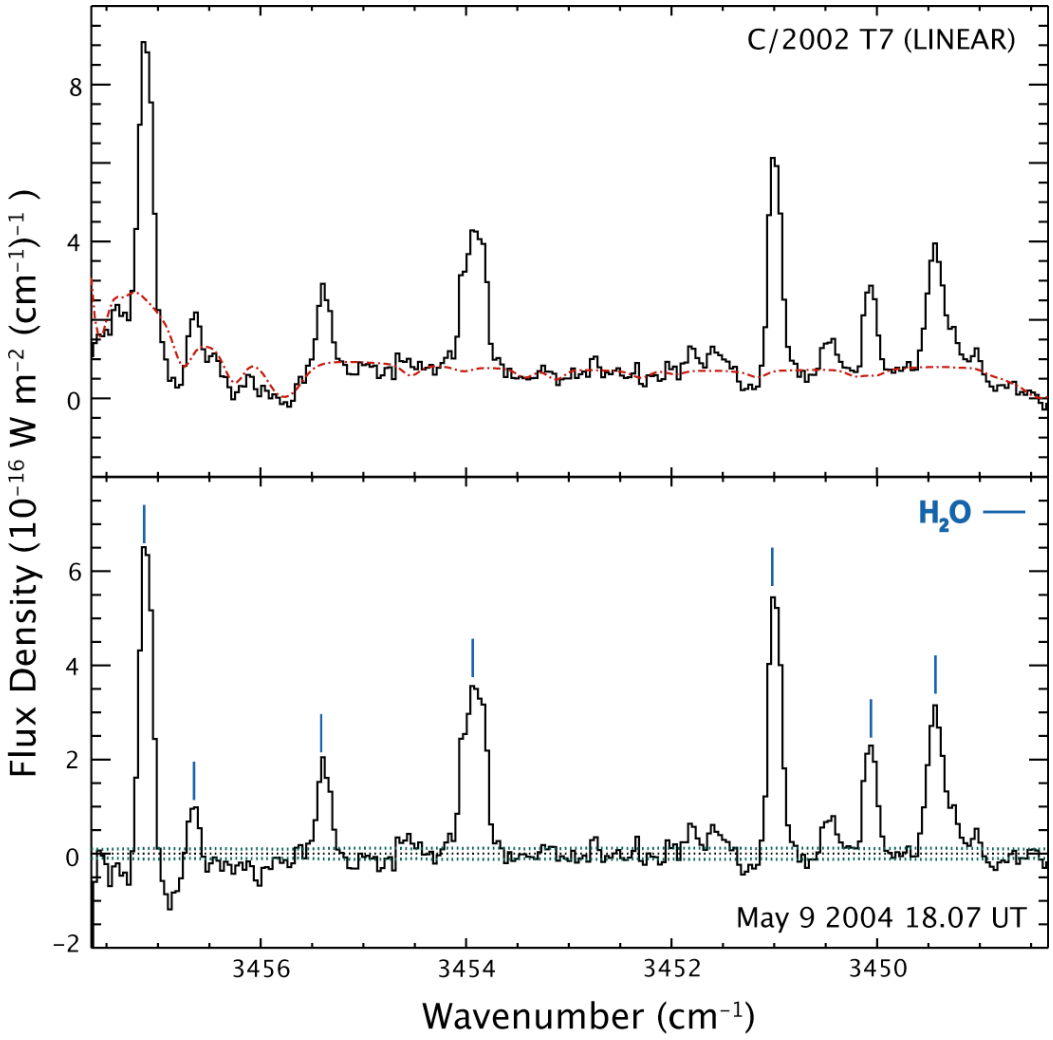

Figure 2.3 (G): Overview of May 9, 2004, 2.9 μm H_2O emission of C/2002 T7 (LINEAR) obtained with CSHELL through the 1 arc-second slit. The spectral revolving power is $\nu/\Delta\nu$ ~25,000. All extracts are centered on the row containing the peak emission. (Top): Comet spectra (solid) and atmospheric model (dotted line). (Bottom): Residuals with line identification and noise level (dotted line).

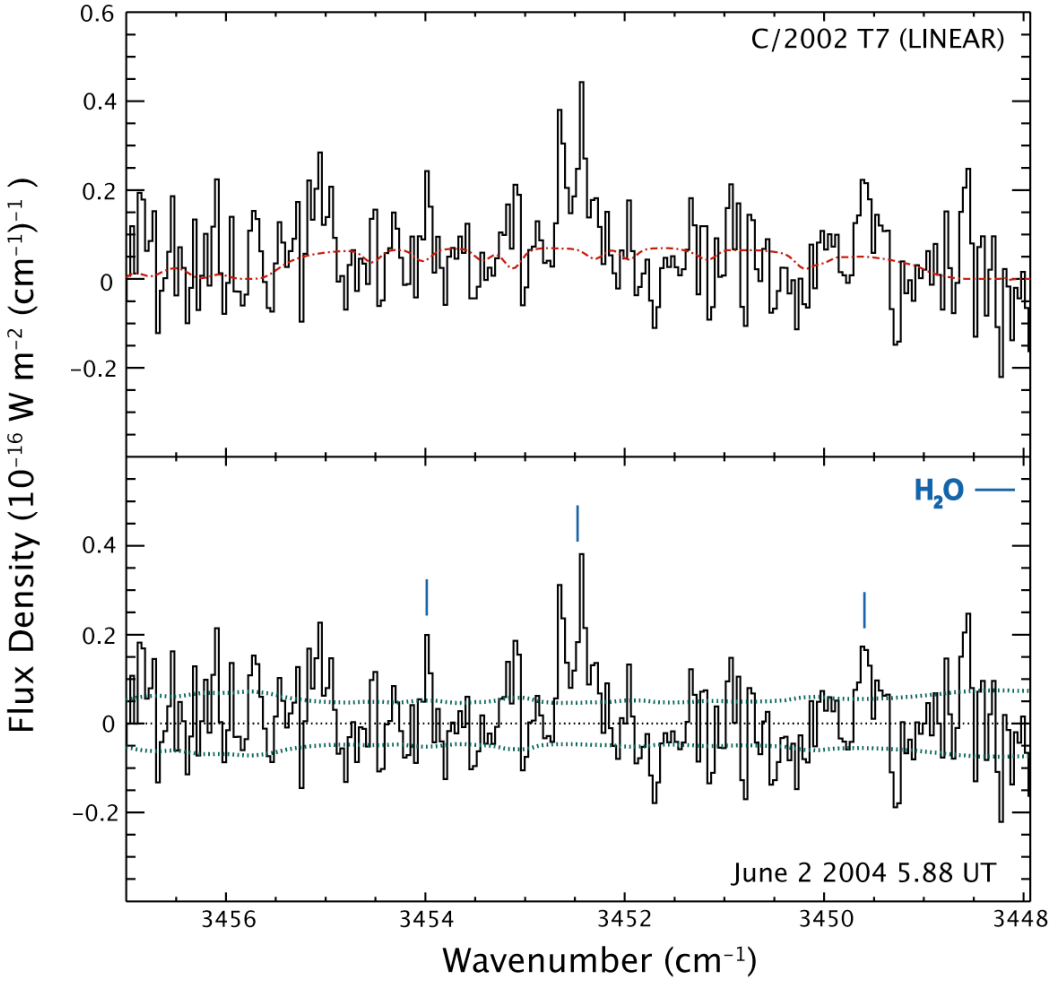

Figure 2.3 (H): Overview of June 2, 2004, 2.9 μm H_2O emission of C/2002 T7 (LINEAR) obtained with CSHELL through the 1 arc-second slit. The spectral revolving power is v/Δv ~25,000. All extracts are centered on the row containing the peak emission. (Top): Comet spectra (solid) and atmospheric model (dotted line). (Bottom): Residuals with line identification and noise level (dotted line).

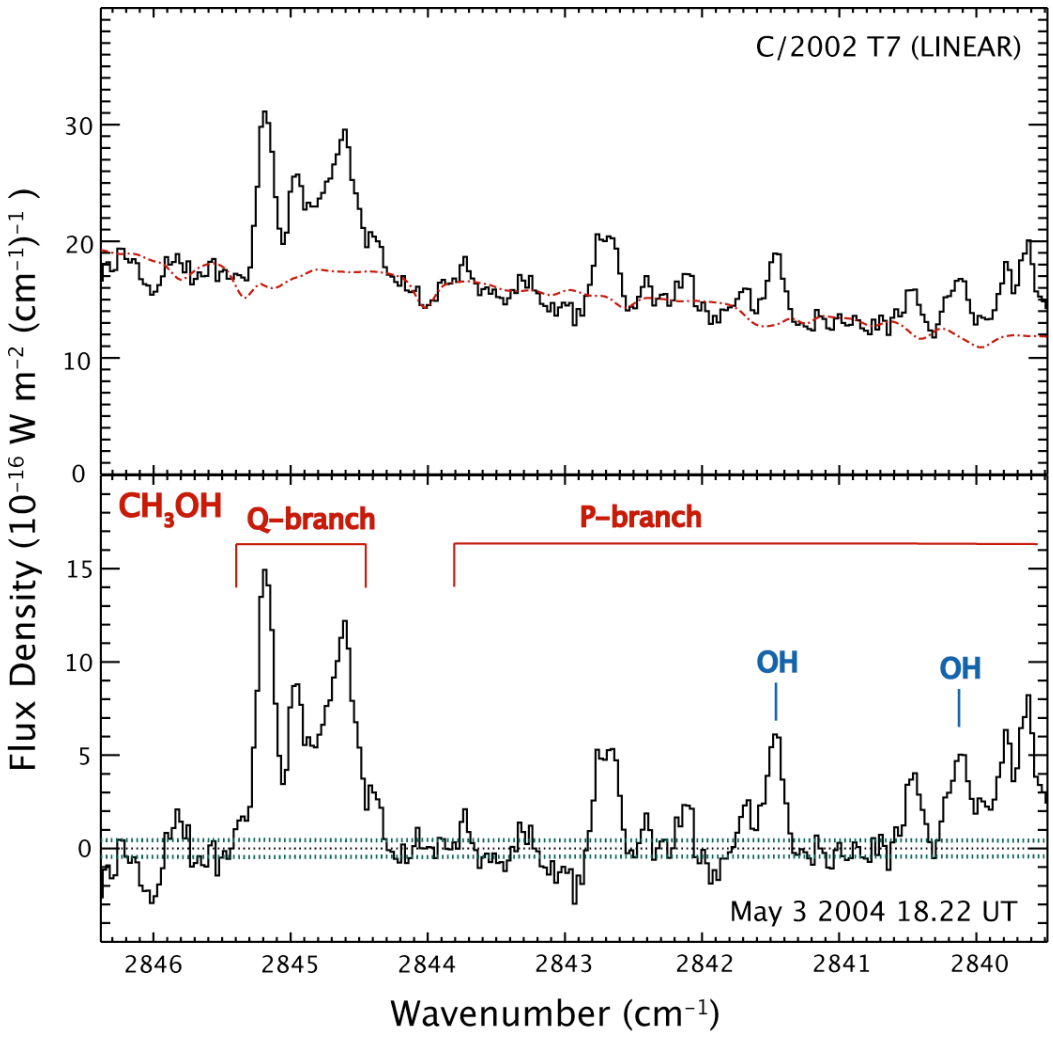

Figure 2.4 (A): Overview of May 3, 2004, CH_3OH Q and P branch gas emission in C/2002 T7 (LINEAR) obtained with CSHELL through the 1 arc-second slit. The spectral revolving power is $\nu/\Delta\nu$ ~25,000. All extracts are centered on the row containing the peak emission. (Top): Comet spectra (solid) and atmospheric model (dotted line). (Bottom): Residuals with line identification and noise level (dotted line).

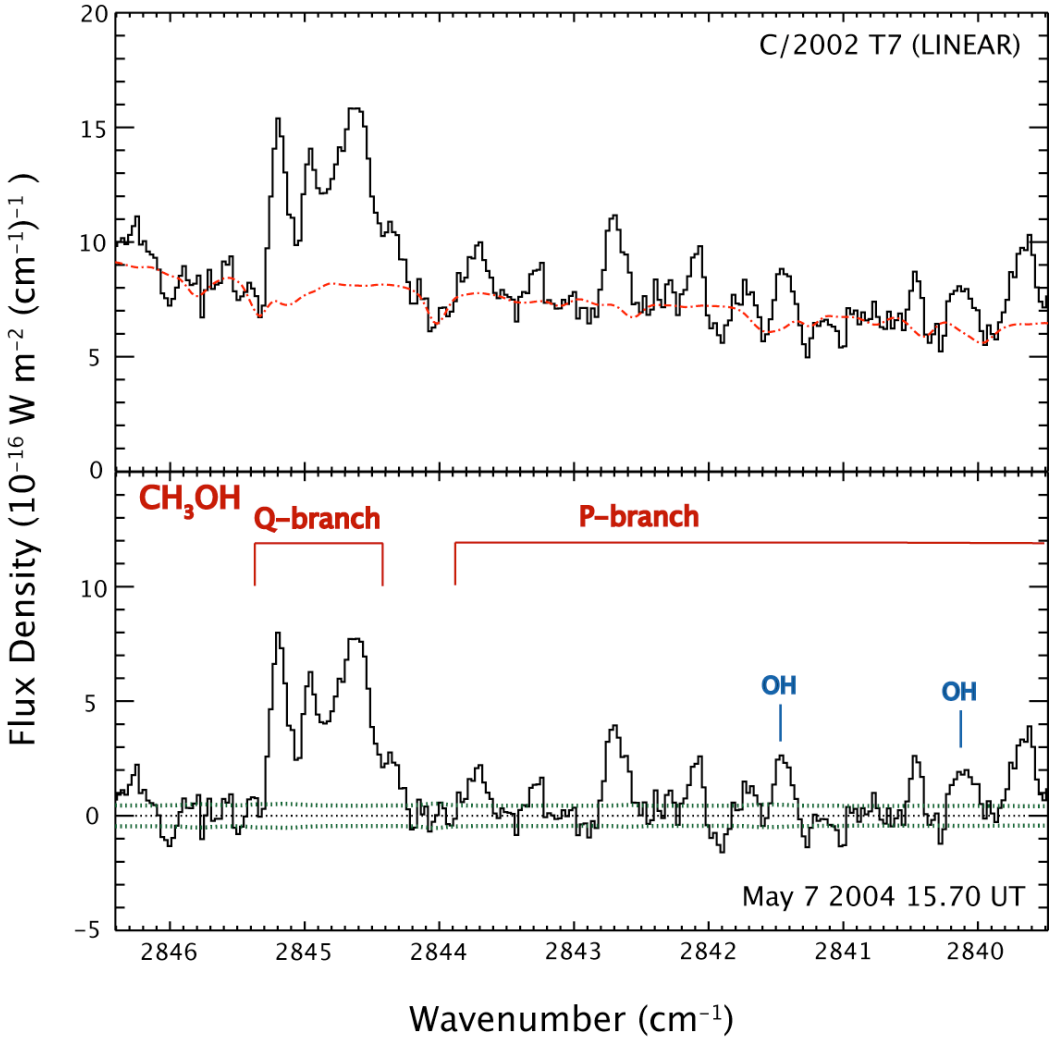

Figure 2.4 (B): Overview of May 7, 2004, CH_3OH Q and P branch gas emission in C/2002 T7 (LINEAR) obtained with CSHELL through the 1 arc-second slit. The spectral revolving power is $\nu/\Delta\nu$ ~25,000. All extracts are centered on the row containing the peak emission. (Top): Comet spectra (solid) and atmospheric model (dotted line). (Bottom): Residuals with line identification and noise level (dotted line).

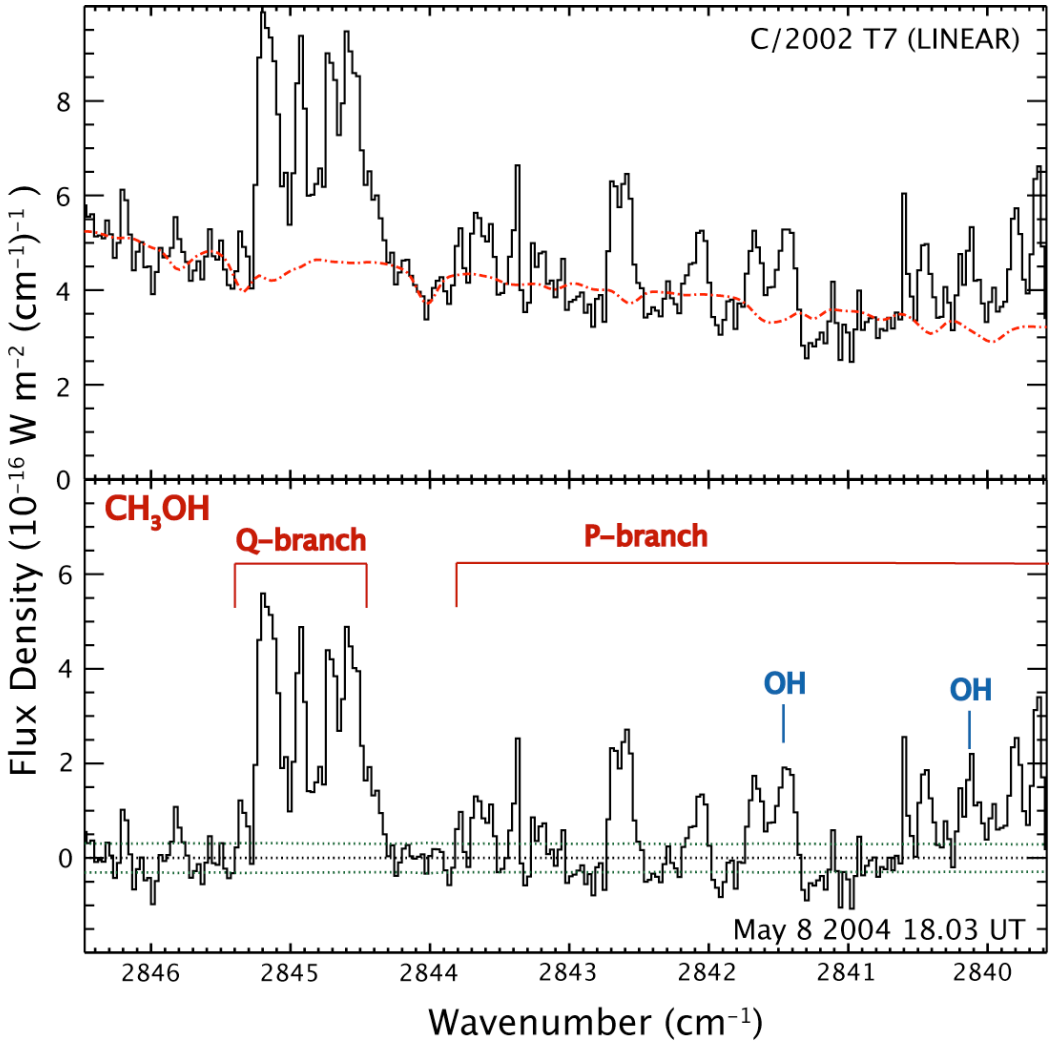

Figure 2.4 (C): Overview of May 8, 2004, CH_3OH Q and P branch gas emission in C/2002 T7 (LINEAR) obtained with CSHELL through the 1 arc-second slit. The spectral revolving power is $v/\Delta v$ ~25,000. All extracts are centered on the row containing the peak emission. (Top): Comet spectra (solid) and atmospheric model (dotted line). (Bottom): Residuals with line identification and noise level (dotted line).

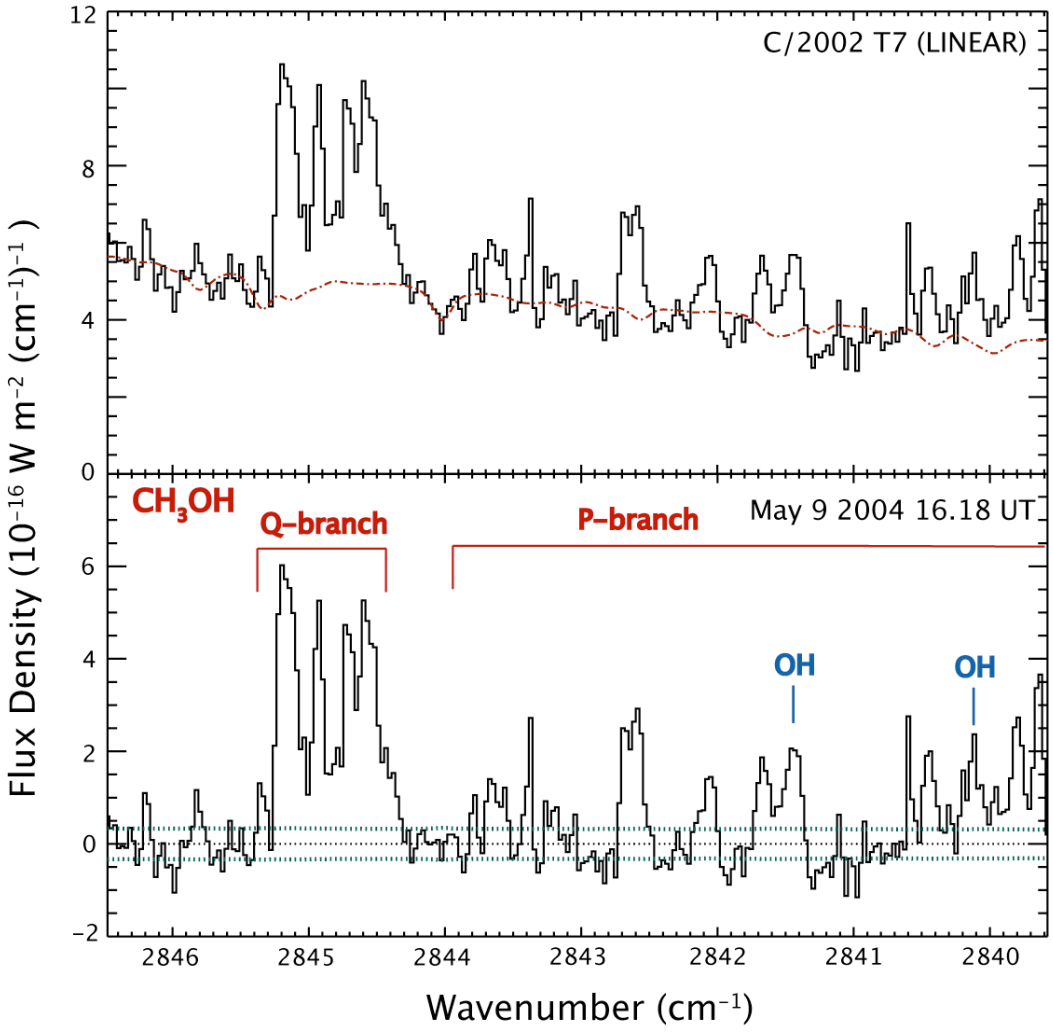

Figure 2.4 (D): Overview of May 9, 2004, CH_3OH Q and P branch gas emission in C/2002 T7 (LINEAR) obtained with CSHELL through the 1 arc-second slit. The spectral revolving power is $\nu/\Delta\nu$ ~25,000. All extracts are centered on the row containing the peak emission. (Top): Comet spectra (solid) and atmospheric model (dotted line). (Bottom): Residuals with line identification and noise level (dotted line).

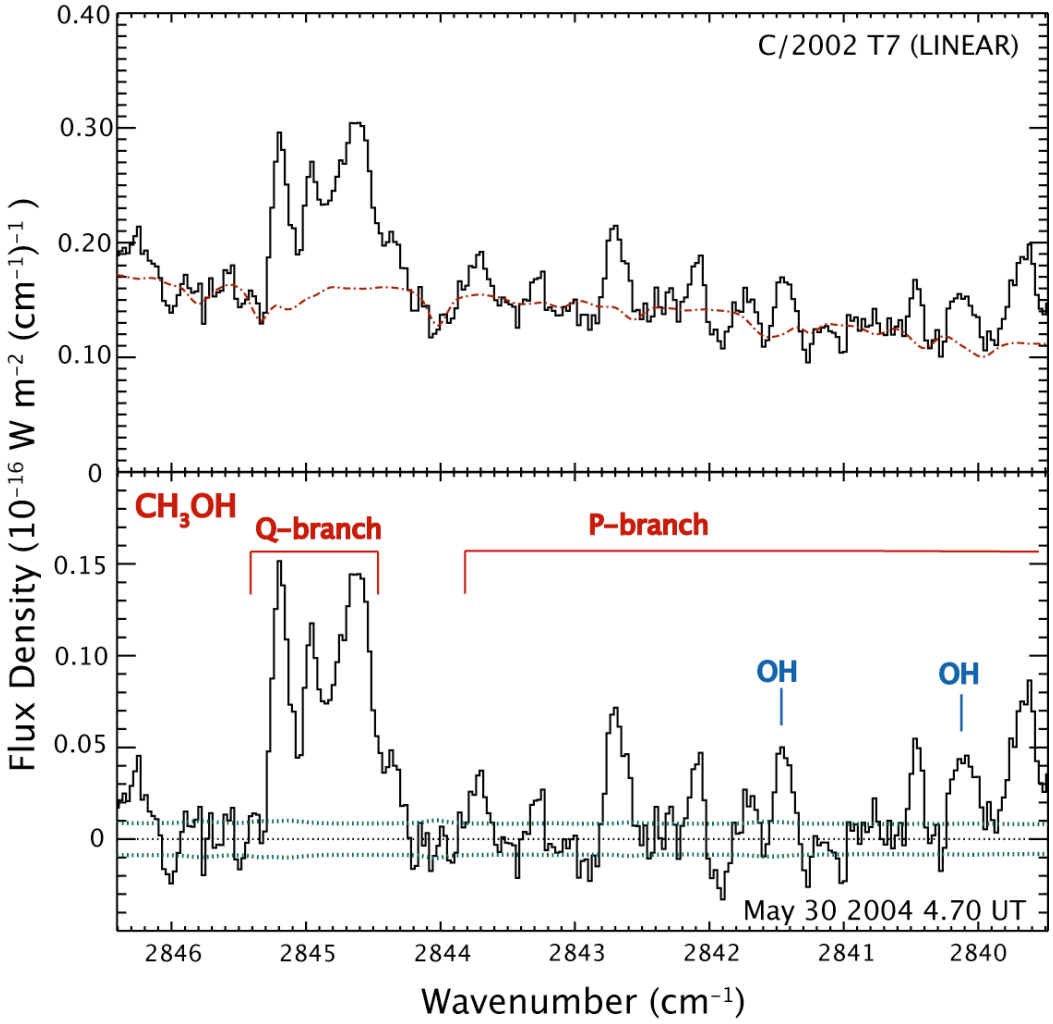

Figure 2.4 (E): Overview of May 30, 2004, CH_3OH Q and P branch gas emission in C/2002 T7 (LINEAR) obtained with CSHELL through the 1 arc-second slit. The spectral revolving power is $\nu/\Delta\nu$ ~25,000. All extracts are centered on the row containing the peak emission. (Top): Comet spectra (solid) and atmospheric model (dotted line). (Bottom): Residuals with line identification and noise level (dotted line).

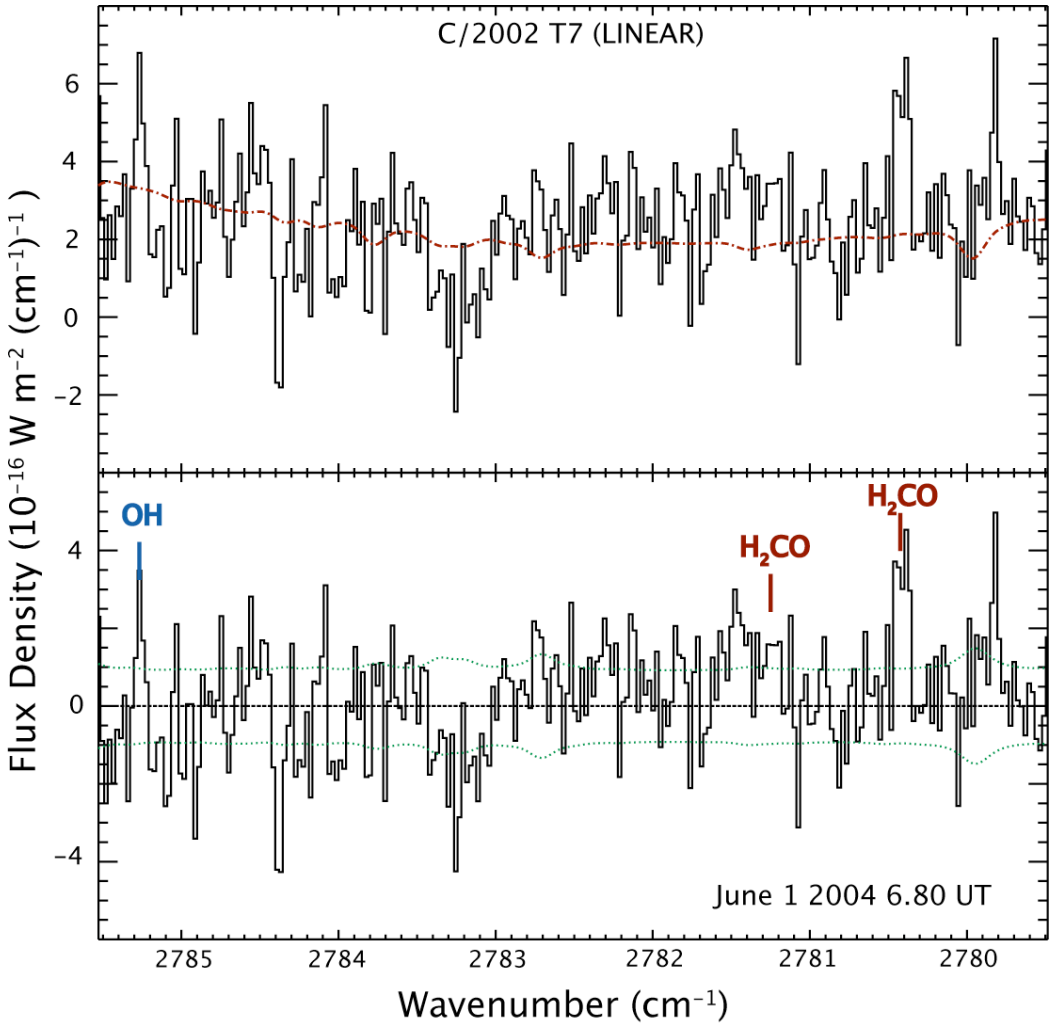

Figure 2.5 (A): Overview of June 1, 2004, H_2CO gas emission in C/2002 T7 (LINEAR) obtained with CSHELL through the 1 arc-second slit. The spectral revolving power is $v/\Delta v$ ~25,000. All extracts are centered on the row containing the peak emission.
(Top): Comet spectra (solid) and atmospheric model (dotted line).
(Bottom): Residuals with line identification and noise level (dotted line).

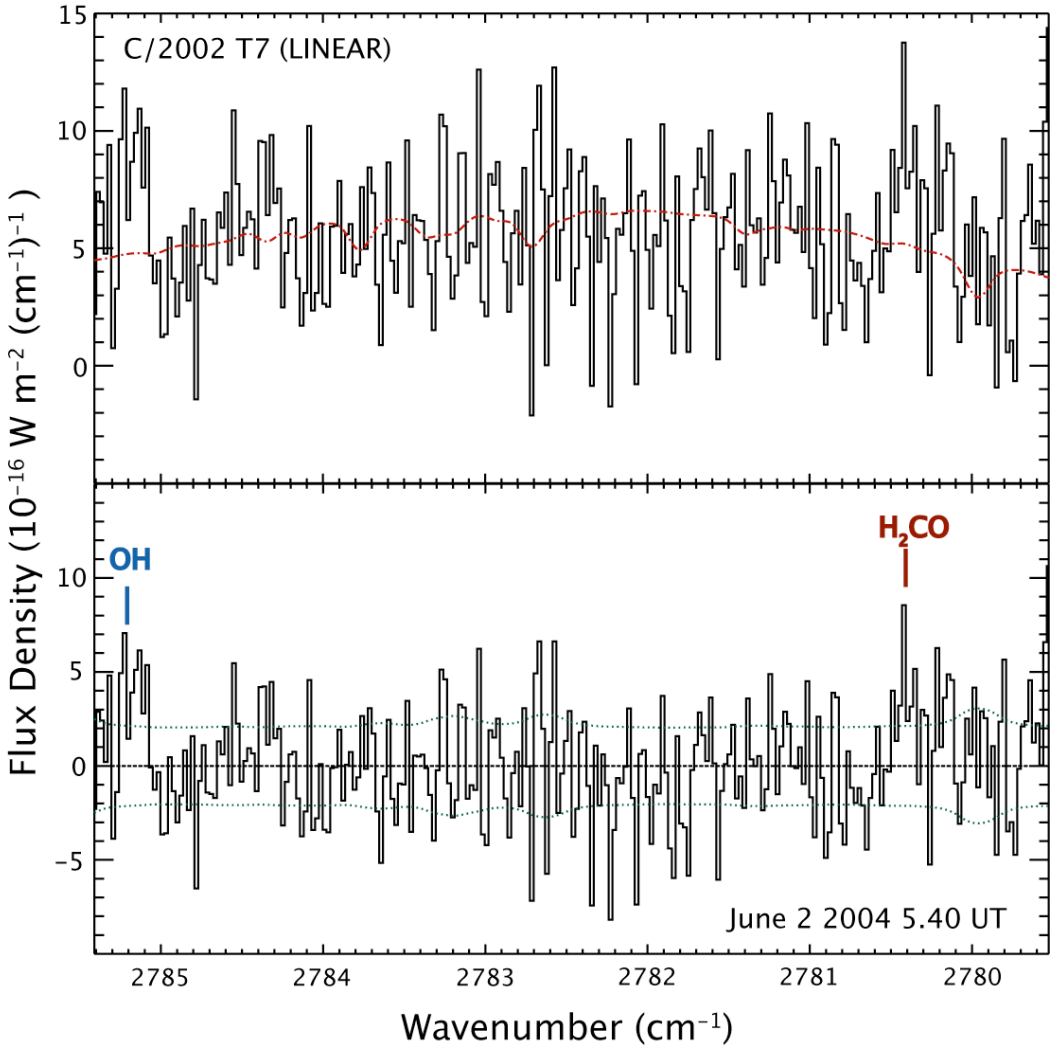

Figure 2.5 (B): Overview of June 2, 2004, H_2CO gas emission in C/2002 T7 (LINEAR) obtained with CSHELL through the 1 arc-second slit. The spectral revolving power is $v/\Delta v$ ~25,000. All extracts are centered on the row containing the peak emission.
(Top): Comet spectra (solid) and atmospheric model (dotted line).
(Bottom): Residuals with line identification and noise level (dotted line).

CHAPTER III

METHODOLOGY FOR DETERMING ROTATIONAL TEMPERATURES AND PRODUCTION RATES THROUGH THE USE OF GROWTH FACTORS

3.1. INTRODUCTION

The main goal of this chapter is to describe the analytical techniques used to obtain quantitative properties of the parent volatiles of C/2002 T7 (LINEAR). I introduce the concept of spherical and symmetric production rates, and present methodology for obtaining rotational temperatures (T_{rot}) of parent volatiles, required for calculating accurate production rates. While T_{rot} can be determined for H_2O and H_2CO using individual settings (see below), as mentioned previously (Chapter 2) this is not the case for CO because only two lines are encompassed per setting. However, an accurate measure of T_{rot} for CO is provided by coupling separate CSHELL settings that together span a range in CO rotational quantum number.

3.2. THE PRODUCTION RATE

The abundance of a parent volatile in comets is expressed through its apparent "spherical" production rate (Q, *molecules* s^{-1}). For a particular spectral line "i" at frequency ν (cm^{-1}):

$$Q_i = \frac{4\pi\Delta^2 F_i}{hc\nu(\tau g_i \kappa_i)_{1AU} f(x)} \quad (3.1)$$

where Δ is the geometric distance (m), F_l(W m^{-2}) is the observed line flux , $hc\nu$ is the energy per photon (J), τ and g_l are the photo-dissociation lifetime (s) and line fluorescence g-factor (photon s^{-1} mol^{-1}), both evaluated at heliocentric distance R_h = 1 AU, κ_i is the monochromatic transmittance through the terrestrial atmosphere at the

Doppler-shifted line center frequency, and f(x) is the fraction of the total number of molecules of the parent in the beam (see the Appendix of Hoban et al., 1991 for the case of square pixels). The wavenumber, ν, is commonly used in infrared spectroscopy and is equal to the inverse of the photon wavelength.

A "spherical Q curve" is generated by stepping a 1x1 arc-second aperture along the slit and calculating Q at each step, assuming uniform spherical outflow from the nucleus. The "symmetric Q" is the mean of spherical Q's at corresponding distances to either side of the nucleus (Magee-Sauer et al. 1999; DiSanti et al. 2001). The "nucleus-centered" production rate (Q_{nc}) corresponds to the flux contained in the central 15 spatial pixels (i.e., in a 1x3 arc-second aperture; the spatial size of a pixel in CSHELL is 0.2" and 1" bin size of contains the signal measured from 0.5" to 1.5" left and right of the comet nucleus) centered on the nucleus. The symmetric Q versus offset distance from the nucleus is referred to as a "Q-curve" (Fig. 3.1). Because of slit losses (due primarily to seeing), Q is invariably lower on the nucleus, increasing to a constant value (the "global" Q or "terminal" production rate, Q_{term}) farther from the nucleus, outside the effective PSF. The growth factor (GF) is defined as the ratio of terminal to nucleus-centered production rates (see Bonev 2005 and references therein):

(3.2) $$GF = \frac{Q_{term}}{Q_{nc}}$$

For the C/2002 T7 (LINEAR) observations Q_{term} represents the weighted mean symmetric production rate 2 – 6 arc-seconds (technically 1.5 – 6.5 arc-seconds) from the

nucleus (Fig. 3.1). In practice, GF is established by generating a Q-curve for the summed profile of multiple lines (e.g., as in the 2.9-μm water setting shown in Fig. 3.2) or, if this is not possible, for a single strong line (e.g., as for the H_2O line at 2137 cm^{-1}; see Fig. 3.5 and accompanying discussion). The GF so determined is then applied to the Q_{nuc} measured for each individual line within a setting, thereby yielding line-by-line values of Q_{term}. The weighted mean of these Q_{term} then corresponds to the overall global production rate of the molecule. Because emission intensities peak near the nucleus, Q_{nuc} for a given line has higher signal-to-noise than does the corresponding Q_{term} based on the Q-curve method. Therefore, scaling individual Q_{nuc} as outlined gives more consistent results (i.e., more consistent line-by-line values of Q_{term}; see discussions in DiSanti et al. 2001, and Dello Russo, et al. 2004).

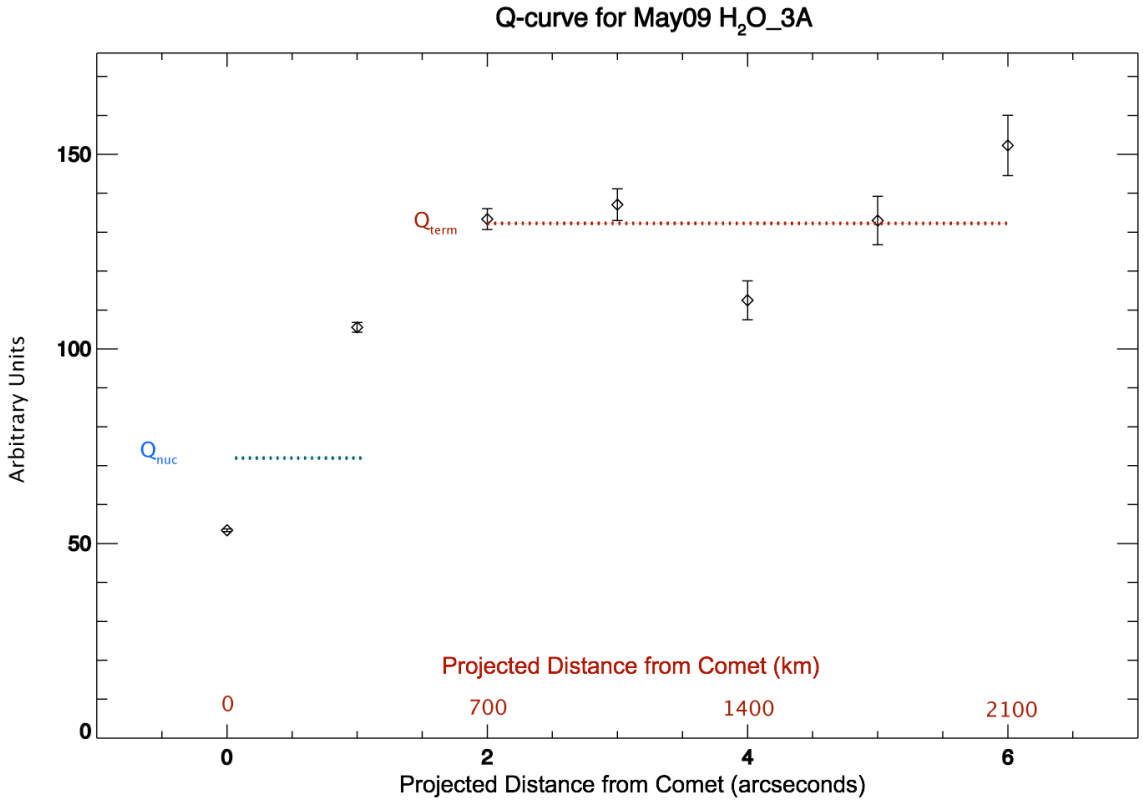

Figure 3.1: Q-curve plot for water measured in the H_2O_3A Setting on May 9 2004. The blue line represents the nuclear centered production rate. The red line represents the terminal production measured from 2 to 6 arc-seconds off the comet's nucleus.

3.3. MODELING OF FLUORESCENT EMISSION

Ideally, to measure Q one would want to observe an entire vibrational band, since the band intensity (i.e., the band g-factor) is (largely) independent of the rotational excitation (i.e., T_{rot}) of the molecule. However, this is generally not possible due to limited spectral coverage and atmospheric opacity. In particular, with its limited spectral grasp per setting, CSHELL is typically able to sample only a small fraction of the total

band intensity. Fig. 3.2 shows the positions of four CO settings used on May 9, 2004 UT, “CO_C”, “CO_D, “CO_G”, and “CO_H,” that together sample a range in rotational energy that is sufficient to provide a robust measure of T_{rot}. A single CSHELL setting is only able to cover two CO lines. As I will detail later in this chapter, multiple lines with a sufficiently wide range in rotational quantum number need to be combined are needed to calculate an accurate value for a gas rotational temperature. This makes it necessary to utilize multiple CSHELL settings.

As mentioned, the limited grasp of CSHELL translates to only two CO lines being encompassed per setting, and this is insufficient to measure T_{rot} for CO.. Molecular lines observed with different CSHELL settings can not be simply used together. There will be a time difference between observations with each setting. Comets naturally have gas and dust emission that may effect their orbital parameters, making than more difficult to track and keep in telescope view than other celestial object. Between spectrometer readings, the comet must be imaged through the CVF to recenter the comet with the field of the slit. Differences in the sensitivity of CSHELL varies with different wavelength and echelle grating angle relative to blaze. As a result of these differences, there will be difference in the flux recorded by CSHELL. Also with separate observations for each setting, additional sources of uncertainty may be introduced do to changes in the observing conditions. These differences must be accounted for when combining observations of different CSHELL settings.

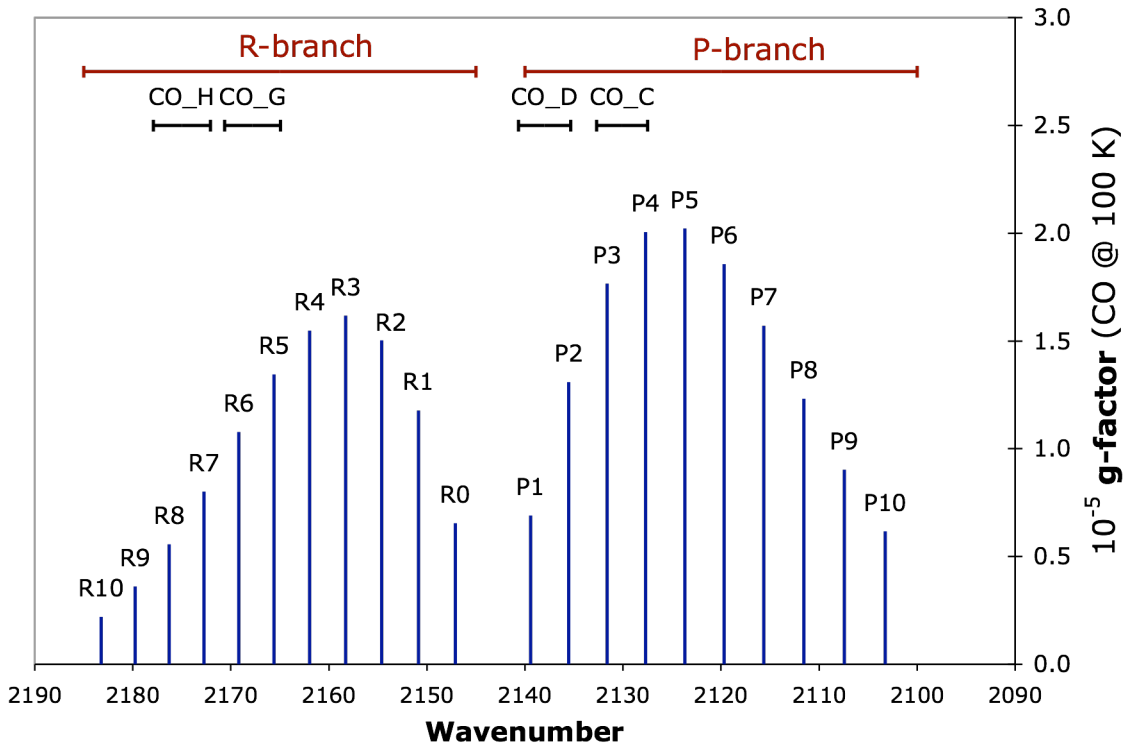

Figure 3.2: R and P branch lines of the CO v = 0-1 band with corresponding wavenumber and flourscence g-factor at a rotational temperature of 100 K. The spectral grasp of the CSHELL settings (CO_C, CO_D, CO_G, and CO_H) are shown, covering two CO lines each.

3.4. TREATING MULTIPLE CSHELL SETTINGS

A method has been developed to account for these differences. This section details how the rotational analyses described previously (and exemplified for the H_2O_3A setting) can be extended to multiple CO settings, as required to determine its T_{rot}. To show this, the observations on May 9 are used, as these sample a broad range in rotational quantum number (from J' = 0 to J' = 9 in the upper vibrational state, v' = 1; see observing log, Table 2.1).

The most notable difference among these settings is the amount of slit loss – because of the relatively narrow slit width (1 arc-second) required to achieve the desired spectral resolving power (RP ~ 2.5 x 10^4), a fraction of the incident flux is blocked by the slit jaws and is therefore lost. The amount of slit loss depends primarily on the seeing averaged over the duration of the observation, and to some extent placement of the comet photo-center relative to the slit mid-plane. For the case of release directly from the nucleus (i.e., for parent volatiles), the correction for this effect is given by the factor GF (see Fig. 3.3 and previous discussion regarding Q-curves).

Ideally, the GF can be determined for each setting from the sum of spatial profiles for CO lines (and H_2O lines, when present), however this approach introduces uncertainties into each GF that are dominated by uncertainties in Q_{term}. To minimize these, Q-curves are generated from the spatial distribution of continuum emission in each setting, since the continuum profiles have much higher signal-to-noise (Fig. 3.3).

The ratio of the nucleus-centered dust continuum production rates for two settings provides a means of establishing their relative scaling, through a correction factor (CF):

(3.3) $$CF = \frac{Q_{0\text{-}1 \text{ setting 2 cont}}}{Q_{0\text{-}1 \text{ setting 1 cont}}}$$

We can also define a “corrected” growth factor by multiplying a growth factor by the continuum-based CF.

(3.4) $$CGF = GF \times CF$$

The inherent assumption with this formalism is that the dust and parent volatile profiles (and therefore GF) maintain a constant ratio over the time interval encompassing the relevant settings (also see A.1 in the Appendix).

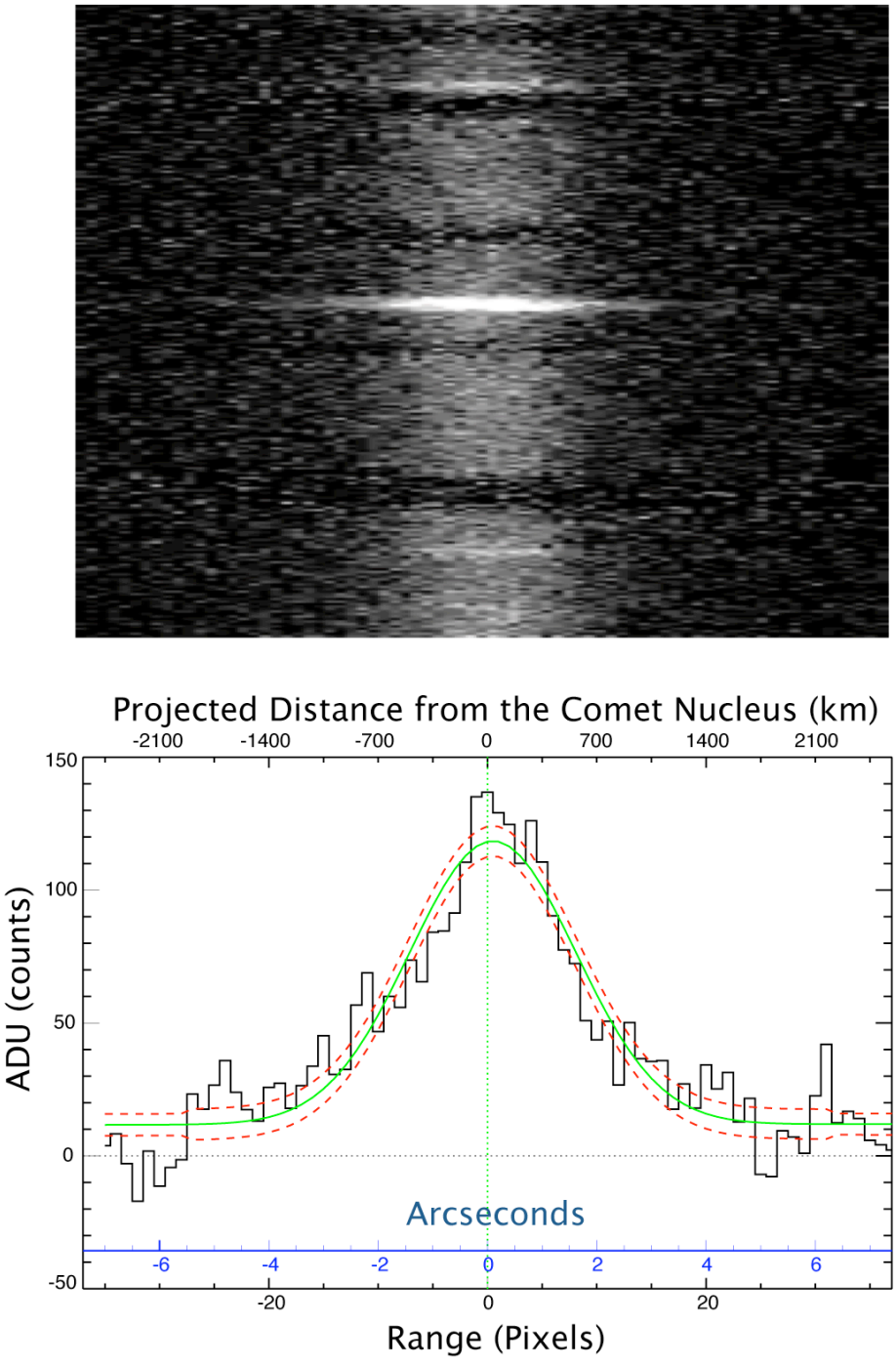

Figure 3.3: (top) Difference frame for combined CO_D setting observations on May 9, 2004 show in relation to spatial dimension. (bottom) Corresponding spatial profile for central water line near 2137 cm^{-1}. Observed flux, Gaussian model fitted to flux, and 1-σ dashed error lines are shown.

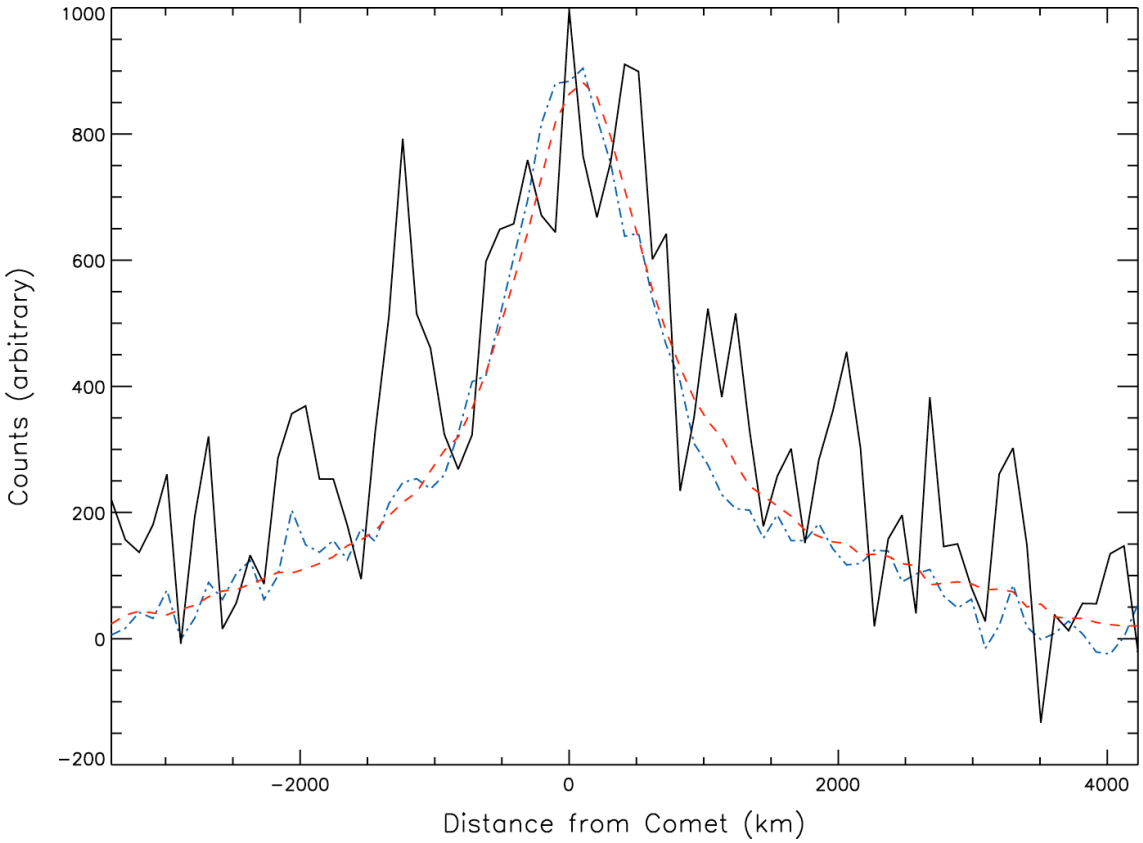

Figure 3.4: Comparison of spatial profiles for CO lines (solid black), H_2O (dash red), and the dust continuum (dot-dash blue) from May 3, 2004 observations. The H_2O profile closely follows the dust continuum. The CO profile is little broader than H_2O profile. Based on accepted scale lengths of CO (based on Giotto Observations of 1P/Halley; Eberhardt, 1999), this difference is likely due to the position of the comet off center, not an extended source, and could be corrected by a relatively small nod (15 arc-second) of the instrument.

3.5. CONVENTIONAL BOLTZMANN ANALYSIS FOR LINEAR MOLECULES

With the lines from different CSHELL setting inter-calibrated, the next step is to determine the rotational temperature for CO. As individual line g-factors are highly dependent on the rotational temperature, rotational temperature is needed before reliable gas production rates can be found.

DiSanti et al. (2001), in detail, describes that the rotation temperature of simple linear molecules can be determined from the intensities of a number of ro-vibrational lines and derives the following equation:

$$(3.5) \qquad (k/hcB') (-1/ T_{rot}) = \ln [F_{line} / \nu^4 (J' + J'' + 1)] / J'(J' + 1)$$

where ν is the line frequency (cm^{-1}), h is Planck's constant, c is the speed of light, and k is Boltzmann's constant. The quantum numbers (J', J") refer to the upper and lower rotational states of the transition. B' is the rotational constant of the upper vibrational state (v = v' = 1), which equals 1.97 cm^{-1} for CO (Herzberg, 1950). F_{line} is the transmittance-corrected line flux (W m^{-2}).

Figures 3.5 and 3.6 are displayed as examples of the Boltzmann method. On May 03, observations produced a CO rotational temperature of 113 +/- 7 K. On May 09, observations produced a CO rotational temperature of 105 +/- 6 K. Each plot point represents the east-west average of the line fluxes for the terminal region of the Q-curve. The error bars of each point represent 1 σ error. The rotational temperature is also show in the lower left with +/- 1 σ error.

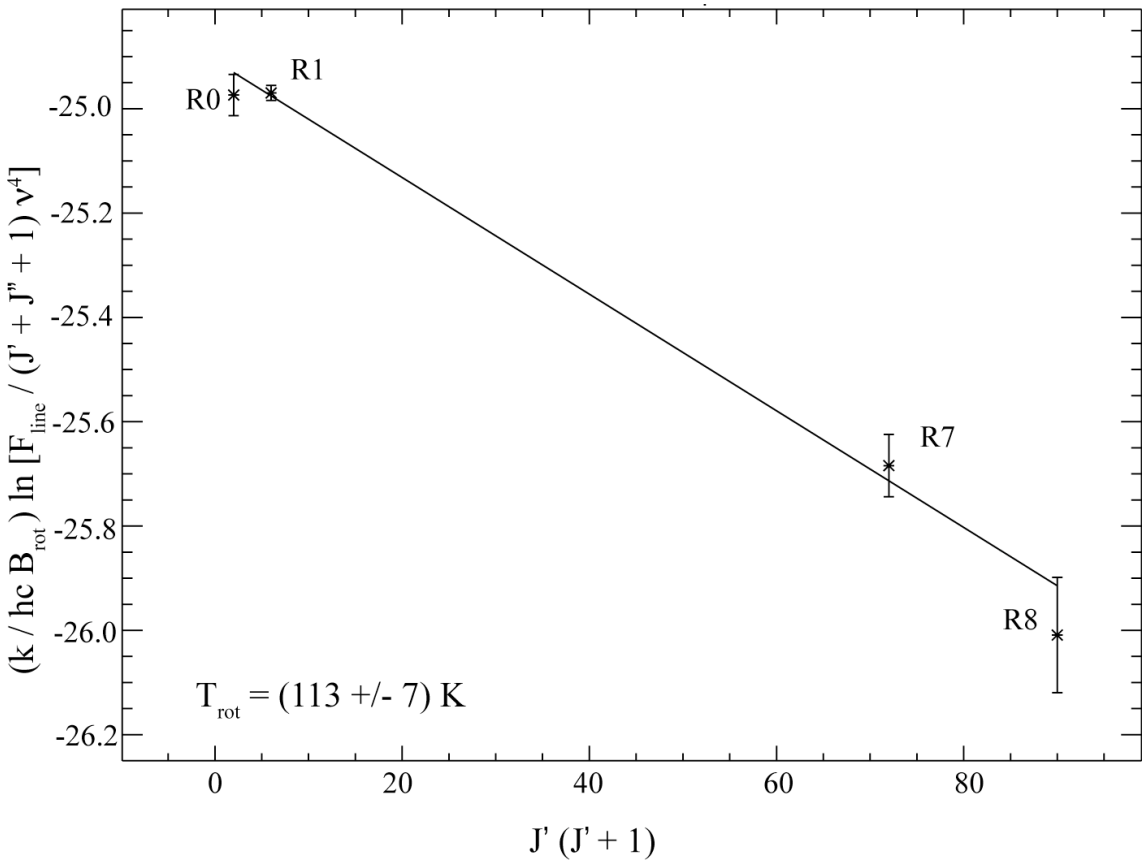

Figure 3.5: The determination of rotational temperature (T_{rot}) based on the intensities of several CO lines observed on May 3, 2004. Each plot represents the east-west average of the line fluxes for the terminal region of the Q-curve. The error bars of each point represent 1 σ error. The rotational temperature is also show in the lower left with +/- 1 σ error.

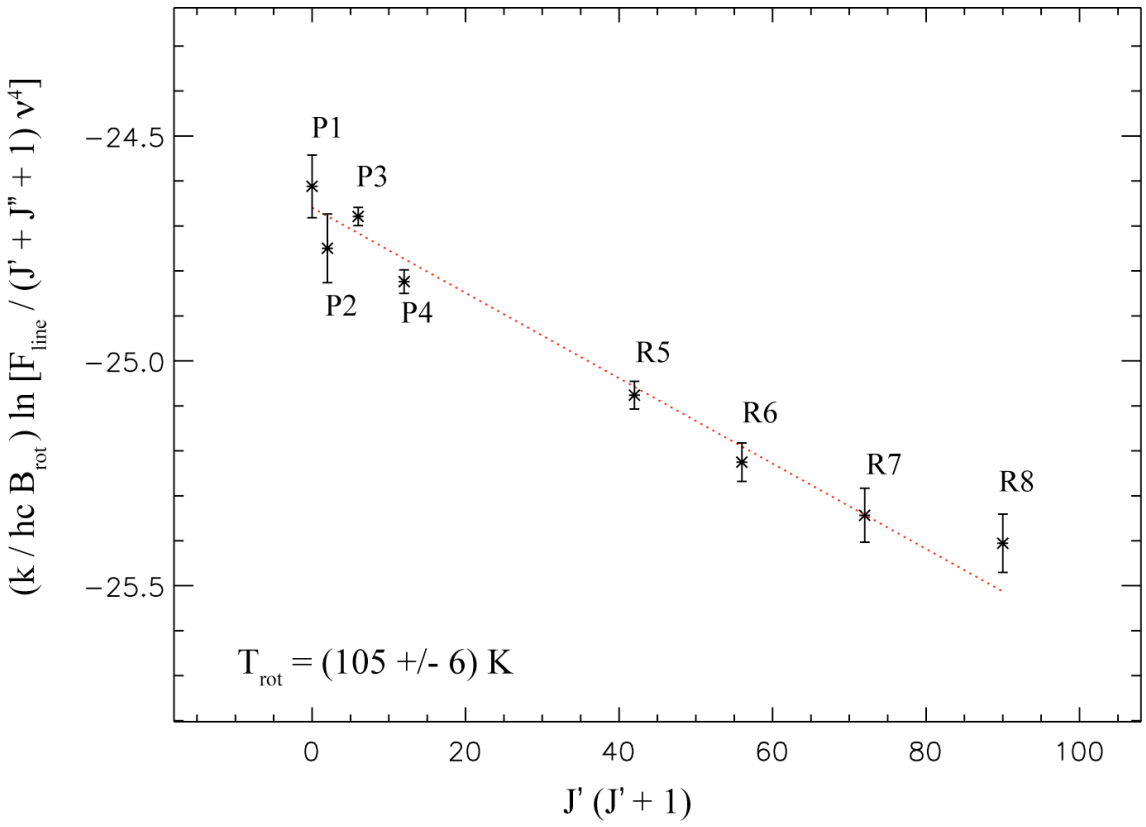

Figure 3.6: The determination of rotational temperature (T_{rot}) based on the intensities of several CO lines observed on May 9, 2004. Each plot represents the east-west average of the line fluxes for the terminal region of the Q-curve. The error bars of each point represent 1 σ error. The rotational temperature is also show in the lower left with +/- 1 σ error.

With the Boltzmann method, it may require a number of steps to result in a final rotational temperature. An estimate of the rotation temperature must be first applied (for example, 100 K) to generate an initial set of the molecular g-factors and corresponding transmittance-corrected line fluxes. In turn, a slope and a new rotational temperature is calculated from the Boltzmann method. The new rotational temperature is then used to fix molecular g-factors and calculate a new set of transmittance-corrected line fluxes. The cycle continues until the process truncates on a final rotational temperature.

Day-by-day rotational temperature values for CO are shown in the following chapter. It would be ideal to compare the rotational temperature of CO with other native molecules ejected from the comet nucleus, in particular water. Unfortunately, the previously described Boltzmann method only can be applied to linear molecules. An alternative approach is necessary to find the rotational temperature of other interesting molecules.

3.6. CORRELATION AND EXCITATION ANALYSIS METHODS FOR ROTATIONAL TEMPERATURE

DiSanti et al. (2006) describes to two alternate methods for determining rotation temperatures of molecular comet emission (DiSanti et al., 2006, particularly focuses on formaldehyde) which can be used for nonlinear molecules. The first is a correlation

method which compares observed molecular lines with a simulated modeled based on g-factor at particular rotational temperature. The second method uses excitation analysis to compare the ratio of line flux and g-factor against lower state energy for a series of molecular lines.

DiSanti et al. (2006) devised an algorithm that allow both complementary methods to be run simultaneously. In the correlation analysis, observed comet residuals are compared with a fluorescence model (convolved to the RP of the comet residuals) and the correlation coefficient, R, between the two is calculated. The process is performed over a range of temperatures (e.g., 50-200 K) in small steps (1 K), and the correlation coefficient is measured at each step. The maximum value of R corresponds to the most probable rotational temperature and the sharpness of the peak is proportional to how well T_{rot} is constrained (Fig. 3.8; see DiSanti et al. 2006 for a detailed discussion).

The correlation analysis is useful as R shows the overall agreement between the observed data and the synthetic model. Unfortunately, it is not easy to analytically determine error using this method. This approach has the drawback of weighting all the individual lines equally (stronger molecular lines should be given a greater weight as they will have correspondingly smaller relative uncertainties due to their larger signal-to-noise ratios) nor does it factor in the spread in rotational energies between the measured lines.

These shortcomings are remedied by the excitation analysis. Modeled line g-factors vary with rotational temperature. Multiplying the g-factor of each individual line

by the fully resolved transmittance κ (at its Doppler shifted line-center frequency) permits direct comparison with its observed flux (F_{line}) as measured from the comet residuals (Eq. 3.1). Examining the ratio F_{line}/g for a number of lines covering a range in rotational energy can be used to measure T_{rot} and also to obtain a statistical measure of its uncertainty. The foundation of the excitation analysis is based on a weighted linear least-squares fit to F_{line}/g vs. rotational energy. At the optimal rotational temperature, F_{line}/g is independent of rotational energy (Dello Russo et al. 2004, 2005; Bonev 2005) and hence the least squares slope equals zero. The F_{line} is the observed flux in the comet residuals, summed over the spread of spectral points across each line. For an isolated CO line, E_{low} represents its lower state energy. In the case of blended lines (such as with some H_2O and H_2CO lines), E_{low} is their weighted mean lower state energy.

Uncertainties in T_{rot} (σ_{Trot}) are based on corresponding uncertainties in the best-fit slope, as developed in previous analyses of cometary H_2O non-resonant fluorescent emission (Dello Russo et al. 2005; Bonev 2005). The larger of the stochastic error or standard error is used to calculate σ_{Trot}. The stochastic error refers to the signal-to-noise ratio of the data (associated with photon noise, and depicted by the error bars on each data point in Fig. 3.8). The standard error pertains to the dispersion of the individual values (weighted by their stochastic errors) about the mean (dotted line in Fig. 3.7). Both types of uncertainty depend on the spread in rotation energy of the sampled lines. Generally speaking, the broader the range in energy, the better the temperature will be constrained. For the CO observations on May 3 and 9, both low- and high-energy lines are encompassed, thereby providing tight constraints on T_{rot}. Because of the high signal-

to-noise of these observations, the standard error in this set of observations of C/2002 T7 LINEAR dominates over the stochastic error (Table 3.1).

The classical Boltzmann method produces a CO rotational temperature of 113 +/- 7 K for May 3, 2004. The rotational temperature, extracted from the excitation method for the same date (114 +/- 7 K) agrees to well within one standard deviation. This demonstrates that the excitation method is producing the correct rotational temperature within error and can be used for other (including nonlinear) molecules, such as water, for which the classical Boltzmann cannot be used (see Section 3.7).

Further verification between the classical Boltzmann and excitation methods can tested by comparing the CO rotational temperatures found by both methods for the May 9 observations. The four CSHELL settings used to observe CO in C/2002 T7 (LINEAR) on May 9, 2004, cover eight CO individual lines (P1, P2, P3, P4, R5, R6, R7, R8). Unfortunately, the CO P2 and P3 lines are each blended with cometary water lines. It will be necessary to carefully extract the signal due to water before the P2 and P3 lines can be included in the correlation and excitation analysis methods. Of course, the water line g-factors (and corresponding flux) are dependent on its rotational temperature, so the rotational temperature for H_2O must be known.

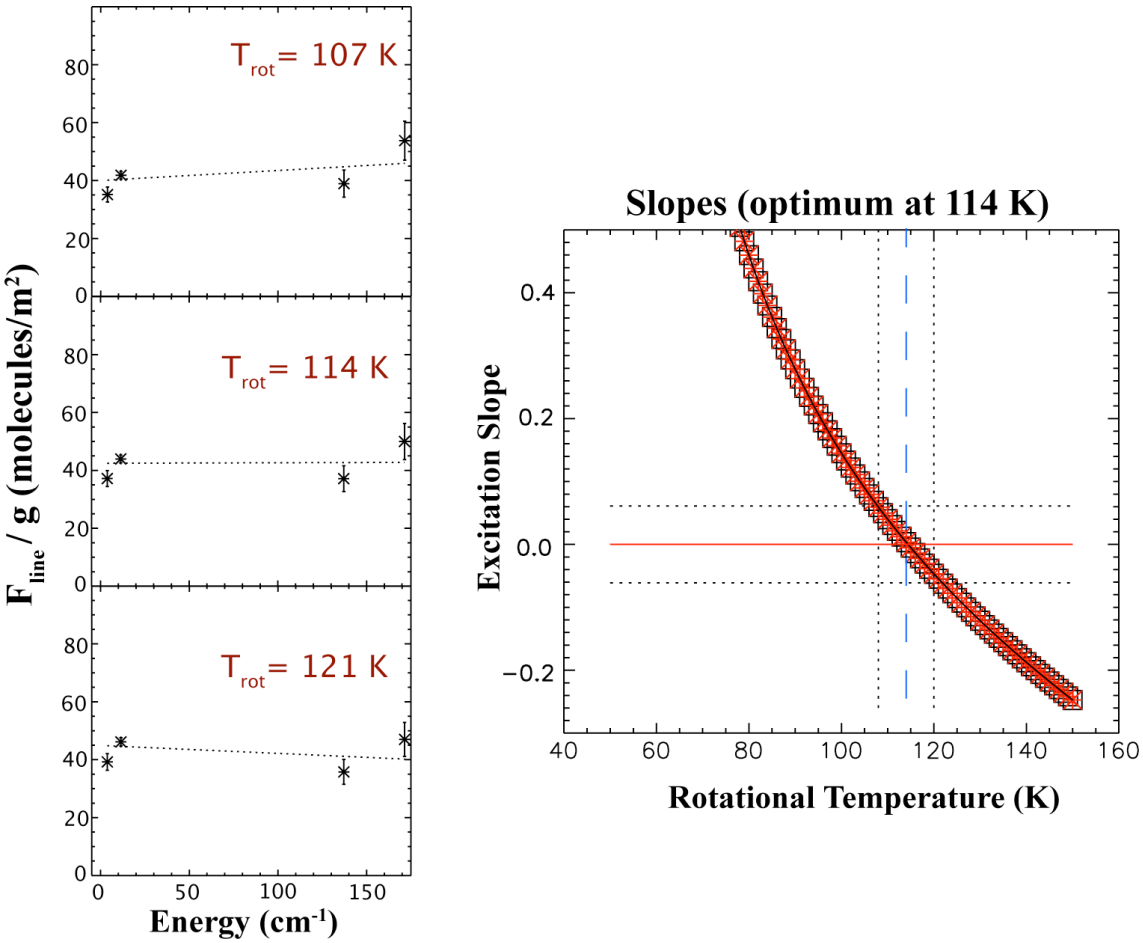

Figure 3.7: Measurement of T_{rot} for CO on UT 2004 May 3. Excitation Method (Left): F/g vs. E_{low} at 97 K, 114 K, and 121 K. These plots permit even small differences in modeled T_{rot} to be visualized. (Right): Best fit slope of F/g vs. E_{low} as a function of T_{rot}, indicating an optimal value of 114 K. The horizontal dotted lines represent +1 σ values in the slope, corresponding to σ_T = +/- 7 K (vertical dotted lines).

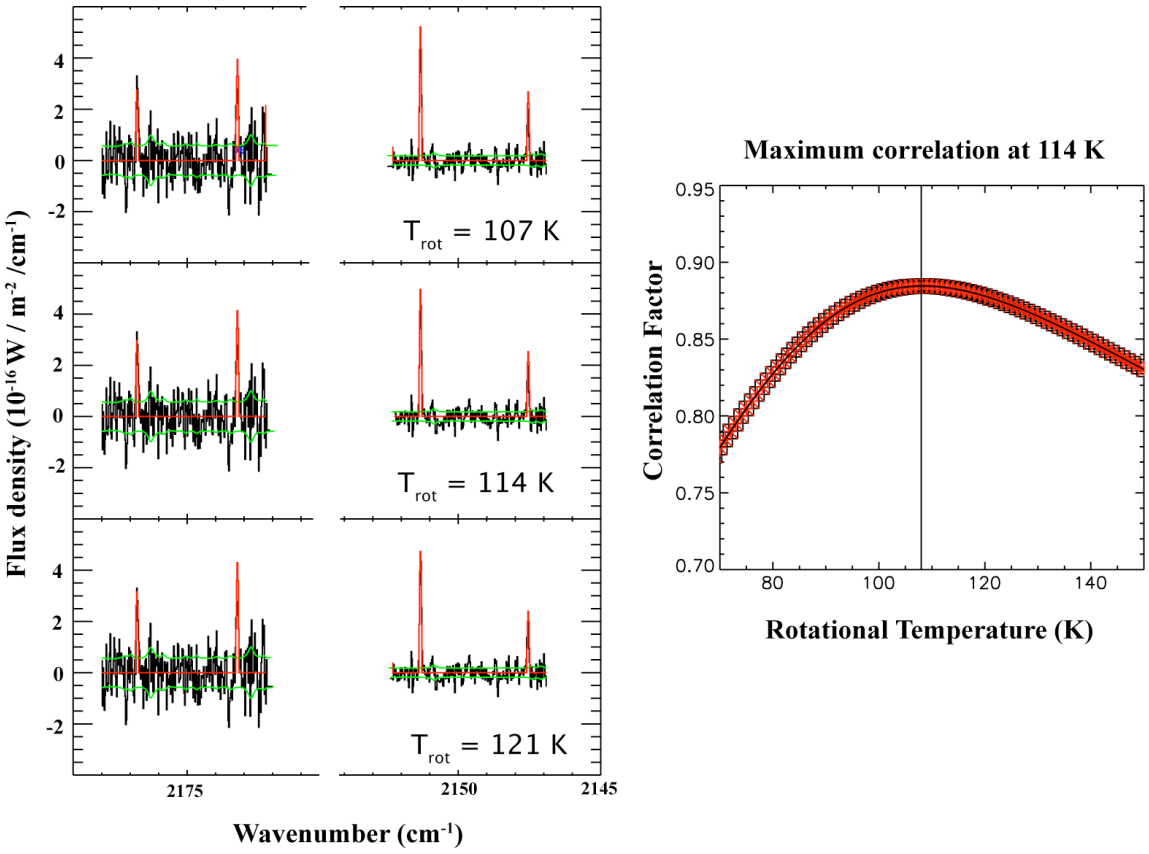

Figure 3.8: Correlation Method (Left) Observed residuals (spectrum minus telluric transmittance function convolved to a resolving power of ~25,000) on May 3, 2004, for a setting that targets CO lines (black traces). Synthetic spectra for water at rotational temperatures of 107, 114 and 121 K (red traces) show variations in modeled line intensities when T_{rot} is varied by ±7 K from the optimum value of 114 K (see Fig. 3.7 and accompanying discussion). In each panel, in this and subsequent figures showing comet residuals, the stochastic (photon) noise (green traces), and the pixels over which the flux of each line was summed (blue traces), are also indicated. (Right) Corresponding correlogram comparing modeled and observed CO emission over a range in rotational temperature.

3.7. ROTATIONAL TEMPERATURE OF H_2O

The CO CSHELL settings contain very few strong water lines, which precludes use of the excitation analysis for water in the 4.7 μm region. The H_2O_3A setting covers a region near 2.9 μm that includes a number of water lines spanning a range in rotational energy. A sample observation from May 9, 2004 (see Fig. 2.3 G) shows that seven water lines are clearly visible. Five of the lines are strong enough and cover a widen enough range in rotational energy to use the correlation (Fig. 3.9) and excitation analysis (Fig. 3.10) to measure the rotational temperature. A sixth strong H_2O line, at rest frequency 3456.5 cm^{-1}, is not included in the analysis due to an inconsistency between modeled and observed intensities, as established previously from observations of comet 153P/Ikeya-Zhang (Dello Russo et al. 2004). The excitation analysis of the 2.9 μm water lines reveals a rotational temperature of 102 +/- 5 K.

The rotational temperature for H_2O can now be applied to the synthetic lines models for H_2O lines contained in the CO Shell settings. Subtraction of modeled H_2O intensities (at T_{rot} = 100 K), scaled to the (isolated) strong water line at rest frequency 2137.37 cm^{-1} in the CO_D setting (Fig. 3.11 A), yields the net signal from the P2 line (Fig. 3.11 B).

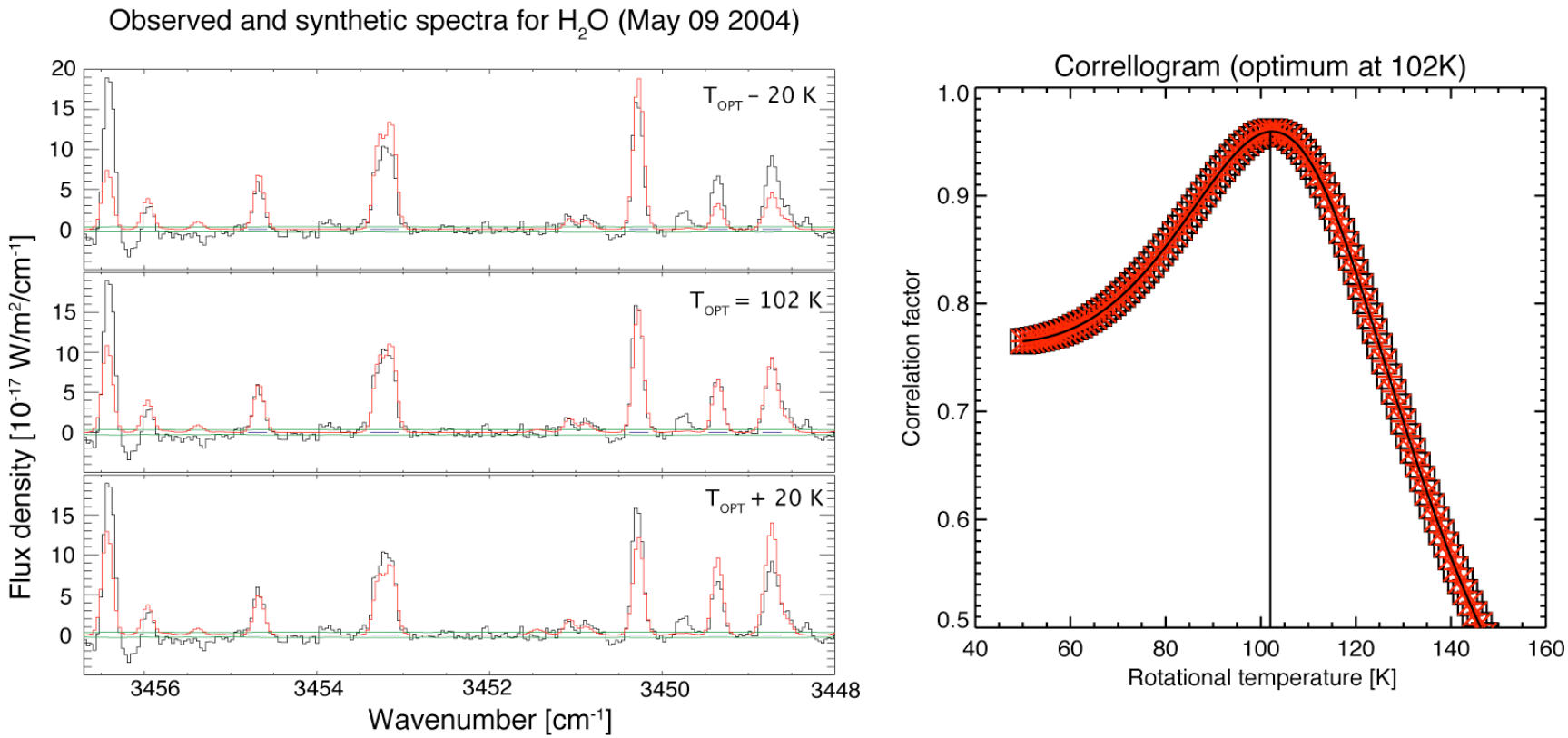

Figure 3.9: (Left) Observed residuals (spectrum minus telluric transmittance function convolved to a resolving power of ~25,000; see previous chapter) on May 9, 2004, for a setting that targets water emission near 2.9 microns (black traces). Synthetic spectra for water at rotational temperatures of 82, 102 and 122 K (red traces) show variations in modeled line intensities when T_{rot} is varied by ±20 K from the optimum value of 102 K. In each panel, in this and subsequent figures showing comet residuals, the stochastic (photon) noise (green traces), and the pixels over which the flux of each line was summed (blue traces), are also indicated. (Right) Corresponding correllogram comparing modeled and observed water emission near 2.9 microns over a range in rotational temperature.

-

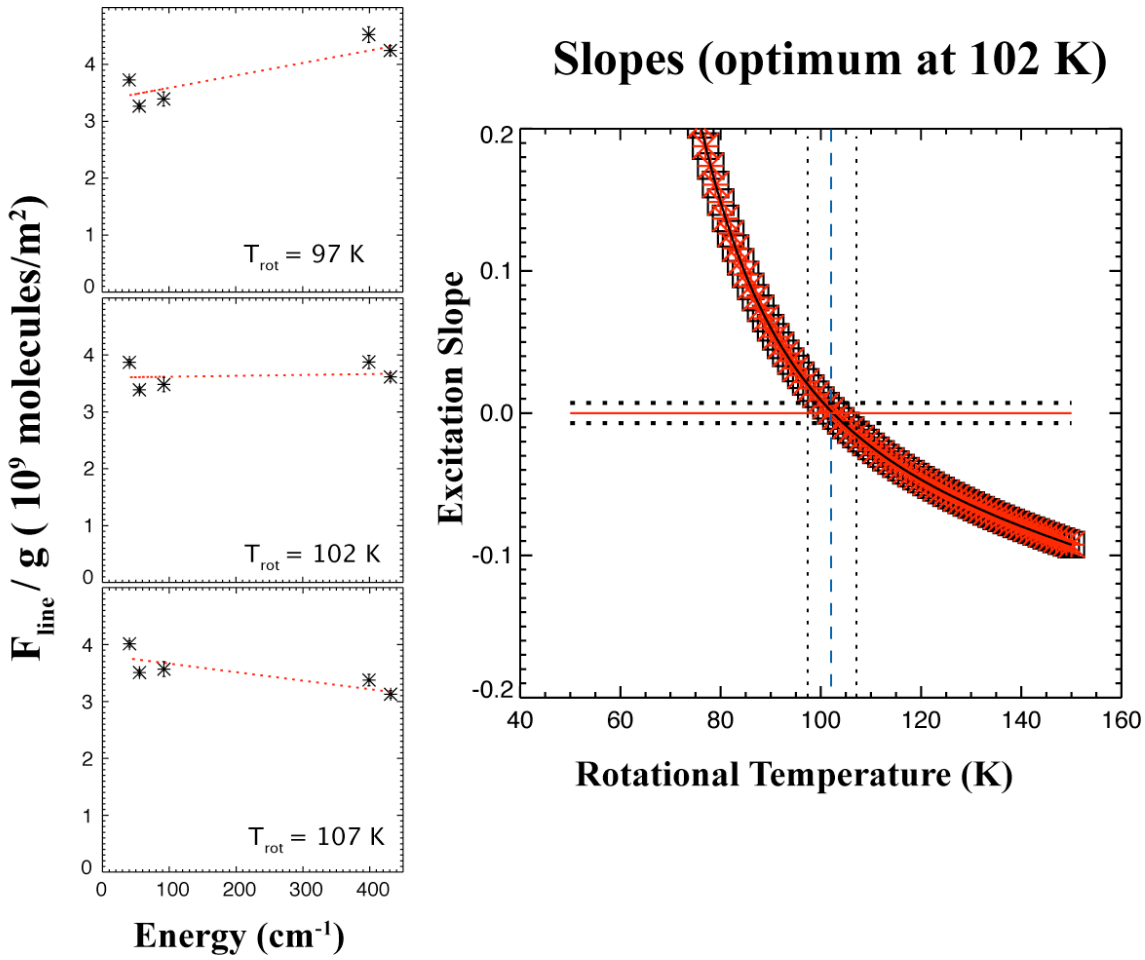

Figure 3.10: (Left): F/g vs. E_{low} at 97 K, 107 K, and 102 K for 2.9 μm H_2O observed on May 9, 2004. These plots permit even small differences in modeled T_{rot} to be visualized. (Right): Best fit slope of F/g vs. E_{low} as a function of T_{rot}, indicating an optimal value of 102 K. The horizontal dotted lines represent +1 σ values in the slope, corresponding to σ_T = +/- 5 K (vertical dotted lines).

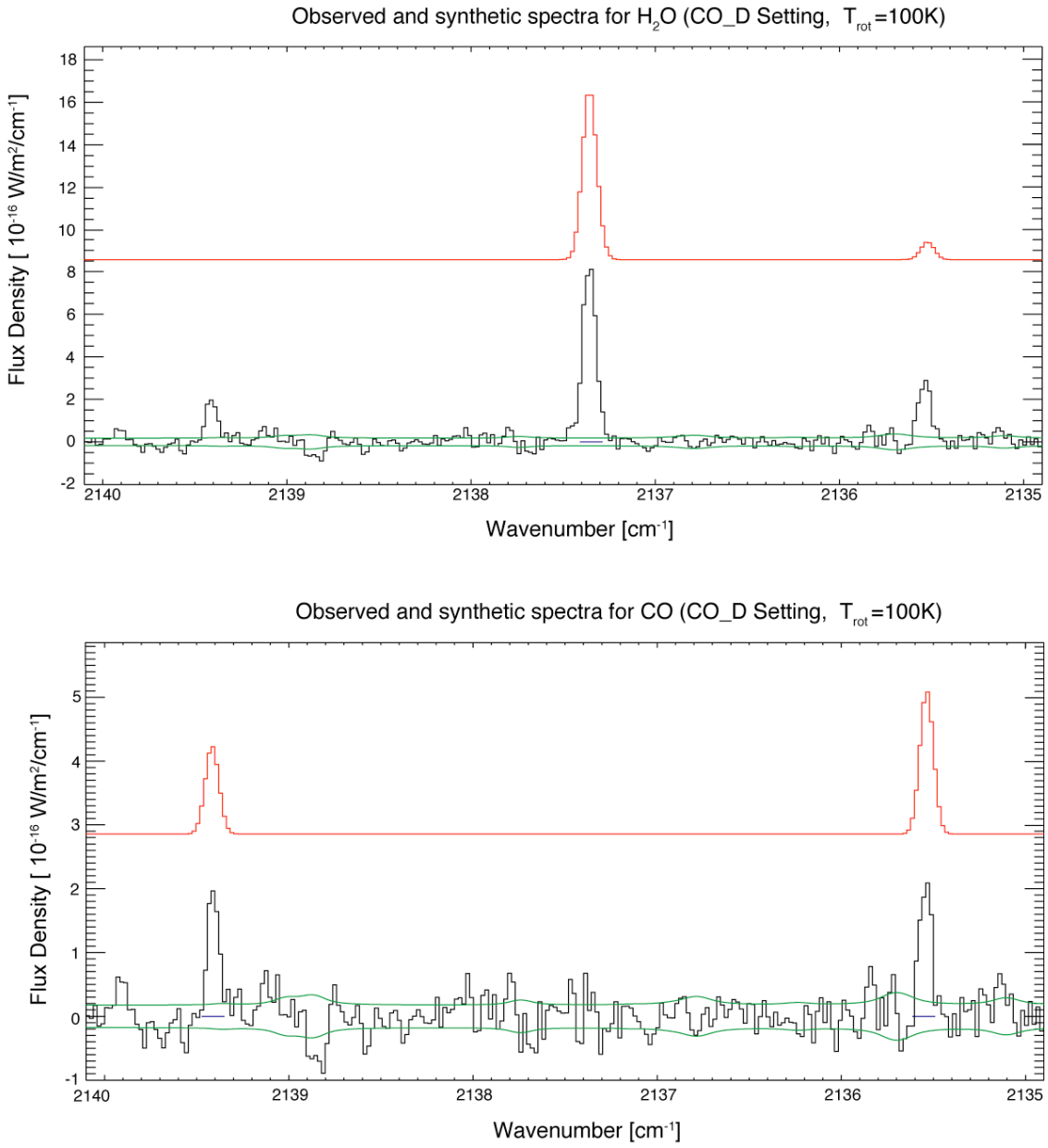

Figure 3.11: (A) Observed comet residuals (black) for CO_D setting on May 09 compared with the H_2O modeled line-by-line g-factors at 100K multiplied by the atmospheric transmittance (red). The bottom graph (B) has the water model subtracted from the observed residuals (black) and the CO synthetic model (red). Stochastic(photon) noise (green). Pixels over which the flux of each line was summed (blue).

An additional weaker H_2O line is blended with the P3 line of CO, which falls in the adjacent CO_C setting. To quantitatively account for the contribution from this water line requires scaling the model based on CGF and other factors:

$$\text{(3.5)} \qquad \text{Scale Factor}_{CO\_C} = \text{Scale Factor}_{CO\_D} \times \left(\frac{\Gamma_{CO\_D}}{\Gamma_{CO\_C}}\right) \times \left(\frac{dw_{0\ CO\_D}}{dw_{0\ CO\_C}}\right) \times \left(\frac{CGF_{CO\_D}}{CGF_{CO\_C}}\right)$$

in which Γ (W m^{-2} $(cm^{-1})^{-1}$ / ADU s^{-1}) is the flux calibration factor, dw_0 is the spectral dispersion (cm^{-1} $pixel^{-1}$). Scale $Factor_{CO\_D}$ is the model scale factor from the CO_D setting, which is derived from running the synthetic fluorescence model alone to correlate with the strongest water line in the CO_D setting. The new scale factor will correct for differences in sensitivity between the two settings (as described earlier), such that the synthetic fluorescence water lines models for both setting are comparable and thus the water contribution can be subtracted from the blended CO lines correctly.

An example of a scale factor calculation from the May 9 Data:

Scale $Factor_{CO\_D} = 4.5208246 \times 10^{30}$

Scale $Factor_{CO\_C} = 4.5208246 \times 10^{30}$ x (2.14837/2.11093) x (0.0208/0.0202) x (2.024/1.626)

Scale $Factor_{CO\_C} = 5.89732 \times 10^{30}$

In analogy with Fig. 3.11, subtracting the scaled H_2O model then isolates the net observed P3 line (Fig. 3.12 B).

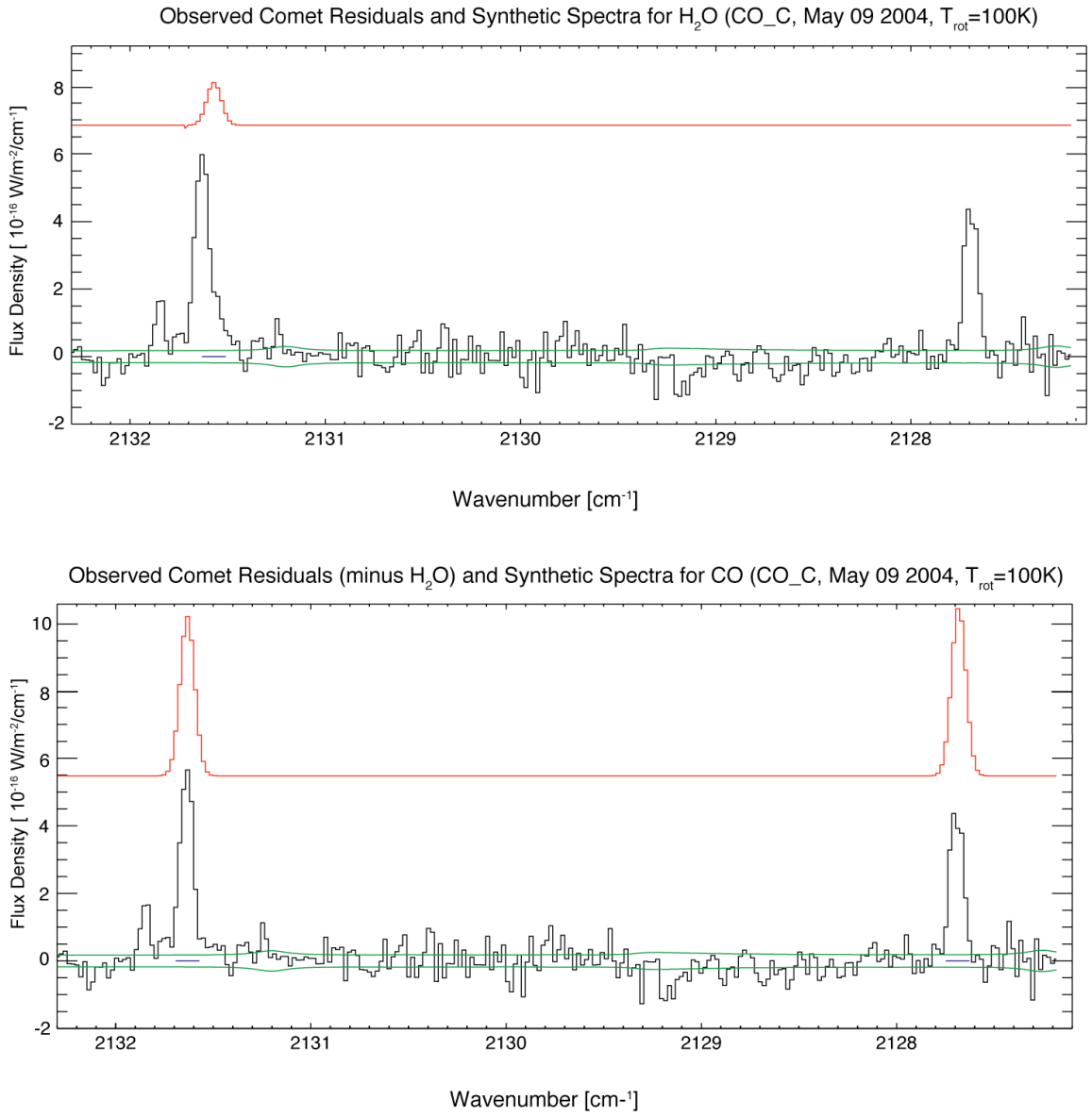

Figure 3.12: (A) Observed comet residuals (black) for the CO_C setting on May 9 along with the transmittance-multiplied H_2O model at 100K (red) scaled according to the intensity of line emission near 2137.4 cm^{-1} in the CO_D setting, as described in the text. (B) Subtraction of the water model from the observed residuals yields the net CO residuals (black). The CO model at 100 K is also shown (red).

3.8. COUPLING MULTIPLE CO SETTINGS

Once the CO lines have been extracted from the blended features, another step is necessary in the analysis process. The separate settings must be combined into a single data set in order to be analyzed with the methods described previously in this chapter The CO model applied to each setting also needs to be scaled in a fashion similar to that applied to the water line in CO_C. Four factors are different within each setting: $f(x)_{0\text{-}1}$, which is the fraction of the total number of parent molecules in the nucleus-centered beam; the flux calibration factor (gamma); dw_0, the single-pixel dispersion (cm^{-1}); and the correction factor. Of these four factors, f(x) has the smallest difference among settings. A mean can be found from all the f(x)'s and then be applied uniformly to each individual line production rate calculation. For the gamma correction and wavenumber dispersion, they are multiplied by the flux count of each individual setting and divided by the integration time. This will give the line flux in units of Wm^{-2}. Finally, the flux from each setting is scaled by the ratio of the setting's corrected growth factor and the average corrected growth factor of all the settings.

$$F_{line\,(Wm^{-2})} = \frac{\sum_{7\,cols} ADU \cdot \Gamma \cdot d\omega_0}{t_{int}} \times \frac{CGF_{setting}}{\langle CGF \rangle} \tag{3.6}$$

With the flux properly scaled, the correlation and excitation analysis can be performed to find the rotational temperature (Fig. 3.14 and 3.15) and then-nuclear centered production rate can be calculated. The CO rotational temperature is found to be

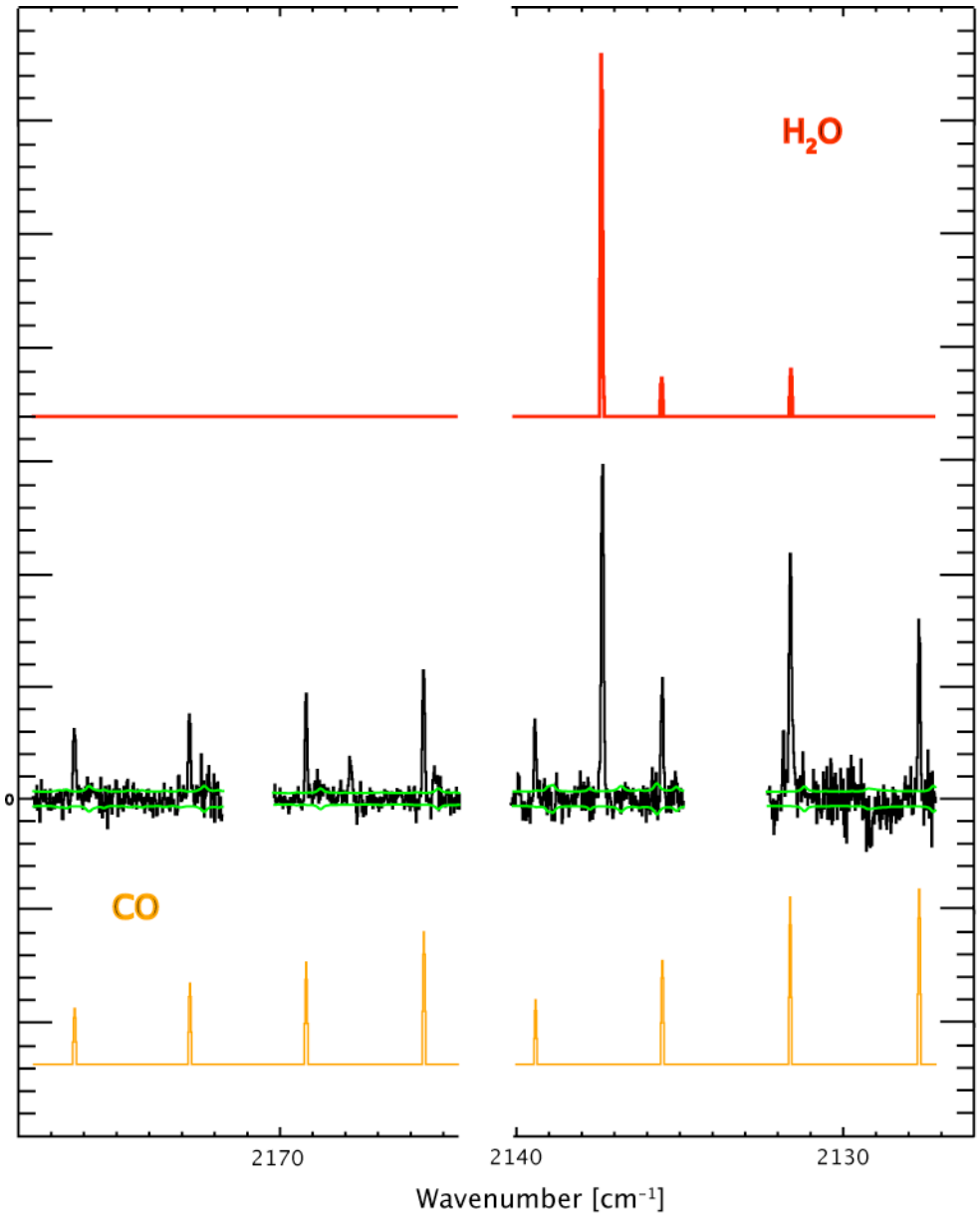

Figure 3.13: The observed comet residual (central black) for the four settings (CO_H, CO_G, CO_C, and CO_D) on May 9 2004 UT, the synthetic model for CO at T_{rot} =103 K (lower orange), the synthetic model for H_2O (upper red] at T_{rot} =103 K, and the stochastic (photon) noise (central green).

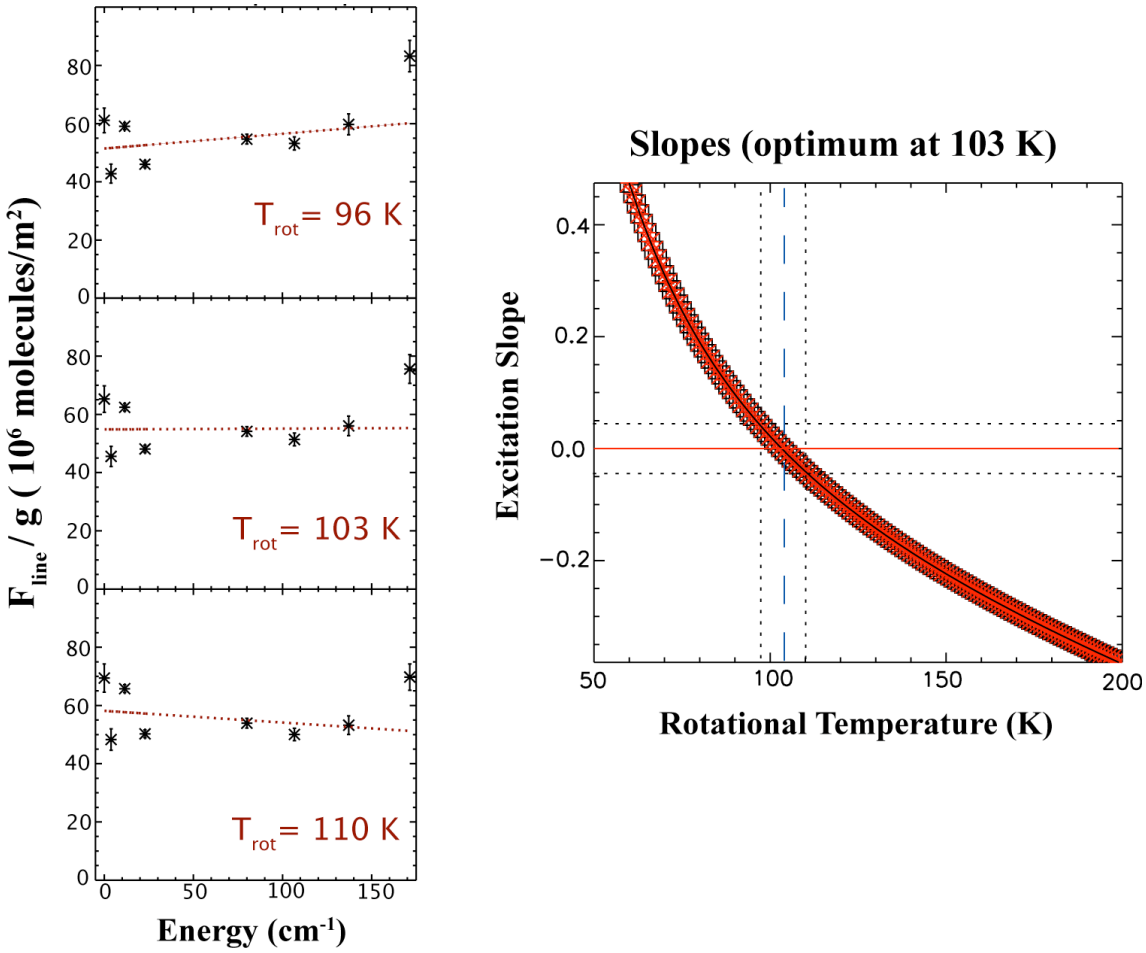

Figure 3.14: Excitation Method (Left): F/g vs. E_{low} at 96 K, 103 K, and 110 K. These plots permit even small differences in modeled T_{rot} to be visualized. (Right): Best fit slope of F/g vs. E_{low} as a function of T_{rot}, indicating an optimal value of 103 K. The horizontal dotted lines represent +1 σ values in the slope, corresponding to σ_T = +/- 7 K (vertical dotted lines).

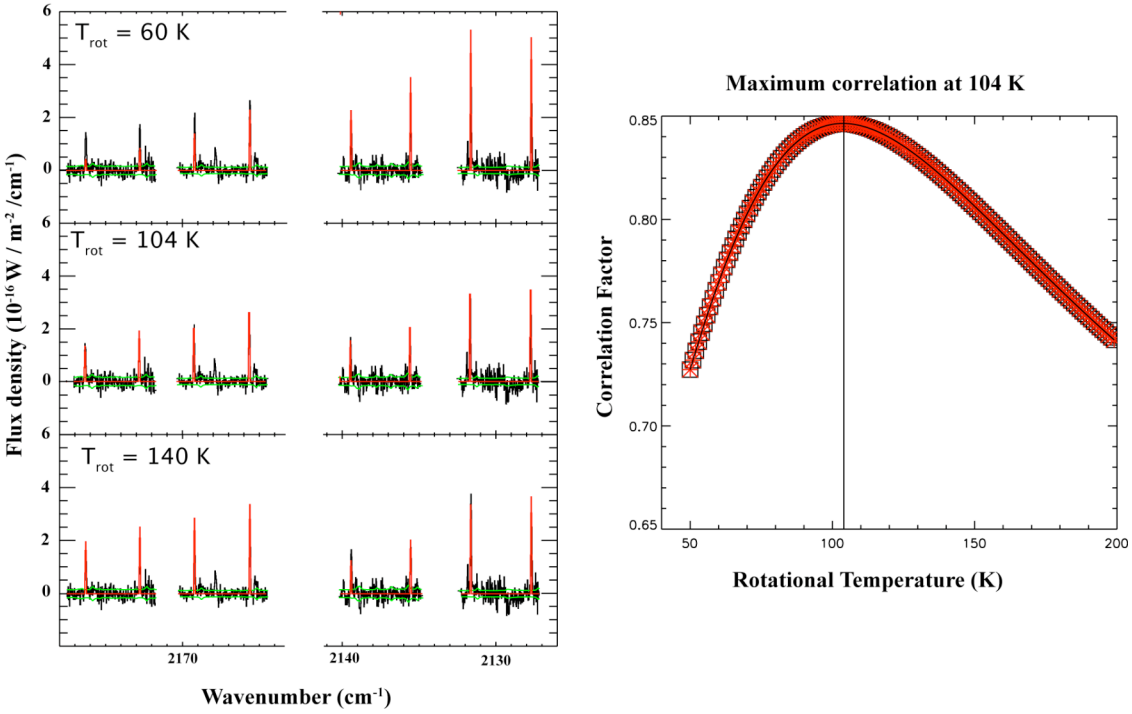

Figure 3.15: Correlation Method (Left) Observed residuals (spectrum minus telluric transmittance function convolved to a resolving power of ~25,000) on May 9, 2004, for a setting that targets CO lines (black traces). Synthetic spectra for CO at rotational temperatures of 60, 104 and 140 K (red traces) show variations in modeled line intensities when T_{rot} is varied about +/-40 K from the optimum value of 114 K. In each panel, in this and subsequent figures showing comet residuals, the stochastic (photon) noise (green traces), and the pixels over which the flux of each line was summed (blue traces), are also indicated. (Right) Corresponding correlogram comparing modeled and observed CO emission over a range in rotational temperature.

104 +/- 7 K, which is within one standard error of the rotational temperature found with the classical Boltzmann method (Fig. 3.5). The nuclear centered production rate now can be calculated:

(3.7) $$Q_{nuc} = \frac{4\pi \cdot \Delta^2 (F_{line} / \kappa)}{f(x)_{0-1} \tau_{co}(g_1)}$$

where Δ is the geometric distance (m), F_{line} (W m^{-2}) is the flux contained in a spectral line, $f(x)_{0\text{-}1}$ is the fraction of the total number of molecules of the parent in the beam as measured from 0 to 1 arc-seconds off the comet's nucleus, τ_{co} and g_1 are the photo-dissociation lifetime (s) and line fluorescence g-factors (W mol^{-1}) at heliocentric distance of R_h = 1 AU, and κ is the atmospheric transmittance at the Doppler-shifted line-center frequency.

The nucleus-centered production rate is determined for each individual line. Then a weighted mean is calculated from all the individual nucleus-centered production rates The terminal production rate is then found by multiplying the weighted mean nucleus-centered production rate by a growth factor, derived from the water measurements of one of the settings, and the average correction factor of all the setting.

(3.8) $$Q_{term} = Q_{nuc} \times \text{GF x } \langle CF \rangle$$

3.9. ADDITIONAL EXCITATION METHOD GRAPHS

The following graphs are additional excitation method plots showing the rotational temperature and mean terminal production rate for H_2O (near 2.9 μm), CO, and H_2CO. Additional information is organized in Tables 4.1-4.3 in the next chapter.

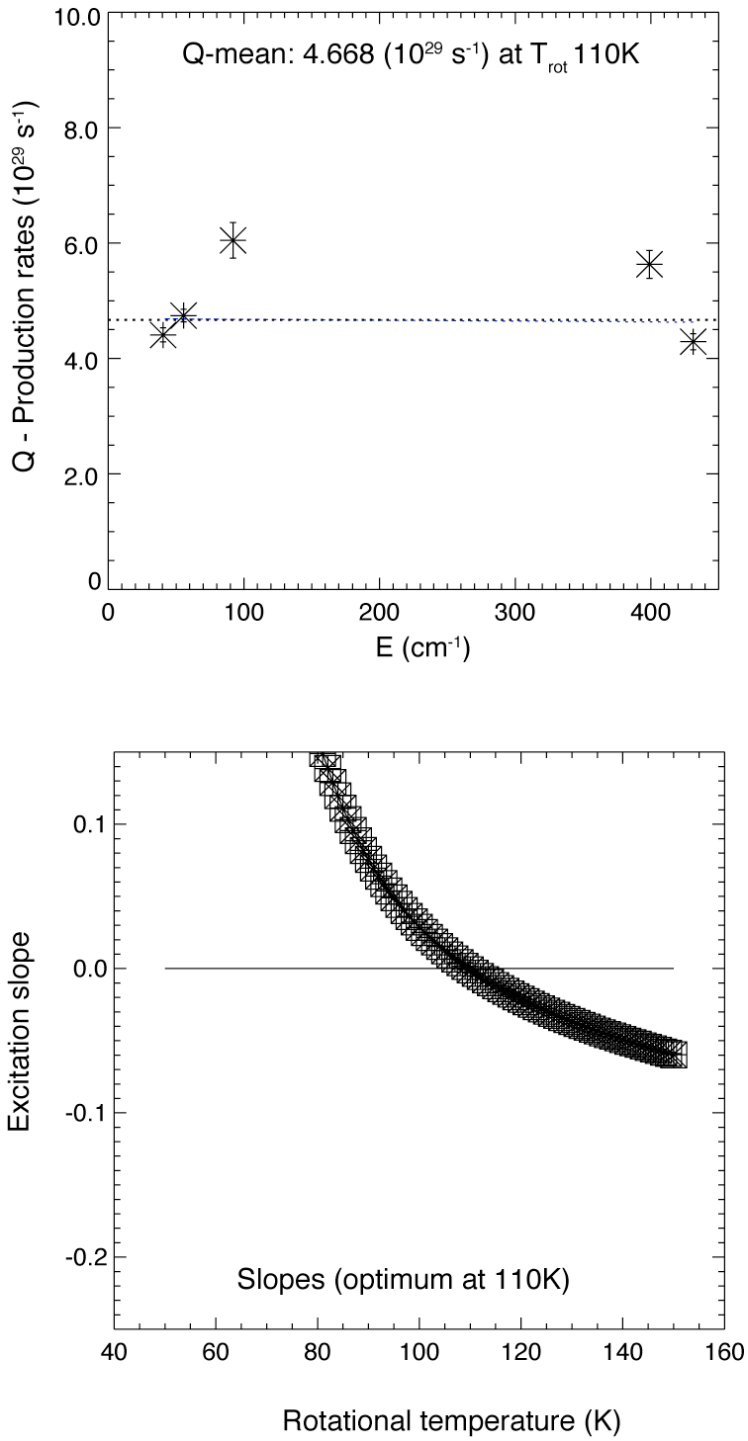

Figure 3.16: Production Rate vs. Energy (top) and excitation slope plot (bottom) for 2.9 μm H_2O observed on May 3, 2004. The rotational temperature was found to be $110\ ^{+4}/_{-4}$ K (1-σ uncertainty; corresponds to spectra in Figure 2.3(A)).

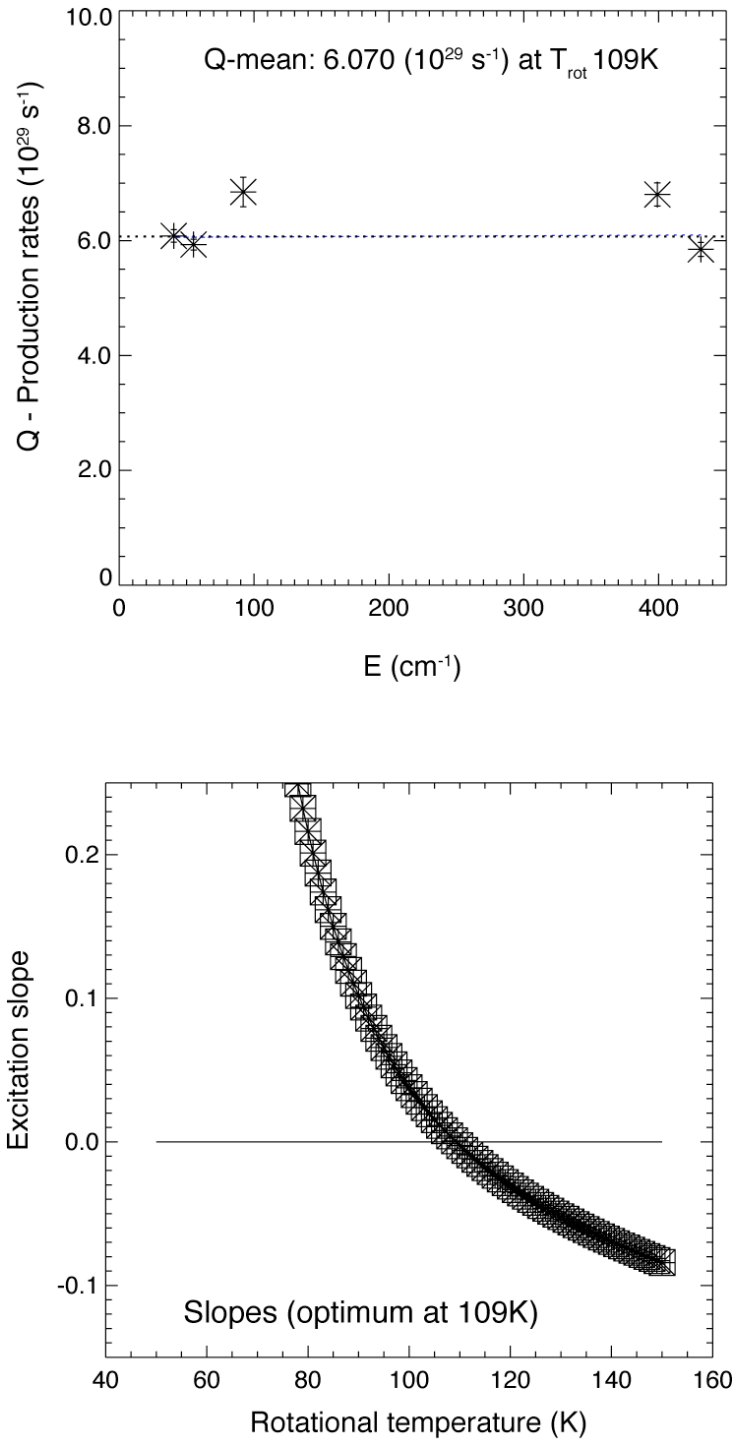

Figure 3.17: Production Rate vs. Energy (top) and excitation slope plot (bottom) for 2.9 μm H_2O observed on May 4, 2004. The rotational temperature was found to be $109\ ^{+2}/_{-1}$ K (1-σ uncertainty; corresponds to spectra in Figure 2.3(B)).

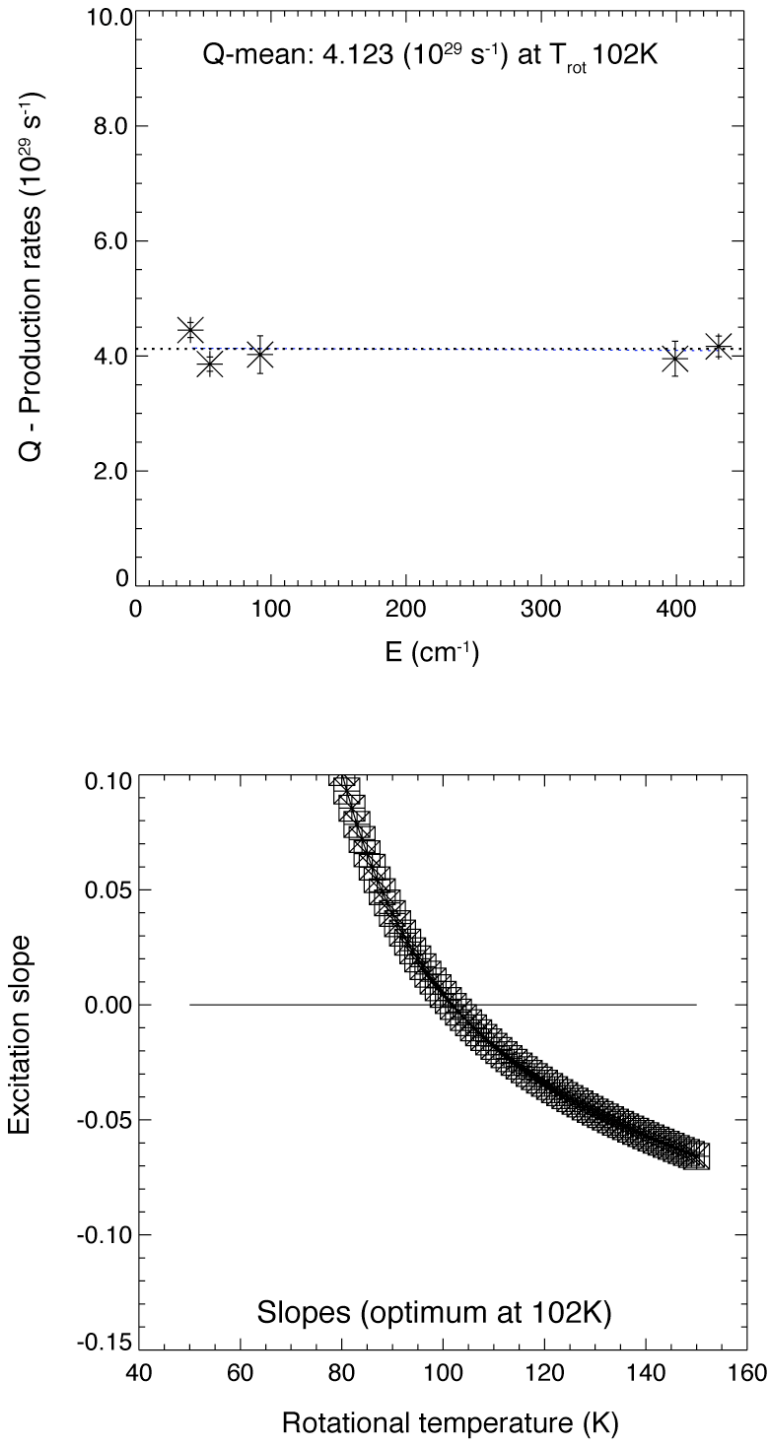

Figure 3.18: Production Rate vs. Energy (top) and excitation slope plot (bottom) for 2.9 μm H_2O observed on May 5, 2004. The rotational temperature was found to be $102\ ^{+2}/_{-2}$ K (1-σ uncertainty; corresponds to spectra in Figure 2.3(C)).

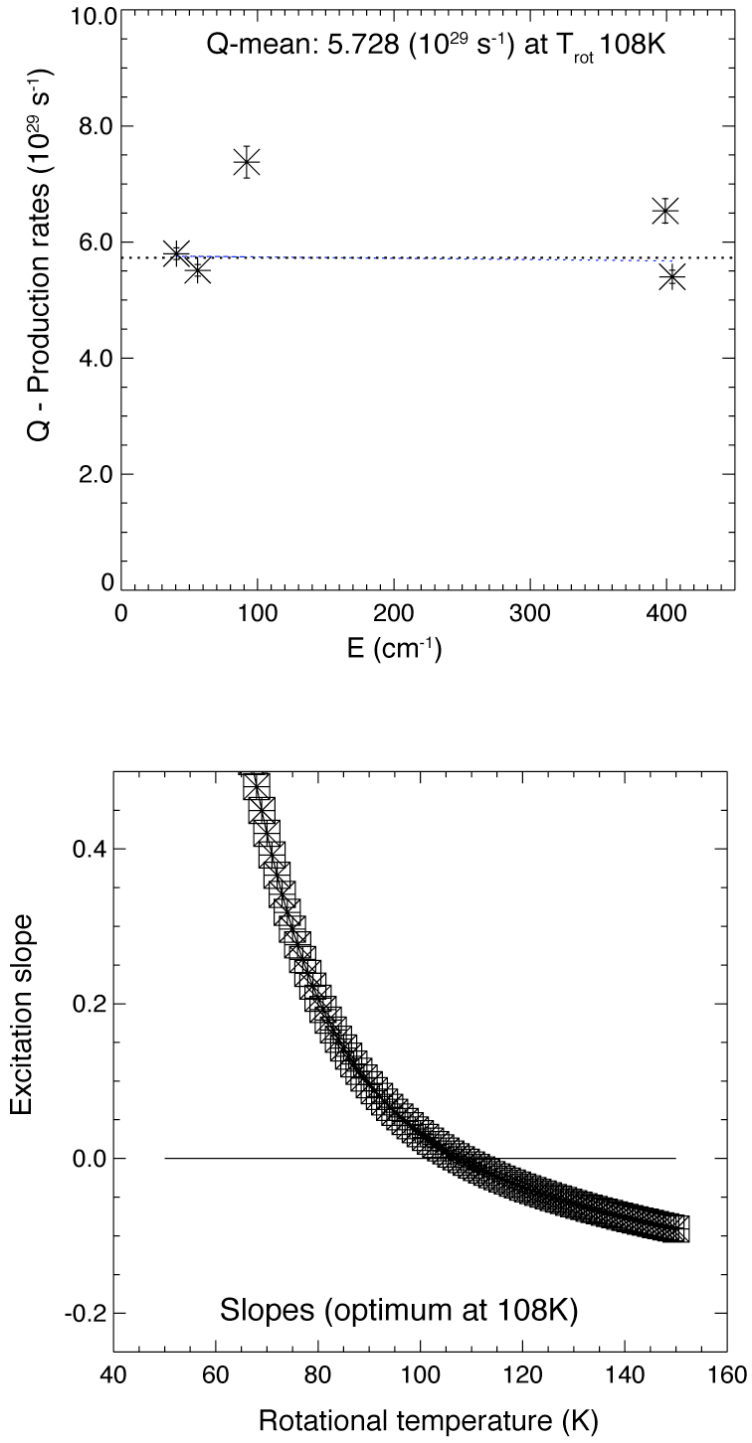

Figure 3.19: Production Rate vs. Energy (top) and excitation slope plot (bottom) for 2.9 μm H_2O observed on May 6, 2004. The rotational temperature was found to be 108 $^{+3}/_{-3}$ K (1-σ uncertainty; corresponds to spectra in Figure 2.3(D)).

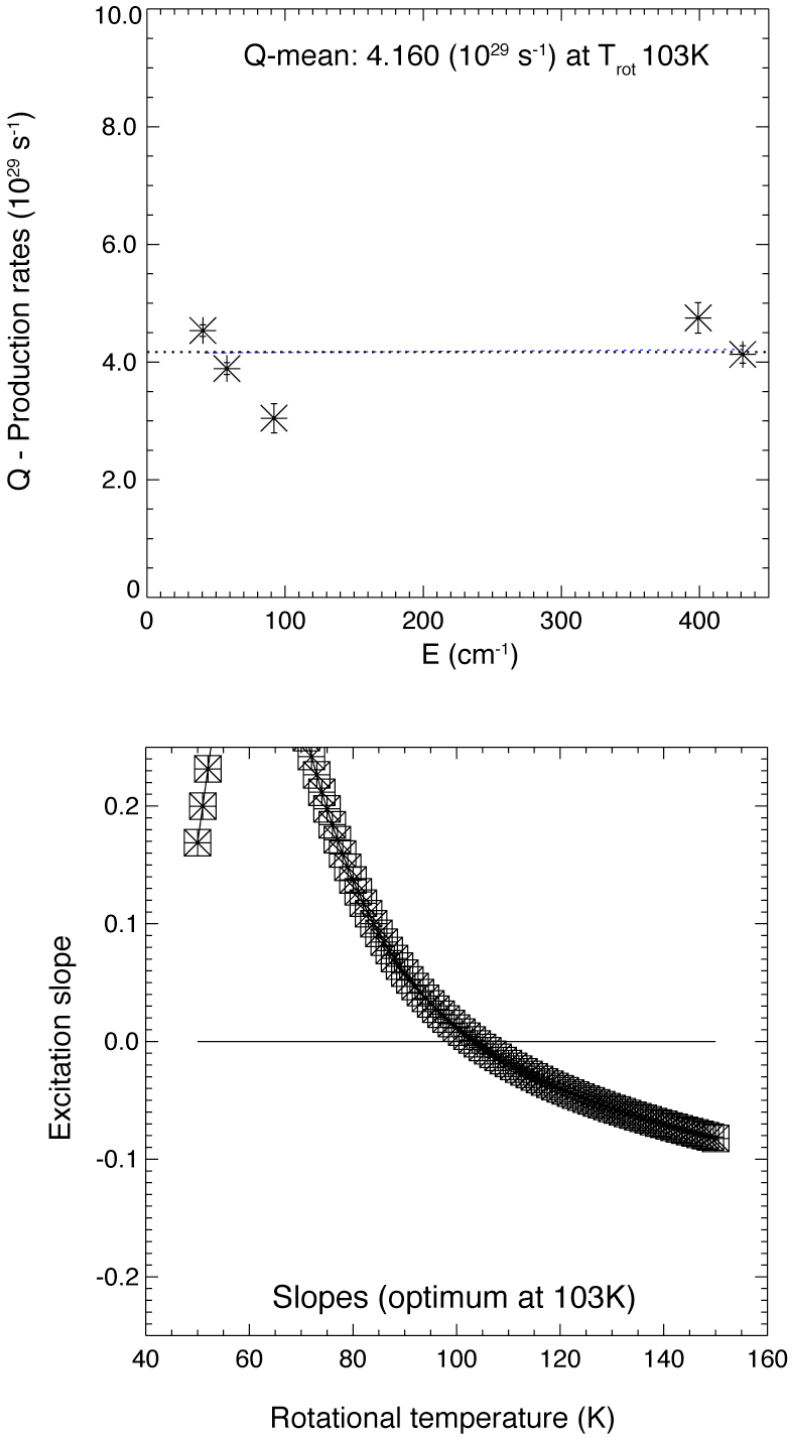

Figure 3.20: Production Rate vs. Energy (top) and excitation slope plot (bottom) for 2.9 μm H_2O observed on May 7, 2004. The rotational temperature was found to be $103\ ^{+4}/_{-3}$ K (1-σ uncertainty; corresponds to spectra in Figure 2.3(E)).

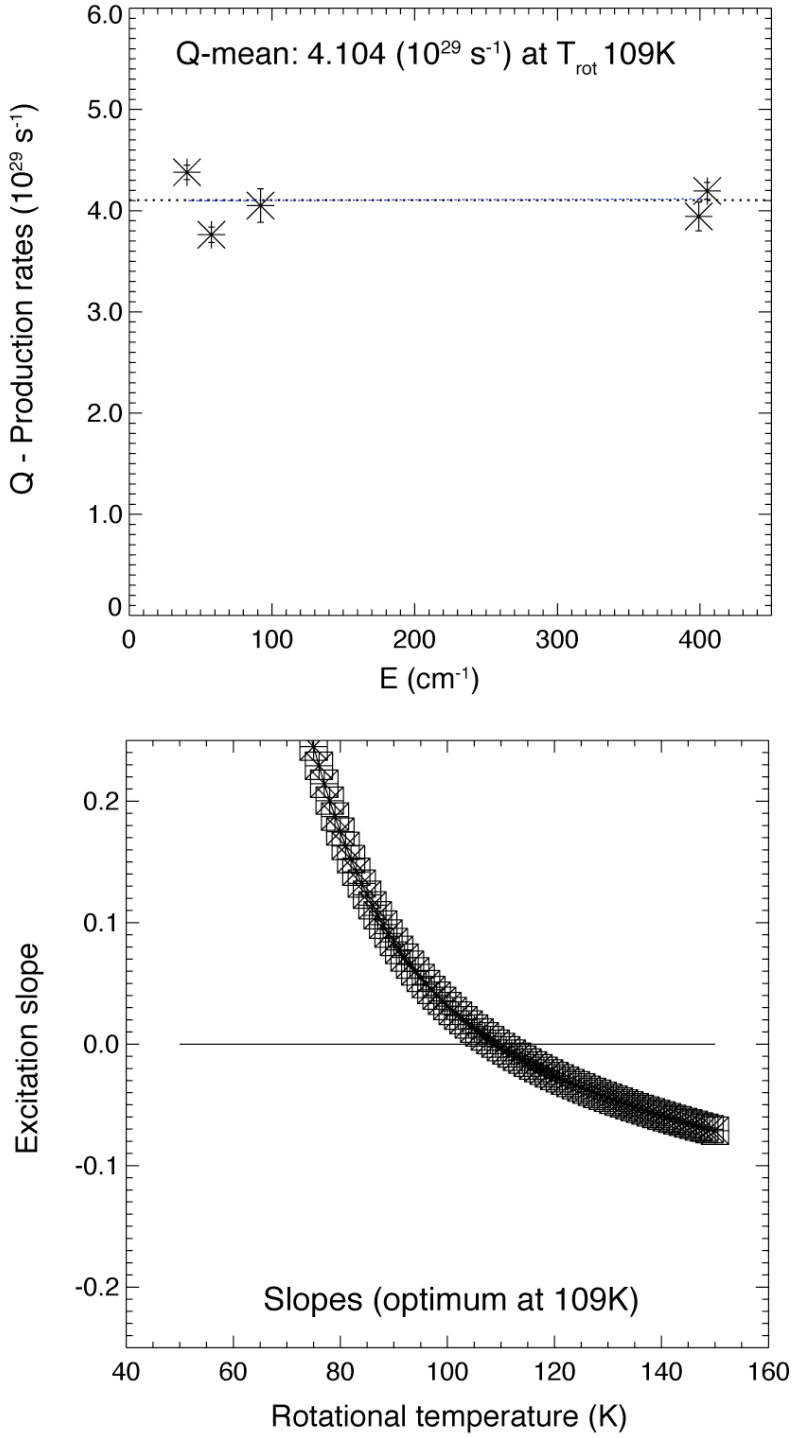

Figure 3.21: Production Rate vs. Energy (top) and excitation slope plot (bottom) for 2.9 μm H_2O observed on May 8, 2004. The rotational temperature was found to be $109\ ^{+3}/_{-2}$ K (1-σ uncertainty; corresponds to spectra in Figure 2.3(F)).

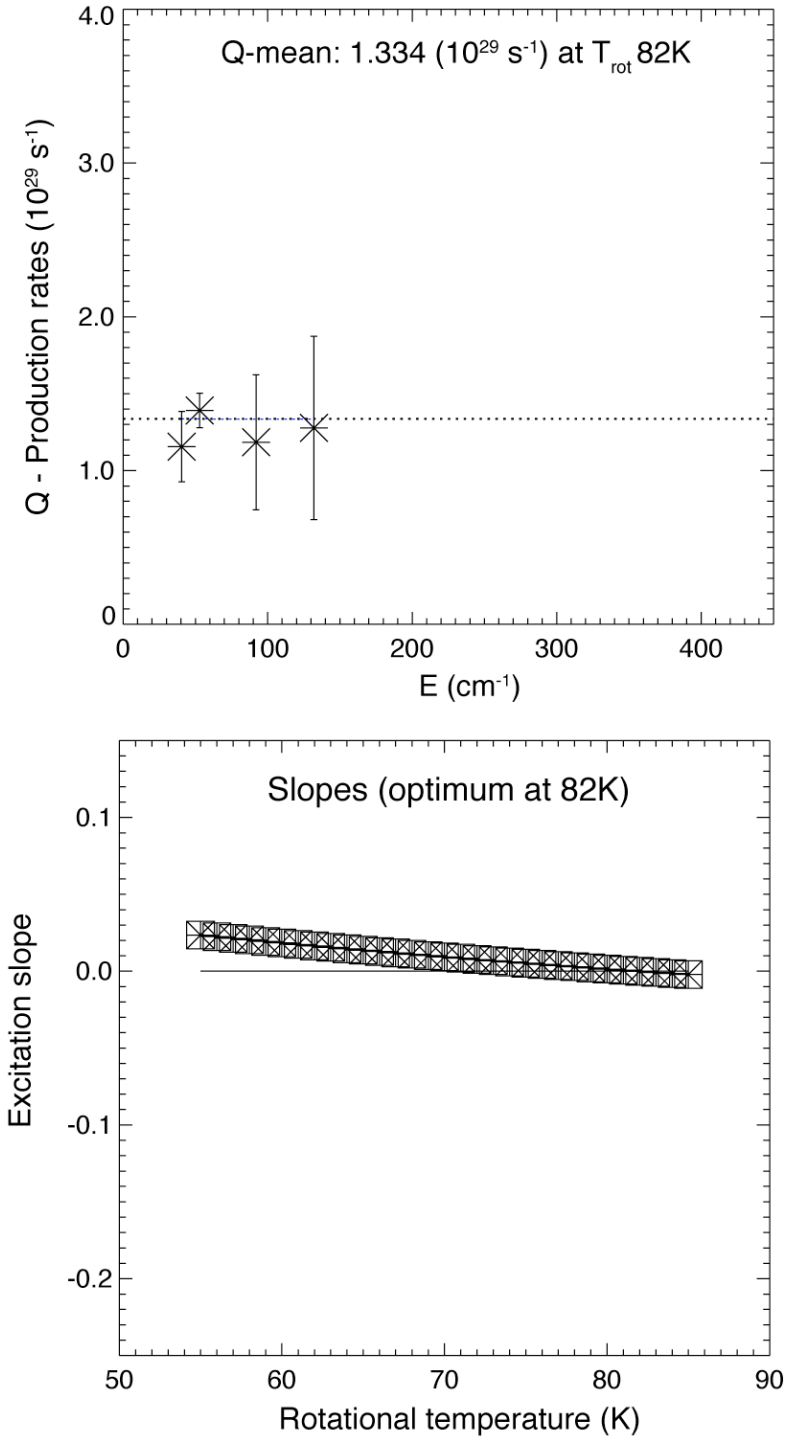

Figure 3.22: Production Rate vs. Energy (top) and excitation slope plot (bottom) for 2.9 μm H_2O observed on June 2, 2004. The rotational temperature was found to be $82\ ^{+32}/_{-27}$ K (1-σ uncertainty; corresponds to spectra in Figure 2.3(H)).

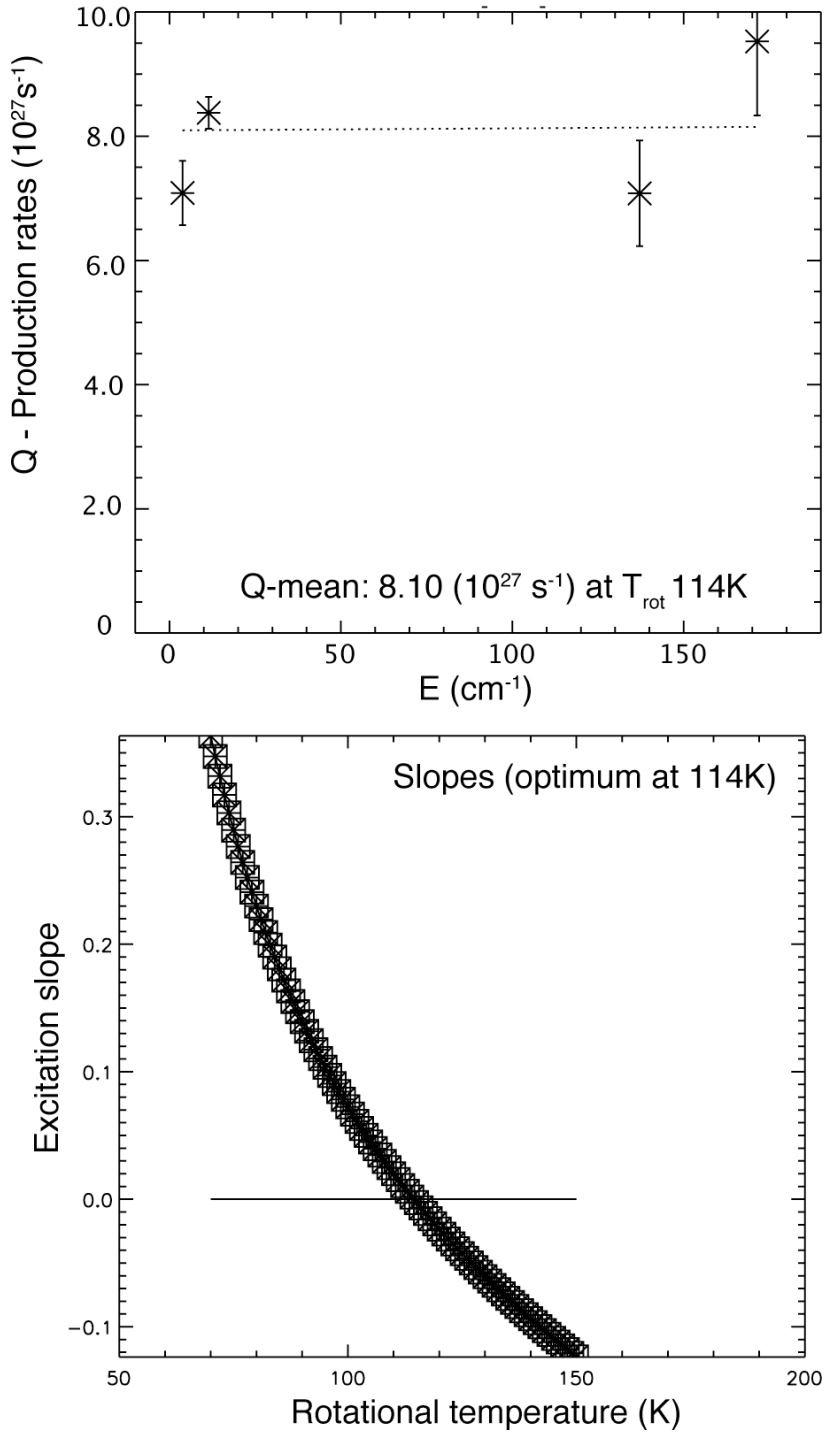

Figure 3.23: Production Rate vs. Energy (top) and excitation slope plot (bottom) for CO observed on May 3, 2004. The rotational temperature was found to be 114 $^{+7}/_{-7}$ K (1-σ uncertainty; corresponds to spectra in Figure 2.2(A)).

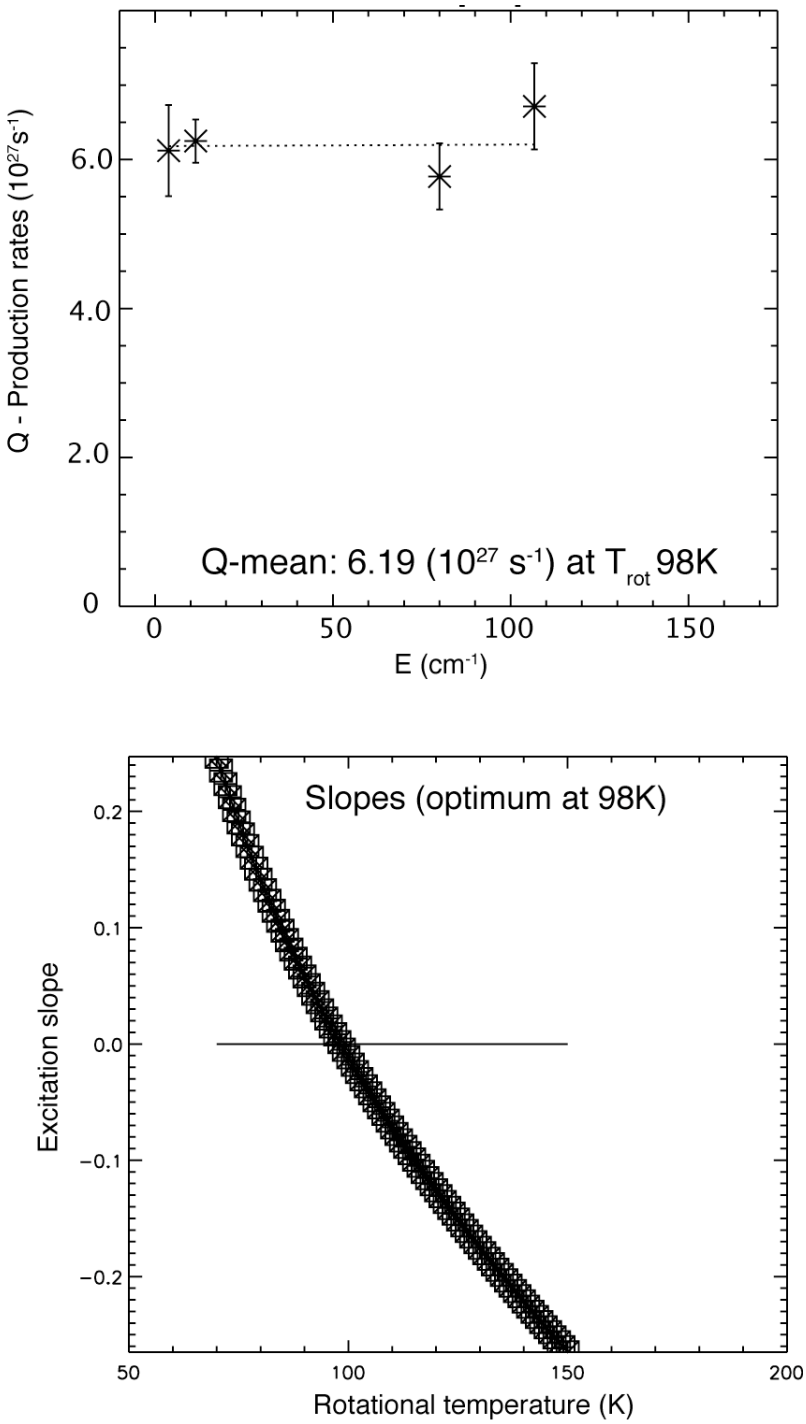

Figure 3.24: Production Rate vs. Energy (top) and excitation slope plot (bottom) for CO observed on May 5, 2004. The rotational temperature was found to be $98\ ^{+7}/_{-6}$ K (1-σ uncertainty; corresponds to spectra in Figure 2.2(C)).

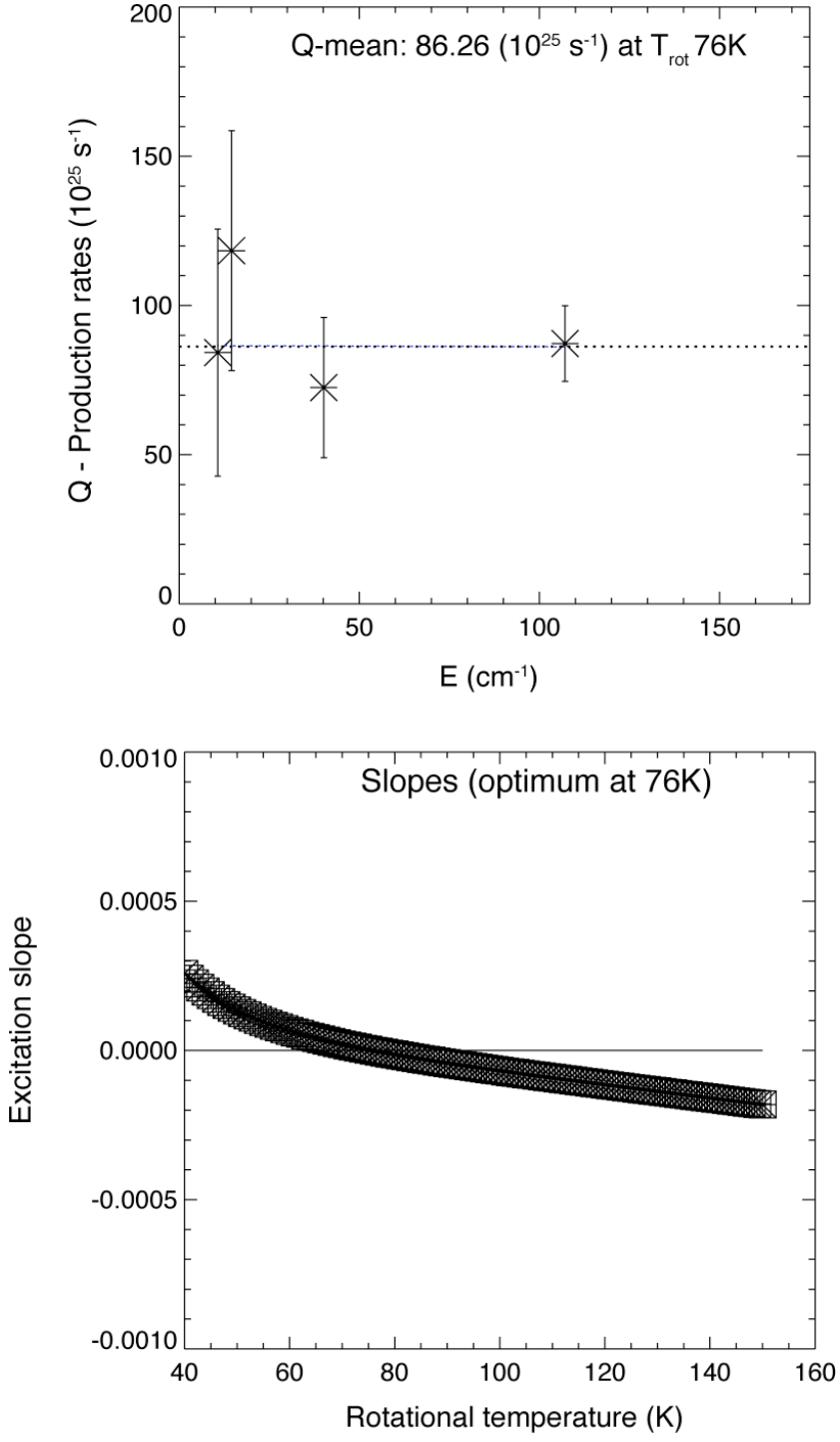

Figure 3.25: Production Rate vs. Energy (top) and excitation slope plot (bottom) for H_2CO observed on June 1, 2004. The rotational temperature was found to be 76 $^{+15}/_{-12}$ K (1-σ uncertainty; corresponds to spectra in Figure 2.5(A)).

CHAPTER IV

RESULTS

4.1. INTRODUCTION

In this chapter I present rotational temperatures and gas production rates for CO, H_2O, CH_3OH, and H_2CO in C/2002 T7 (LINEAR). I also compare production rates at different heliocentric distances (relative to H_2O), and discuss what this reveals about the processing history of the pre-cometary ices.

4.2. WATER IN C/2002 T7 (LINEAR)

Water in C/2002 T7 (LINEAR) was sampled in two separate spectral regions. The first is near 4.7 μm, a region covered by several CO settings and that includes two hot bands of H_2O (ν_1- ν_2 and ν_3- ν_2). Setting CO_D contains a pair of blended water lines from the ν_3-ν_2 band and a weak line (ν_0 = 2135.53 cm^{-1} , 404-313 line of the ν_1-ν_2 band) that is blended with the P2 line of CO. The blended water lines includes one very strong line (000-101) at 2137.37 cm^{-1} and a much weaker line (322-321) at ν_0 = 2137.33 cm^{-1} (the g-factor difference is about a factor of seven at temperature of 100 K; see Table 2.2). Setting CO_E contains two water hot-band lines (2148.19 cm^{-1}, 2151.19 cm^{-1}).

A second region near 2.9 microns contains lines from (at least) six hot bands. Because this region samples lines from several overlapping bands, it is possible to sample a sizeable range in rotational energy within a single CSHELL setting (e.g., H_2O_3A), and thereby obtain a robust measure of rotational temperature that avoids uncertainties associated with the coupling of multiple settings, as is required for CO (previously discussed in Chapter 3; see also the discussion in Dello Russo et al., 2004).

Using hot-band lines near 2.9 μm, rotational temperatures were measured for H_2O on all seven observing dates in early May (Table 5.2). For early June, T_{rot} was measured for water on only one date (Table 5.1). The cometary emissions were much fainter than in early May, and only four of the six 2.9 μm lines were bright enough to include in the excitation analysis.

H_2O production rates for C/2002 T7 (LINEAR) were determined for all seven dates in early May, and for four dates in late May / early June (Table 4.1). The weighted mean H_2O production rate from May 3 - 9 was $4.84 \pm 0.77 \times 10^{29}$ molecules/s. For the period between May 30 and June 2 the corresponding value was $1.20 \pm 0.23 \times 10^{29}$ molecules/s. The uncertainty in terminal production rates includes uncertainties in measured line flux divided by fluorescence g-factor (multiplied by monochromatic transmittance), and in growth factors measured for H_2O. My early May results for the H_2O production rate of C/2002 T7 (LINEAR) are comparable to water production rates derived from OH prompt emission lines (near 3.6 microns) that were also observed using CSHELL on May 5, May 7, and May 9, for which the weighted mean $Q_{(H_2O)} = 3.97 \pm 0.62 \times 10^{29}$ mol/s (DiSanti et al., 2006)

Table 4.1. Production Rates for H_2O in Comet C/2002 T7 (LINEAR)

UT Date 2004	T_{rot} Corr. [a] (K)	T_{rot} Boltz. [b] (K)	f(x) [c]	Setting ID [d]	<F/g> [e] ($x10^9$ molecules/m^2)	Q_{nc} [f] ($x10^{29}$ s^{-1})	GF [g]	Q_{term} [h] ($x10^{29}$ s^{-1})
May 3		114*	0.0175	CO_E	3.10 +/- 0.25	2.80 +/- 0.10	1.61 +/- 0.06	4.51 +/- 0.23
	108	110^{+4}_{-4}	0.0208	H2O_3A	2.76 +/- 0.32	2.41 +/- 0.12	1.93 +/- 0.17	4.67 +/- 0.24
May 4	108	109^{+2}_{-1}	0.0196	H2O_3A	3.86 +/- 0.23	3.26 +/- 0.08	1.86 +/- 0.05	6.09 +/- 0.21
May 5		98*	0.0175	CO_E	2.20 +/- 0.31	1.99 +/- 0.12	1.76 +/- 0.21	3.49 +/-0.48
	103	102^{+2}_{-2}	0.0226	H2O_3A	2.55 +/- 0.19	1.63 +/- 0.05	2.52 +/- 0.23	4.12 +/-0.39
May 6	108	108^{+3}_{-3}	0.0167	H2O_3A	3.94 +/- 0.37	1.63 +/- 0.05	1.88 +/- 0.09	5.73 +/- 0.36
May 7	102	103^{+4}_{-3}	0.0154	H2O_3A	3.13 +/- 0.39	2.44 +/- 0.12	1.70+/- 0.10	4.16 +/- 0.31
May 8	108	109^{+3}_{-2}	0.0142	H2O_3A	3.83 +/- 0.28	2.29 +/- 0.70	1.79 +/- 0.13	4.10 +/- 0.32
May 9		103*	0.0128	CO_D	3.17 +/- 0.04	2.12 +/- 0.03	2.02 +/- 0.16	4.29 +/- 0.35
	102	102^{+2}_{-2}	0.0128	H2O_3A	3.80 +/- 0.34	3.66 +/- 0.17	1.83 +/- 0.06	4.43 +/- 0.20
May 30		80*	0.0085	CO_D	0.356 +/- 0.016	0.41 +/- 0.02	3.58 +/- 0.29	1.50 +/- 0.14
May 31		80*	0.0089	CO_D	0.143 +/- 0.034	0.18 +/- 0.04	4.74 +/- 1.09	0.87 +/- 0.29
June 1		80*	0.0092	CO_D	0.467 +/- 0.028	0.65 +/- 0.04	1.75 +/- 0.14	1.14 +/- 0.07
June 2		80*	0.0096	CO_D	0.135 +/- 0.026	0.20 +/- 0.04	4.27 +/- 0.82	0.87 +/- 0.27
		82^{+32}_{-27}	0.0121	H2O_3A	0.510 +/- 0.058	0.61 +/- 0.08	2.18 +/- 0.24	1.33 +/- 0.18

[a] Optimum rotational temperature based on correlation analysis.

[b] Optimum rotational temperature based on Boltzmann excitation analysis with 1 σ uncertainty

[c] Fraction of all H_2O molecules in a 1" x 3" box based on the photodissociation of lifetime of 7.70 $x10^4$ s for H_2O

[d] Grating setting from Observing Log.

[e] Weighted mean ratio of observed line g-factor times transmittance (10^7 molecules m^{-2}) at the optimum value T_{rot} based on excitation analysis. The uncertainty listed is the larger of the stochastic and standard error.

[f] Nucleus-centered production rate of H_2O (10^{29} molecules s^{-1}) .

[g] Growth factor for the H_2O with 1 σ uncertainty.

[h] Total production rate of H_2O (10^{27} molecules s^{-1}). The error includes the uncertainity in Q_{nc} and the uncertainty in the H_2O growth factor.

* Not enough lines were observed to calculate a rotational tmeperature based on excitation analysis. The rotational temperature calculated for CO on the same date was used for early May observations. For late May/early June observations, a rotational temperature of 80 K was assumed.

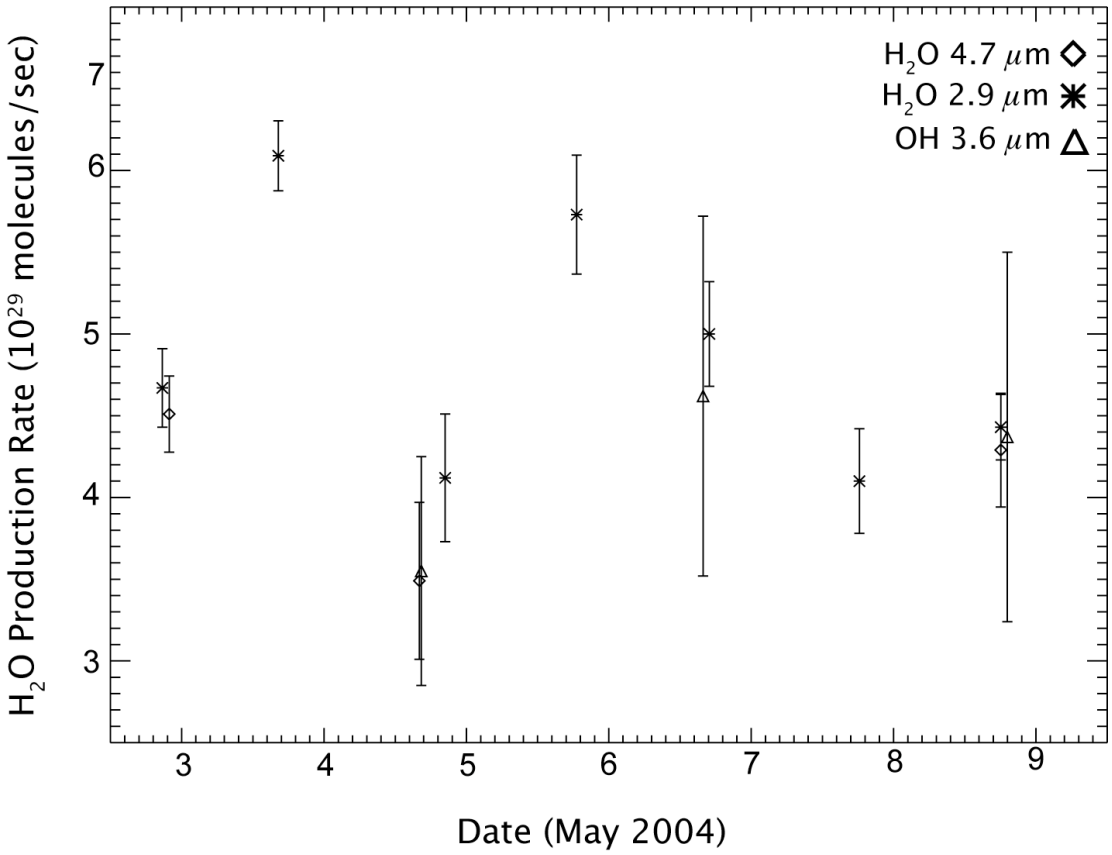

Figure 4.1: Plot of H_2O production rate vs. time for early May observations with 1-σ uncertainty bars. The direct water measurements are from the 4.7 and 2.9 micron regions. The third set of measurements are obtained from the OH lines P(17.5) 1+ and 1- (n_0 =2788.188, 2785.8529 cm^{-1}) stated in DiSanti et al., 2006. This reveals strong agreement in H_2O production rates observed on the same day.

Figure 4.1 compares the individual early May water production rates from these different spectral regions (2.9 μm, 3.6 μm, 4.7 μm). For each day on which H_2O was measured in more than one region, the individual production rates agree within error. The day-to-day water production rates show variability (see section 6.2). My late May / early June H_2O production rates lie within two standard deviations (2σ) of those obtained from sub-millimeter observations in late May 2004 with the 1.1m submillimeter *ODIN* satellite ($Q_{(H_2O)} = 1.92 \pm 0.29 \times 10^{29}$ mol/s, Mean UT: 2004/05/29.2; Biver et al., 2007). Further comparisons with results from other observation of C/2002 T7 (LINEAR) are detailed in Chapter 5.

4.3. CARBON MONOXIDE IN C/2002 T7 (LINEAR)

Observations of C/2002 T7 (LINEAR) were acquired in multiple CO settings on three dates (May 3, 5, and 9). and from these robust rotational temperatures were obtained using the excitation method (Section 3.2). On other dates, only one or two CO rotational lines were observed and T_{rot} could not be determined for CO. Instead, rotational temperatures for water observed on the same date were assumed to apply to CO. This is a reasonable assumption if electron-molecule collisions are the dominant process controlling rotational temperatures in the inner coma (Xie and Mumma, 1992). It is also reasonable given the similar T_{rot} values measured for CO and H_2O when these

were measured independently on the same date (Tables 4.1 and 4.2; see also results presented in Ch. 3).

Rotational temperatures measured independently for CO and H_2O (this work), and for H_2CO (DiSanti et al. 2006), agree within error (Figure 4.2). The early May observations constrain T_{rot} to values between 100 and 110 K (Table 4.1). For late May / early June, the rotational temperature calculations are less reliable because the CO detections were limited to only one or two lines per day. Boltzmann excitation analyses were limited to only two CSHELL settings (H_2CO_B on June 1 and H_2O_3A on June 2; see Table 3.1). Both revealed rotational temperatures consistent with 80 K (76^{+15}_{-12} for H_2CO, 82^{+32}_{-27} for H_2O), although they are relatively poorly constrained compared to the early May results because of lower signal-to-noise ratio (SNR). I adopted $T_{rot} = 80 \pm 20$ K in determining production rates for CO from the late May / early June observations. Table 4.1 lists line-by-line production rates (nucleus-centered and terminal) for CO, along with important parameters used in their calculation (g-factor, observed flux, correction factor, fraction of total number of molecules included within the nucleus-centered beam).

These production rates pertain to native CO, based on the following reasoning. To avoid inclusion of CO produced from (potential) distributed sources (i.e., CO produced in the coma, Meier et al. 1993; DiSanti et al. 1999; 2001), the CO production rate was determined by scaling the nucleus-centered production rate using the growth factor as determined from a water line measured simultaneously within the same CSHELL setting (see Chapter 3 for detailed discussion).

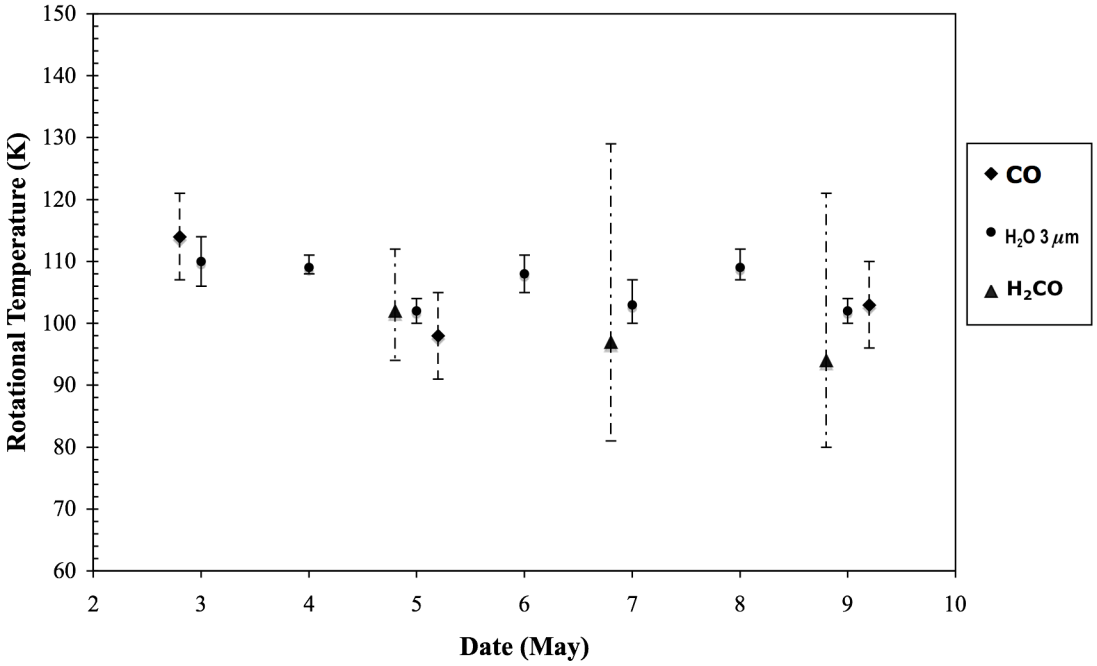

Figure 4.2: CO, H_2O, and H_2CO Rotational Temperatures for Early May 2004 with 1-σ error bars. The CO and H_2O temperatures are from the excitation analysis. The H_2CO temperatures, based on the excitation analysis were presented in DiSanti et al., 2006. Comparing the rotational temperatures for all three molecules indicates that the rotation temperature remained constant during the early May observations.

Table 4.2. Production Rates for CO in Comet C/2002 T7 (LINEAR)

UT Date 2004	T_{rot} Corr. [a] (K)	T_{rot} Boltz. [b] (K)	f(x) [c]	Line	g-factor [d] (10^{-6} ph/s/mol)	F_{line} [e] (10^{-17} W/m^2)	Q_{nc} [f]	CGF [g]	Q_{term} [h] ($x10^{27}$ s^{-1})
May 3	108	114^{+7}_{-7}	0.00102	R0	5.828	0.926 +/- 0.067	4.40 +/- 0.32	1.61+/- 0.06	7.09 +/- 0.58
				R1	10.60	1.995 +/- 0.061	5.20 +/- 0.17		8.37 +/- 0.41
				R7	8.884	1.427 +/- 0.172	2.76 +/- 0.32	2.65 +/- 0.11	7.08 +/- 0.90
				R8	6.621	1.412 +/- 0.177	3.60 +/- 0.45		9.53 +/- 1.25
May 4		109*	0.00103	R2	14.22	1.358 +/- 0.088	6.32 +/- 0.17	1.85 +/- 0.18	11.7 +/- 1.18
				R3	15.56	1.307 +/- 0.085	5.25 +/- 0.16		9.72 +/- 0.99
May 5	101	98^{+7}_{-6}	0.00106	R0	6.667	1.377 +/- 0.138	3.48+/- 0.35	1.76 +/- 0.214	6.12 +/- 0.96
				R1	10.20	2.525 +/- 0.118	3.55 +/- 0.17		6.25 +/- 0.81
				R5	13.42	2.637 +/- 0.203	4.17 +/- 0.32	1.39 +/- 0.332	5.77 +/- 1.45
				R6	10.68	2.444 +/- 0.211	4.85 +/- 0.42		6.72 +/- 1.71
May 7		103*	0.00090	R5	13.35	3.143 +/- 0.124	3.96 +/- 0.16	2.04 +/- 0.08	8.07 +/- 0.46
				R6	11.19	3.374 +/- 0.128	5.23 +/- 0.20		10.7 +/- 0.60
May 8		109*	0.00083	R5	13.55	2.475 +/- 0.351	2.96 +/- 0.42	2.27 +/- 0.36	6.72 +/- 1.42
				R6	11.19	2.541 +/- 0.384	3.68 +/- 0.55		8.36 +/- 1.82
May 9	105	103^{+7}_{-7}	0.00074	P4	19.67	4.010 +/- 0.105	3.21 +/- 0.09	1.63 +/- 0.05	5.68 +/- 0.99
				P3	17.25	4.605 +/- 0.093	4.16 +/- 0.09		7.36 +/- 1.27
				P2	12.76	2.354 +/- 0.190	3.04 +/- 0.23	2.02 +/- 0.16	5.37 +/- 1.01
				P1	6.721	1.848 +/- 0.131	4.35 +/- 0.30		7.70 +/- 1.43
				R5	13.50	3.150 +/- 0.966	3.61 +/- 0.11	1.57 +/- 0.16	6.39 +/- 1.11
				R6	10.93	2.424 +/- 0.104	3.42 +/- 0.15		6.06 +/- 1.07
				R7	8.337	1.994 +/- 0.120	3.74 +/- 0.22	1.86 +/- 0.20	6.61 +/- 1.20
				R8	5.781	1.893 +/- 0.123	5.04 +/- 0.32		8.92 +/- 1.64
May 30		80*	0.00049	P2	15.91	0.516 +/- 0.042	0.900 +/- 0.07	3.58 +/- 0.29	3.20 +/- 0.37
May 31		80*	0.00051	P2	15.91	0.301 +/-0.065	0.569 +/- 0.12	4.74 +/- 1.09	2.70 +/- 0.85
June 1		80*	0.00053	P2	15.91	0.597 +/- 0.052	1.22 +/- 0.11	1.75 +/- 0.14	2.14 +/- 0.19
				P1	8.494	0.501 +/- 0.059	1.92 +/- 0.23		3.36 +/- 0.40
June 2		80*	0.00055	P2	15.91	0.191 +/- 0.053	0.42 +/- 0.12	4.28 +/- 0.821	1.81 +/- 0.61

[a] Optimum rotational temperature based on correlation analysis.
[b] Optimum rotational temperature based on Boltzmann excitation analysis with 1 σ uncertainty
[c] Fraction of all (native) CO molecules in a 1" x 3" box based on the photodissociation lifetime of 1.335 $x10^6$ s for CO.
[d] g-factor of the CO ro-vibrational line at the optimal value of T_{rot}
[e] Transmittance corrected observed line flux.
[f] Nucleus-centered production rate of CO (10^{27} molecules s^{-1})
[g] Corrected growth factor (CGF)for the grating setting with 1-σ uncertainty. The correction factor is based on the observed growth factor of H_2O on the same date and the continuum nuclear-centered ratio of the CO and H_2O grating settings.
[h] Total production rate of CO (10^{27} molecules s^{-1}). The error includes the uncertainity in Q_{nc} and the uncertainty in the setting corrected growth factor.
*Not enough lines were observed to calculate a rotational temperature based on excitation analysis. The rotational temperature calculated for 2.9 μm H_2O on the same date was used for early May observations. For late May/early June observations, a rotational temperature of 80 K was assumed.

4.4. FORMALDEHYDE (H_2CO) and METHYL ALCOHOL (CH_3OH) IN C/2002 T7 (LINEAR)

Formaldehyde (H_2CO) was detected in C/2002 T7 (LINEAR) on two dates in early June (Table 4.3). For 1 June 2004, I retrieved a rotational temperature of $78\ ^{+17}_{-13}$ K for H_2CO, using four spectral regions which each include multiple individual lines (ν_1 and ν_5 Q-branch, central rest frequencies = 2781.01 cm^{-1}; 2781.84 cm^{-1}; 2782.15 cm^{-1}; 2782.46 cm^{-1}; see Fig 4(a)-(c) in Disanti 2006 for details on individual H_2CO lines in this region). The growth factor was determined from a co-measured OH line (ν_0 = 2785.85 cm^{-1}, see Figure 2.4A), which by its nature traces the spatial distribution of their parent (H_2O) molecules (Bonev 2005; Bonev et al. 2006; Mumma et al. 2001a). On 2 June 2004, only one H_2CO emission feature (multiple ν_1 Q-branch lines near 2781.0) could be accurately measured. This was due to lower SNR as there was less on-source observing time compared with the previous day. The weighted mean $Q(H_2CO)$ for these two dates was $(9.43 \pm 1.66) \times 10^{26}$ molecules/s. Early May observations of H_2CO in C/2002 T7 (LINEAR) were published for three dates (DiSanti et al., 2006). I also include those values in my analysis of the H_2CO heliocentric dependence (section 5.2).

Methanol was detected in C/2002 T7 (LINEAR) on five dates in early May and one date in late May (Table 4.3). The CH_3OH setting used encompasses the Q-branch (at 3.516 microns, or 2844 cm^{-1}) and two OH lines (prompt emission). The CH_3OH production rate was found by integrating the flux over the Q-branch (Table 4.3), a

relatively strong and broad feature. I measured very high signal-to-noise spatial profiles for methanol, which resulted in growth factors having low relative uncertainties. The g-factor for the Q-branch is relatively insensitive to rotational temperature, and was taken to be 1.27×10^{-5} at 50 K to 9.54×10^{-6} at 100 K (both in units of photons s^{-1} $molecule^{-1}$). Because of this, and also because of line-by-line inadequacies for the existing fluorescence model, it was not possible to measure rotational temperatures for CH_3OH. Therefore, its T_{rot} was adopted from that measured for other molecules at the respective times (100 K in early May and 80 K in late May).

Table 4.3. Production Rates for CH_3OH and H_2CO in Comet C/2002 T7 (LINEAR)

UT Date 2004	T_{rot} Boltz. [b] (K)	f(x) [c]	Setting ID [d]	g-factor [d] (10^{-6} ph/s/mol)	F_{line} [e] (10^{-17} W/m^2)	Q_{nc} [f]	GF [g]	Q_{term} [h] (x10^{28} s^{-1})
May 3	100	0.01951	CH_3OH_A	9.54	8.07 +/- 0.08	1.30 +/- 0.01	1.61 +/- 0.032	2.10 +/- 0.02
May 5	100	0.01945	CH_3OH_A	9.54	5.44 +/- 0.11	0.80 +/- 0.02	1.66 +/- 0.06	1.32 +/- 0.06
May 7	100	0.01438	CH_3OH_A	9.54	5.40 +/- 0.09	0.74 +/- 0.01	2.65 +/- 0.05	1.96 +/- 0.05
May 8	100	0.00420	CH_3OH_A	9.54	3.15 +/- 0.05	1.35 +/- 0.22	1.49 +/- 0.13	1.92 +/- 0.35
May 9	100	0.01202	CH_3OH_A	9.54	5.981 +/- 0.08	0.72 +/- 0.01	2.18 +/- 0.04	1.57 +/- 0.04
May 30	80	0.00787	CH_3OH_A	10.1	0.766 +/-0.022	0.156 +/- 0.006	2.88 +/- 0.11	0.450 +/- 0.024
June 1	76^{+15}_{-12}	0.1367	H_2CO_B	21.8	0.171 +/- 0.044	0.0232 +/-0.0028	3.73 +/- 0.95	0.0865 +/- 0.0244
June 2	76*	0.1365	H_2CO_B	11.0	0.120 +/- 0.024	0.0353 +/- 0.0071	3.12 +/- 0.76	0.110 +/- 0.0347

[a] Optimum rotational temperature based on correlation analysis.

[b] Optimum rotational temperature based on Boltzmann excitation analysis with 1 σ uncertainty

[c] Fraction of all H_2CO or CH_3OH molecules in a 1" x 3" box based on the photodissociation of lifetime of 4.5 x10^3 s for H_2CO and 8.3 x10^4 s for CH_3OH.

[d] Grating setting from Observing Log.

[d] Total sum of g-factors of selected molecular at the optimal value of T_{rot}

[e] Total transmittance corrected observed line flux.

[f] Nucleus-centered production rate of H_2O (10^{29} molecules s^{-1}) .

[g] Growth factor with 1 σ uncertainty.

[h] Total production rate of H_2CO or CH_3OH (10^{28} mol s^{-1}). The error includes the uncertainity in Q_{nc} but not the uncertainty in the GF

* Not enough lines were observed to calculate a rotational temperature based on excitation analysis. A rotational temperatures of 100 K and 75 K were used for CH_3OH based on rotational temperatures of CO and H_2O. For the June 2 H_2CO observation, the June 1 H_2CO rotational temperature was used.

4.5. MIXING RATIOS RELATIVE TO WATER

Water is the dominant parent volatile in comets. For this reason, volatile abundances of minor species are often described in terms of the "mixing ratio" between that volatile species and H_2O (Hoban, et al. 1993; Mumma et al., 1996; Bonev, 2005):

(4.1) $$MR(X) = \frac{Q(X)}{Q(H_2O)}$$

The mixing ratio of a species is useful because it represents a measure of the comet's chemistry that is independent of overall activity. The global production rates are highly dependent on a number of factors, many of which do not directly relate to composition. These factors include heliocentric distance, orbital position (e.g., pre- or post-perihelion), fractional active surface of the nucleus, and dynamical class. On the contrary, mixing ratios can reveal information regarding formation temperature and ice processing history (Mumma, Weissman, & Stern, 1993).

The mixing ratios of CO, CH_3OH, and H_2CO for individual dates are given in Table 4.4, and the weighted mean values for Early May and late May/ early June are listed in Table 4.5.

Table 4.4. Mixing Ratios in Comet C/2002 T7 (LINEAR)

UT Date 2004	Q(CO) [a] ($x10^{27}$ s^{-1})	Q(H_2CO) [b] ($x10^{27}$ s^{-1})	Q(CH_3OH) [c] ($x10^{28}$ s^{-1})	Q(H_2O) [d] ($x10^{29}$ s^{-1})	MR(CO) [e]	MR(H_2CO) [f]	MR(CH_3OH) [g]	MR(CO) [e] / MR(CH_3OH) [g]
May 3	8.10 +/- 0.58		2.10 +/- 0.02	4.59 +/- 0.17	1.76 +/- 0.14		4.58 +/- 0.18	0.38 +/- 0.034
May 4	10.6 +/- 1.43			6.09 +/- 0.21	1.74 +/- 0.24			
May 5	6.19 +/- 1.68		1.32 +/- 0.06	3.78 +/- 0.45	1.63 +/- 0.48	0.75 +/- 0.12 [h]	3.49 +/- 0.44	0.47 +/- 0.15
May 6				5.73 +/- 0.36				
May 7	9.06 +/- 1.31		1.96 +/- 0.05	4.16 +/- 0.31	2.17 +/- 0.35	0.94 +/- 0.20 [h]	4.71 +/- 0.37	0.46 +/- 0.083
May 8	7.32 +/- 1.39		1.92 +/- 0.35	4.10 +/- 0.32	1.79 +/- 0.37		4.68 +/- 0.93	0.38 +/- 0.11
May 9	6.48 +/- 0.79		1.57 +/- 0.04	4.40 +/- 0.17	1.48 +/- 0.19	0.76 +/- 0.15 [h]	3.57 +/- 0.17	0.41 +/- 0.057
May 30	3.20 +/- 0.37		0.450 +/- 0.024	1.50 +/- 0.14	2.13 +/- 0.32		3.00 +/- 0.32	0.71 +/- 0.13
May 31	2.70 +/- 0.85			0.87 +/- 0.29	3.10 +/- 1.42			
June 1	2.35 +/- 0.85	0.865 +/- 0.244		1.13 +/- 0.07	2.08 +/- 0.76	0.77 +/- 0.22		
June 2	1.81 +/- 0.61	1.10 +/- 0.347		1.19 +/- 0.33	1.52 +/- 0.66	0.92 +/- 0.39		

[a] Weighted mean of the daily production rate of native carbon monoxide (10^{27} molecules s^{-1}).
[b] Weighted mean of the daily production rate of native formaldehyde (10^{27} molecules s^{-1}).
[c] Weighted mean of the daily production rate of methanol (10^{28} molecules s^{-1}).
[d] Weighted mean of the daily production rate of (10^{29} molecules s^{-1}).
[e] Abundance of carbon monoxide relative to water (percent).
[f] Abundance of formaldehyde relative to water (percent).
[g] Abundance of methanol relative to water (percent).
[h] from DiSanti et al., 2006, ApJ, 650, 470-483.

Table 4.5. Mean Mixing Ratios in Comet C/2002 T7 (LINEAR)

	X(CO) [a]	X(H_2CO) [b]	X(CH_3OH) [c]
Early May	1.72 +/- 0.20	0.79 +/- 0.09 [d]	4.00 +/- 0.57
Late May/ Early June	2.06 +/- 0.42	0.81 +/- 0.11	3.00 +/- 0.32

[a] Mean abundance of carbon monoxide relative to water (percent).
[b] Mean abundance of formaldehyde relative to water (percent).
[c] Mean abundance of methanol relative to water (percent).
[d] from DiSanti et al., 2006, ApJ, 650, 470-483.

4.6. Summary

Water, carbon monoxide, formaldehyde, and methanol were all detected in comet C/2002 T7 (LINEAR) on several dates. The H_2O production rate averaged 4.84 +/- 0.77 x 10^{29} molecules/s in Early May and 1.20 +/- 0.23 x10^{29} molecules/s in late May/early June. Water production rates from different spectral regions (2.9 micron; 4.7 micron; OH lines around 3.6 microns) agreed within error when take on the same date. Independent rotational temperatures were measured for both CO and H_2O in early May. Both agreed within error, and fell in the range of 100 -115 K. Rotational temperatures for H_2CO and H_2O were around 80 K for early June. The day-to-day H_2O production showed variability in early May. Late May and early June provided less observations with larger errors, so it is difficult to determine if the day-to-day variability continued at that later time. The mixing ratios for CO were 1.70 ± 0.14% (early May) and 2.06 ± 0.42% (late May/early June). The mixing ratios of H_2CO were 0.79 ± 0.09% (early May; DiSanti et al. 2006) and 0.81 ± 0.11%. Methanol was enhanced in C/2002 T7 (LINEAR) with mixing ratios of 4.00 ± 0.57% (early May) and 3.00 ± 0.32% (late May/early June). The agreement (within error) of mixing ratios between $R_h \sim 0.6$ and 1.0 AU suggests that the composition of Comet C/2002 T7 (LINEAR) remained constant with depth in the nucleus (further discussed in Chapter 5).

CHAPTER V

Discussion of the Chemistry of C/2002 T7 (LINEAR)

5.1. INTRODUCTION

This chapter presents a discussion of the scientific conclusions that can be drawn from the observational results of C/2002 T7 (LINEAR). First, I examine the daily variability of the production rates and respective mixing ratios of H_2O, CO, H_2CO, and CH_3OH, to explore potential short-term changes in the comet's chemistry. Second, I present the production rates in terms of heliocentric distance, and look for any long-term heterogeneity in the nucleus. Finally, I compare and contrast the abundances of oxidized carbon in C/2002 T7 (LINEAR) with those reported in the refereed literature for other comets, and examine how the results presented in this thesis add to the overall picture of creating a cometary taxonomy based on chemistry.

5.2. HELOCENTRIC DEPENDENCE OF THE PRODUCTION RATES

Comet C/2002 T7 (LINEAR) was observed over a range of heliocentric distances, allowing a test for longer-term post-perihelion changes in chemistry. As a comet travels through the inner Solar System, its surface (or near-surface) ice sublimates, exposing deeper layers. If a comet formed in one region of the early Solar System was then ejected to another part (such as the Oort cloud) and exposed to a different radiative environment (in particular interstellar cosmic ray processing), some heterogeneity in nucleus composition might be expected.

The first analysis step was to determine if the individual native molecular production rates change with heliocentric distance. A log-log plot was used to establish a best-fit

slope. Daily mean production rates are shown; for H_2O, those from the 2.9 and 4.7 μm regions are indicated by separate points. The resulting solution for water was found to be $Q(H_2O) = 10^{29.11 \pm 0.02} r^{-3.41 \pm 0.12}$. It is important to emphasize that this represents the mean water production rate – it does not account for the overall short term variability seen in early May (see Section 6.2). Nonetheless this information can be used to establish how the water production rate decreases with increasing heliocentric distance. This can then be applied together with a sinusoid, to better fit the water production data points (see Figure 5.4). Similar calculations were performed for CO, H_2CO, and CH_3OH. The resulting heliocentric dependences were: $Q(CO) = 10^{27.45 \pm 0.04} r^{-2.47 \pm 0.28}$; $Q(H_2CO) = 10^{27.04 \pm 0.08} r^{-2.73 \pm 0.53}$; and $Q(CH_3OH) = 10^{27.65 \pm 0.02} r^{-3.66 \pm 0.12}$.

The four molecular production rate functions now can be used to test for changes in mixing ratios with heliocentric distance. For example, the CO mixing ratio would be $Q(CO)\{r\}/Q(H_2O)\{r\}$, its uncertainty based on the errors in slopes and intercepts of the two production rate functions. The results for CO, H_2CO, and CH_3OH are shown in the lower plots in Figures 6.5 -6.7, with 1-σ error bars. As an additional check, the mean early May and early June mixing ratios from Table 4.5 are plotted as well. Both CO and H_2CO strongly show a flat slope in term of mixing ratio vs. heliocentric distance. There is no evidence that that there is any heterogeneity in C/2002 T7 (LINEAR) in reference to carbon monoxide or formaldehyde. Methanol is also consistent with no change in its mixing ratio between early May and late May 2004, however this interpretation is limited as only one measurement of methanol was obtained for late May. If the methanol

observed from C/2002 T7 (LINEAR) happened to be abnormally high or low on May 30, 2004, this would greatly affect the mixing ratio.

Comet C/2002 T7 (LINEAR) is a dynamically new comet from the Oort cloud (Mardsen, 2003; Nakano, 2003, 2006). Cometary nuclei in the Oort cloud are exposed to cosmic ray irradiation and are expected to develop an outer "crust" of nonvolatile material to depth about 100 g cm^{-2} (Johnson, et al., 1987). Sufficiently rapid thermal increase on a comet during close approach to the Sun can break the radiation-processed "crust", releasing volatiles and giving rise to a cometary burst (Johnson et al., 1987). The early May and early June 2004 observations occurred after perihelion, so it is likely that this outer "crust" had been eroded away as a result of sustained solar insolation. Indeed, this appears to be the case based on no observed change in the composition of oxidized carbon between R_h = 0.66 and 1.03 AU. It is possible that C/2002 T7 (LINEAR) lost its radiation-processed crust earlier in its orbit, prior to it reaching perihelion at R_h = 0.62 AU in late April 2004. Thus it may be reasonable to expect homogeneity in the comet nucleus post-perihelion.

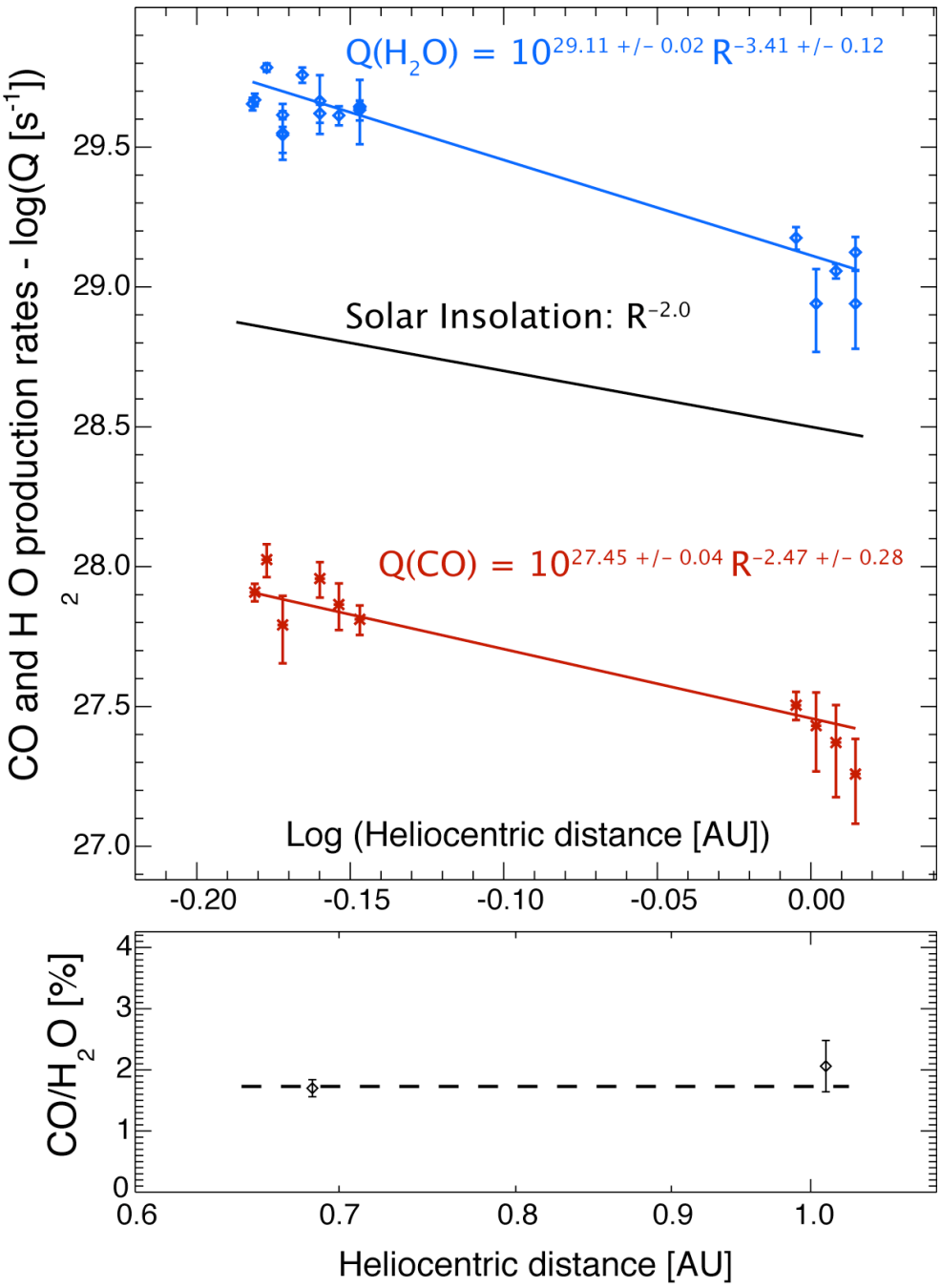

Figure 5.1: (Top) Log of CO (bottom) and H_2O (top) production rate vs. log comet heliocentric distance. The third line (center) represents the slope corresponding to solar insolation (R^{-2}). (Bottom): CO/H_2O mixing ratio vs. Heliocentric distance. The points represent the weighted mean of early May and late May/early June CO/H_2O mixing ratios with 1-σ error bars. The mixing ratio does not seem have changed between the two observing periods.

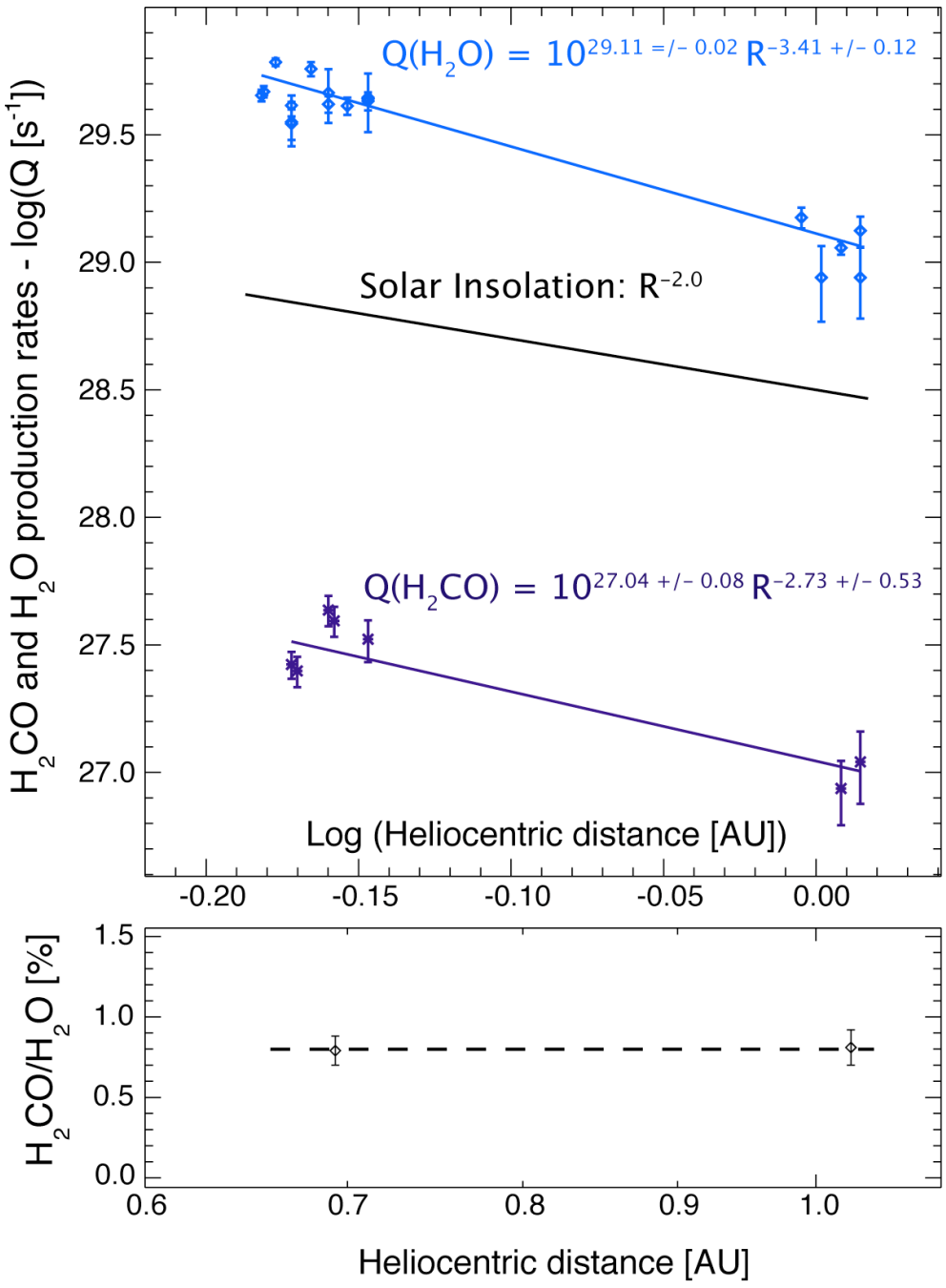

Figure 5.2: (Top) Log of H_2CO (bottom) and H_2O (top) production rate vs. log comet heliocentric distance. The third line (center) represents the slope corresponding to solar insolation (R^{-2}). (Bottom): H_2CO/H_2O mixing ratio vs. heliocentric distance. The points represent the weighted mean of early May and late May/early June CO/H_2O mixing ratios with 1-σ error bars. The mixing ratio does not seem have changed between the two observing periods.

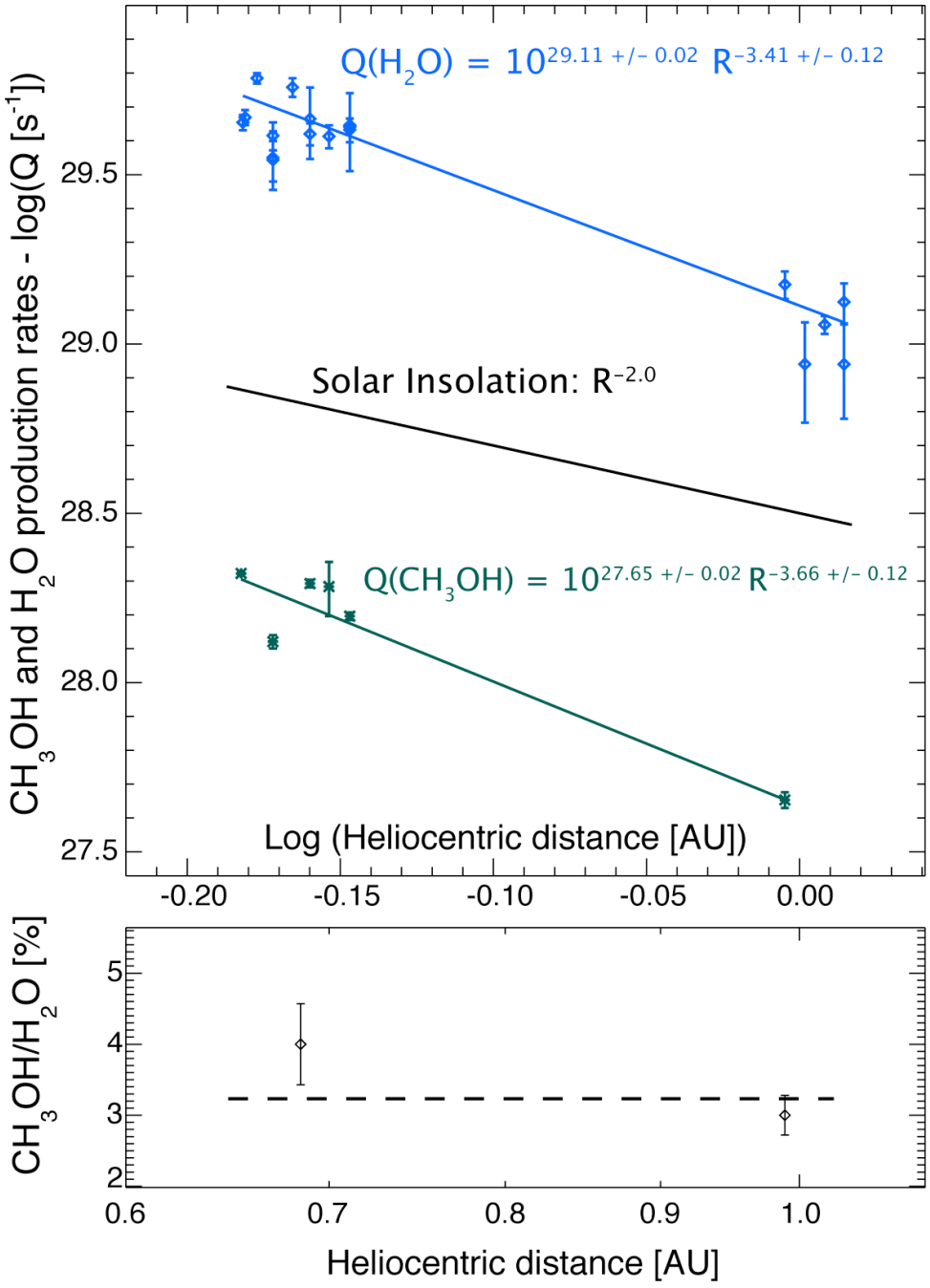

Figure 5.3: (Top) Log of CH_3OH (bottom) and H_2O (top) production rate vs. log comet heliocentric distance. The third line (center) represents the slope corresponding to solar insolation (R^{-2}). (Bottom): CO/H_2O mixing ratio vs. heliocentric distance. The points represent the weighted mean of early May and late May/early June CO/H_2O mixing ratios with 1-σ error bars. The mixing ratio does not seem have changed between the two observing periods.

5.3. DAILY VARIABILITY OF COMET C/2002 T7 (LINEAR)

The early May H_2O production rates from C/2002 T7 (LINEAR) show some variability from day to day. The variability did not look irregular, so I tested for possible periodicity. For example, if there were a part of the comet's surface that was more active, there would be an increase in the observed production when that part of the comet nucleus was exposed to the incident solar radiation. Another possible situation is a nucleus having a non-spherical shape; for an elongated nucleus, the surface area exposed to the Sun varies over its rotation and this could produce noticeable differences in gas production.

The seven daily weighted mean H_2O production rates from May 3 to May 9 were plotted against their mean mid UT date. I applied a sine curve with a decreasing slope based on the change in overall H_2O production rate with heliocentric distance (see Figure 5.5). The sine curve parameters were adjusted to find the best reduced χ^2 fit. A period of 2.32 days provided the best match with a reduced $\chi^2 = 0.27$ (Figure 5.4). A sine curve without a decreasing slope and a (LINEAR) fit was also applied to the data, but these produced poor fits (reduced χ^2 of 39 and 190). The sine curve with the decreasing slope produced a rotational period of 2.32 days for a hot spot on the nucleus, or a rotational period of 4.64 days for a non-spherical, elongated comet nucleus with uniform gas production per unit surface area. Normally, a reduced χ^2 should be close to one. Lower reduced χ^2 values indicate that the individual errors are overestimated. Since some of the daily values include average production rates and observations combining 2.9 μm and 4.7

μm H_2O measurements, this could introduce additional uncertainties when calculating the daily mean Q (H_2O). I recalculated the reduced χ^2 using the individual daily values of both 2.9 μm and 4.7 μm H_2O measurements including their respective times of observation. The result was a higher reduced χ^2 of 0.61, compared than just the 2.9 μm and 4.7 μm H_2O measurements alone. This is still less than one, but it indicates a good fit between the fitted decreasing sine function and the data. Additional systematic errors may have inadvertently added in the calculation of the terminal production rates, as errors from both nucleus-centered production rates and growth factors (see Table 4.1, 4.2, and Appendix) were included.

The following step was performed to examine the variability of CO and CH_3OH in early May. If the periodicity of the early May H_2O production rates was caused by rotation of a non-spherical nucleus or non-uniform activity of a chemically homogeneous spherical nucleus, similar variability should be seen in the other parent molecules. The early May CO, H_2CO, CH_3OH production rates were both scaled by their respective weighted mean mixing ratios (see Table 4.4) (with their uncertainties based both on the original standard error in the production rates and the uncertainties in the mixing ratios). These scaled production rates were grouped with the early May water production rates and a new reduced χ^2 calculation was preformed to see how well all four (H_2O, CO, H_2CO and CH_3OH) molecules matched the sine curve. The molecular production rates of oxidized carbon were scaled by their corresponding daily mixing ratios. The new reduced χ^2 was 0.58 (0.66 if individual daily 2.9 μm and 4.7 μm H_2O measurements were used),

showing that the proposed period of 2.32 days does match the short-term variation of H_2O, CO, and CH_3OH production rates (Figure 5.5).

The dust continuum from the May 3-9 H_2O_3A setting observations were examined to see if they also showed the same periodic rate. The dust continuum in the H_2O_3A was very low (see Figure 2.3 A-H) but I was able to retrieve relative production rates for each date. A best fit sine curve with a period of 2.65 days match the first six days (May 3-8), with a reduced χ^2 of 1.9. The last data point from May 9 does not fit the sine curve, so a decaying factor may be needed to applied to the sine curve, as was done with H_2O (Figure 5.1, slope of decreasing Q for H_2O with increasing R_h). I attempted to scale the decay factor from H_2O to the dust, but I could not find a good fit for all seven days.

A short term periodicity of cometary H_2O production has been reported (Biver, et al. 2009). Based on observations of C/2001 Q4 (NEAT) with the Odin satellite between March 6 and May 16, 2004 targeting the H_2O (0_{10}-1_{01}) line at 557 GHz, Biver et al. (2009) fitted the observed H_2O production rate with a first order sine wave having a period of about 0.82 days and reduced χ^2 of 1.4. However, the results reported here represent the first measure of daily variations in the production rates for multiple parent volatiles.

Throughout early May, carbon monoxide did not change in abundance relative to water. For each of the six days in early May that CO was measured, the daily CO mixing

ratios are within 1-σ of their weighted mean and the CO mixing ratios matched a constant value of 1.8% with a reduced χ^2 of 1.02. The daily early May CH_3OH mixing ratios are not as consistent as CO. Most of the individual daily mixing ratios are more than 2-σ away from their weighted mean. However, the errors in methanol mixing ratios may be understated. Accurate synthetic models for methanol do not exist (as they for H_2O, CO and H_2CO). Also a comparison of the early May CO and CH_3OH mixing ratios (MR(CO) / MR(CH_3OH) in Table 4.4) does not indicate any daily change in the abundances of CH_3OH in relation to CO. A future test, to see if the methanol mixing ratios are accurate, is to examine the production rate of OH lines within the CSHELL methanol setting to establish whether they lines produce the similar water production rates. However, these are co-mingled with lines of methanol so that an accurate CH_3OH fluorescence model is needed to accurately quantify Q (H_2O) based on the intensities of these OH lines. An additional test involves measuring Q(CH_3OH) from lines that are measured simultaneously with ethane, using empirically-determined g-factors.

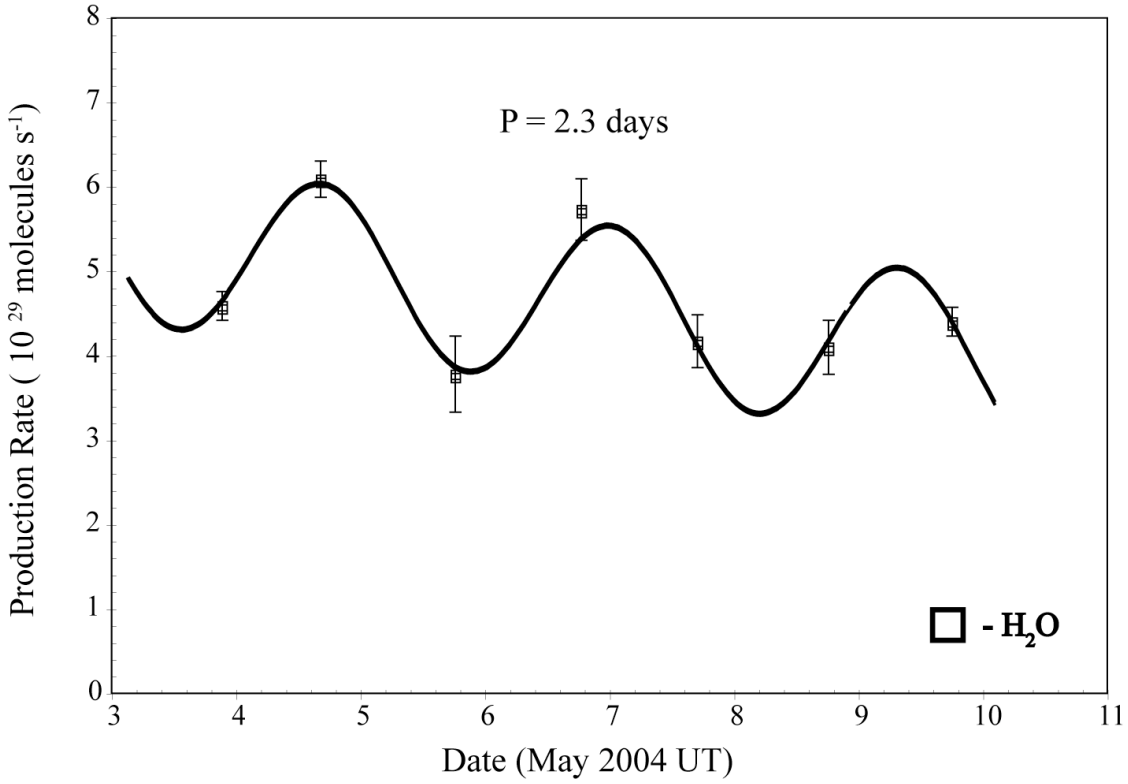

Figure 5.4: Daily average production rate for H_2O in C/2002 T7 (LINEAR) in Early May 2004. The solid line is a best fit sine wave with a period of 2.32 days with a decreasing slope based on the overall decrease of water production rate with heliocentric distance.

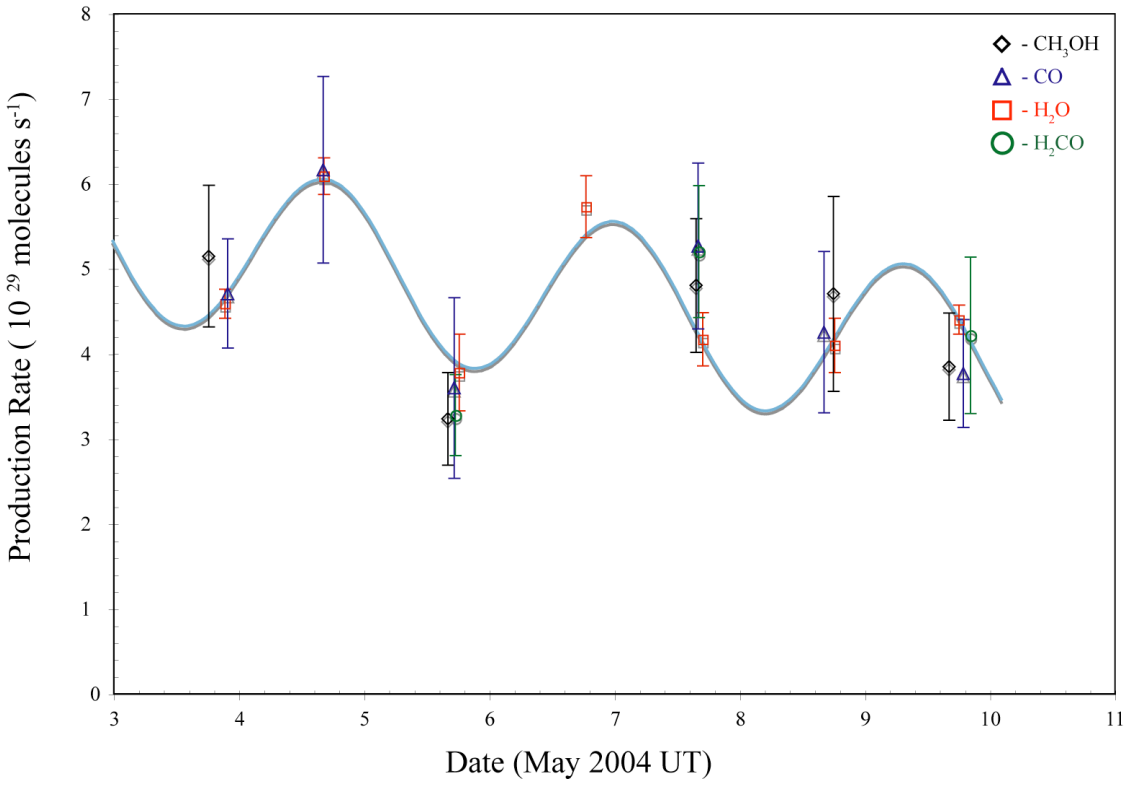

Figure 5.5: Daily average production rate for H_2O, CO, H_2CO, and CH_3OH in C/2002 T7 (LINEAR) in Early May 2004. CO and CH_3OH are both scaled by their mean respective early May mixing ratios. The solid line is a best fit sine wave with a period of 2.32 days with a decreasing slope based on the overall decrease of water production rate with heliocentric distance.

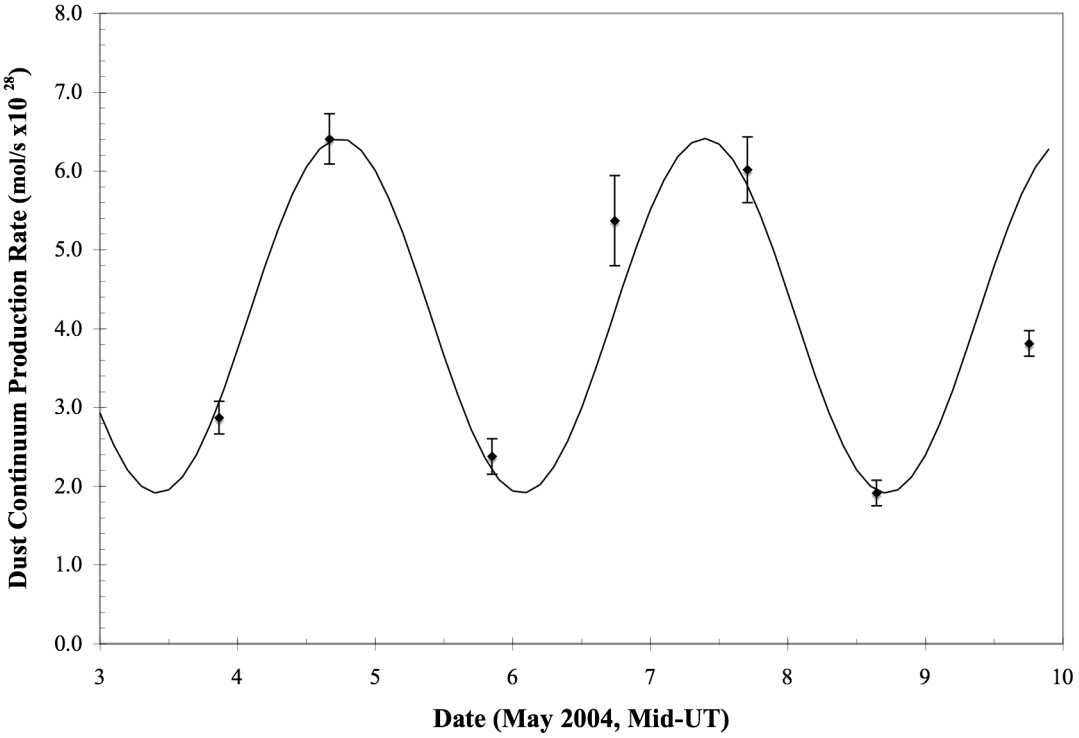

Figure 5.6: Relative Dust Continuum production rate from the H_2O_3A CSHELL setting for early May 2004. The solid line is a best fit sine wave with a period of 2.65 days. The sine wave fits the data from May 3 to May 8 with a reduced χ^2 of 1.9 .

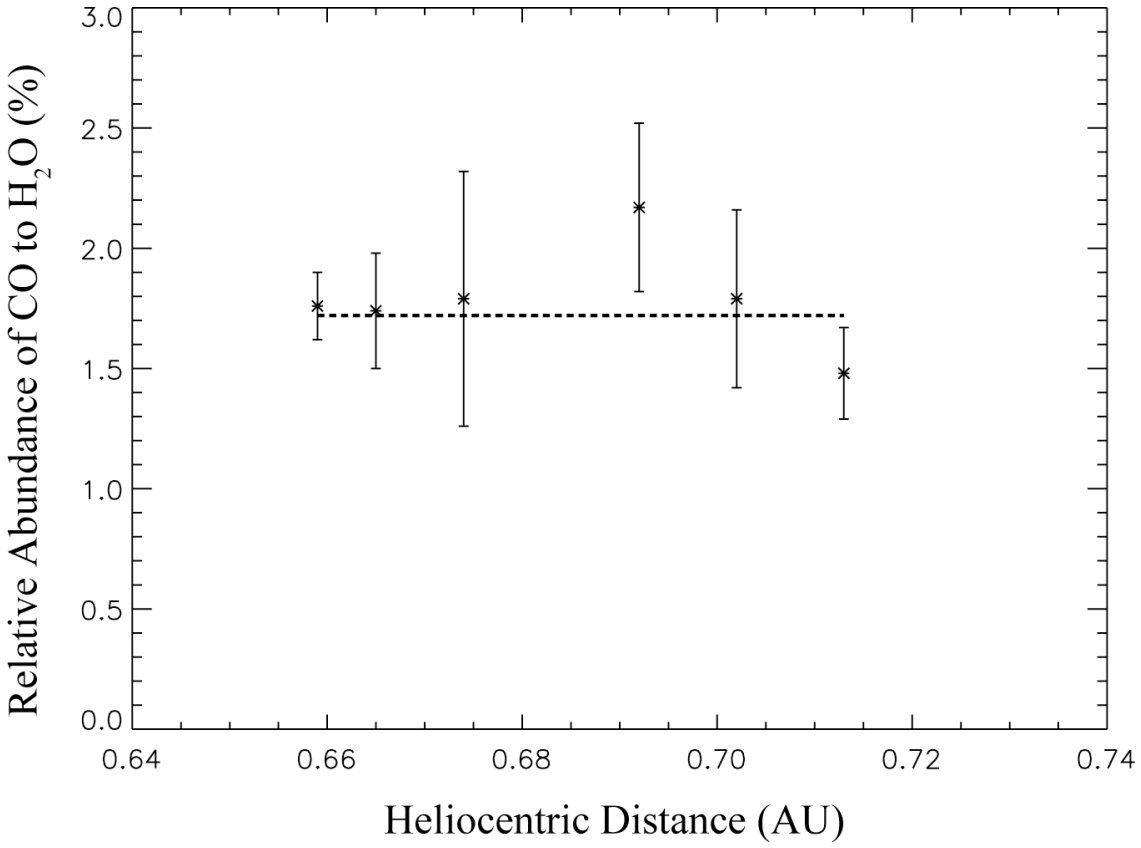

Figure 5.7: Daily abundance of CO relative to H_2O in C/2002 T7 (LINEAR) for early May 2004, with 1-σ uncertainty bars and the weighted mean (dashed line) of the 6 dates.

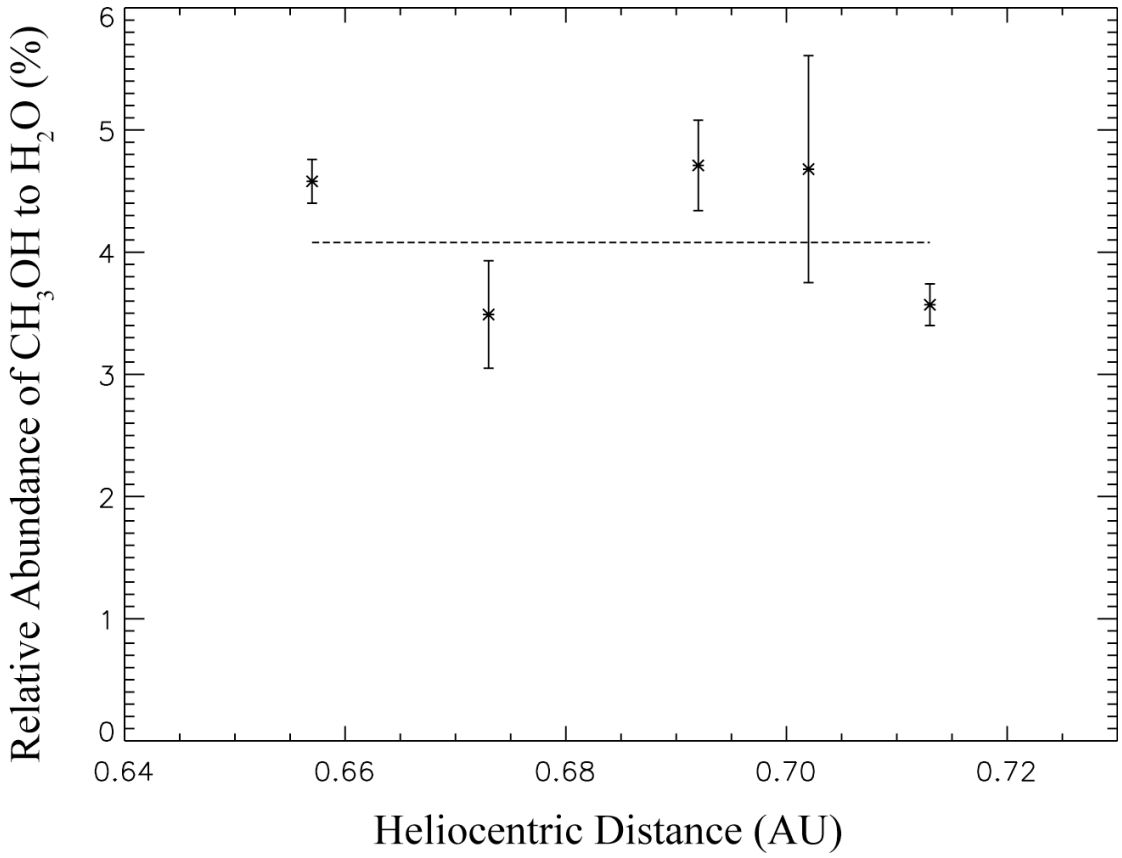

Figure 5.8: Daily abundance of CH_3OH relative to H_2O in C/2002 T7 (LINEAR) for early May 2004, with 1-σ uncertainty bars and the weighted mean (dashed line).

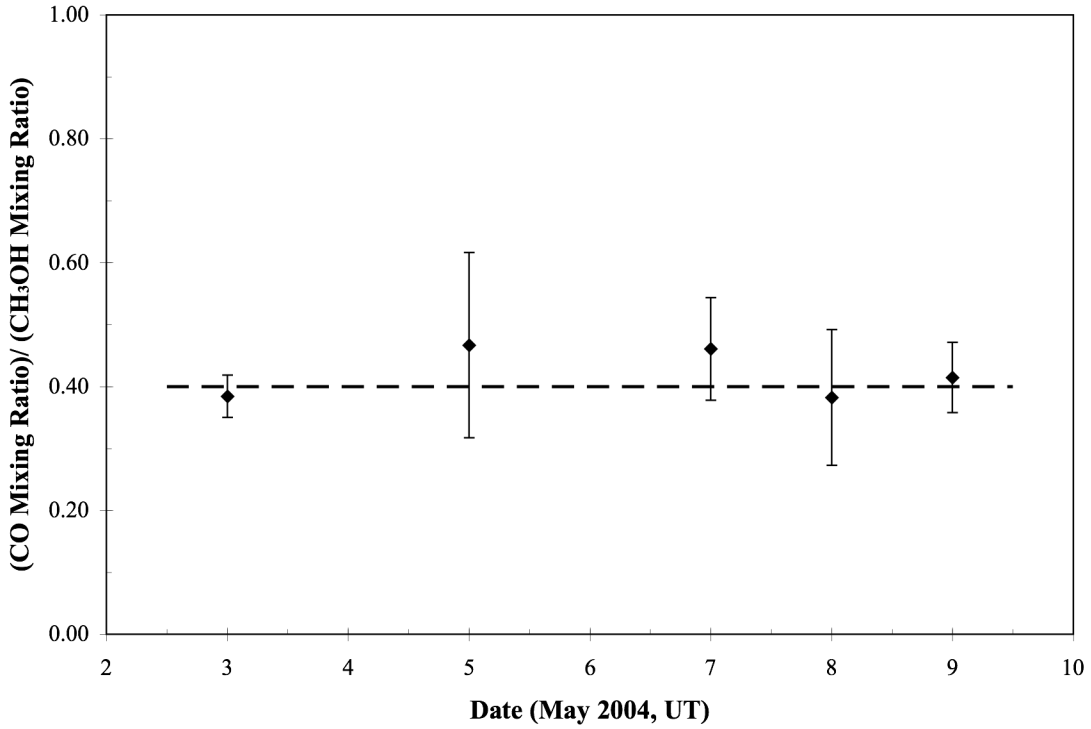

Figure 5.9: Ratio of CO Mixing Ratio to CH_3OH Mixing Ratio (relative to H_2O) in C/2002 T7 (LINEAR) for early May 2004, with 1-σ uncertainty bars and the weighted mean (dashed line). The ratio is consistent for the observing period within 1-σ uncertainty.

5.4. COMPARISON WITH OTHER OBSERVATIONS OF C/2002 T7 (LINEAR)

C/2002 T7 (LINEAR) was the subject of other observation studies during its time within the inner Solar System. These observations were mostly performed at optical and radio wavelengths and some produced gas production rates for a number of molecular species. This section will briefly cover these other observational results and compare them with the results from the infrared observations previously presented in this paper.

From optical observations, D. G. Schleicher estimated the H_2O production rate to be around 2 $x10^{29}$ mol/s for May 11, 2004 (listed as a private communication within Friedel et al., 2005). This is about a factor of two to three lower than the early May production rates determined with CSHELL (4-6 $x10^{29}$ mol/s). Friedel et al. (2005) uses Schleicher's H_2O production rate (as determined from fluorescent OH) to calculate HCN mixing ratios for C/2002 T7 (0.33 +/- 0.11 %). The characteristics of Schleicher's observations of C/2002 T7 are not yet published, so it is difficult to examine the cause of the difference, aside from the general advantage that in the infrared we observe native H_2O directly. Infrared observational techniques have a much small beam size than optical, allowing one to measure much closer to the nucleus. Infrared observational techniques can also measure directly multiple water lines and determine an accurate rotational temperature (as previously described in Chapter 3). Fink (2009) discloses a taxonomic survey of comets using optical CCD spectroscopy, which details a method of deriving H_2O production rates. Due to telluric absorption, optical surveys rely on observing daughter products of water, such as OI (1D) or fluorescent OH, both produced

after the released native water has been photo-dissociated. The scaling factor between OI and H_2O depends on the level of solar UV activity (i.e., on the solar cycle), and can introduce uncertainties of up to 25% (Fink, 2009).

Water ice grains were detected in the coma of C/2002 T7 (LINEAR) as far back in September 2003, at a pre-perihelion distance of 3.52 AU (Kawakita, et al., 2004). Sharp variations (ranging between 1 and 2 magnitudes) in the overall brightness of C/2002 T7 (LINEAR) were detected in November-December 2003 (Filonenko, private communication as cited in Rosenbush, et al. 2005), which could indicate a cometary burst, perhaps resulting from C/2002 T7 (LINEAR) losing its "crust".

The Odin satellite is space-based instrument that has been used to observe comets in the sub-millimeter region of the spectrum. Odin was lunched in 2001 and is equipped with a 1.1-m primary mirror and five receivers at 119 GHz. Between 2001 and 2005, the Odin satellite was used to observe the 557 GHz water line in 12 comets. C/2002 T7 (LINEAR) was observed 4 times. The two observations in late May (May 25.9 and 29.2 UT) yielded water production rate of 2.18 +/- 0.23 $x10^{29}$ mol/s and 1.92 +/- 0.29 $x10^{29}$ mol/s, respectively. These values are consistent with the late May H_2O production rate from CSHELL observations (May 30: 1.50 +/- 0.14), after incorporating the heliocentric dependence in $Q(H_2O)$ ($\sim R_h^{-3.41+/-0.12}$; see above and Fig. 5.10). Radio observations such as ODIN sample only a single line over a larger range of release time from the nucleus. Infrared observing techniques have the advantage of a much smaller beam size (+/-1.5 arc-seconds for a 15-row extract) than radio telescopes (Odin beam size is 2.2' at 557

GHz; Biver et al., 2007). The much more concentrated IR beam allows for a more accurate measurement of parent volatiles. Also, with only a single line, the rotation temperature is poorly constrained. Biver et al. (2007) states that another source of uncertainty with their calculated production rates is due to asymmetric outgassing detected on May 25.

Remijan et al. (2006) report radio observations of C/2002 T7 (LINEAR) using the Berkeley-Illinois-Maryland Association (BIMA) array taken between May 11-15, 2004 ($r_h \sim 0.75$ AU). Remijan et al. measured the J = 3 $_{1,3}$ – 4 $_{0,4}$ A^+ CH_3OH line at 107.013 GHz, using a rotation temperature of 115 K. A CH_3OH production rate of 7.5 (+/-1.5) $x10^{27}$ mol/s was determined as well as a CH_3OH mixing ratio of 3.8 (+/- 0.8)%, using the H_2O production rate of 2.0 $x10^{29}$ mol/s determined by Schleicher. The CH_3OH production rate is within 2-σ error of the CSHELL results, including the heliocentric distance for CH_3OH production (Figure 5.2). Remijan's CH_3OH mixing ratio (3.8+/-0.8 %) is also in agreement with the value calculated from the infrared observation for early May (4.08 +/- 0.66%; see Tables 4.4 and 4.5).

Remijan et al. (2008) also observed C/2002 T7 (LINEAR) on May 20, 2004, with the 12m National Radio Astronomy Observatory (NRAO). The beam size was 40 arc-seconds and the comet was at a heliocentric distance R_h = 0.865 AU. Remijan targeted 4 single CH_3OH lines (6 $_{0,6}$ - 6$_{-1,6}$ E; 1 $_{0,1}$ – 1 $_{-1,1}$ E; 3 $_{0,3}$ – 3 $_{1,3}$ E; 2 $_{0,2}$ – 2 $_{-1,2}$ E; near 157,270 MHz) and derived an excitation temperature of 35+/- 5 K. Remijan calculated a CH_3OH production rate of 2.0 $x10^{27}$ mol/s and CH_3OH mixing ratio of 1.5%. This

differed from my late May CH_3OH findings by a factor of 1.5 in the production rate and a factor of 2 in the CH_3OH mixing ratio. Remijan bases the CH_3OH mixing ratio on a value of 1.3 $x10^{29}$ mol/s for the H_2O production rate cited from Lecacheux, et al. (2004; IAUC 8304). This appears to be an error as Leacheux states 1.3 $x10^{29}$ mol/s as the H_2O production rate for C/2001 Q4 NEAT, not C/2002 T7 (LINEAR), based on 556.936 GHz line measurements taken by the ODIN satellite in March 2004. Remijan may be assuming C/2002 T7 (LINEAR) has the same production as C/2001 Q4 (NEAT). As described in Chapter 3, because the rotational temperature of the CH_3OH lines could not be directly measured, my CH_3OH calculations adopted the rotational temperature measured for H_2O (~ 100 K in early May, ~ 80 K in late May) to establish g-factors for multiple (combined) Q-branch lines. If correct, the lower 35 K temperature would result in a higher CH_3OH g-factor for the Q-branch lines and thus reduce the calculated production rates, however this should be considered unlikely.

On two dates (15 May 2010 and 25 May 2010), C/2002 T7 (LINEAR) was observed at the 12m National Radio Astronomy Observatory (NRAO) by Milam et al. (2006). Three transitions of H_2CO were sampled (May 15: $3_{0,3}$ - $2_{0,2}$ and $3_{1,2}$ - $2_{1,1}$; May 25: $3_{1,3}$ - $2_{1,2}$). Native production rates (May 15: 3.9 $x10^{26}$, 2.52 $x10^{26}$; May 25: 1.03 $x10^{26}$) and mixing ratios (May 15: 0.2% and 0.1%; May 25: 0.1%) were also calculated. These production rates are lower by a factor of two compared with DiSanti et al. (2006) for early May, and also with my early June 2004 results for $Q(H_2CO)$. Milam et al. (2006) calculated the native production rates through finding an overall column density from the full beam size. The large beam size would include any extended source of

H_2CO. An assumed rotational temperature of 50 K was also used by Milam et al. This is much lower than the 94-108 K range found in early May by DiSanti et al. (2006), or 80 K used for my early June calculations.

Schulz, et al. (2006) discloses BVRI observations of C/2002 T7 (LINEAR) with the European Space Agency's (ESA) 1m, Optical Ground Station (OGS) telescope. Schulz calculated B, V, R, and I coma profiles and stated the profiles shows short-term variation in the comet's activity. Schulz also states C/2002 T7 (LINEAR) displays a non-uniform coma with distinct features, including a prominent structure extending from the nucleus in the tailwind hemisphere. Schulz suggests that the features could be produced through active areas on a rotating nucleus. These observations and conclusion would be in agreement with the infrared observations presented here.

TABLE 5.1

Table 5.1. Comparison of Observational Results of C/2002 T7 (LINEAR)

Molecule	Region	Date	Production Rate (mol/s)	Mixing Ratio[a]	T_{rot}
H_2O	IR	May 3-9	4.1 - 6.1 $x10^{29}$	----	102-110 K
		May 5-9	3.55 - 4.62 $x10^{29}$ [d]	----	
		May 30-June 2	0.87 - 1.5 $x10^{29}$	----	82 $^{+32}_{-27}$ K
	Optical	May 11	2.0 $x10^{29}$ [b]	----	
	Radio	May 25.9	2.18 +/- 0.23 $x10^{29}$ [c]	----	
		May 29.2	1.92 +/- 0.29 $x10^{29}$ [c]	----	
CO	IR	May 3-9	6.2 - 10.6 $x10^{27}$	1.72 +/- 0.20	98-114 K
		May 30-June 2	1.8 - 3.2 $x10^{27}$	2.06 +/- 0.42	80 K
H_2CO	IR	May 3-9	2.5 - 4.3 $x10^{27}$ [d]	0.79 +/- 0.09 [d]	94-102 K [d]
		May 30-June 2	0.87 - 1.1 $x10^{27}$	0.81 +/- 0.11	76 $^{+15}_{-12}$ K
	Radio	May 15	3.9 $x10^{26}$ [e]	0.2 [e]	50 K [e]
			2.52 $x10^{26}$ [e]	0.1 [e]	
		May 25	1.03 $x10^{26}$ [e]	0.1 [e]	50 K [e]
CH_3OH	IR	May 3-9	1.32 - 2.1 $x10^{28}$	4.00 +/- 0.57	100 K
		May 30	4.5 +/- 0.24 $x10^{27}$	3.00 +/- 0.32	80 K
	Radio	May 11-15	7.5 +/- 1.5 $x10^{27}$ [f]	3.8 +/- 0.8 [f]	115 K [f]
		20-May	2.0 $x10^{27}$ [g]	1.5 [g]	35+/- 5 K [g]

[a] Mean abundance relative to water (percent).

[b] private communication from D. Schleicher, cited in Friedel, (2005).

[c] Biver et al. (2006).

[d] DiSanti et al. (2006); H_2O production rate based on OH lines in H_2CO_B setting.

[e] Milam et al. (2006).

[f] Remijan et al. (2006).

[g] Remijan et al. (2008).

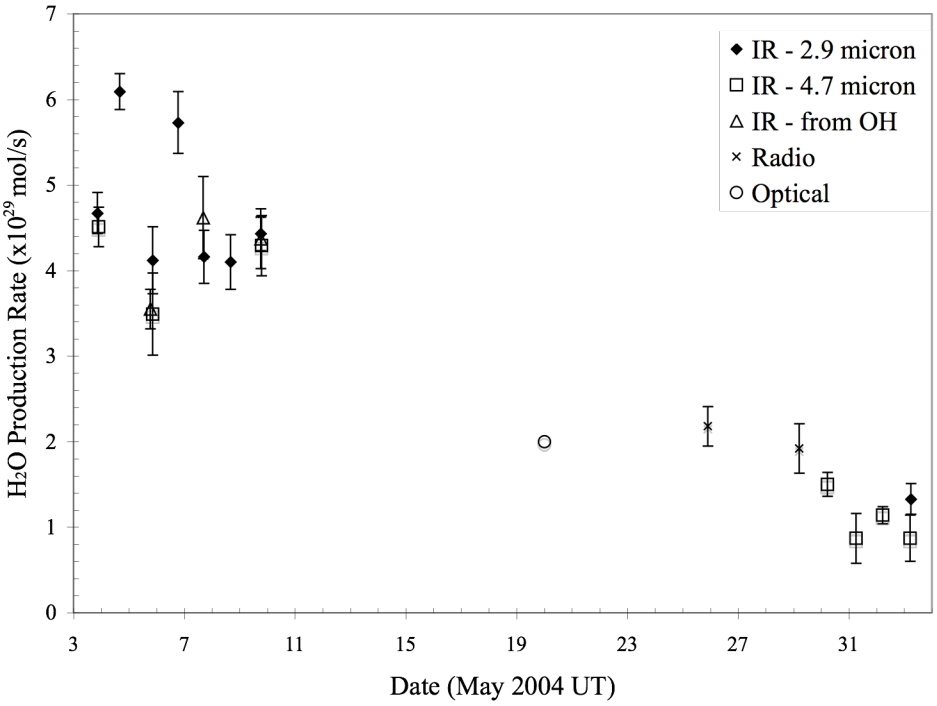

Figure 5.10: A comparison of H_2O production rates in C/2002 T7 (LINEAR) from infrared (2.9 μm, 4.7 μm, and OH), radio, and optical observations. The data points with error bars are shown with 1-σ uncertainty.

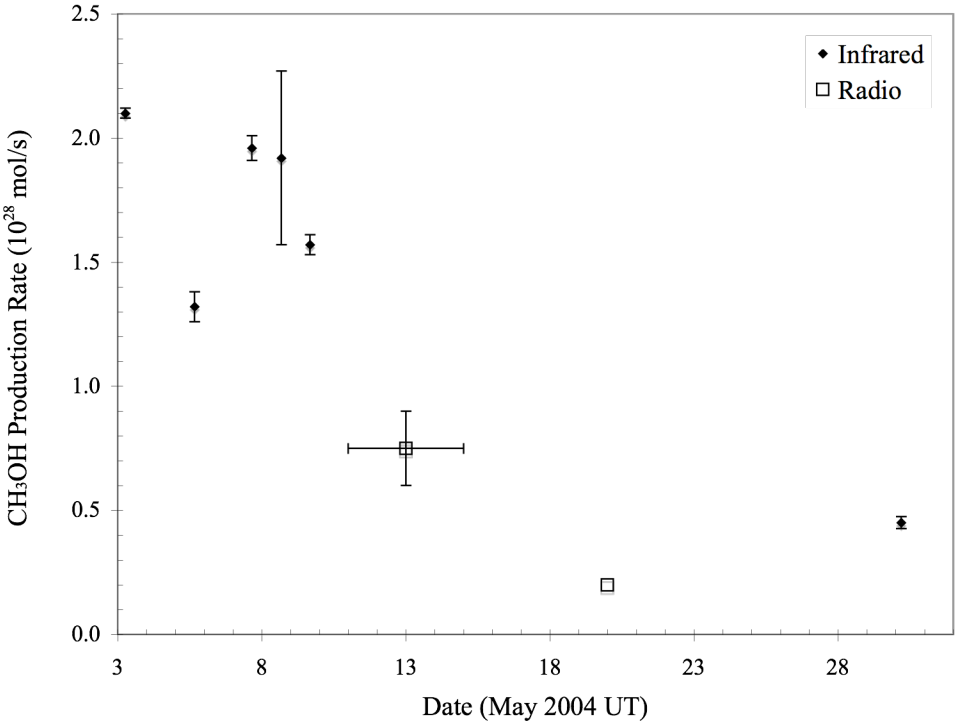

Figure 5.11: A comparison of CH_3OH production rates of C/2002 T7 (LINEAR) from infrared and radio observations. The data points with vertical error bars are shown with 1-σ uncertainty. Horizontal error bars represent a range in date where observations were taken and combined.

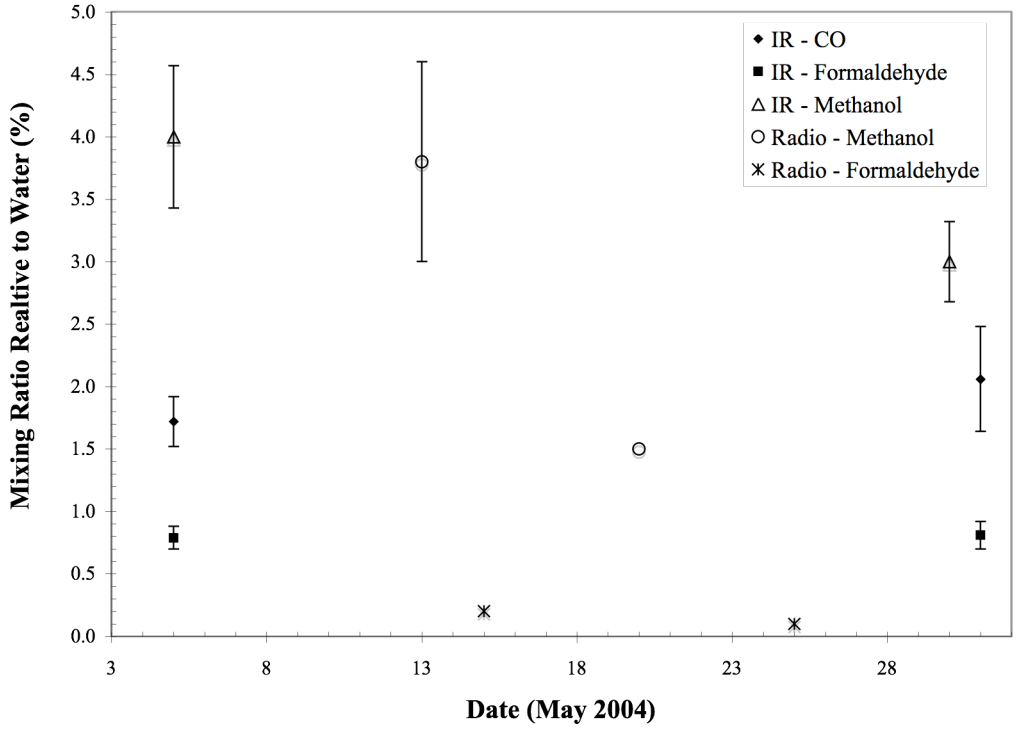

Figure 5.12: A comparison of mixing ratios of C/2002 T7 (LINEAR) from infrared and radio observations. The data points with error bars are shown with 1-σ uncertainty.

5.5. COMPARISON OF CHEMISTRY BETWEEN C/2002 T7 (LINEAR) AND OTHER OBSERVED COMETS

Establishing cometary taxonomy based on chemistry is a key goal in the field of comet science. A number of ongoing comet observing campaigns are being carried out in optical (Schleicher et al., 2008; Fink, 2009), infrared (Mumma et al., 2003; DiSanti & Mumma, 2008; Dello Russo et al. 2009) and radio (Biver et al., 2002; Bockelée-Morvan et al., 2005; Croviser, 2007; Remijan et al, 2008) regions of spectrum to provide the necessary information to characterize comets into different categories. The observations of C/2002 T7 (LINEAR) presented in this paper now add aspects of an additional comet to this growing database. Previous analysis of oxidized carbon in isotropic or ecliptic comets has enabled the classification of comets into preliminary classes based on abundances: organic "rich"; organic "normal"; or organic "depleted" (Mumma et al., 2003; DiSanti & Mumma, 2008). At the time of dissertation, it is uncertainly whether these classes are distinct or representative as part of a more continuous range in compositions.

Within this study, C/2002 T7 (LINEAR) has been found to have a mean CO mixing ratio of 1.78 +/- 0.18 and a mean CH_3OH mixing ratio of 3.24 +/- 0.90. Four OC comets (C/1996 B2 Hyakutake, C/1995 O1 Hale-Bopp, C/1999 H1 Lee, and 153 P/Ikeya –Zhang) have grouped together based on having similar abundances of C_2H_6, C_2H_2, HCN, and CH_3OH. In relation to the molecules relative to this dissertation, the four OC comets have a CO mixing ratio range of 1.8% -15% and mean CH_3OH mixing ratio of

2.2 +/- 0.2 % (DiSanti & Mumma, 2008). These four OC comets form a basis for the organics "normal" class. Organic "normal" comets have similar abundances as those detected within dense interstellar molecular clouds (Mumma, et al. 2003; DiSanti et al., 2009). Ices that formed into the nuclei of these comets would have been processed at very low temperatures (e.g., ~ 10 – 20 K for H-atom addition reactions; see discussion in Section 1.10).

The other two classes are based on abundances that are more ("enriched") or less ("depleted") compared to organic "normal". C/1999 S4 (LINEAR) contains very low abundances of CO and CH_3OH relative to water (0.9 +/- 0.3 %, less than 0.15%, respectively) and characterizes the organics "depleted" class (Mumma et al., 2003). 73 P/ Schwassmann-Wachmann 3C would be placed in organics "depleted" class as well. C/2001 A2 (LINEAR) contains a CO mixing ratio of 3.9 +/-1.1% and CH_3OH mixing ratio of 3.9 +/- 0.4% and would be in the organics "enriched" class based on CH_3OH, reflecting a more interstellar chemistry (DiSanti, et al, 2009).

There are a couple comets (C/2006 M4 (SWAN) and 8P/Tuttle) that do not fit the current three categories (Bonev et al., 2008; DiSanti et al, 2009). These two comets that are depleted in CO, but have organic "normal" level abundances of CH_3OH. A low CO/CH_3OH ratio could indicate an environment that enabled higher conversion of CO to CH_3OH through H-atom addition. An environment of higher density (or longer exposure time) of atomic hydrogen would lead to an excess of CH_3OH while depleting CO (DiSanti et al., 2009).

Compared to organics "normal" comets, C/2002 T7 (LINEAR) has borderline "normal" CO abundance and "enriched" CH_3OH abundance relative to water. C/2002 T7 (LINEAR) could be placed in the "enriched" class along with C/2001 A2 (LINEAR). The low CO/CH_3OH ratio found for C/2002 T7 (LINEAR) could also place it with C/2006 M4 (SWAN). The H_2CO mixing ratio found for C/2002 T7 (LINEAR) (0.80 +/- 0.9) was relatively high compared to the limited sample of comets with native H_2CO abundance measured, with only 153 P/Ikeya-Zhang having a similar value among the values reported to date.

Table 5.2. Organic Parent Volatile Abundances in Comets

Name	X (CO) [a]	X (H_2CO) [b]	X (CH_3OH) [c]	Class
Oort Cloud Comets				
C/2002 T7 (LINEAR) [d]	1.78 +/- 0.18	0.80 +/- 0.09	3.24 +/- 0.90	Enriched
C/1996 B2 Hyakutake	15 +/- 1.9 [o]		1.7 +/- 0.4 [e]	Normal
C/1995 O1 Hale Bopp	12 +/- 0.4 [o]	0.3 - 2.2 [u]	2.4 +/- 0.3 [e f]	Normal
C/1999 H1 Lee [h]	1.8 +/- 0.2		2.1 +/- 0.5	Normal
C/2001 Q4 (NEAT) [u]			0.1 - 0.5	---
C/2006 M4 (SWAN) [v]	0.48 +/- 0.15		3.4 +/- 0.69	---
C/2000 WM_1 (LINEAR) [s]	0.52 +/- 0.12	0.20 +/- 0.03	1.30 +/- 0.08	Depleted
C/2001 A2 (LINEAR)[j]	3.9 +/- 1.1	0.24 +/- 0.05	3.9 +/- 0.4	Enriched
C/1999 T1 McN-Hartley [i]	~17			Normal
C/1999 S4 (LINEAR)[o]	0.9 +/- 0.3		< 0.15	Depleted
1P/Halley	3.5 [k]		1.7 +/- 0.4 [l]	Normal
8P/ Tuttle	0.45 +/- 0.09 [w]		2.7 +/- 0.30 [x]	---
153P Ikeya-Zhang [g]	4.7 +/- 0.8	0.62 +/- 0.18	2.5 +/- 0.5	Normal
Jupiter Family Comets				
9P/ Tempel 1 (Preimpact)[t]			1.3 +/- 0.20	Normal
9P/ Tempel 1 (Postimpact)	4.3 +/- 1.7		0.99 +/- 0.17	Normal
17 P/ Holmes [p]			2.25 +/- 0.43	Normal
73 P/S-W 3-C	0.53 +/- 0.13 [q]	0.147 +/- 0.033[r]	0.149 +/-0.029[r]	Depleted

Table 5.3. Reference Notes for Table 5.2.

[a] Mean abundance of native carbon monoxide relative to water (percent).
[b] Mean abundance of formaldehyde relative to water (percent).
[c] Mean abundance of methanol relative to water (percent).
[d] Weighted mean of early May and late May/early June 2004 mixing ratios.
[e] Biver et al. (2002).
[f] Bockelée-Morvan et al.(2000).
[g] DiSanti et al. (2002).
[h] Mumma et al. (2001a).
[i] Mumma et al. (2001b).
[j] Magee-Sauer et al. (2008).
[k] Eberhardt (1999).
[l] Eberhardt (1987).
[m] DiSanti et al. (2001).
[n] Dello Russo et al. (2001).
[o] Mumma et al. (2003).
[p] Dello Russo et al. (2008).
[q] DiSanti et al. (2007).
[r] Dello Russo et al. (2007).
[s] Radava et al. (2010).
[t] Mumma et al. (2005).
[u] Milam et al. (2006).
[v] DiSanti et al. (2008).
[w] Böhnhardt et al. (2008).
[x] mean of abundance from Böhnhardt et al. (2008) and Bonev et al. (2008).

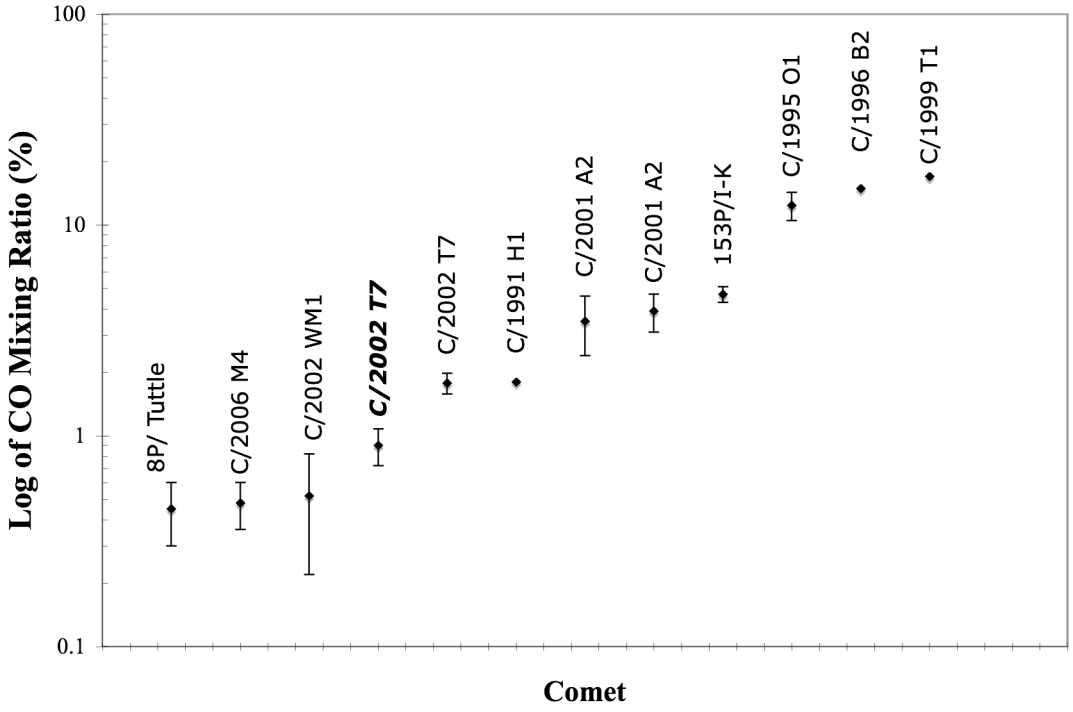

Figure 5.13: A comparison of CO mixing ratios observed in Oort cloud comets. C/2002 T7 (LINEAR) is in bold. The Y-axis is in logarithmic format. C/2002 T7 (LINEAR) is borderline depleted in CO compared with other Oort cloud comets. Error bars represent 1-σ uncertainties.

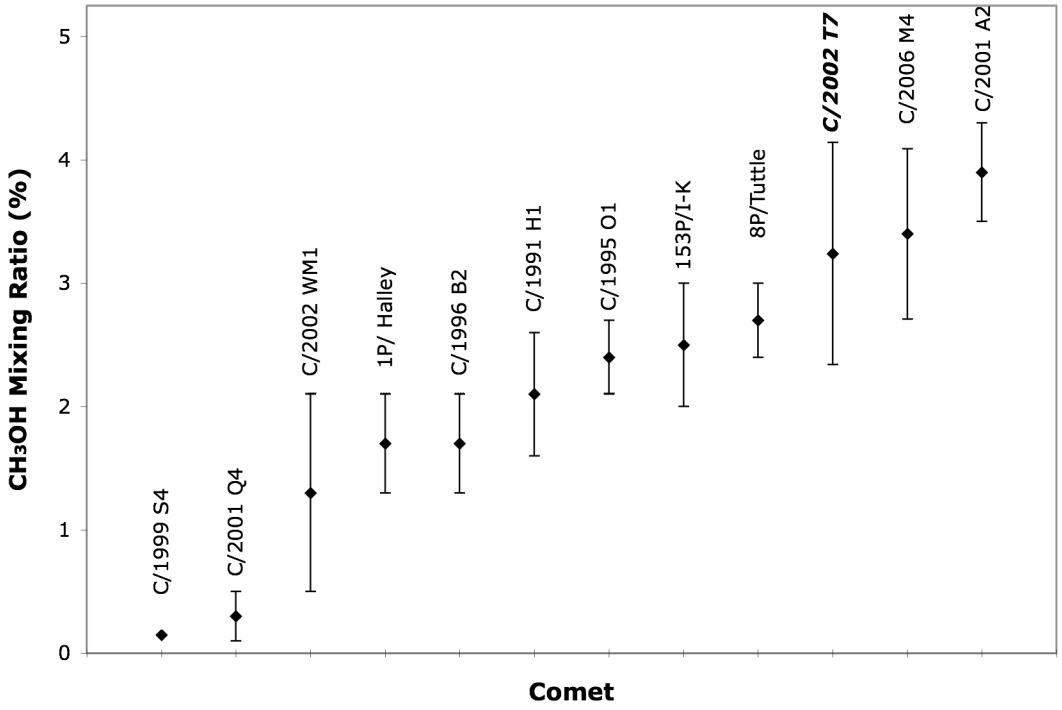

Figure 5.14: A comparison of CH_3OH mixing ratios observed in Oort cloud comets. C/2002 T7 (LINEAR) is relatively enhanced in CH_3OH compared with other Oort cloud comets.

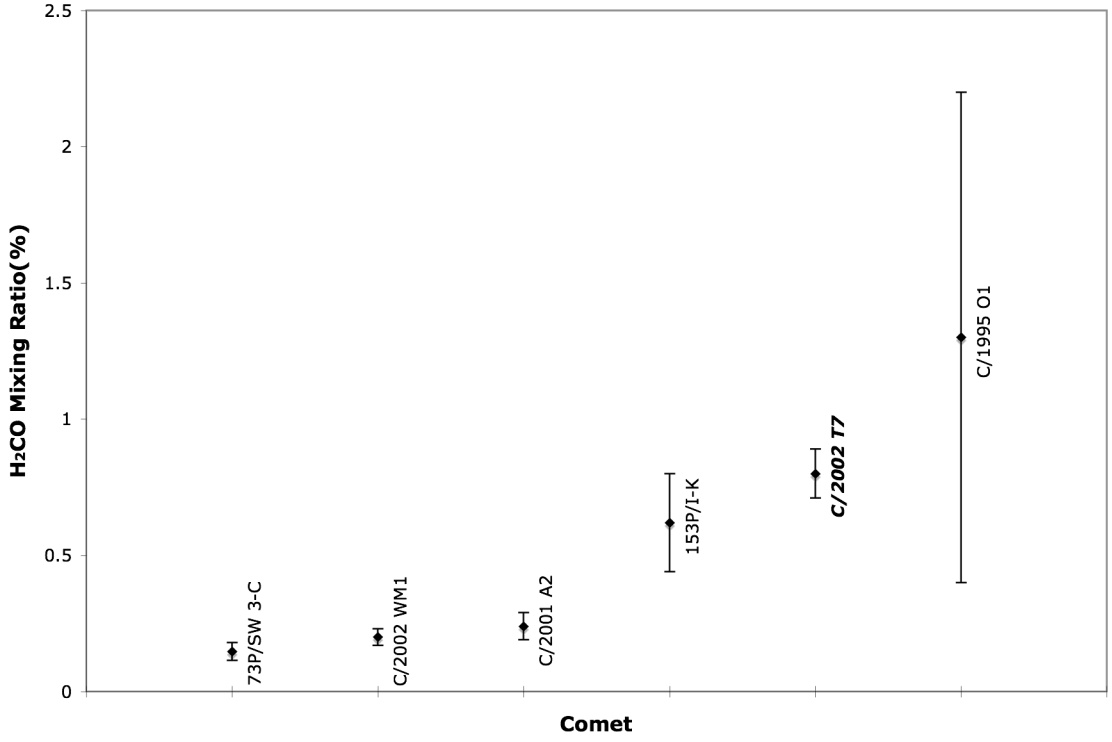

Figure 5.15: A comparison of H_2CO mixing ratios observed in comets. C/2002 T7 (LINEAR) appears to be normal in H_2CO compared with the limited sample of comets where H_2CO has been measured.

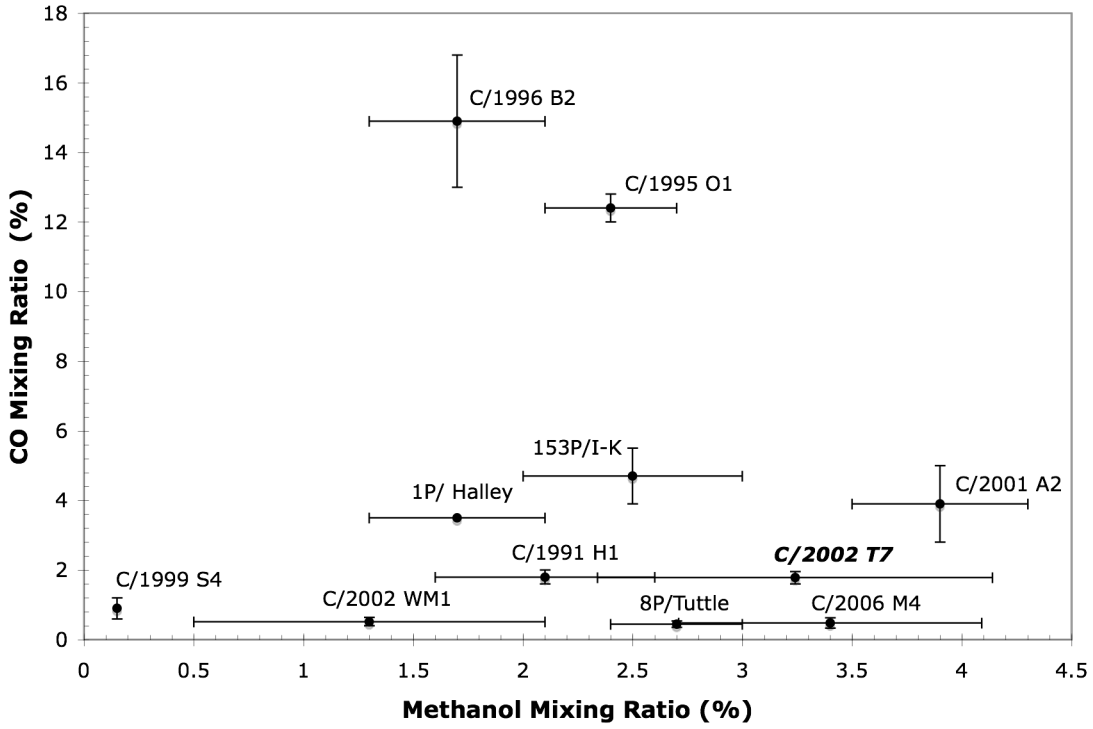

Figure 5.16: CH_3OH mixing ratio vs. CO mixing ratio observed in Oort cloud comets. C/2002 T7 (LINEAR) is borderline depleted in CO and enhanced in methanol.

CHAPTER VI

CONCLUSIONS

CONCLUSIONS AND FUTURE WORK

C/2002 T7 (LINEAR) has provided a wonderful opportunity to add to cometary science. The early May and late May/early June 2004 observations of C/2002 T7 (LINEAR) from the NASA IRTF allowed an in-depth study of daily oxidized carbon production rates using accurate rotational temperatures that were derived daily through multiple molecular lines and (on some dates) for more than one parent molecule. The observations also allowed a detailed attempt to examine the heliocentric dependence of oxidized carbon of an Oort cloud comet, albeit over a limited range in R. C/2002 T7 (LINEAR) proved to be a very interesting object with a robust chemistry. It was enriched in methanol (early May: $4.00 \pm 0.57\%$, late May/early June: $3.00 \pm 0.32\%$) and formaldehyde (early May: $0.79 \pm 0.09\%$, late May/early June: $0.81 \pm 0.11\%$) while being depleted in carbon monoxide (early May: $1.70 \pm 0.14\%$, late May/early June: $2.06 \pm 0.42\%$) compared to most Oort cloud comets studied to date. In terms of CO and H_2CO, C/2002 T7 LINEAR had abundances similar to C/1991 H1 Lee, although its mixing ratio of methanol was twice that in C/1999 H1.

The early May observations of C/2002 T7 LINEAR showed a periodic variation in the production rate of all four molecules (water, CO, H_2CO, and CH_3OH). I was able to obtain a rigorous fit to the combined daily average production rates of each molecule using a decaying sine curve with a period of 2.32 days. As there appeared to be no change in the day-to–day mixing ratios, I concluded that the variation was possibly due to

C/2002 T7 LINEAR having a non-uniform gas production rate. This could arise for example from one hemisphere of a spherical nucleus being more productive, or alternatively from more uniform production per unit area from an irregularly shaped nucleus that presents a varying cross-section, or some combination of these.

C/2002 T7 (LINEAR) was also examined for any long-term changes in oxidized carbon abundances by comparing mixing ratios at different heliocentric distances. There is no evidence of any heterogeneity in the cometary nucleus composition. Given the comet's orbital characteristics, this was C/2002 T7 LINEAR first and only trip into the inner Solar System (Nanako, 2003, 2006). It is possible that the observed abundances of oxidized carbon in C/2002 T7 (LINEAR) are representative of conditions in the cold molecular cloud from which the solar system formed, although some degree of processing in the proto-solar nebula cannot be ruled out.

The methodology derived for finding the cometary gas production rates and rotational temperature worked sufficiently and was verified through a secondary method. Both the correlation and excitation analysis method were used to determine the rotational temperatures of CO, H_2O and H_2CO. The CO rotational temperatures were comparable with rotational temperature values calculated with the classical Boltzmann method. The use of the water (and OH) growth factors produced accurate measurements for the native CO and H_2CO production rates of C/2002 T7 (LINEAR). The differences in continuum growth factors could be used to calibrate and combine different CSHELL settings to

calculate accurate rotational temperatures. This methodology will be useful for future comet observations with CSHELL and other high-resolution IR spectrometers.

While much work has been done in this dissertation on comet C/2002 T7 (LINEAR), several additional avenues of research can be pursued with these data. For example, the decaying sine curve can extrapolated to the late May/early June to see if it matches there as well. Considerations such as changes in phase angle can be combined with the observed daily light curve to better constrain the rotation rate and perhaps pole orientation. The focus of this work was solely on the native oxidized carbon from C/2002 T7 (LINEAR). So far, no extended sources of the targeted molecules (CO, H_2CO, CH_3OH) were detected in current analysis of the CSHELL data. Additional native ices, in particular CH_4, C_2H_6 and HCN, can be examined to determine whether their production rates also track those of the molecules studied here. Finally, there is also some remaining CSHELL settings that target other organic molecules, specifically CH_4, C_2H_6 (also containing additional lines of CH_3OH), HCN, and C_2H_2) that need to be processed and analyzed in order to more completely assess the parent volatile composition of C/2002 T7 (LINEAR).

Appendix

A.1. Growth Factors and Correction Factors: CO

This section concerns use of growth factors in the cometary native gas production rates. Early in my analysis of the C/2002 T7 (LINEAR) early May observations, I discovered that the CO on May 3 did not produce consistent line-by-line terminal production rates, even as measured at the correct rotational temperature using the Boltzmann method. Theoretically, the terminal production rates of each line should be within error of each other based on modeled fluorescence g-factors. The terminal production rates could be affected if there was another source of flux. One possibility was an extended source of CO in the comet's coma, the CO being produced through degradation of a more complex progenitor species.

Since this study was focused on the native CO production rate of C/2002 T7 (LINEAR), a method would have to be used to either remove or exclude the possible extended CO source flux. One way is to measure extremely close to the comet nucleus. The IRTF/CSHELL long slit and high (up to seeing-limited) spatial resolution permitted studying emissions in the inner coma. The terminal production rate is measured from 1 to 6.5 arc-second from the nucleus. A nucleus-centered production rate can be measured just from 0 to 1 arc-seconds from the nucleus, thereby minimizing contributions from (potential) extended sources. Unfortunately, at this close to the comet nucleus, there is the problem of slit loss and a global production rate from just the nucleus-centered flux will underestimate the true production rate.

To solve this second problem, the concept of a growth factor was introduced (see Bonev, 2005, and references therein).The growth factor is the ratio of the terminal production rate to the nuclear-centered production factor. The presence of an extended source will increase the observed terminal production rate and thus increase the apparent growth factor. Other factors, such as the telescope not on source, could increase the apparent growth factor. If the nuclear-centered production rate of CO can be scaled by a correct growth factor that not affected by an extended source, then the native CO terminal production rate can be found. Water is the dominant volatile in comets and is not expected to have an extended source in the coma. The growth factor of water should match the proper growth factor of the native CO.

To test the suitability of using the growth factor of water, I calculated and compared the growth factors for individual lines of water and CO for May 3, 5, and 9 of 2004. For the terminal productions, values were found using both offsets and no offsets (applied to the Q-curve). I also calculated a growth factor for the dust continuum as well for each CSHELL setting of each date, as they would be needed to scale difference in seeing between settings. On all three dates, the H_2O (May 3: 1.61 +/- 0.062; May 5: 1.76 +/- 0.214; May 9: 2.02 +/- 0.081) showed a lower growth factor with smaller relative errors than CO (May 3: 2.32 +/- 0.112; May 5: 3.01 +/- 0.416; May 9: 2.43 +/- 0.337) CO growth factors also were higher than the dust continuum growth factors. The spatial profiles for CO, H_2O, and dust are shown in Fig. 3.4. H_2O and dust are about the same. The CO profile is little broader than H_2O profile. Based on accepted scale lengths of CO (based on Giotto Observations of 1P/Halley; Eberhardt, 1999), this difference is likely

due to the position of the comet off center, not an extended source, and could be corrected by a relatively small nod (15 arc-second) of the instrument.

The following step is to determine if calculating individual line terminal production rates from the water growth factor and the CO nuclear-centered production rates produced better agreement between the CO lines. Figure A1 shows a comparison between individual terminal production rates derived from the measured CO flux 1.5 to 6.5 arc-seconds from the comet, and Figure A.2 shows the CO lines derived from its nuclear-centered flux and water growth factor measured for the same date (May 9, 2004). It is clear that using the water growth factor provides better agreement among the measured lines.

Although improved, the terminal production rate (Q_{term}) for individual CO lines as shown in Figure A2 are still not consistent within error. As the different settings were taken at slight different times, the effects of differences in observing conditions (e.g., seeing and/or positioning in the slit) between frames could lead to differences in observed cometary line flux. Since these differences would also affect the continuum background, a possible correction could be found through comparing the difference in the nucleus-centered production rate ($Q_{0\text{-}1}$) of the continuum in each setting. As seen in Table A1, there is a noticeable difference in the nucleus-centered production rate and continuum growth factor for different settings. Setting CO_D is chosen as the base setting, as it contains the strong water line used to determine the H_2O growth factor. The other settings are scaled, as shown in Table A.2, by a correction factor based on the ratio of continuum

nucleus-centered production rates. Figure A.3 shows terminal production rates after incorporating both the water growth factor and this continuum correction factor. After the correction factor, the individual lines are in even better agreement, showing both the H_2O growth factor and the continuum based correction factor are required in the calculation of line-by-line CO terminal production rates.

Table A.1. Calculation of growth factors for CO, H_2O and dust continuum

Date	Setting	Target	$Q_{0\text{-}1}$	$\sigma_{0\text{-}1}$	$Q_{2\text{-}6}$	$\sigma_{stochastic}$	$\sigma_{standard}$	GF	σ_{GF}
May 3									
	CO_E	CO	4.45E+27	1.05E+26	1.03E+28	4.85E+26	2.62E+26	2.32	0.122
		H_2O	2.44E+29	2.73E+27	3.94E+29	9.66E+27	1.46E+28	**1.61**	**0.062**
		Continuum	3.25E+28	1.86E+26	5.79E+28	4.07E+26	1.92E+27	1.78	0.060
	CO_H	Continuum	1.33E+28	1.85E+26	5.15E+28	9.21E+26	2.84E+27	3.88	0.088
May 5									
	CO_E	CO	2.90E+27	1.65E+26	8.73E+27	8.88E+26	1.10E+27	3.01	0.416
		H_2O	1.85E+29	5.84E+27	3.27E+29	2.13E+28	3.83E+28	**1.76**	**0.214**
		Continuum	1.28E+28	4.25E+26	2.31E+28	2.83E+27	1.53E+27	1.81	0.134
	CO_G	Continuum	1.96E+28	5.77E+26	4.66E+28	6.07E+26	2.16E+27	2.38	0.115
	CO_I	Continuum	2.74E+27	2.33E+25	6.60E+27	1.12E+26	4.49E+26	2.41	0.171
May 9	CO_D	CO	2.24E+27	9.98E+25	5.43E+27	3.67E+26	7.14E+26	2.426	0.337
		H_2O	1.33E+29	2.56E+27	2.68E+29	5.63E+27	9.37E+27	**2.024**	**0.081**
		Continuum	1.25E+28	2.09E+26	2.25E+28	5.25E+26	2.25E+27	1.802	0.180
	CO_C	Continuum	1.99E+28	1.32E+26	3.69E+28	3.29E+26	4.28E+26	1.852	0.025
	CO_G	Continuum	2.22E+28	1.71E+26	4.14E+28	4.43E+26	2.00E+26	1.865	0.025
	CO_H	Continuum	1.86E+28	8.99E+25	4.08E+28	2.89E+26	2.17E+26	2.195	0.019

Calculation of growth factors for CO, H_2O and dust continuum for multiple CSHELL settings on May 3, 5, and 9 2004. The nuclear-center production rates ($Q_{0\text{-}1}$) are shown with 1-σ error. Terminal production rates ($Q_{2\text{-}6}$) are calculated with both 1-σ standard and stochastic errors. The growth factors of H_2O selected are in bold.

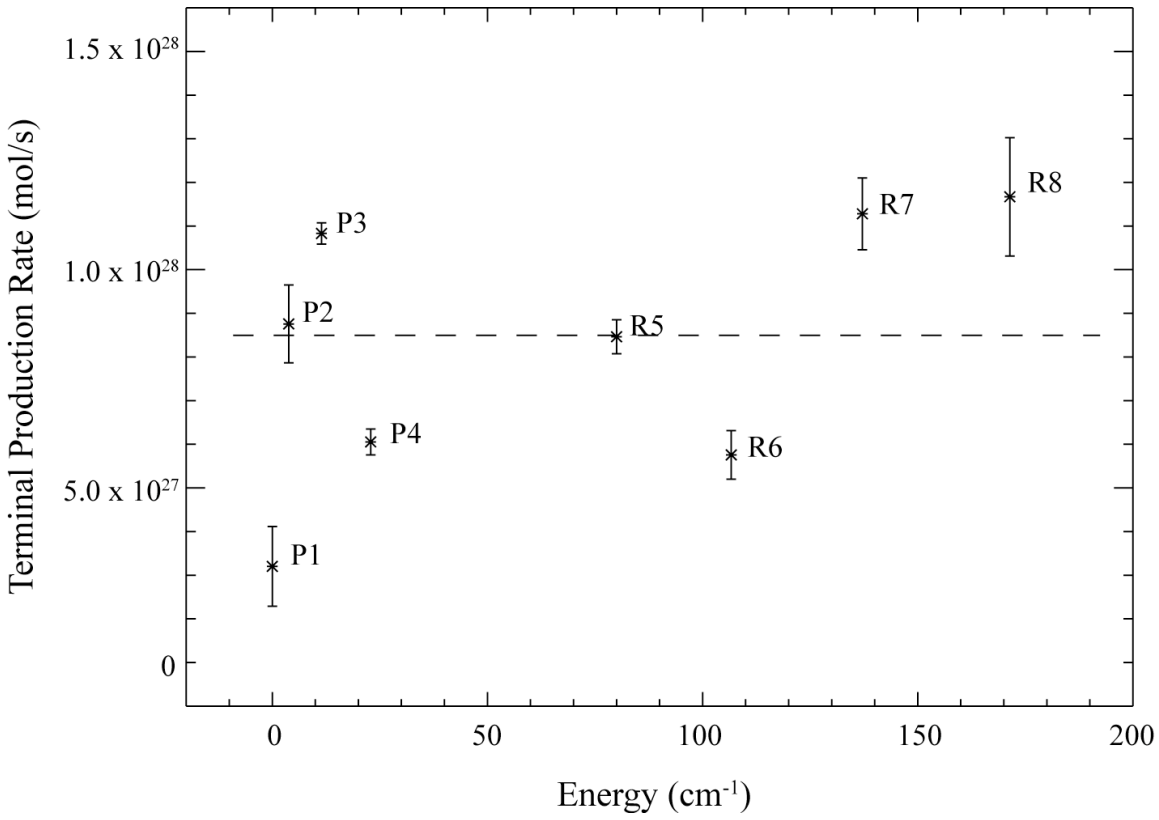

Figure A.1: Terminal production rate of individual CO lines for May 9, 2004, based on observed CO flux from 1.5 to 6.5 arc-seconds from the comet nucleus, vs. energy (cm-1) of the individual line. The dashed line is the weighted mean of the terminal production rates (8.55 +/- 3.56 x10^{27} mol/s).

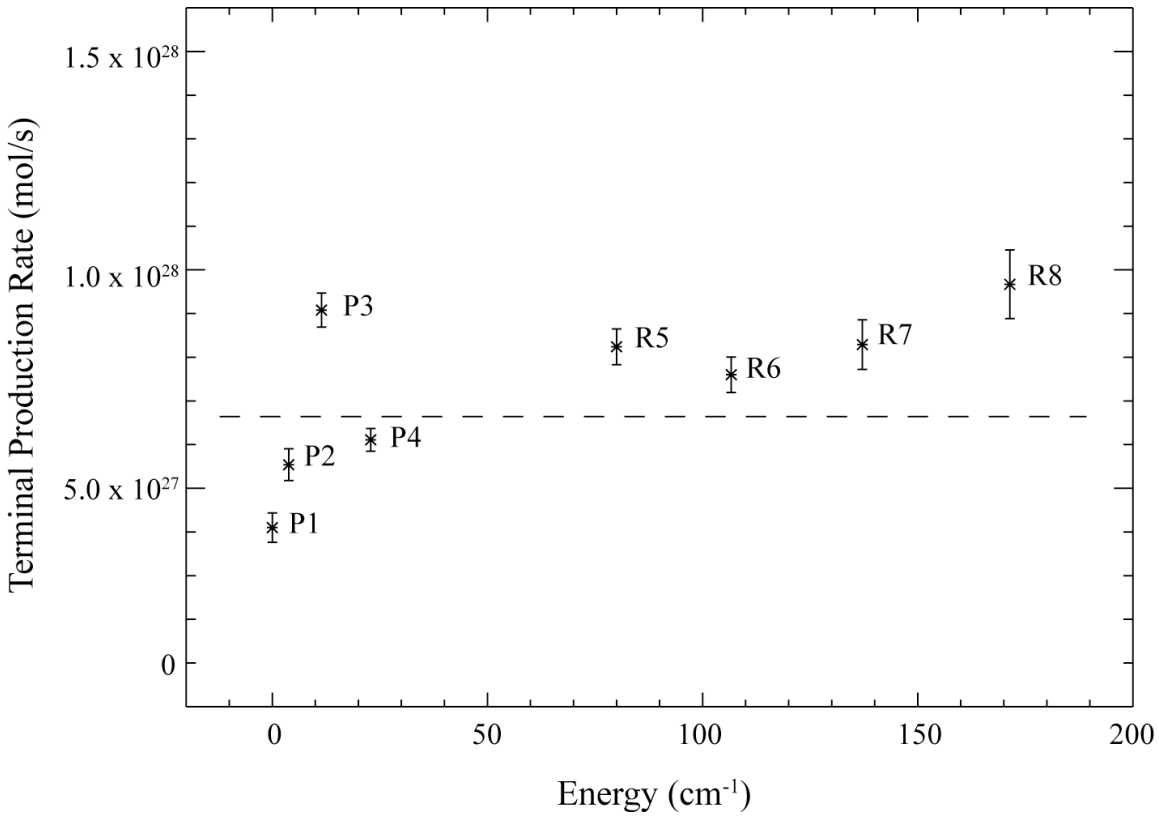

Figure A.2: Terminal production rate of individual CO lines for May 9, 2004, based on observed CO nucleus-centered flux (0 to 1 arc-second) and the growth factor of H_2O (observed in CO_D setting), vs. energy (cm-1) of the individual line. The dashed line is the weighted mean of the terminal production rates (6.69 +/- 2.02 x10^{27} mol/s).

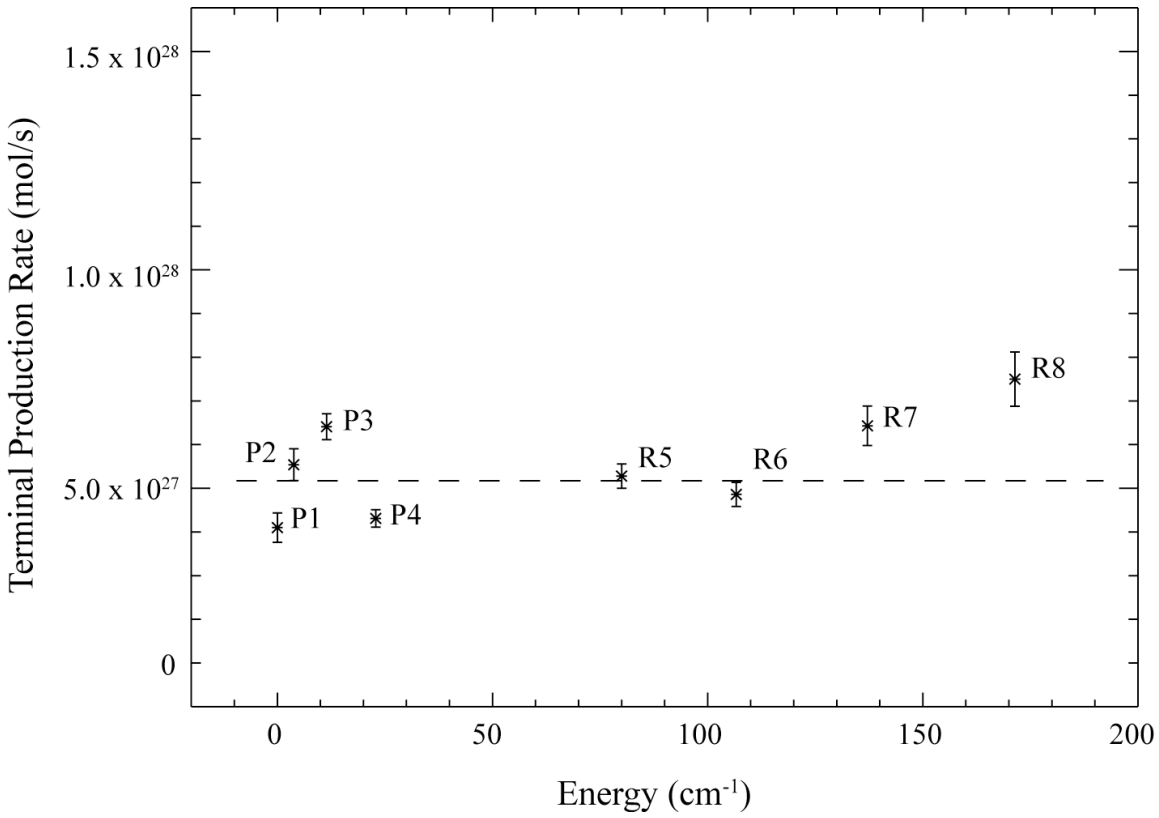

Figure A.3: Terminal production rate of individual CO lines for May 9, 2004, based on observed CO nucleus-centered flux (0 to 1 arc-second), the growth factor of H_2O (observed in CO_D setting), and a correction factor based on the ratio of continuum nucleus-centered production rates between different CSHELL settings, vs. energy (cm^{-1}) of the individual line. The dashed line is the weighted mean of the terminal production rates (5.11 +/- 1.45 $x10^{27}$ mol/s).

Table A.2. The calcualtions of the individual CO line terminal production rates using the H_2O growth factor and correction factors from the differences in the continuum growth factors.

Line	Energy (cm^{-1})	Q_{0-1} ($x10^{27}$)	σ_{0-1} ($x10^{27}$)	GF	σ_{GF}	$Q_{2-6\ (calc)}$ ($x10^{27}$)	$\sigma_{2-6\ (calc)}$ ($x10^{27}$)	CF	σ_{CF}	$Q_{2-6\ (calc * CF)}$ ($x10^{27}$)	$\sigma_{2-6\ (calc * CF)}$ ($x10^{27}$)	$Q_{2-6(measured)}$ ($x10^{27}$)	$\sigma_{2-6\ (measured)}$ ($x10^{27}$)
P1	0	2.03	0.15	2.02	0.062	4.10	0.337	1.00		4.10	0.337	3.20	0.914
P2	3.8	2.74	0.14	2.02	0.062	5.54	0.365	1.00		5.54	0.365	8.76	0.894
P3	11.4	4.49	0.07	2.02	0.062	9.08	0.391	0.71	0.012	6.41	0.297	10.83	0.243
P4	22.9	3.02	0.05	2.02	0.062	6.11	0.261	0.71	0.012	4.31	0.199	6.05	0.296
R5	80.0	4.07	0.12	2.02	0.062	8.24	0.410	0.64	0.011	5.28	0.279	8.46	0.391
R6	106.7	3.75	0.13	2.02	0.062	7.60	0.407	0.64	0.011	4.86	0.275	5.76	0.558
R7	137.1	4.10	0.23	2.02	0.062	8.29	0.568	0.78	0.013	6.43	0.453	11.28	0.822
R8	171.4	4.78	0.34	2.02	0.062	9.67	0.786	0.78	0.013	7.50	0.621	11.67	1.357

A.2. Growth Factors: H_2O_3A setting

Another possible way to test the suitability of using continuum growth factors to scale lines from different is to compare the daily H_2O growth factors from the H_2O_3A CSHELL setting observations and the corresponding dust continuum growth factors. If the continuum growth factors can correct for the different observing conditions and the dust continuum matches any short-term changes in water production, the ratio of the water and continuum growth factors should remain about the same day to day.

Figures 2.3 (A-H) show the observed spectra taken with the H_2O_3A setting between May 3 and May 9, 2004. Unfortunately, an odd drawback to having excellent observing conditions is that the signal of dust continuum is very low compared to the H_2O lines. Relative terminal and nuclear-center production rates of the dust continuum and the resulting growth factors were calculated (Table A.3), but the values had higher error than the continuum growth factors previously calculated for the CO settings. Daily growth factors were calculated for the combined flux of H_2O lines within the H_2O_3A setting and compared the dust continuum growth factors (Table A.4).

The ratio of the dust continuum growth factors and the 2.9 micron H_2O appears to be consistent within 2–σ error throughout the May 3-9 observing period. It does seem based on the C/2002 T7 (LINEAR) observations that the growth factors of the continuum is following the difference in observation conditions and could be used to scale different settings to a common ground. Similar analysis with other CHSELL comet observations

should be done to see if this method is applicable to other comet beyond C/2002 T7 (LINEAR) .

Table A.3. The calculation of the H_2O_3A setting, dust continuum growth factor and nuclear-centered production rates.

May mid-UT	Q_{0-1} (x 10^{27})	σ_{0-1} (x 10^{27})	Q_{2-6} (x 10^{27})	σ_{2-6} (x 10^{27})	GF continuum	σ_{GF}
3.86	9.98	2.06	28.68	2.08	2.87	0.63
4.67	29.29	1.26	64.06	3.21	2.19	0.14
5.85	6.28	0.91	23.77	2.25	3.78	0.65
6.74	19.69	0.54	53.69	5.71	2.73	0.30
7.71	25.85	0.97	60.15	4.18	2.33	0.18
8.64	8.73	0.24	19.13	1.61	2.19	0.19
9.75	11.54	1.00	38.10	1.61	3.30	0.32

Table A.4. Comparison of dust continuum growth factors with combined H_2O growth factors.

May mid-UT	GF continuum	σ_{GF} continuum	GF H_2O_3A	σ_{GF} H_2O_3A	Ratio of GFs	$\sigma_{Ratio-GF}$
3.86	2.87	0.63	1.93	0.17	1.49	0.35
4.67	2.19	0.14	1.86	0.05	1.18	0.08
5.85	3.78	0.65	2.52	0.23	1.50	0.29
6.74	2.73	0.30	1.88	0.09	1.45	0.17
7.71	2.33	0.18	1.70	0.10	1.37	0.13
8.64	2.19	0.19	1.79	0.13	1.22	0.14
9.75	3.30	0.32	1.83	0.06	1.80	0.18

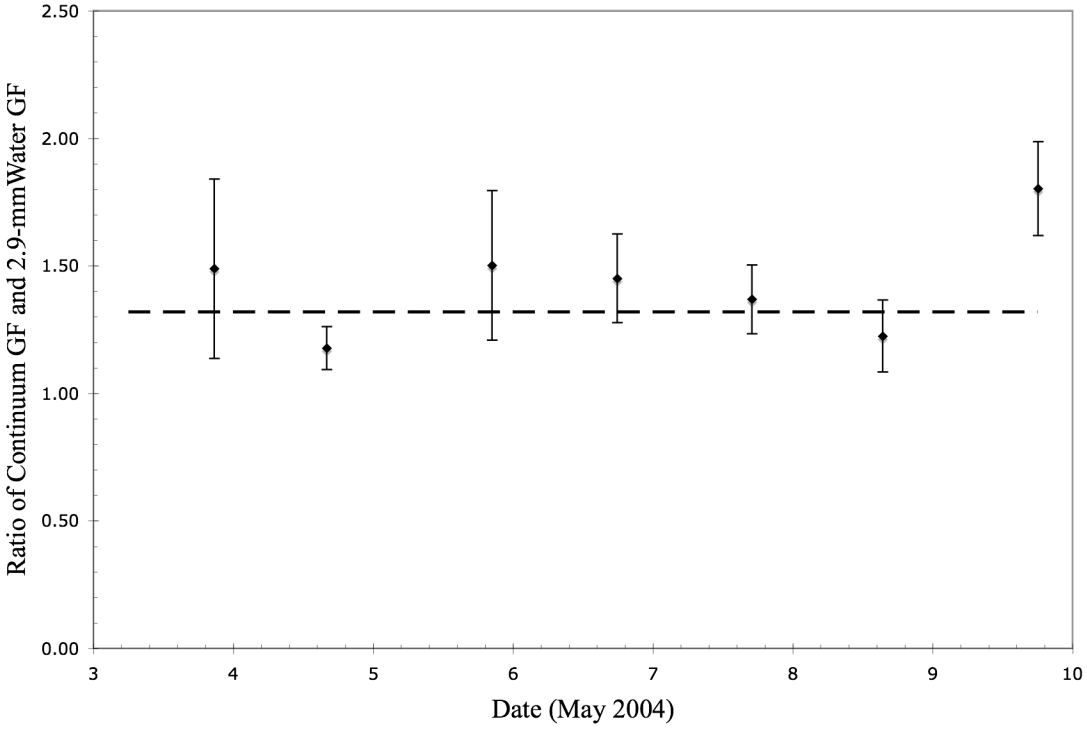

Figure A.4: The ratio of the continuum growth factors and 3-micron water growth factors from the H_2O_3A settings. The ratio are shown with 1-σ error bars and appears to be consistent within error between May 3 and May 9. The weighted mean of the ratios is 1.32 +/- 0.27.

A.3. Grating Angle and Gamma Table

Table A.5. Grating Setting Angles and Gamma (Γ) Flux Corrections

Date	Setting	Angle	Δ θ	Gamma
May 3	H2O_3A	60.796	2.704	6.07E-17
	CO_E	62.320	1.180	2.01E-17
	CO_H	61.070	2.430	2.47E-17
May 4	H2O_3A	60.796	2.704	6.45E-17
	CO_F	61.952	1.548	2.43E-17
May 5	H2O_3A	60.796	2.704	5.37E-17
	CO_E	62.320	1.180	2.05E-17
	CO_G	61.416	2.084	1.95E-17
	CO_I	60.706	2.794	2.17E-17
May 6	H2O_3A	60.796	2.704	5.37E-17
May 7	H2O_3A	60.796	2.704	5.67E-17
	CO_G	61.416	2.084	2.11E-17
May 8	H2O_3A	60.796	2.704	5.26E-17
	CO_G	61.416	2.084	1.94E-17
May 9	H2O_3A	60.796	2.704	5.56E-17
	CO_C	63.337	0.163	2.11E-17
	CO_D	62.918	0.582	2.15E-17
	CO_G	61.416	2.084	1.95E-17
	CO_H	61.070	2.430	2.05E-17
May 30	CO_D	62.965	0.535	4.24E-17
	CH3OH_A	63.270	0.230	4.24E-17
May 31	CO_D	62.965	0.535	4.71E-17
June 1	CO_D	62.965	0.535	4.50E-17
	CO_F	61.997	1.503	3.96E-17
	H2CO_B	65.802	2.302	5.14E-17
June 2	H2O_3A	60.808	2.692	5.60E-17
	CO_D	62.965	0.535	4.75E-17
	H2CO_B	65.802	2.302	5.14E-17

Table A.5. is a comparison table of the grating angle setting for selected CSHELL settings, the difference from the grating angle from blaze angle (θ_b =63.5 deg.) and Gamma correction calculated from observed standard stars. The Gamma and grating angles were examined to find any errors in grating setting during the observation of standard stars. None were found with the settings I examined.

References

Birtwhistle, P., Spahr, T. B. 2002. COMET C/2002 T7 (LINEAR*), IAU Circ.* **8003**, 1.

Biver, N., et al. 2002a. The 1995-2002 long term monitoring of Comet C/1995 O1 (Hale-Bopp) at radio wavelength. *Earth, Moon, & Planets.* **90**. 5-14.

Biver, N., et al. 2002b. Chemical composition diversity among 24 comets at radio wavelengths. *Earth, Moon, & Planets.* **90**. 323-333.

Biver, N, et al. 2007. Submillimetre observations of comets with Odin: 2001-2005, *Planetary and Space Science*, **55**, 1058-1068.

Biver, N., et al. 2009. Periodic variation in the water production of comet C/2001 Q4 (NEAT) observed with the Odin satellite, *Astron. & Astrophysics* **501**, 359-366.

Bockelée-Morvan et al. 1991., Microwave detection hydrogen sulfide and methanol in comet Austin (1989c1). *Nature*, **350**, 318-320.

Bockelée-Morvan et al. 2000. New molecules found in comet C/1995 O1 (Hale-Bopp), Investigating the link between cometary and interstellar material. *Astron. & Astrophysics* **353**, 1101-1114.

Bockelée-Morvan et al. 2005. The composition of cometary volatiles, in Comets II, ed. by Festou, M. C., Keller, H. U.,. Weaver, H.A., University of Arizona Press, Tucson, 391-423.

Böhnhardt, H., Mumma, M.J., Villanueva, G.L., DiSanti, M.A., Lippi, M., and Kaufl, H.U. 2008. The unusual volatile composition of Halley-type Comet 8P/Tuttle; Addressing the existence of an inner Oort Cloud. *Astrophys. J.* **683**, L71-L74.

Bonev, B. P. 2005. Towards a chemical taxonomy of comets: Infrared spectroscopic methods for quantitative measurements of cometary water (with an independent chapter of Mars polar science). Ph.D. Thesis (U. Toledo). http://astrobiology.gsfc.nasa.gov/Bonev_thesis.pdf

Bonev, B.P., Mumma, M.J., Radeva, Y.L., DiSanti, M.A., Gibb, E.L., and Villanueva, G.L. 2008. The particular volatile composition of Comet 8P/Tuttle: A contact binary of chemically distinct cometesimals? *Astrophys. J.* **680**, L61-L64.

Chair, J.E., et al. 1995. High resolution studies of solid CO in the Taurus dark cloud: Characterizing the ices in the quiescent clouds. *Astrophys. J.* **455**, 234-243.

Chiar, J.E., et al. 1998. Processing the icy mantles in protostellar envelopes. *Astrophys. J.* **498**, 716-727.

Crovisier, J. 2007. Cometary diversity and cometary families. Proceedings of the XVIII`emes Rencontres de Blois: Planetary Science: Challenges and Discoveries, 28th May - 2nd June 2006, Blois, France. arXiv:astro-ph/0703785.

Dello Russo, N. DiSanti, M.A., Magee-Sauer, K., Gibb, E.L., Mumma, M.J., Barber, R.J., and Tennyson, J. 2004. Water production and release in comet 153P/Ikeya-Zhang (C/2002 C1): Accurate rotational temperature retrievals from hot band lines near 2.9 μm. *Icarus* **168**, 186-200.

Dello Russo, N., Bonev, B. P., DiSanti, M.A., Mumma, M.J., Gibb, E.L., Magee-Sauer, K., Barber, R.J., and Tennyson, J. 2005. Production rates, rotational temperatures, and spin temperatures in comets C/1999 H1 (Lee), C/1999 S4, and C/2001 A2. *Astrophys. J.* **621**, 537-544.

Dello Russo. N., Vervack, R.J., Weaver, H.A., Kawakita, H., Kobayashi, H., Biver, N., Bockelée-Morvan, D., and Crovisier, J. 2009. The Parent Volatile Composition of 6p/d'Arrest and a Chemical Comparison of Jupiter-Family Comets Measured at Infrared Wavelengths. *Astrophys. J.* **703**, 187-197.

DiSanti, M. A., Mumma, M. J., et al. 1999. Identification of two sources of carbon monoxide in comet Hale-Bopp. *Nature*, **399**, 662-665.

DiSanti, M.A., Mumma, M.J., Dello Russo, N., and Magee-Sauer, K. 2001. Carbon monoxide production and excitation in Comet C/1995 O1 (Hale-Bopp): Isolation of native and distributed CO sources, *Icarus* **153**, 361-390.

DiSanti, M. A., Dello Russo, N., Mumma M. J., Magee-Sauer, K., et al. 2002. *Proceedings of Asteroids, Comets, Meteors - ACM 2002. International Conference*, 689-692.

DiSanti, M.A., Mumma, M. J., Dello Russo, N., Magee-Sauer, K., and Griep, D.M. 2003. Evidence for a dominant native source of carbon monoxide in Comet C/1996 B2 (Hyakutake), *J. Geophysical Research* **108**, 15(1-19).

DiSanti, M. A., et al. 2006. Detection of Formaldehyde Emission in Comet C/2002 T7 LINEAR at Infrared Wavelengths: Line-by-Line Validation of Modeled Fluorescence Intensities. *Astrophys. J.* **650**, pg. 470-483.

DiSanti, M.A., Anderson Jr., W. M., Villanueva, G.L., Bonev, B.P., Magee-Sauer, K., Gibb, E.L., and Mumma, M.J. 2007. Depleted carbon monoxide in the Jupiter Family Comet 73 P/ Schwassmann-Wachmann 3-C. *Astrophys. J.* **661**, L101-104.

DiSanti, M.A. and Mumma, M. J. 2008. Reservoirs for Comets: Compositional Differences Based on Infrared Observations. *Space Sci. Rev.* **138**, 127-145.

DiSanti, M.A., Villanueva, G.L., Milam, S. N., Zack, L.N., Bonev, B.P. Mumma, M.J., Ziurys, L.M., and Anderson Jr., W.M. 2009. A multi-wavelength study of parent volatile abundances in Comet C/2006 M4 (SWAN). *Icarus* **203**, 589-598.

Duncan, M., Quinn, T., and Tremaine, S. 1988. The origin of short period comets. *Astrophys. J. Letters* **328**, L69.

Edwards, D. P. 1992. GENLN2: A General Line-by-Line Atmospheric Transmittance and Radiance Model (Version 3.0 Description and Users Guide). *NCAR Tech.* Note NCAR/TN-367 STR.

Eberhardt, P., et al. 1987. The CO and N_2 abundance in comet P/Halley, *Astron. Astrophys*. **187**, 481-484.

Eberhardt, P. 1999. Comet Halley's gas composition and extended sources: Results from the neutral spectrometer on Giotto. *Space Sci. Rev.* **90**, 45-52.

Festou, M.C., Keller, H.U., and Weaver., H.A. 2004. A brief conceptual history of cometary science. in Comets II, ed. by Festou, M.C., Keller, H.U.,. Weaver, H.A.,University of Arizona Press, Tucson, 3-16.

Fink, U. 2009. A taxonomic survey of comet composition 1985-2004 using CCD spectroscopy. *Icarus*, **201**, 311-334.

Friedel, D.N., Remijan, A.J., and et al. 2005. BIMA Array Detections of HCN in Comets LINEAR (C/2002 T7) and NEAT (C/2001 Q4). *Astrophys. J.* **630**, 623-630.

Feldman, P.D., and Brune, W.H., 1976. Carbon Production in Comet West. *Astrophys. J.* **209**, L45-L48.

Gibb, E.L., Mumma, M.J., Dello Russo, N., DiSanti, M.A., and Magee-Sauer, K., 2003. Methane in Oort cloud comets. *Icarus*, **165**, 391-406.

Gibb, E.L., et al. 2004. Interstellar Ice: The Infrared Space Observatory Legacy, *Astrophys. J. Sup. Series* **151**, 35-73.

Gladman, B. 2005. The Kuiper Belt and the Solar System's Comet Disk, *Science* **307**, 71-75

Gomes, R., Levision, H.F., Tsiganis, K., and Morbidelli, A. 2005. Origin of the cataclysmic Late Heavy Bombardment period of the terrestrial planets. *Nature* **435**, 466-469.

Greene, Thomas P., Tokunaga, Alan T.,Toomey, Douglas W., Carr, Jonathan B. 1993. CSHELL: a high spectral resolution 1-5 um cryogenic echelle spectrograph for the IRTF, *Proc. SPIE* **1946**, 313-324.

Herzberg. G. 1950. Spectra of Diatomic Molecules, Von Nostrand Reinhold, New York.

Hiraoka, K., et al. 2002. Formation of formaldehyde by the tunneling reaction of H with solid CO at 10 K revisited. *Astrophys. J.,* **577**, pg. 265-270.

Hoban, S., Mumma, M. J., et al. 1991. A Tentative Identification of Methanol as the Progenitor of the 3.52 –mm Emission Feature in Several Comets. *Icarus,* **93**, 122-134.

Hoban, S., Reuter, D. C., Disanti, M. A., Mumma, M. J., and Elston, R. 1993. Infrared observations of methanol in Comet P/Swift-Tuttle, *Icarus*, **105**, 548.

Hudson, R.L., and Moore, M.H.1999. Laboratory Studies of the Formation of Methanol and Other Organic Molecules by Water+Carbon Monoxide Radiolysis: Relevance to Comets, Icy Satellites, and Interstellar Ices. *Icarus*, **140**, 451-461.

Huebner, W.F. 2008. Origins of Cometary Materials. *Space Sci.. Rev.* **138**, 5-25.

JPL HORIZONS System, 2010. Generated ephemeris of C/2002 T7 (LINEAR). http://ssd.jpl.nasa.gov/?horizons

Johnson, R. E., Cooper, J. F., Lanzerotti, L. J., and Strazzulla, G. 1987. Radiation Formation of a Non-Volatile Comet*, Astron. Astrophys*. **187**, 889-892.

Kawakita, H., Watanabe, J., et al. 2004. Evidence of Icy Grains in Comet C/2002 T7 (LINEAR) at 3.52 AU, *Astrophys. J.* **601**, L191-194.

Kunde, V. R., Maguire, W. C. 1974. Direct integration transmittance model, *J. Quant. Spectrosc. Radiat. Transfer*, **14***,* 803-817.

Levison, H.F., and Duncan, M. 1990. Search for proto-comets in the outer regions of the solar system. *Astrophys. J.* **100**. 1669L.

Levison, H.F., and Morbidelli, A. 2003. The formation of the Kuiper belt by outward transport of bodies during Neptune's migration. *Nature,* **426**, pg. 419-421.

Marsden, B.G. 2003. Comet C/2002 T7 (LINEAR), *Minor Planet Electronic Circ*., 2003-R06.

Meier et al. 1993. The extended formaldehyde source in comet P/Halley. *Astron. Astrophys.* **277**, 677-690.

Magee-Sauer et al. 2008. The organic composition of comet C/2001 A2 (LINEAR). *Icarus*. **142**. 347-358.

Milam, S., et al., 2006. Formaldehyde in Comet C/1995 O1 (Hale-Bopp), C/2002 T7 (LINEAR), and C/2001 Q4 (NEAT): Investigating the Cometary Origin of H_2CO. *Astrophys, J.*, **649**, 1169-1177.

Morbidelli, A., Levison, H.F., and Gomes, R. 2008. The Dynamical Structure of the Kuiper Belt and Its Primordial Origin. The Solar System Beyond Neptune, University of Arizona Press, Tucson, 275-292

Mumma, M.J., and Reuter, D.C. 1989. On the identification of formaldehyde in Halley's comet. *Astrophys, J.*, **344**, 940-948.

Mumma, M. J., Weissman, P. R., and Stern, S. A. 1993. Comets and the origin of the solar system – Reading the Rosetta Stone. Protostars and Planets III, ed. by Levy, E., et al. University of Arizona Press, Tucson. 1177-1252.

Mumma, M. J., et al. (2001a). A survey of organic volatile species in comet C/1999 H1 (Lee) using NIRSPEC at the Keck Observatory. *Astrophys. J.* **546**. 1183-1193.

Mumma, M. J., et al. (2001b). Organic composition of C/1999 S4 (LINEAR): A comet formed near Jupiter? *Science.* **292**. 1334-1339.

Mumma, M. J., M. A. DiSanti, N. Dello Russo, K. Magee-Sauer, E. L. Gibb, and R. Novak. 2003. Remote infrared observations of parent volatiles in comets: A window on the early Solar System. *Advances in Space Research*. **31**, 2563-2575.

Nanako, S. 2003. NK 929. Nanako Note, http://www.oaa.gr.jp/~oaacs/nk/nk929.htm

Nanako, S. 2006. NK 1438. Nanako Note, http://www.oaa.gr.jp/~oaacs/nk/nk1438.htm

Oort, J. H. 1950. The structure of the cloud of comets surrounding the Solar System and a hypothesis concerning its origin, *Bull. Astron. Inst. Neth.* **11**, 91-110.

Radeva, Y., et al. 2010. The organic composition of Comet C/2000 WM1 (LINEAR) revealed through infrared spectroscopy. *Icarus*, **206**, 764-777.

Rank, et al. 1971. Interstellar molecules and dense clouds. *Science*, **174**, 1083-1101.

Remijan, A., et al. 2006. A BIMA Array Survey of Molecules in Comets LINEAR (C/2002 T7) and NEAT (C/2001 Q4). *Astrophys. J.* **643**, 567-574.

Remijan, A., et al. 2008. The Distribution, Excitation and Formation of Cometary Molecules: Methanol, Methyl Cyanide, and Ethylene Glycol. *Astrophys. J.* **661**, 613-621.

Rosenbush, V.K. 2006. Comet C/2002 T7 (LINEAR): Polarimetric and Photometric Studies, *Solar System Research*, Vol. 40, No. 3, pgs 230-238.

Rothman, L. S., et al. 2005. The HITRAN 2004 molecular spectroscopic database, *J. Quant. Spectrosc. Radiat. Transfer*, **96**, 139-204.

Schulz, et al. 2005. Coma Morphology of Three Non-periodic Comets. *Earth, Moon, and Planets*, **97**, 387-397

Seiichi Yoshida, 2008. C/2002 T7 (LINEAR). Gary W. Kronk's Cometography. http://cometography.com/lcomets/2002t7.html

Stern, S. A., 2003. The evolution of comets in the Oort Cloud and Kuiper Belt. *Nature,* **424**, 639-642.

Tisserand, F., 1896. Truite de Mechanique Celeste. **4**: 203. Paris: Gauthier-Villas.

Tokunaga, A.T., Toomey, D.W., Carr, J., Hall, D.N., and Epps, H. W. 1990. Design for a 1-5 micron cryogenic echelle spectrometer. *Proc. SPIE.,* **1235**, 131-143.

Tsiganis, K., Gomes, R., Morbidelli, A., and Levison, H.F. 2005. Origin of the orbital architecture of the giant planets of the Solar System. *Nature*, 435, 459–461.

Turner, B. E. 1989. Recent progress in astrochemistry. *Space Sci. Rev*., **51**, 235-337.

Watanabe, N., et al. 2004. Hydrogenation of CO on pure solid CO and CO-H_2O mixed ice. *Astrophys. J.,* **616**, 638-642.

Weaver, H.A. and Mumma, M.J. 1984. Infrared molecular emission from comets, *Astrophys. J.,* **276**, 782-797.

Whittet et al. 1996. An ISO view of interstellar ice: first results. *Astron. & Astrophys*., **315**, L357-L360.

Whipple, F. L. 1950. A comet model. The acceleration of Comet Encke, *Astrophys. J.,* **111**, 375-394.